UNIVERSITAT DE BARCELONA

Genome architecture and function in tissue regeneration

Palmira Llorens Giralt

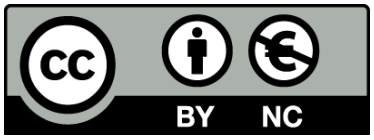

Genome architecture and function in tissue regeneration

Doctoral Thesis

Palmira Llorens Giralt

Universitat de Barcelona

Tesi Doctoral

Genome architecture and function in tissue regeneration

Arquitectura i funció del genoma en la regeneració de teixits

Memòria presentada per

Palmira Llorens Giralt

Per optar al grau de

Doctora per la Universitat de Barcelona

Programa de Doctorat en Genètica

Departament de Genètica, Microbiologia i Estadística,

Facultat de Biologia, Universitat de Barcelona

Directora i tutora: Montserrat Corominas Guiu

Doctorand: Palmira Llorens Giralt

Barcelona, maig 2025

Sobre la portada

Una ferida obre una escletxa en un teixit, trencant-ne l'arquitectura i desorganitzant momentàniament les cèl·lules que l'envolten. En aquest caos aparent, s'hi amaga una resposta coordinada a nivell genòmic, que es reconfigura per tal d'obrir regions ocultes i establir noves interaccions. És l'inici d'una coreografia transcripcional, que permetrà guarir el dany i restaurar l'equilibri perdut.

About the front cover

A wound opens a crack in a tissue, disrupting its architecture and temporarily disorganizing the surrounding cells. Amid this apparent chaos lies a coordinated genomic response, reconfiguring itself to unveil hidden regions and establish new interactions. Thus begins a transcriptional choreography that will heal the damage and restore the lost balance.

ACKNOWLEDGEMENTS

La meva directora de tesi sempre diu que un doctorat és un procés d'aprenentatge, per explorar models i perfeccionar noves tècniques i protocols, però, sobretot, per aprendre a gestionar la frustració. I si alguna cosa he sentit durant aquests més de quatre anys, és frustració constant. Però, ara que s'acaba i miro enrere, me n'adono que de la frustració també en neix l'agraïment. Perquè he tingut la sort de compartir aquesta travessia, a falta d'una paraula millor, amb persones que m'han donat suport i ànims, tant a nivell personal com professional, a les quals m'agradaria donar les gràcies.

En primer lloc, vull donar les gràcies a la Montse, per la llibertat que m'has donat, tant a nivell de projectes com a nivell personal. Vull agrair-te, especialment, l'oportunitat de formar-me en altres laboratoris (i visitar altres països!). Gràcies per tenir sempre la porta oberta i fer-me sentir que podíem parlar de tot. I, sobretot, per creure més en mi que jo mateixa.

Moltes gràcies a en Florenci, no només per aquests quatre anys d'acompanyament amb mirada crítica, però sobretot divertida i amable, sinó també per obrir-me les portes al camp de la biologia del desenvolupament, ets un superprofe;). També a la Marta, per les preguntes i l'interès constant en el projecte.

Em fa especial il·lusió agrair també a un seguit de dones que, per atzar o per fortuna, han sigut claus en el desenvolupament de la meva tesi, com a col·laboradores, mentores i amigues. A la Paula, amb qui va començar tot, gràcies per ensenyar-me tant i, sobretot, per tractar-me com una igual des del primer dia. T'he trobat molt a faltar. També vull donar les gràcies a la Sílvia Pérez, la Tània Quesada, la Silvina Nacht, i, especialment, a la Maria Martí, l'Esther Bertran i la Marina Ruiz, per acollir-me als seus laboratoris i ajudar-me a tirar endavant, sempre amb un somriure i una mà estesa. Els vostres grups tenen molta sort de comptar amb vosaltres.

A la gent del lab, present i passada, així com als doctorands dels labs veïns, mil gràcies per acompanyar-me i ser font inesgotable de xafarderies i riures constants. Especialment, gràcies al José, el meu compi de congressos i copes de vi, per ser insuportablement necessari, i al Carlos, sense el qual no sé com hauria acabat aquesta tesi. També vull agrair a les compis dels labs intermitents, perquè les estades amb elles han sigut com un petit oasi. A Bellvitge, Gemma, Anna i Paula, m'heu donat mooolta vida aquest últim any. Also, a special thanks to the people in Durham, and especially Pierre and David, who taught me extraordinary things and were incredibly kind. To Erin, with all my heart, thank you for allowing me to live the American Dream. I will never forget the Duke games, crashing at your place for a Sunday grill or a Halloween party, joining your family for Thanksgiving, and just making me feel like I belonged. I miss you! You will always have a place here in Barcelona. Also, thanks to Margot, Bruno, Melissa, Colleen, Hunter and Nick, for an amazing ride, and Amy and Kelsey, for your help and friendship. I am also grateful to Jenisha in Lausanne, for a cheerful collaboration.

I would like to express my deepest gratitude to Dr. Kenneth Poss for an incredible and enriching experience at Duke University. I am also very grateful to Dr. Maria Cristina Gambetta, for welcoming me into her lab in Lausanne and providing a much-needed boost to my project.

Me gustaría agradecer a la Dra. Isabel Fabregat, por acogerme en su laboratorio y darme la oportunidad de expandir mi tesis en un campo muy emocionante. També vull agrair al Dr. Marc Martí-Renom, per l'ajuda indispensable pel projecte del Hi-C, ja sigui acollint-me al seu laboratori, analitzant dades o ensenyant-me a analitzar-les jo mateixa. Y agradecer también al Dr. Guillermo Vicent, por su ayuda y asesoramiento en el proyecto de hígado.

A nivell personal, no sé ni per on començar. Milions de gràcies a les Gipsiqueens, i especialment a les Diosas: Figui, Geor, Bea, Carla, Aida, Escu, Paula i Jana (a qui vull agrair especialment l'ajuda amb la portada). Heu sigut la constant d'aquests anys i em sento molt afortunada de tenir-vos. Sou més que un equip, sou família. I especialment a l'Alba, per ser la germana gran que mai he tingut. Gràcies per escoltar-me quan més ho necessitava i fer-me saber que tenia altres opcions, t'estimo. Als de Pastuira, per ser un món a part, i especialment al Miqui i l'Ona, sou casa. A la Cris i totes les de ball, per ser la millor font de desconnexió. Mil gràcies a les de la uni, Berta, Júlia, Laies Beni i Carbi, Laura, Llu, Mary i Patri, em sento increïblement afortunada d'haver-vos trobat i poder fer juntes aquest camí, gràcies per compartir les meves pors i celebrar, sempre i de manera incondicional, els meus petits èxits; m'omple d'orgull ser la vostra amiga. I a la Naira, la Carlota, l'Alba i la Berta, em feu ser una persona més atrevida, més feliç i més viva, us estimo molt!

Finalment, a la meva família, gràcies per donar-me la constància i amor necessaris per atrevir-me a volar lluny. Mariona i Natxo, no trobo paraules per agrair-vos cada dia dels tres mesos que vaig ser amb vosaltres, gràcies per acollir-me i fer-me veure món. A la Cris i l'Anna, pel vostre suport incondicional, sobretot a base de *tuppers*;) I especialment a la Cinta i la Rosa, per cuidar-me tant (a mi i a tota la família) i fer-me sentir sempre com a casa. Als avis, pels records tendres que perduren. I a l'àvia Mercè, per ser la pionera científica i mimar-me sempre amb dolçor i trapelleria, i a l'àvia Maria, per escalfar-me les mans quan fa fred i gaudir cada dia des de la tranquil·litat i l'amor a la família. I, especialment, a en Quim, a qui admiro profundament i amb qui no calen paraules, i als meus pares, per haver posat sempre la nostra educació al davant, però, sobretot, la nostra felicitat en primer lloc. Em sento orgullosa de formar part d'aquesta petita família, us estimo molt. La sort que tinc de poder comptar amb vosaltres és infinita.

I a en Pol, amb qui he après a gaudir de cada moment i a valorar les petites coses. Gràcies per donar-me estabilitat i seguretat, però alhora, ser capaç de treure el meu costat més infantil i intrèpid. Em fas immensament feliç.
Cada dia amb tu és una aventura, i les que encara ens esperen. T'estimo.

This work was supported first by the Agència de Gestió d'Ajuts Universitaris de Recerca through FI grant No. FI-B100235 and next by the Spanish Ministry of Universities through FPU grant No. FPU20/01473. The research stay at Duke University was supported by the "Ayuda de Movilidad para Estancias Breves FPU 2023" EST23/00461, while the research visit at the UNIL in Lausanne was supported by the Doctoral School of the University of Barcelona.

Als meus pares, per prioritzar-nos sempre.

A en Pol, per les teves ganes de viure intensament.

I de l'engruna en treus una altra festa.

—Eva Piquer, *Aterratge*

RESUM

La capacitat regenerativa és molt diversa al món animal, no només entre espècies, sinó també entre diferents òrgans i estadis del desenvolupament d'un mateix organisme. Entendre per què existeix aquesta variabilitat continua sent un dels grans reptes de la biologia del desenvolupament. Estudis en animals amb gran capacitat regenerativa han demostrat que els gens implicats en el desenvolupament sovint es reactiven durant la regeneració i solen estar conservats a nivell evolutiu. Per tant, les diferències en el potencial regeneratiu podrien dependre de la capacitat d'un teixit determinat per reactivar aquests programes en un context específic, més que de la presència o absència dels gens necessaris. Aquesta reactivació transcripcional inclou múltiples nivells de regulació, com ara l'activitat de factors de transcripció, elements d'ADN *cis*-reguladors, remodelatge de la cromatina, modificacions d'histones i l'organització tridimensional (3D) del genoma.

En aquest treball, explorem com l'organització de la cromatina i l'activitat del genoma influencien les respostes regeneratives mitjançant l'estudi de dos teixits epitelials que es regeneren per proliferació compensatòria. Primer, fem servir un model mamífer amb gran capacitat regenerativa, l'hepatectomia parcial de dos terços en fetge de ratolí, per estudiar canvis en l'estructura de la cromatina durant la regeneració. Integrant dades d'accessibilitat de la cromatina i transcriptòmiques, mostrem que la reprogramació transcriptional està mediada per una àmplia gamma d'elements *cis*-reguladors, incloent-hi elements reguladors sensibles a la regeneració (RREs). Aquests RREs, que inclouen tant potenciadors específics de regeneració com potenciadors del desenvolupament reactivats, indueixen l'expressió de gens implicats en la preparació i proliferació d'hepatòcits. En canvi, es reprimeixen potenciadors associats a funcions energèticament costoses típiques dels hepatòcits quiescents, cosa que comporta una disminució de l'expressió de gens metabòlics, especialment aquells relacionats amb el metabolisme lipídic. A més, construïm una xarxa reguladora gènica que revela una cascada d'activació de factors de transcripció que modulen l'expressió de gens de regeneració de manera temporalment específica. En conjunt, oferim un atles a escala genòmica de les interaccions entre potenciadors i gens que aporta noves perspectives sobre els mecanismes reguladors que determinen la regeneració hepàtica.

Per tal d'investigar si i com l'estructura de la cromatina i l'arquitectura 3D del genoma influeixen en el potencial de regeneració, un àmbit encara poc explorat, utilitzem el disc imaginal d'ala de *Drosophila melanogaster* com a model. Descobrim que l'organització espacial del genoma en les cèl·lules del disc d'ala canvia de manera subtil però significativament durant la regeneració, incloent una reducció de la compartimentalització. Notablement, observem un augment en la freqüència de contacte en tres interaccions de llarga distància, anomenades *meta-loops*, els extrems dels quals es troben a més de 3 megabases. Mitjançant deficiències cromosòmiques i delecions dirigides per CRISPR/Cas9, demostrem que aquests *meta-loops* són essencials per a la regeneració però prescindibles durant el desenvolupament. Finalment, identifiquem la proteïna architectural Cp190 com un factor clau en la formació d'aquests *meta-loops*.

Els resultats d'aquesta tesi revelen que l'estat de la cromatina i l'arquitectura genòmica tenen rols crítics durant la regeneració, posant en relleu la conservació de principis reguladors de la reparació tissular.

Paraules clau

Regeneració; Dinàmica de la cromatina; Organització 3D del genoma; Potenciadors; Desenvolupament; Ratolí; Fetge; *Drosophila melanogaster*; Disc imaginal de l'ala

ABSTRACT

Regenerative capacity differs not only across species, but also between organs and developmental stages within the same organism. Understanding why this variability exists remains a major challenge in developmental biology. Studies in regenerative animals have shown that genes involved in development are often re-expressed during regeneration and tend to be evolutionary conserved. Therefore, differences in regenerative potential may depend on the ability of a given tissue to reactivate these programs in a context-dependent manner, rather than on the presence or absence of necessary genes. This transcriptional reactivation is orchestrated through multiple layers of regulation, including transcription factor activity, *cis*-regulatory DNA elements, chromatin remodeling, histone modifications, and the three-dimensional organization of the genome.

In this work, we explore how chromatin organization and genome activity influence regenerative responses by studying two epithelial tissues that regenerate through compensatory proliferation. First, we use a highly regenerative mammalian model, the two-thirds partial hepatectomy in mouse liver, to study changes in chromatin structure during regeneration. By integrating chromatin accessibility and transcriptomic data, we show that transcriptional reprogramming is driven by a wide range of *cis*-regulatory elements, including regeneration-responsive regulatory elements (RREs). These RREs, which comprise both regeneration-specific and reactivated developmental enhancers, activate genes involved in hepatocyte priming and proliferation. In contrast, enhancers linked to energy-intensive functions of quiescent hepatocytes become repressed, leading to the downregulation of metabolic genes, particularly those involved in lipid metabolism. We further construct a gene regulatory network that uncovers a cascade of transcription factor activation, which modulates expression of repair genes in a time-specific manner. Altogether, we provide a genome-wide atlas of enhancer-gene interactions that offers new insights into the regulatory mechanisms driving liver regeneration.

To investigate whether and how chromatin structure and genome folding influence regenerative potential, an area that remains largely unexplored, we use the wing imaginal disc of *Drosophila melanogaster* as a model. We find that the spatial organization of the genome in wing disc cells undergoes subtle but significant reorganization during regeneration, including reduced compartmentalization. Notably, we observe increased contact frequency across three long-range chromatin loops, termed meta-loops, whose anchors span over 3 megabases. Using chromosomal deficiencies and CRISPR/Cas9-mediated knockouts, we demonstrate that these loops are required for regeneration but are dispensable during development. Finally, we identify the architectural protein Cp190 as a key factor in the formation of these meta-loops.

The results of this thesis reveal critical roles for chromatin states and higher-order genome architecture in regeneration, highlighting conserved regulatory principles underlying tissue repair.

Keywords

Regeneration; Chromatin dynamics; 3D Genome organization; Enhancers; Development; Mouse; Liver; *Drosophila melanogaster*; Wing imaginal disc

TABLE OF CONTENTS

ABBREVIATIONS

3D	Three-dimensional
ABC	Activity-by-Contact algorithm
ATAC-seq	Assay for Transposase-Accessible Chromatin followed by sequencing
ChIP-seq	Chromatin Immunoprecipitation followed by sequencing
Chr	Chromosome
CRISPR	Clustered Regularly Interspaced Short Palindromic Repeats
CTRL	Control
DRRE	Damage Responsive Regulatory Element
DEG	Differentially Expressed Gene
Df	Deficiency
FC	Fold Change
GRN	Gene Regulatory Network
H3K4me1/3	Histone H3 Lysine K4 mono or trimethylation
H3K27ac	Histone H3 Lysine K27 acetylation
Hi-C	High-throughput chromosome conformation capture followed by sequencing
NDA	Non-Differentially Accessible
PHx	Partial Hepatectomy
REG	Regeneration
RNAi	RNA of interference
RRE	Regeneration Responsive regulatory Element
TAD	Topologically Associating Domain
TF	Transcription Factor
WT	Wild-type

INTRODUCTION

“If there were no regeneration, there would be no life.
If everything regenerated, there would be no death.”

—R.J. Goss, *Principles of Regeneration* (1969)

1. REGENERATION

1.1 The history of regeneration

Regeneration, the ability to restore lost or injured body parts, is a fundamental property of multicellular life that has captivated scientists for centuries. While regenerative capacity is widespread across the animal kingdom, its uneven distribution raises intriguing questions about its evolutionary origins and underlying developmental mechanisms. Understanding why some organisms can regenerate while others cannot remains a major challenge in biological research.

The concept of regeneration can be traced back to ancient Greek mythology. In Greek legends, the Hydra was a serpent-like creature that could regrow its severed heads, while Prometheus, punished by Zeus for giving fire to humanity, endured the daily regeneration of his liver after being repeatedly devoured by an eagle (Goss, 1991). These myths may reflect early observations of regenerative potential in nature, long before scientific exploration of the topic began.

The first documented experimental studies on regeneration were conducted by Abraham Trembley in the 1700s, where he characterized the remarkable regenerative abilities of the hydra. By sectioning these invertebrate polyps along various axes, Trembley observed that each part could regenerate into a complete individual, eventually creating a seven-headed organism. This inspired him to name these animals after the Greek mythological monster (reviewed in Goss, 1991; Bely and Nyberg, 2010; Galliot, 2012).

Another hallmark in regenerative biology was the publication of *Regeneration* (1901) by Thomas Hunt Morgan. In this work, Morgan explored the parallels between embryological growth and regenerative processes, proposing that regeneration could serve as a model for studying development and the mechanisms of differentiation. He also challenged existing developmental theories, which failed to explain the full spectrum of regenerative phenomena, thus opening new research lines in embryology. One of Morgan's key contributions was the establishment of a dual classification for regeneration: epimorphis and morphallaxis. **Epimorphosis** involves cell proliferation and/or the formation of a blastema, a mass of undifferentiated cells that forms at the wound site and later develops into the missing body part, as exemplified by salamander limb regeneration. Conversely, **morphallaxis** occurs through the repatterning or remodeling of existing tissue, with little or no cell proliferation, as seen in *Hydra* regeneration (reviewed in Bely and Nyberg, 2010; Sunderland, 2010; Mehta and Singh, 2019).

Currently, three regenerative modes have been proposed: regeneration by (1) rearrangement of pre-existing tissue, (2) use of adult somatic stem cells, and (3) dedifferentiation and/or transdifferentiation of cells (reviewed in Alvarado and Tsonis, 2006; Mehta and Singh, 2019). Although distinct in nature, these mechanisms can overlap and coexist, with animals with regenerative potential often employing one or a combination of them (Bideau *et al*., 2021). Furthermore, regeneration occurs at different levels of biological organization, ranging from individual cells to complex organs and even whole-body regeneration. These regenerative strategies and hierarchical levels vary among taxa, and

even closely related species can exhibit different degrees of regenerative capacity (reviewed in Bely and Nyberg, 2010; Mehta and Singh, 2019).

1.2 Regeneration in metazoans

The ability to regenerate is found across all phyla, with high regenerative potential, including whole-body regeneration, present in all basal metazoan lineages. However, despite its presumed advantages, regeneration is not universal (Bely and Nyberg, 2010; Iismaa *et al*., 2018; Bideau *et al*., 2021) (Fig. 1). For example, while many ecdysozoan phyla, including multiple arthropod species, can regenerate limbs and antennae, none are capable of regenerating an entire body or primary body axis. Even closely related species can exhibit striking differences in regenerative potential. For instance, planarians can regenerate their entire body from tiny tissue fragments, whereas other platyhelminthes cannot regenerate their heads after amputation. Similarly, the spiny mouse *Acomys* can regenerate ear hole punches and large wounds in the skin, while the common laboratory mouse *Mus musculus* lacks this ability (Bely and Nyberg, 2010; Alvarado, 2000; Poss and Tanaka, 2024).

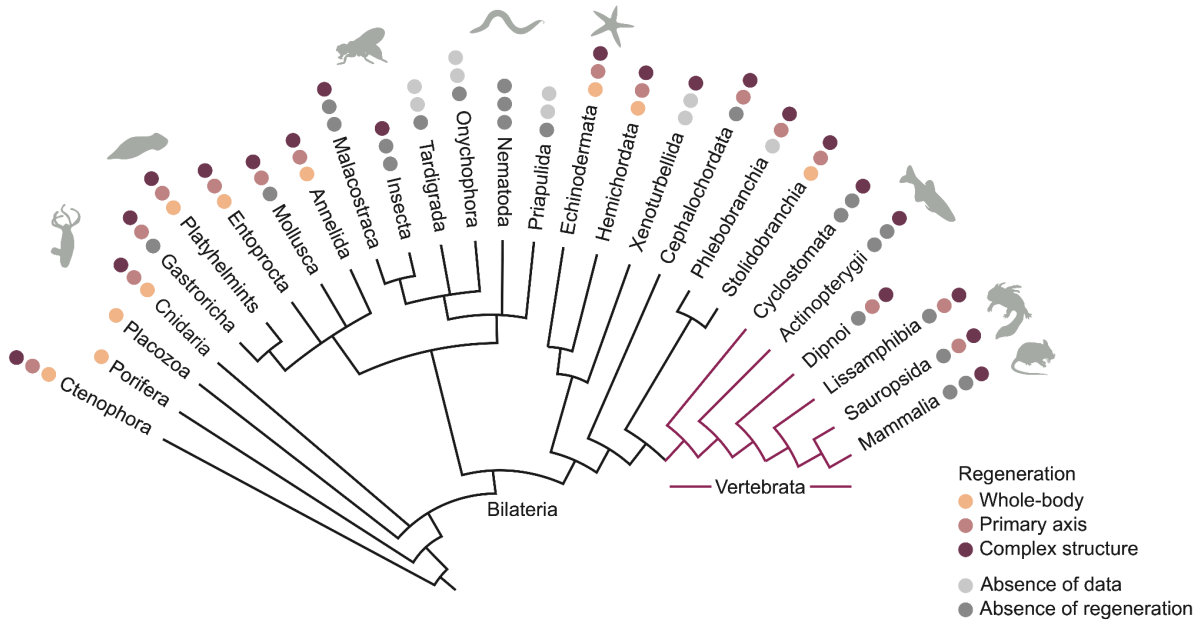

Figure 1. Phylogenetic distribution of regeneration across Metazoa. The regenerative abilities of each taxon are mapped on the metazoan phylogenetic tree with colored circles, based on at least one substantiated report, but not necessarily for all species in the taxon. Light grey indicates a lack of substantiated data, while dark grey denotes the absence of regenerative capacity. Typical model organisms used in developmental and regeneration studies are depicted as silhouettes next to their respective taxa, including hydra (*Hydra vulgaris*), planarian (*Schmidtea mediterranea*), fruit fly (*Drosophila melanogaster*), nematode (*Caenorhabditis elegans*), sea star (*Asterias rubens*), zebrafish (*Danio rerio*), axolotl (*Ambystoma mexicanum*), and mouse (*Mus musculus*).
Data and tree topologies adapted from Bely and Nyberg (2010); Bideau et al. (2021).

One explanation for this diversity is that the common ancestor of metazoans was capable of regeneration, but this trait was selected against during evolution, as uncontrolled proliferation can lead to tumor formation and compromise long-term survival (Bely and Nyberg, 2010; Alvarado, 2000). Alternatively, the absence of selective pressure for regeneration could have led to the loss of this trait over time (Alvarado, 2000; Chen and Poss, 2017). Either way, if the hypothesis of a **common regenerative ancestor** is correct, then all regenerative processes share a fundamental basis, underscoring the relevance of studying regeneration in non-mammalian organisms to advance in regenerative medicine. On the other hand, an alternative hypothesis proposes that regeneration evolved independently multiple times through positive selection as an adaptation to environmental pressures. This would imply that regenerative mechanisms vary across species, limiting the applicability of studies on non-mammalian organisms for developing therapies to reinduce regeneration in human tissues lacking this ability (Alvarado, 2000; Bely and Nyberg, 2010; Maden, 2018).

Notably, regenerative capacity varies greatly not only among species but also across organs and developmental stages within the same species. For instance, while fetal and neonatal mice can regenerate their hearts following cardiac injury, this capacity is lost in adulthood (Poss and Tanaka, 2024). Similarly, *Drosophila* larvae can regenerate imaginal discs—larval epithelial sacs that give rise to adult body structures such as eyes, wings, and genitalia—but this ability is lost with the onset of metamorphosis (reviewed in Hariharan and Serras, 2017).

1.3 Mechanisms of regeneration

Regeneration has long been a central focus of biological research, with studies across diverse model organisms providing valuable insights into its underlying mechanisms. While regenerative processes vary widely among species, key aspects of tissue repair appear to be conserved. Based on these observations, Poss and Tanaka (2024) recently proposed four **hallmarks of regeneration** that typically occur in response to acute injury: (1) activation of a competent cellular source to replace lost tissue, (2) initiation of regeneration programs, (3) productive interactions among supporting cell types, and (4) functional integration of newly formed cells to restore tissue size and shape.

The first hallmark, activation of a competent cellular source, functions through different mechanisms depending on the origin of new cells. Regenerative strategies include the use of stem cells, transdifferentiation, dedifferentiation, proliferation of differentiated cells, and endoreplication (Fig. 2A). For instance, planarians regenerate by forming a blastema through the proliferation of neoblasts, pre-existing somatic **stem cells** (Alvarado and Tsonis, 2006). **Transdifferentiation**, which involves the direct transition of one differentiated cell type into another without an intermediate undifferentiated state, is best exemplified by lens regeneration in newts. **Dedifferentiation** is a hallmark of zebrafish heart regeneration, where cardiomyocytes revert to a fetal-like state and regain proliferative capacity in response to injury. In other cases, regeneration relies on the division of differentiated cells, such as the **compensatory proliferation** of hepatocytes during liver regeneration. Alternatively, regeneration can occur without cell division, as observed in mammalian skeletal muscle recovery through myoblast fusion, or in the abdominal epidermis of *Drosophila*, where epithelial cells undergo **endoreplication** and fuse to form a syncytium in response to wounding (Tanaka and Reddien, 2011; Bideau *et al*., 2021; Poss and Tanaka, 2024).

In addition, five hierarchical levels of regeneration can be defined based on the complexity of the regenerated structure: (a) **whole-body** regeneration, such as the restoration of an entire planarian from a tiny tissue fragment; (b) regeneration of **complex structures**, including limbs, fins, antennae or tails, observed in some arthropods and vertebrates; (c) **organ** regeneration, such as the regeneration of heart and liver in zebrafish; (d) **tissue** regeneration, characterized by the closure of gaps in epithelia like the epidermis or gut; and (e) **cellular** regeneration, exemplified by axonal regeneration (Bely and Nyberg, 2010; Slack, 2017; Mehta and Singh, 2019) (Fig. 2B).

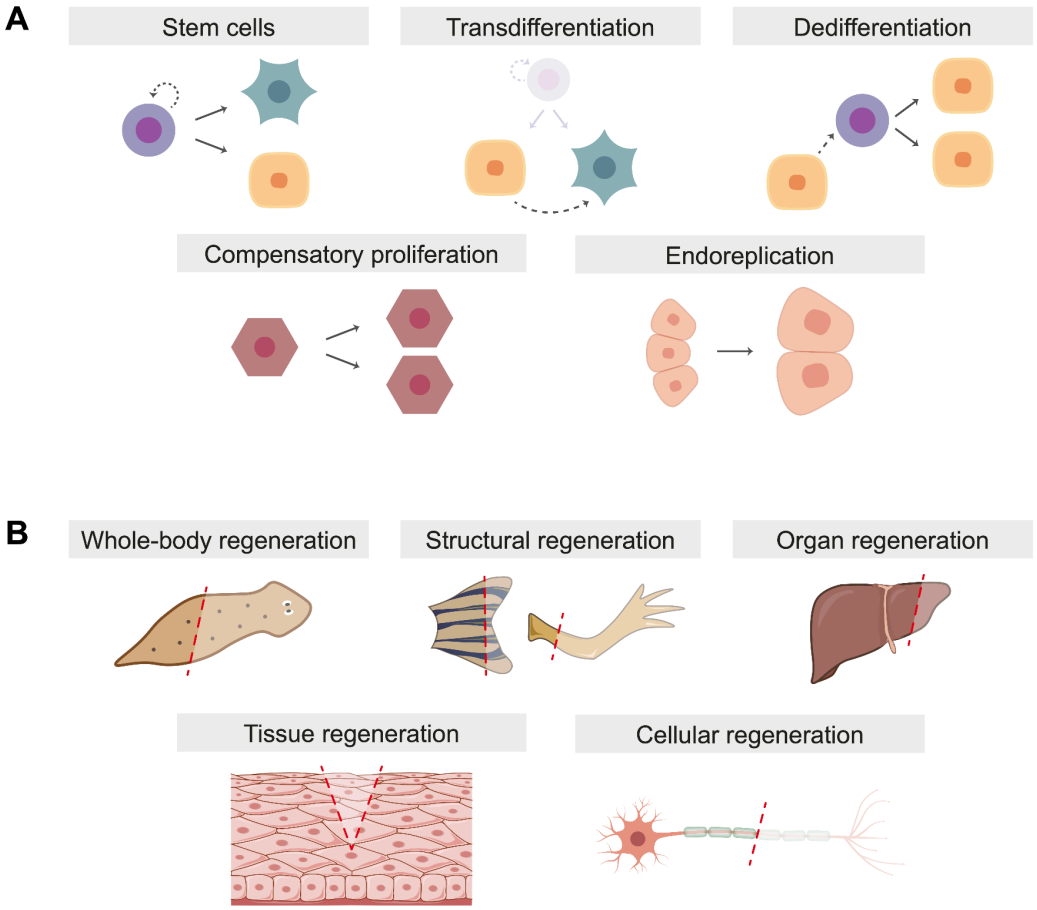

Figure 2. Types of regeneration. (A) Regenerative strategies based on the source of new cells: stem cells, transdifferentiation, dedifferentiation, compensatory proliferation, or endoreplication. **(B)** Biological levels of regeneration based on structural complexity: whole-body regeneration (e.g. planarians); regeneration of complex structures (e.g. zebrafish fins, salamander limbs); organ regeneration (e.g. mammalian liver); tissue regeneration (e.g. epidermal wound healing); and cellular regeneration (e.g. axonal repair). *Adapted from Slack (2017); Bely and Nyberg (2010).*

1.4 Models of regeneration

Liver regeneration and *Drosophila* imaginal discs provide valuable model systems to study the fundamental mechanisms underlying regenerative processes.

1.4.1 Liver regeneration

The mammalian liver exhibits remarkable regenerative capabilities after injury or resection. As the largest internal organ in the human body, the liver is responsible for essential functions including the production of serum proteins, the synthesis, storage and redistribution of nutrients, and the detoxification of both internal and external wastes. Its critical role in systemic homeostasis has driven the evolution of multiple regenerative mechanisms that safeguard against liver failure (reviewed in Taub, 2004; Michalopoulos and Bhushan, 2021).

Liver architecture and function

The liver is a highly specialized organ with a complex architecture that supports its diverse physiological functions. It is composed of various cell types, each derived from different embryological lineages. Hepatocytes, the principal parenchymal cells, account for nearly 80% of the liver mass and are responsible for most metabolic and synthetic activities. The second most abundant cell population are cholangiocytes, or biliary epithelial cells (BECs), which line the bile ducts and are involved in bile transport and modification. Both hepatocytes and cholangiocytes arise from hepatoblasts, a common embryonic precursor with endodermal origin. Other non-parenchymal liver cells include liver sinusoidal endothelial cells (LSECs), which are fenestrated endothelial cells lining the sinusoids; Kupffer cells, the resident liver macrophages; and hepatic stellate cells (HSCs), which serve as vitamin A reservoirs and secrete cytokines and growth factors in response to injury (Taub, 2004; Si-Tayeb *et al*., 2010; Trefts *et al*., 2017; López-Luque and Fabregat, 2018; Arias *et al*., 2020).

Liver cells are organized into functional architectural units known as hepatic lobules, hexagonal structures with hepatocytes arranged radially around a central hepatic vein (Trefts *et al*., 2017) (Fig. 3A). Each lobule has a portal triad at each corner, consisting of a bile duct, portal vein, and hepatic artery, which transport bile and supply blood to the liver, respectively. Portal blood, rich in nutrients, toxins, and hormones, mixes with oxygenated arterial blood as it flows through the sinusoids within the lobules (Si-Tayeb *et al*., 2010; Abu Rmilah *et al*., 2019; Arias *et al*., 2020). This dual blood supply creates gradients in oxygen, nutrients, and metabolic byproducts, establishing a **metabolic zonation** that partitions the lobule into distinct functional zones (Fig. 3B). Periportal hepatocytes, receiving oxygen- and nutrient-rich blood, are specialized in gluconeogenesis and β-oxidation, whereas centrilobular hepatocytes, exposed to lower oxygen levels, are more active in glycolysis and lipogenesis (Kaestner, 2009; Hijmans *et al*., 2014; Trefts *et al*., 2017).

The liver is essential for numerous physiological processes, such as the regulation of carbohydrate, lipid, and protein homeostasis. It maintains blood glucose levels by synthesizing and storing glycogen, as well as by producing glucose via gluconeogenesis during hypoglycemia. As a central hub for lipid metabolism, the liver is responsible for cholesterol synthesis, triglyceride production, and lipoproteins assembly. Hepatocytes also synthesize many plasma proteins, such as albumin (Rui *et al*., 2014; Abu Rmilah, 2019). In addition, the liver exhibits both endocrine and exocrine functions, secreting hormones like insulin-like growth factors and synthesizing bile acids to facilitate the emulsification and absorption of dietary fats (Arias *et al*., 2020). Furthermore, the liver plays a critical role in

detoxification, neutralizing toxic substances from both endogenous and exogenous sources, such as metabolic byproducts or drugs. Hepatocytes convert these toxins into hydrophilic metabolites through cytochrome P450 enzymes for excretion via bile, urine, or stool (Stanger, 2015; Abu Rmilah, 2019).

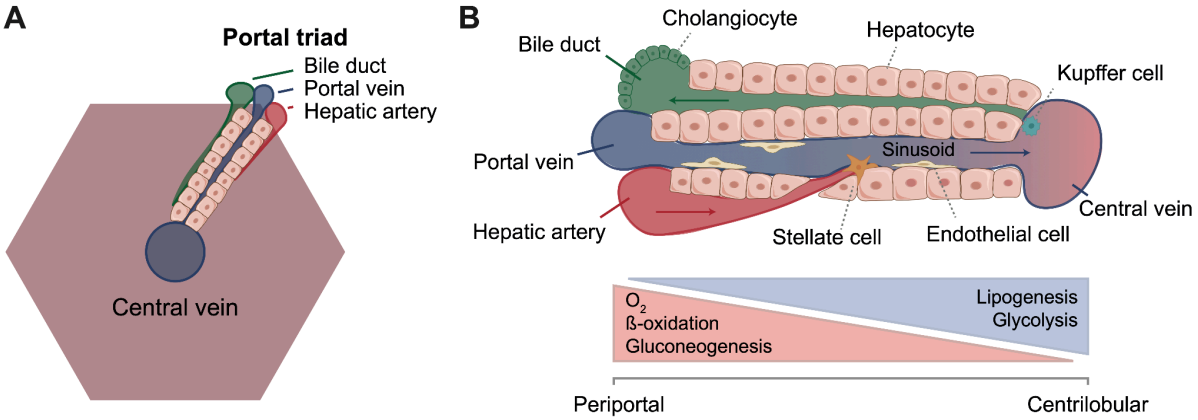

Figure 3. Liver architecture and metabolic zonation. (A) Representation of the hepatic lobule, functional unit of the liver with hexagonal shape. Hepatocytes are arranged radially around a central vein, with a portal triad (bile duct, portal vein and hepatic artery) at each corner. **(B)** Representation of a sinusoid and the corresponding zonation of metabolic processes. Blood from the hepatic artery (oxygen-rich) and portal vein (nutrient-rich) mixes in the sinusoids and flows toward the central vein. This generates an oxygen, nutrient, and waste gradient that defines a metabolic zonation: periportal hepatocytes specialize in gluconeogenesis and β-oxidation, while centrilobular hepatocytes perform glycolysis and lipogenesis. Arrows indicate fluid flow direction. *Adapted from Trefts et al., (2017)*.

Liver regeneration models: 2/3 partial hepatectomy

Several experimental models have been used to understand liver regeneration, including multiple animal models and different methods to induce damage. Traditionally, liver regeneration has been studied in rodents (rats and mice), although the zebrafish has recently emerged as a cost-effective alternative. Liver injury models in rodents include the widely used two-thirds partial hepatectomy (2/3 PHx) and chemically-induced hepatotoxicities, such as the administration of the well-established hepatotoxin carbon tetrachloride (CCl_4) (Forbes and Newsome, 2016; López-Luque and Fabregat, 2018; Bangru and Kalsotra, 2020).

The **2/3 PHx** model, in particular, takes advantage of the multilobar structure of the rodent liver (Michalopoulos and Bhushan, 2021). First described by Higgins and Anderson (1931), this method involves the surgical removal of the median and left lateral lobes, which together constitute approximately 70% of the liver (Fig. 4A). Following PHx, the remaining liver restores its original mass and size within 20 days. However, the resected lobes are not reconstructed; instead, cells in the remnant tissue undergo compensatory hypertrophy and hyperplasia. Thus, the term “regeneration” may not be entirely accurate in this context and is better described as compensatory proliferation (Taub, 2004; Michalopoulos, 2020). Cell proliferation after PHx generally follows phenotypic fidelity, meaning hepatocytes generate hepatocytes, and the same applies for cholangiocytes, endothelial cells, hepatic stellate cells and Kupffer cells (Michalopoulos and Bhushan, 2021).

The classical model of PHx offers several advantages, including low perioperative mortality, the absence of necrosis in the residual tissue, a simple and reproducible surgical procedure, and a well-characterized sequence of events. Following PHx, liver regeneration proceeds through three sequential phases: an initiation or “priming” phase, a proliferation or progression phase, and a termination phase (reviewed in López-Luque and Fabregat, 2018; Abu Rmilah *et al*., 2019; Michalopoulos, 2020; Ozaki, 2020) (Fig. 4B).

The **priming phase** of liver regeneration occurs within the first four hours after PHx. During this period, quiescent hepatocytes (in the G0 phase) are primed into a state of replicative competence by a cytokine network. Approximately 95% of hepatic cells rapidly and synchronously enter the cell cycle, with DNA synthesis peaking around 36 hours post-PHx (reviewed in Taub, 2004; Bangru and Kalsotra, 2020). Immediately after surgery, increased portal vein flow per liver volume exerts mechanical stress on endothelial cells, triggering the activity of urokinase plasminogen activator (uPA). In turn, uPA mediates the conversion of plasminogen into plasmin, which activates matrix metalloproteinases (MMPs). These MMPs remodel the extracellular matrix (ECM) and activate hepatocyte growth factor (HGF), which is present in the hepatic ECM (Abu Rmilah *et al*., 2019; Ozaki, 2020; Michalopoulos and Bhushan, 2021).

Concurrently, gut-derived factors such as lipopolysaccharide (LPS) reach the liver and activate Kupffer cells, inducing the secretion of Tumour Necrosis Factor-alpha (TNFα) and interleukin 6 (IL-6). This results in increased levels of circulating cytokines in peripheral blood, along with elevated concentrations of other molecules involved in liver regeneration, such as leptin and serotonin (Bangru and Kalsotra, 2020; Michalopoulos and Bhushan, 2021; Ma *et al*., 2025). These proinflammatory signals activate key transcription factors (TFs) in hepatocytes, including Signal Transducer and Activator of Transcription 3 (STAT3) and Nuclear Factor-kappa B (NF-κB), mediated by IL-6 and TNFα, respectively. This activation triggers the expression of several immediate-early genes related to hepatocyte proliferation, including *c-Fos*, *c-Jun* and *c-Myc* (Taub, 1996; López-Luque and Fabregat, 2018; Michalopoulos, 2020; Ozaki, 2020; Blake and Steer, 2023) (Fig. 4B).

After priming, hepatocytes transition into the **progression phase**, during which mitogenic growth factors such as Epidermal Growth Factor (EGF) and HGF bind to their respective receptors (EGFR and c-Met), activating intracellular signalling pathways, including MAPK, STAT3, PI3K/Akt, and ERK. These signals, together with the induction of early-delayed genes like cyclins and Cyclin-Dependent Kinases (CDKs), promote cell cycle progression, allowing hepatocytes to enter the S phase (DNA synthesis) 36 hours post-PHx and undergo mitosis at 48 hours post-PHx (Fig. 4B). Non-parenchymal cells divide sequentially after hepatocytes, with Kupffer cells proliferating first, followed by cholangiocytes, and finally endothelial cells (Taub, 2004; López-Luque and Fabregat, 2018; Abu Rmilah *et al*., 2019; Michalopoulos, 2020; Ozaki 2020).

Once liver regeneration has compensated for the lost tissue, growth must be tightly regulated to prevent excessive proliferation. The **termination phase**, responsible for restoring liver size and homeostasis, is mediated by several factors, including Transforming Growth Factor (TGF)-ß, IL-1 and tumour suppressor genes (p53 and p21), which promote proliferation arrest (Fig. 4B). Although these factors play a key role during the latest stage of liver regeneration, they are expressed within the first hours after PHx (López-Luque and Fabregat, 2018; Bangru and Kalsotra, 2020).

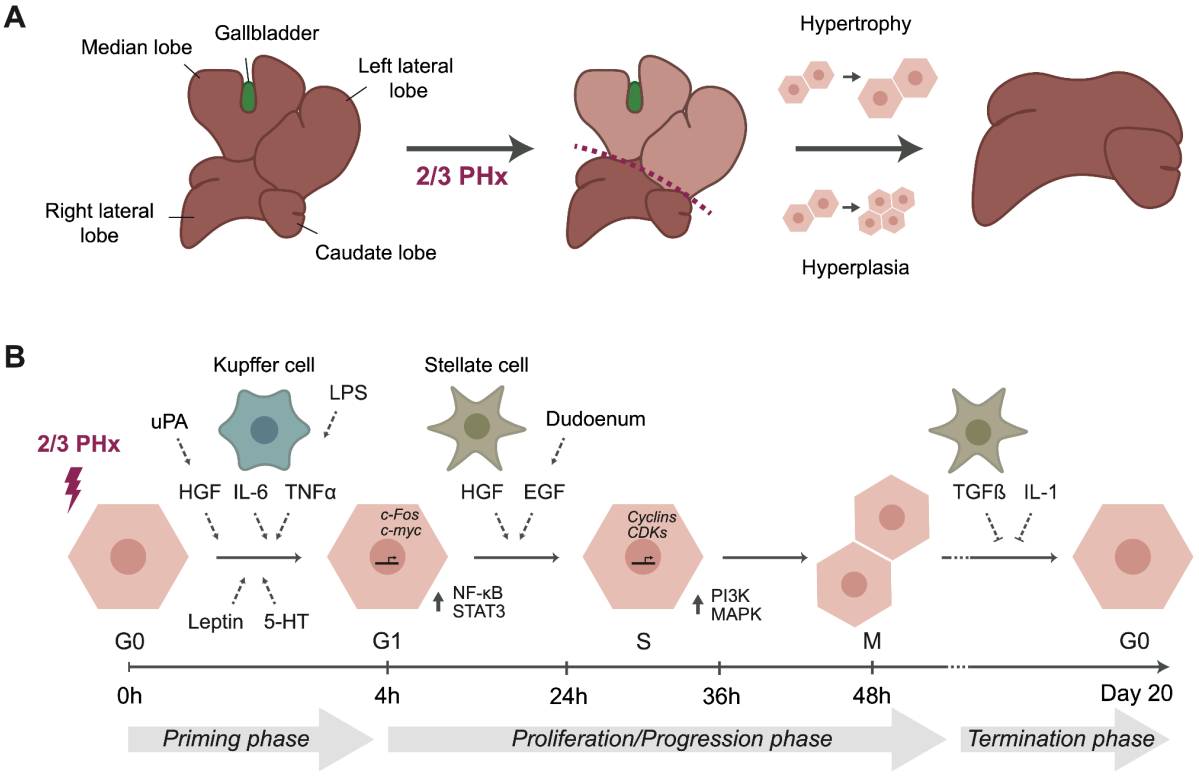

Figure 4. Liver regeneration after partial hepatectomy (PHx). (A) Schematic of the 2/3 PHx model in rodents: the median and left lateral lobes are surgically removed, and the remaining lobes regenerate to restore original liver mass via compensatory hypertrophy and hyperplasia. **(B)** Timeline of liver regeneration through three phases: priming, proliferation, and termination. Gut-derived factors like lipopolysaccharide (LPS) activate Kupffer and stellate cells and increase tumour necrosis factor (TNF)α and interleukin (IL)-6 production. These, along with circulating factors like leptin and serotonin (5-HT), prime hepatocytes to re-enter the cell cycle. TNFα and IL-6 activate the transcription factors Nuclear Factor-kappa B (NF-κB) and Signal Transducer and Activator of Transcription 3 (STAT3), respectively, inducing the expression of genes such as *c-fos* and *c-myc*. In the progression phase, duodenum-derived epidermal growth factor (EGF) and hepatocyte growth factor (HGF) secreted by stellate cells, promote hepatocyte proliferation. Finally, transforming growth factor β (TGFβ) signaling induces proliferation arrest, marking the termination phase of regeneration.

Metabolic reprogramming during liver regeneration

As a central organ in regulating glucose, lipid, and protein homeostasis, the liver undergoes metabolic remodeling to adapt its cellular activity and functional demands in response to injury. These reprogrammed metabolic networks are essential not only for meeting systemic energy needs but also for providing anabolic precursors and generating molecular signals that regulate liver regeneration (Caldez *et al*., 2018; Solhi *et al*., 2021; Ma *et al*., 2025).

Within hours after PHx, one of the earliest metabolic changes is hypoglycemia, likely resulting from depleted glycogen stores and reduced gluconeogenic capacity due to liver mass loss. Hypoglycemia acts as a pro-regenerative signal, promoting *cyclin D* expression, while glucose supplementation has been shown to inhibit hepatic regeneration (Huang and Rudnick 2014; Solhi *et al*., 2021; Ma *et al*., 2025). As a result, fatty acid oxidation becomes the primary energy source during regeneration. Increased lipolysis in adipose tissue

enhances fatty acid uptake by hepatocytes, leading to transient steatosis in the regenerating liver (Shteyer *et al*., 2004; Solhi *et al*., 2021). In addition, bile acids play a regulatory role in liver regeneration by acting as metabolic signals to promote proliferation. After PHx, bile acid levels temporarily increase in the liver, but this overload is subsequently controlled by the inhibition of CYP7A1, a rate-limiting enzyme in the synthesis of bile acids (Csanaky *et al*., 2009; Zhang *et al*., 2009; Fan *et al*., 2015).

Liver injuries: a ductular source for hepatocytes

When liver injury is severe and prolonged, hepatocyte proliferation may be inhibited. Under these conditions, bipotential liver progenitor cells (LPCs) could serve an alternative source for new hepatocytes (Huch *et al*., 2013; Miyajima *et al*., 2014; Li *et al*., 2020; Bangru and Kalsotra, 2020). These LPCs, commonly referred to as oval cells, are believed to originate from the canals of Hering, structures that form a transition zone between hepatocytes and bile ducts (Wang *et al*., 2003; Blake and Steer, 2023). During liver damage, oval cells are thought to expand through a ductular reaction and differentiate into hepatocytes or cholangiocytes, thereby contributing to liver repopulation (Lázaro *et al*., 1998; Lu *et al*., 2015). However, the existence of a dedicated liver stem cell population remains a subject of ongoing debate (Grompe, 2015).

1.4.2 *Drosophila* regeneration

Historically, *Drosophila melanogaster* has been a key model organism for studying developmental biology. Its numerous advantages, including a short lifespan, rapid life cycle, and an extensive repertoire of genetic tools, enable efficient, high-throughput experiments such as genetic screenings and functional genomics (Beira and Paro, 2016).

Beyond its contributions to this field, the fruit fly also serves as an excellent experimental system for regeneration research. Although adult flies cannot regenerate appendages after metamorphosis, **imaginal discs**—the larval precursors of adult structures—are capable of regenerative growth following injury or cell death. Much of the research on *Drosophila* regeneration has focused on imaginal discs, though more recent studies have also investigated adult structures that depend on stem cells, such as the midgut and germline, to gain deeper insights into tissue repair and homeostasis (reviewed in Bergantiños *et al*., 2010a; Hariharan and Serras, 2017; Fox *et al*., 2020).

Imaginal discs as a model for regeneration

Imaginal discs are epidermal, sac-like structures that give rise to adult body structures of the “imago” (the adult sexually mature stage), hence the name. There are 19 discs in the larva, each arising from a cluster of a few embryonic ectodermal cells that mature by proliferating extensively and invaginating during the larval stages to form the imaginal disc (Fig. 5A). Cell fates in the imaginal disc epithelia are largely specified during the third larval instar stage. Upon metamorphosis, the discs undergo eversion and significant morphogenetic changes, developing into adult cuticular structures such as the legs, wings, antennae and eyes. This process is triggered by the ecdysone hormonal cascade (Cohen, 1993; Fristrom and Fristrom, 1993; Aldaz and Escudero, 2010; Beira and Paro, 2016).

Morphologically, imaginal discs consist of two epithelial sheets with their apical surfaces facing each other: the peripodial membrane, an outer layer composed of squamous cells, and the disc proper, which is formed by a single columnar epithelial layer (Fig. 5B). Adult structures originate from the disc proper, with minimal contribution from the peripodial membrane (Haynie and Bryant, 1986; Beira and Paro, 2016). During early development, some of these primordia are subdivided into functional regions of restricted lineage, known as compartments. Compartments are stable domains, separated by boundaries that prevent cell mixing between adjacent regions. They include the Anterior and Posterior compartments, as well as the Dorsal and Ventral regions. The wing disc is further divided into the trunk region (Notum) and the appendage regions (Hinge and Wing pouch) (Garcia-Bellido *et al.*, 1973; recently reviewed in Morata and Lawrence, 2022) (Fig. 5B).

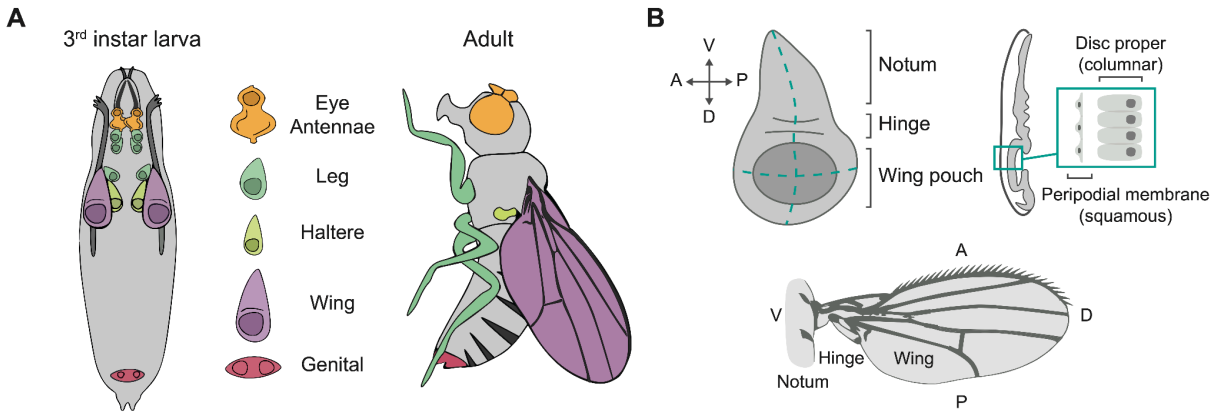

Figure 5. Imaginal discs in *Drosophila melanogaster*. (A) Illustration of the imaginal discs present in the third-instar larva (left) and the corresponding structures they give rise to in the adult fly (right). **(B)** Morphology of the wing imaginal disc, highlighting its compartmentalization along the Antero-Posterior (AP) and Dorso-Ventral (DV) axes (top left). A lateral view (top right) illustrates its epithelial composition, including the peripodial membrane and the disc proper. (Bottom) Adult fly wing depicting the regions derived from the wing imaginal disc.

The regenerative capacity of imaginal disc was first demonstrated by culturing disc fragments in the abdomens of adult female flies (Hadorn, 1965; Bryant, 1971). These experiments revealed the remarkable plasticity of imaginal discs, which not only exhibit regenerative growth but also undergo transdetermination—a process in which determined cells adopt the fate of other imaginal discs (Hadorn, 1965; Schubiger 1971; Hadorn, 1978; Maves and Schubiger, 1995; Bergantiños *et al.*, 2010a; Worley *et al.*, 2012). Additional studies further demonstrated that discs were capable of compensatory proliferation after X-ray irradiation, restoring their original size and enabling the development of normal adult flies even after the loss of half their cells (Haynie and Bryant, 1977).

More recently, the development of advanced genetic tools has enabled precise *in vivo* ablation of specific regions within imaginal discs, improving reproducibility and allowing larger-scale experiments. This approach involves driving the expression of a pro-apoptotic gene, such as *reaper* (*rpr*) or *eiger* (*egr*), in targeted areas of the disc using the Gal4/UAS system under the control of tissue-specific regulatory elements (Smith-Bolton *et al.*, 2009; Bergantiños *et al.*, 2010b). Temporal regulation of Gal4 activity is achieved by using the thermo-sensitive Gal80 ($Gal80^{ts}$), expressed under a ubiquitous promoter. At lower

temperatures, Gal80^{ts} represses Gal4, but at restrictive temperatures (over 29ºC), Gal80^{ts} becomes inactive, allowing precise **induction of apoptosis** both temporally (via temperature) and spatially (via the choice of the Gal4 upstream regulatory element) (Smith-Bolton *et al*., 2009; Bergantiños *et al*., 2010b; Repiso *et al*., 2011) (Fig. 6A). This system can be further complemented with other genetic tools that allow controlled expression of transgenes. For instance, the LexA/Gal4 hybrid (LHG) system can be used to spatially control the expression of *rpr* while simultaneously using Gal4/UAS to induce RNAi-mediated knockdown of candidate regeneration genes (Santabárbara-Ruiz *et al*., 2015) (Fig. 6B).

These experiments have been fundamental in identifying the key molecular mechanisms underlying *Drosophila* imaginal disc regeneration, including early signals that trigger tissue repair, signaling pathways that restore disc patterning and size, and the source of new cells that replenish lost areas.

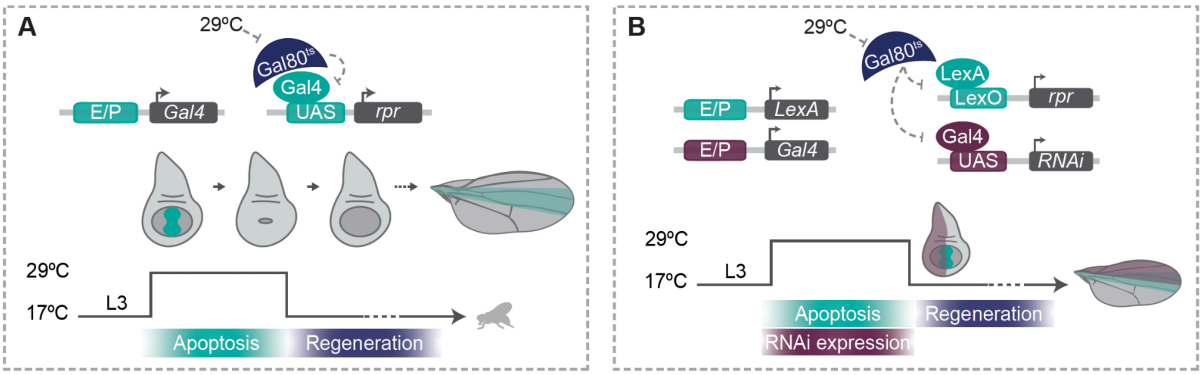

Figure 6. Gal4/LexA transactivation system for genetically induced cell death in the wing disc. **(A)** At 17ºC, the thermo-sensitive Gal80 (Gal80^{ts}), expressed under a ubiquitous promoter, inhibits Gal4 activity. At 29ºC, Gal80^{ts} becomes inactive, allowing Gal4 to induce the expression of the pro-apoptotic gene *reaper* (*rpr*) in a specific region of the wing imaginal disc of 3rd instar larvae. When the temperature is shifted back to 17ºC, larvae can regenerate the damaged tissue, giving rise to normal adult wings. **(B)** Dual transactivation system in which Gal80^{ts} represses both LexA and Gal4 at 17ºC. At 29ºC, LexA binds to the LexO sequence to activate *rpr* expression, while Gal4 binds to the UAS sequence to drive RNAi expression, each in specific areas of the wing disc.

Signals and mechanisms in wing imaginal disc regeneration

Upon injury, damaged cells release reactive oxygen species, calcium waves, and biolectrical stimuli (Restrepo and Basler, 2016; Santabárbara-Ruiz *et al*., 2019; Esteban-Collado *et al*., 2024). These early signals, along with cytokines secreted by immune cells, are sensed as pro-regenerative cues by neighboring living cells (Vizcaya-Molina *et al*., 2020) (Fig. 7). Together, they activate multiple signaling pathways essential for proper regeneration, including JNK and p38 MAP kinases (Bosch *et al*., 2005; Lee *et al*., 2005; Mattila *et al*., 2005; Bergantiños *et al*., 2010b; Santabárbara-Ruiz *et al*., 2015); Jak/STAT (Katsuyama *et al*., 2015; La Fortezza *et al*., 2016), Pi3K/Akt/Ask1 (Santabárbara-Ruiz *et al*., 2019; Esteban-Collado *et al*., 2021), TNF receptor Wgn (Esteban-Collado *et al*., 2024), WNT (Smith-Bolton *et al*., 2009; Harris *et al*., 2016; Verghese and Sun, 2016), and Hippo (Sun and Irvine, 2011). Upon activation, the downstream effectors of these signaling pathways

translocate to the nucleus and initiate the transcriptional programs of regeneration (Vizcaya-Molina *et al*., 2020; Camilleri-Robles *et al*., 2024) (Fig. 7).

Early studies using surgical injury and *in vivo* culture of imaginal discs revealed the appearance of a blastema around the wound site, where proliferative cells accumulated to restore lost tissue (Hadorn *et al*., 1968, Karpen and Schubiger, 1981). More recently, genetic ablation experiments in the wing disc confirmed the formation of a blastema at the injury site, showing that tissue damage leads to a localized loss of patterning and cell fate expression, similar to the de-differentiated blastema cells observed in vertebrate regeneration (Smith-Bolton *et al*., 2009; Bergantiños *et al*., 2010a; Worley *et al*., 2022). These studies revealed that reprogrammed cells can adopt new identities, such as vein or intervein cells, and even cross compartment boundaries (Repiso *et al*., 2013, Herrera and Morata, 2014, Worley *et al*., 2022). Importantly, the disc blastema does not originate from stem cells but rather from proximally fated cells that undergo reprogramming and proliferate through **compensatory cell proliferation** to replace lost tissue (Smith-Bolton *et al*., 2009; Sun and Irvine, 2011; Worley *et al*., 2022).

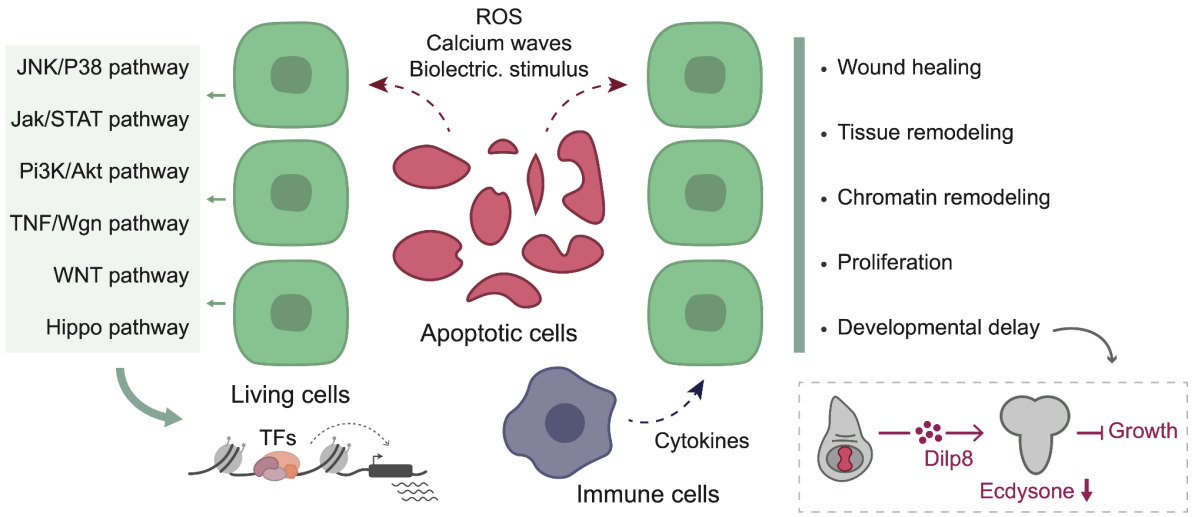

Figure 7. Signals and mechanisms in imaginal disc regeneration. Upon injury, apoptotic cells release reactive oxygen species (ROS), calcium waves, and bioelectrical stimuli, while immune cells secrete cytokines, all of which are sensed as pro-regenerative cues by neighboring living cells. These signals collectively activate key signaling pathways (left), which ultimately converge on the nucleus to drive the transcriptional programs required for regeneration. Regeneration proceeds through a sequence of events (right), including a delay in pupariation. This delay is mediated by the insulin-like peptide Dipl8, which is secreted by the damaged disc and acts remotely on the brain to suppress ecdysone signaling, thereby extending the developmental window for tissue repair.

Complete regeneration of injured discs requires a delay in pupariation, with the duration of this delay correlating with the extent of tissue damage (Smith-Bolton *et al*., 2009). This developmental pause, also observed when disc growth is impaired, is mostly mediated by the insulin-like peptide Dipl8 (Fig. 7). Secreted by the disc, Dilp8 acts remotely on the brain to suppress ecdysone production and activity, thereby postponing metamorphosis and allowing additional time for tissue repair (Colombani *et al*., 2012; Garelli *et al*., 2012). After pupariation, regenerative competence is generally lost, with only adult tissues capable of

stem cell-based homeostatic renewal, such as the midgut and germline, retaining regenerative potential (Fox *et al*., 2020).

2. TRANSCRIPTIONAL REGULATION AND GENOME TOPOLOGY

One of the hallmarks of tissue regeneration is the **activation of regenerative programs** (Poss and Tanaka, 2024). Following injury, cells surrounding the damage site integrate signals from the wound, initiating transcriptional reprogramming and widespread chromatin remodeling to enable effective tissue repair. This transcriptional response is tightly regulated by transcription factors that either activate or repress specific genes, enhancers and silencers that fine-tune transcriptional efficiency, and chromatin modifications that influence gene accessibility. Non-coding RNAs further contribute to transcriptional control, while 3D genome organization facilitates interactions between regulatory elements. Together, these mechanisms ensure the precise and coordinated modulation of gene expression, driving the activation of pro-regenerative, developmental, and patterning genes essential for the reconstruction of damaged tissue.

2.1 Transcriptional regulation by enhancers

Enhancers are noncoding DNA *cis*-regulatory elements that control the spatial and temporal specificity of gene expression in response to various stimuli. They regulate transcription independently of their orientation or proximity to the target gene, residing anywhere from a few base pairs upstream of the gene to within introns or even several kilobases away (reviewed in Catarino and Stark, 2018; Kawasaki and Fukaya, 2024). Enhancers contain short consensus motifs that are specifically recognized by transcription factors (TFs). Binding of TFs to these motifs recruits cofactors, which can either activate or repress the transcription of target genes. Among these cofactors are chromatin remodelers, which displace histones to increase DNA accessibility, and histone-modifying enzymes, which add post-translational modifications to histones. The coordinated activity of these coactivators establishes a unique chromatin signature characteristic of active enhancers (Thomas and Buecker, 2023).

Advances in high-throughput technologies have facilitated the functional annotation of cis-regulatory elements by leveraging their distinct **chromatin signature** (Pundhir *et al*., 2015) (Fig. 8A). While inactive enhancers are typically occupied by nucleosomes, active enhancers are found in nucleosome-free regions. These accessible regions are often flanked by histones bearing specific post-translational modifications (PTMs), such as H3K27ac and H3K4me1, whereas silent chromatin is usually marked by H3K27me3 and heterochromatin by H3K9me3 (Pundhir *et al*., 2015; Catarino and Stark, 2018). As a result, next-generation sequencing techniques, including the Assay for Transposase-Accessible Chromatin (ATAC-seq) to map open chromatin regions and Chromatin Immunoprecipitation (ChIP-seq) to profile histone modifications, are commonly employed for **enhancer predictions** within a cell type of interest (Thomas and Buecker, 2023) (Fig. 8B). However, while DNA accessibility and active histone marks are strong predictors of enhancers, other genomic regions, such as insulators, are also depleted of nucleosomes. Moreover, although

many PTMs correlate with enhancer activity, they are not always functionally required (Catarino and Stark, 2018).

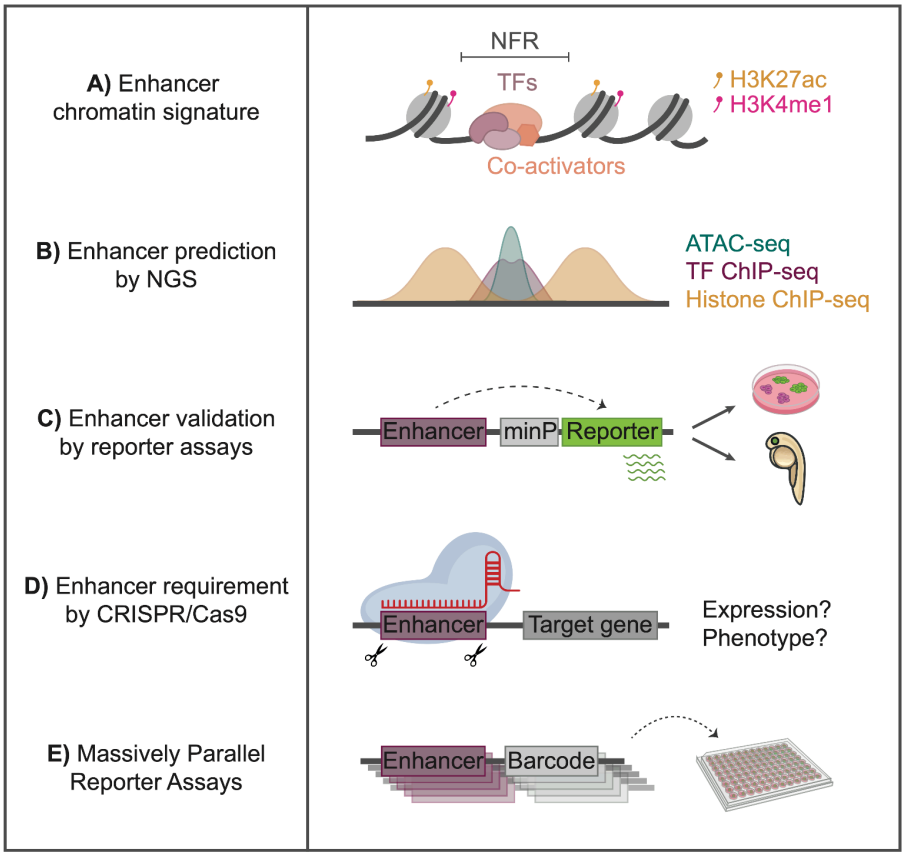

Figure 8. Strategies for functional annotation and validation of enhancers. (A) Active enhancers reside in nucleosome-free regions (NFRs), are bound by transcription factors (TFs) and co-activators, and are typically flanked by histones with specific post-translational modifications (PTMs), such as H3K27ac and H3K4me1. **(B)** Next-generation sequencing (NGS) techniques for enhancer identification include ATAC-seq, which maps open chromatin regions, and ChIP-seq, which profiles histone modifications or TF binding. **(C)** Candidate enhancers are validated using reporter assays, either *in vitro* in cell cultures or *in vivo* in transgenic reporter animals. **(D)** CRISPR/Cas9 deletion evaluates enhancer necessity for endogenous gene expression or biological functions. **(E)** Massively parallel reporter assays (MPRAs) enable high-throughput measurement of enhancer activity.

Therefore, candidate enhancers identified based on chromatin traits should be validated through functional experiments. A common approach involves assessing the ability of candidate regulatory elements to drive reporter gene expression. **Reporter assays to validate** enhancers can be performed *in vitro* by cloning the candidate enhancer upstream of a luciferase gene and transfecting it into cell cultures (Fig. 8C). Alternatively, enhancers can be validated in their endogenous context (*in vivo*) using transgenic reporter animals, where the regulatory element is cloned to drive green fluorescent protein (GFP) expression (Field and Adelman, 2020; Goldman and Poss 2020). Another approach is to use clustered regularly interspaced short palindromic repeat interference (**CRISPR**)/**Cas9-mediated deletion** of candidate enhancers to evaluate their **requirement** for endogenous gene expression or specific biological functions (Catarino and Stark, 2018) (Fig. 8D).

The scalability of enhancer validation has greatly improved with the development of **massively parallel reporter assays** (**MPRAs**) (Fig. 8E). MPRAs are high-throughput methods that measure the activity of thousands of candidate regulatory elements by linking each sequence to a unique barcoded reporter transcript and using next-generation sequencing to quantify barcode-containing transcripts. An alternative approach is the self-transcribing active regulatory region sequencing (STARR-seq) method, which eliminates the need for barcodes by using the enhancer sequence itself as its identifier. Additionally, rather than using a reporter library, a pool of guide RNAs can be designed to delete or disrupt putative enhancers, allowing functional screening based on selectable phenotypes such as cell growth or drug resistance (Catarino and Stark, 2018; Field and Adelman, 2020).

2.2 Genome architecture in gene expression regulation

Over the past two decades, interest in the **three-dimensional (3D) organization of the genome** and its active role in gene expression regulation has grown significantly. Advances in technologies for mapping and visualizing genome topology have provided valuable insights into chromatin structure across different species and cell types. Historically, the spatial organization of chromosomes, domains, and specific loci within the nucleus was studied using microscopy-based techniques, such as fluorescent in situ hybridization (FISH). The advent of chromosome conformation capture (3C)-based approaches revolutionized the field by enabling the detection of DNA fragments that preferentially interact in 3D space (reviewed in Bonev and Cavalli, 2016; Rowley and Corces 2018; and Lizana and Schwartz, 2024). Originally developed in 2002, the 3C assay measures interaction frequencies between pairs of genomic loci (Dekker *et al*., 2002). This method was later refined and expanded into **Hi-C**, a high-throughput technique that enables the unbiased mapping of chromatin interactions across entire genomes (Lieberman-Aiden *et al*., 2009). Hi-C combines proximity-based ligation—where chromatin is crosslinked, digested with a restriction enzyme, and ligated under dilute conditions to favor ligation between interacting DNA fragments—with biotin-mediated purification of ligation products and massively parallel sequencing. Analysis of the resulting genome-wide contact matrix has revealed key principles of chromatin folding in the eukaryotic genome (Lieberman-Aiden *et al*., 2009; Dekker *et al*., 2013) (Fig. 9).

At the highest level of genome organization, chromosomes occupy discrete territories within the nucleus (Cremer and Cremer, 2001). This is evidenced in Hi-C matrices, where loci on the same chromosome (cis) show higher interaction frequencies than those on different chromosomes (trans) (Lajoie *et al*., 2015). Further analysis of the contact matrix using computational correlation and principal component analysis has revealed that the genome is partitioned into two **compartments** with distinct transcriptional activities and chromatin features (Lieberman-Aiden *et al*., 2009; Sexton *et al*., 2012). This compartmentalization appears as a checkerboard-like pattern in the Hi-C matrix, alternating between A and B compartments that preferentially interact with other compartments of the same type (Fig. 9). Active (A) compartments are gene-dense, transcriptionally active, more accessible and enriched for activating chromatin marks. In contrast, inactive (B) compartments are defined as gene-poor, heterochromatic regions (Lieberman-Aiden *et al*., 2009; Lajoie *et al*., 2015; Rowley and Corces, 2018).

The genome is further organized into **Topologically Associating Domains** (**TADs**), sub-megabase regions characterized by higher interaction frequencies within the domain than outside it (Nora *et al*., 2012; Dixon *et al*., 2012; Sexton *et al*., 2012; Hou *et al*., 2012) (Fig. 9). In mammals, TADs typically span several hundred kilobases, whereas in *Drosophila*, they are usually no larger than a hundred kilobases (reviewed in Rowley and Corces, 2018; Llorens-Giralt *et al*., 2021). The prevailing model for TAD formation in mammals suggests that they arise from multiple loop extrusion events mediated by the cohesin complex (Wutz *et al*., 2017; Fudenberg *et al*., 2016). TADs are separated by sharp boundaries enriched with CTCF-binding sites in a head-to-head orientation (Dixon *et al*., 2012), which act as barriers to cohesin and insulate the domains from neighboring regions (Dekker and Mirny, 2016). Consistent with this model, cohesin depletion leads to the disruption of most TADs (Rao *et al*., 2017), while deleting or inverting CTCF-binding sites weakens TAD insulation and facilitates crosstalk between neighboring TADs (de Wit *et al*., 2015; Hanssen *et al*., 2017; Nora *et al*., 2017).

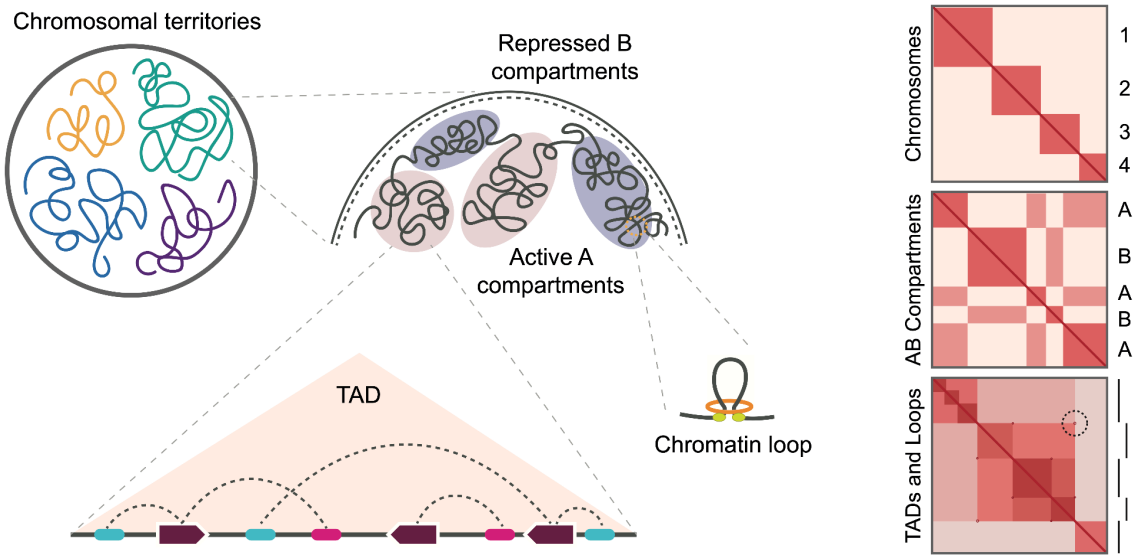

Figure 9. Three-dimensional (3D) genome organization. Chromosomes occupy discrete nuclear territories and are partitioned into active, gene-rich A compartments and gene-poor, heterochromatic B compartments. The genome is further organized into topologically associating domains (TADs) and chromatin loops, bound by cohesin and CTCF in mammals. On the right, Hi-C matrices illustrate these chromosomal features. *Adapted from Eagen (2018)*; *Jerkovic´and Cavalli (2021).*

In *Drosophila*, TADs have been shown to be physical units that correlate well with domains of distinct chromatin states, such as polycomb-repressed, heterochromatin or active regions (Rowley *et al*., 2017; Szabo *et al*., 2018; Ulianov *et al*., 2021; Llorens-Giralt *et al*., 2021; Denaud *et al*., 2025). Unlike in mammals, *Drosophila* TAD boundaries are predominantly enriched with active promoters or small domains containing individual genes, rather than CTCF (Rowley *et al*., 2017; Ramírez *et al*., 2018). Accordingly, the loss of CTCF has minimal impact on domain boundaries, as observed in *Drosophila* neurons (Kaushal *et al*., 2021).

Whether TADs exist as functional units with a regulatory role or simply reflect statistical frequencies of chromatin interactions across cell populations remains an open question, with evidence supporting both perspectives. On one hand, studies combining super-resolution

microscopy with DNA-labeling by FISH have identified globular domains that correspond to distinct chromatin states, such as small, compact polycomb-repressed domains and less condensed active domains (Boettiger *et al*., 2016; Szabo *et al*., 2018). Moreover, disruption of TAD boundaries has been linked to gene expression dysregulation, sometimes leading to pathogenic phenotypes such as limb developmental abnormalities in both humans and mice (Lupiáñez *et al*., 2015). On the other hand, systematic analysis of gene expression in *Drosophila* balancers, highly rearranged chromosomes, has shown that, despite major TAD disruptions, only a subset of genes exhibited moderate changes in expression (Ghavi-Helm *et al*., 2019). Moreover, TADs are generally maintained across cell types during fly embryonic development, even as transcriptional profiles undergo significant changes (Ing-Simmons *et al*., 2021). Furthermore, single-cell Hi-C maps have revealed substantial cell-to-cell variability in TAD structures. While chromatin compartments are observed in individual nuclei, TADs only emerge as distinct domains when single-cell maps are aggregated (Flyamer *et al*., 2017; Cattoni *et al*., 2017).

Another architectural feature present in the genome of most organisms is the formation of **chromatin loops** (Rowley and Corces, 2018; Kim *et al*., 2025). Chromatin loops consist of pairs of loci in close physical proximity that appear as focal peaks of contact enrichment in Hi-C matrices (Eagen, 2018) (Fig. 9). In mammals, loop anchors are primarily bound by cohesin or CTCF and are typically located at TAD borders (Wutz *et al*., 2017). In contrast, chromatin loops in *Drosophila* form within TADs and generally independently of CTCF (Rowley *et al*., 2017; Ramírez *et al*., 2018). Loops can vary in length, from short-range interactions between enhancers and their target promoters, spanning tens to hundreds of kilobases, to long-range loops extending across several megabases (Dekker and Misteli, 2015; Misteli, 2020). These larger loops often contribute to genome compaction or facilitate the precise temporal and spatial regulation of developmental genes (Loubiere *et al.*, 2020; Pollex *et al*., 2024; reviewed in Paldi and Cavalli, 2025; Zunjarrao and Gambetta, 2025). For instance, in *Drosophila* neurons, high-frequency loops have been shown to connect specific pairs of TADs, forming meta-domains that, in some cases, regulate the expression of neural genes (Mohana *et al*., 2023).

2.3 Functional annotation of enhancer-promoter interactions

As enhancer annotations become increasingly accurate and comprehensive, and technologies for studying genome organization continue to improve in resolution, identifying enhancer-promoter interactions has become a critical step in understanding gene regulatory networks in both physiology and disease. Since enhancers can regulate target genes over large genomic distances, their spatial proximity to promoters can be exploited to predict enhancer-promoter pairs (Shlyueva *et al*., 2014). Chromatin conformation capture technologies, such as those discussed earlier, enable genome-wide mapping of physical interactions between regulatory elements and their target promoters. These methods can be combined with chromatin immunoprecipitation-based techniques, such as ChIA-PET and HiChIP, to study interactions involving specific proteins (Leung and Nagano, 2022). While these approaches are powerful, chromatin interaction matrices have limitations in accurately linking regulatory elements to their target genes. To overcome these challenges, computational models have been developed to predict enhancer-gene interactions based on correlations between gene expression and chromatin features (Dekker *et al*., 2013). For

instance, the Activity-by-Contact (ABC) algorithm, integrates enhancer activity and 3D genome organization data to map regulatory interactions on a genome-wide scale (Fulco *et al*., 2019).

These predictions can be functionally validated using CRISPR-based approaches, which offer both precision and scalability. Endogenous perturbation of candidate regulatory elements can be achieved by knocking out enhancer regions and assessing their effect on target genes (reviewed in Catarino and Stark, 2018) (Fig. 8D). Alternatively, catalytically inactive Cas9 (dCas9), when fused to repressors or activators, enables high-throughput screening of candidate enhancers via CRISPR interference (CRSPRi) and CRISPR activation (CRISPRa) assays Fulco *et al*., 2019; Leung and Nagano, 2022).

3. CHROMATIN REGULATORY LANDSCAPE OF REGENERATION

Chromatin regulation has been extensively studied in development and homeostasis, but its role in regeneration remains less well understood. Recent research exploring how chromatin states influence regeneration across different species, cell types, and injury contexts suggests that chromatin modifications and enhancer activity are closely linked to regenerative competency. These factors determine whether a tissue can successfully initiate and sustain a regenerative response (Goldman and Poss, 2020; Jia *et al*., 2023).

Among the different regulatory mechanisms, injury-associated enhancers, also known as **regeneration-responsive enhancers** (**RREs**), have emerged as key regulators of transcriptional activation following tissue damage. These cis-regulatory DNA elements are specifically induced upon injury to control the expression of genes essential for regeneration (Rodríguez and Kang, 2020; Yang and Kang, 2019; Suzuki and Ochi 2020; Harris, 2022). Genome-wide chromatin profiling studies have uncovered RREs across multiple regenerative contexts, including zebrafish heart, fin, and spinal cord regeneration (Goldman *et al*., 2017; Begeman *et al*., 2020; Kang *et al*., 2016; Wang *et al*., 2020a; Mokalled *et al*., 2016). A well-characterized example is the *leptin b* enhancer (LEN), which strongly upregulates *leptin b* after injury in the heart and fins (Kang *et al*., 2016). LEN consists of distinct regulatory modules that confer tissue specificity, ensuring activation exclusively in regenerating tissues without affecting normal development (Kang *et al*., 2016). These findings suggest that RREs could be engineered to direct the expression of pro-regenerative factors to injured tissues with spatial and temporal precision, minimizing the risks of tumorigenic growth.

In mammals, regeneration-associated enhancers have been identified in skeletal muscle injury (Aguilar *et al*., 2016), cardiac repair (Vieira *et al*., 2017), and skin regeneration (Ge *et al*., 2017). Beyond vertebrates, studies in *Drosophila* wing imaginal discs have uncovered **damage-responsive regulatory elements** (**DRREs**) that control the expression of regeneration-associated genes (Vizcaya *et al*., 2018; Harris *et al*., 2020). DRREs contain binding sites for transcription factors that are upregulated during tissue repair and functionally conserved across species, including zebrafish and mice (Vizcaya *et al*., 2018). Based on their chromatin accessibility in uninjured tissue, DRREs are classified into two categories: increasing DRREs (iDRREs), which are already accessible in wild-type tissue,

and emerging DRREs (eDRREs), which become accessible only upon injury. Some eDRREs are repurposed from developmental programs (*reused* DRREs), while others are uniquely activated during regeneration (*novel* eDRREs) (Vizcaya *et al*., 2018). A well-studied example of an iDRRE is BRV118, an enhancer regulated by the JNK/AP-1 pathway that drives *wingless* expression in response to tissue damage (Harris *et al*., 2016). Notably, this enhancer is silenced by Polycomb-mediated H3K27 trimethylation as development progresses, coinciding with the loss of regenerative potential (Harris *et al*., 2016). In addition, its deletion impairs regeneration but does not affect normal wing development, highlighting the specificity of RREs in injury responses.

Since many developmental and regenerative genes are evolutionarily conserved, differences in regenerative capacity across tissues and species may depend on the presence, accessibility, and activity of RREs. Understanding how these enhancers function in various regenerative contexts is critical for uncovering the chromatin regulatory mechanisms underlying regeneration. Moreover, as regeneration-responsive enhancers become better characterized, future studies should investigate how chromatin structure and 3D genome architecture influence regenerative potential, an area that remains largely unexplored. A deeper understanding of the interplay between injury-induced signaling, RREs, and 3D chromatin organization could provide fundamental insights into why some organisms and tissues can regenerate while others cannot. While regenerative medicine has traditionally focused on the therapeutic potential of transplanted stem cells, future strategies may instead harness endogenous repair mechanisms by employing RREs to drive controlled expression of pro-regenerative factors in injured tissues, as previously suggested (Chen and Poss, 2017; Yan *et al*., 2023).

OBJECTIVES

OBJECTIVES

Regenerative capacity differs not only across species, but also between organs and developmental stages within the same organism. This variability suggests that regenerative potential is more likely determined by the spatiotemporal regulation of genome activity and transcriptional programs, rather than solely by the genome sequence or the presence or absence of specific genes. Building on these observations, the **main objective** of this thesis is to elucidate the role of enhancers and 3D genome organization in orchestrating the gene expression programs involved in tissue regeneration.

The specific objectives are the following:

Chapter I. Enhancer regulation in liver regeneration

- Identify and characterize *cis*-regulatory DNA elements involved in early liver regeneration after partial hepatectomy.
- Investigate the gene regulatory networks and transcriptional regulators that govern the regenerative response in the liver.
- Examine the reuse of developmental enhancers during liver regeneration.

Chapter II. Three-dimensional genome architecture in wing disc regeneration

- Characterize changes in 3D genome organization following damage to *Drosophila* wing imaginal discs.
- Determine the role and requirement of long-range chromatin loops during wing disc regeneration.
- Identify the architectural protein mediating meta-loop formation during regeneration.

RESULTS

CHAPTER I.
Enhancer regulation in liver regeneration

The results presented in this Chapter I have recently been accepted for publication in *Cell Genomics.*

Below, the graphical abstract and highlights of the published manuscript. See the full copy of the Llorens-Giralt *et al*. (2025) article as Appendix I.

Cell Genomics

Article

Sequential activation of transcription factors promotes liver regeneration through specific and developmental enhancers

Graphical abstract

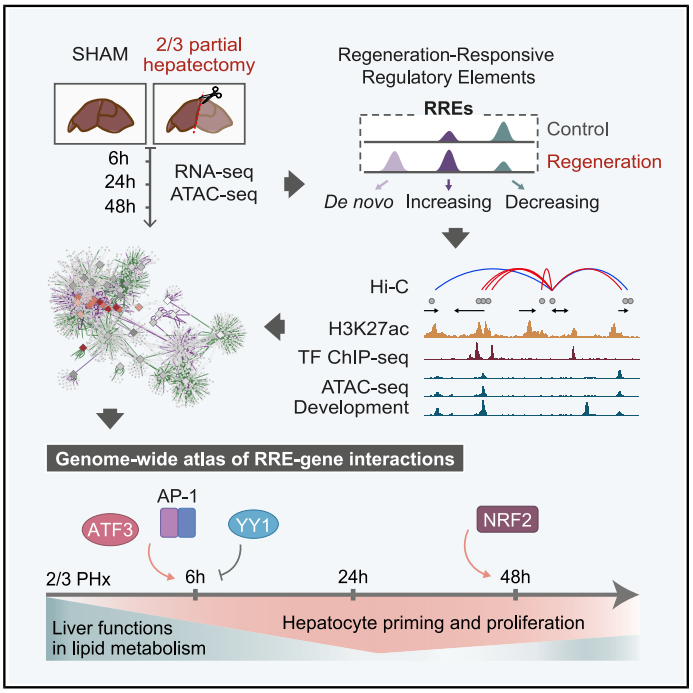

Highlights

- Regeneration-responsive regulatory elements (RREs) were identified in early liver regeneration
- RRE-gene interaction atlas reveals shift from lipid metabolism to proliferative programs
- RREs comprise both regeneration-specific and reactivated developmental enhancers
- Integrative genomic analysis generates GRN with a transcription-factor-activation cascade

Authors

Palmira Llorens-Giralt, Marina Ruiz-Romero, Ramil Nurtdinov, ..., Florenci Serras, Isabel Fabregat, Montserrat Corominas

Correspondence

mcorominas@ub.edu

In brief

Llorens-Giralt et al. study how liver cells respond to partial hepatectomy by examining changes in gene activity and chromatin accessibility. They create a functional regulatory map of early liver regeneration and identify key elements controlling specific gene programs essential for liver repair and growth.

Llorens-Giralt et al., 2025, Cell Genomics *5*, 100887
July 9, 2025
https://doi.org/10.1016/j.xgen.2025.100887

CellPress

Sequential activation of transcription factors promotes liver regeneration through specific and developmental enhancers

Palmira Llorens-Giralt[1,5], Marina Ruiz-Romero[2,5], Ramil Nurtdinov[2], Macarena Herranz-Itúrbide[3], Guillermo P Vicent[4], Florenci Serras[1], Isabel Fabregat[3], Montserrat Corominas[1,6,*].

[1]Department of Genetics, Microbiology and Statistics, Faculty of Biology and Institute of Biomedicine (IBUB), University of Barcelona, Barcelona, Catalonia, Spain.
[2]Centre for Genomic Regulation (CRG), The Barcelona Institute for Science and Technology (BIST), Barcelona, Catalonia, Spain.
[3]TGF-beta and Cancer Group, Oncobell Program, Bellvitge Biomedical Research Institute (IDIBELL), L'Hospitalet de Llobregat, Barcelona, Spain; Oncology Program, National Biomedical Research Institute on Liver and Gastrointestinal Diseases (CIBEREHD), Instituto de Salud Carlos III, Madrid, Spain.
[4]Molecular Biology Institute of Barcelona, Consejo Superior de Investigaciones Científicas (IBMB-CSIC), Barcelona, Spain.
[5]These authors contributed equally to this work
[6]Lead contact
*Correspondence: mcorominas@ub.edu

SUMMARY

The mammalian liver exhibits remarkable regenerative capabilities after injury or resection. Central to this process is the precise modulation of gene expression, driven by changes in chromatin structure and the temporal activation of distal regulatory elements. In this study, we integrate chromatin accessibility and transcriptomic data following partial hepatectomy in mice. We show that the expression of crucial regeneration genes is orchestrated by a diverse array of *cis*-regulatory elements, including regeneration-specific enhancers and enhancers repurposed from various developmental stages. These enhancers collaborate to activate the transcriptional programs required for hepatocyte priming and proliferation, with their activity initially regulated by the AP-1 complex and ATF3, and subsequently by NRF2 during proliferation. Our results also indicate that hepatic regeneration involves repression of enhancers regulating liver-specific metabolic functions, particularly those involved in lipid metabolism. This study provides a genome-wide atlas of enhancer-gene interactions, offering new insights into the regulatory mechanisms underlying liver regeneration.

KEYWORDS

Liver; Regeneration; Chromatin dynamics, Enhancers, Transcription factors, Development

INTRODUCTION

Regenerative capacity varies greatly, not only across species but also between tissues, organs, and developmental stages within the same species. The evolutionary conservation of regeneration-associated genes suggests that variation in regenerative ability arises from differences in how these genes are regulated following injury, rather than simply whether they are present[1,2]. Genome-wide chromatin profiling has identified *cis*-regulatory elements activated by injury that orchestrate regenerative transcriptional programmes. These regeneration-responsive elements have been characterized in regenerating zebrafish heart[3,4], fins[5,6], and spinal cord[7], as well as *Drosophila* wing imaginal discs[8,9]. In mice, similar enhancer activity has been observed in skeletal muscle[10], Schwann cells[11], skin stem cells[12,13], and heart[14,15]. Recent studies show that regeneration-responsive enhancers

can be engineered to drive pro-regenerative gene expression specifically in damaged tissues via transgenic models or viral vectors[5,16]. These elements are transiently activated after injury and deactivate once repair is complete, minimising potential tumourigenic risk.

In vertebrates, the liver has remarkable regenerative capacity, fully restoring mass and function after injury or partial hepatectomy (PHx)[17,18]. Under normal conditions, hepatocytes are quiescent, but within 4 hours after PHx, about 95% re-enter the cell cycle[19,20]. This is triggered by a cytokine-driven priming phase, which induces proliferation genes and represses liver-specific differentiation genes[21]. Growth factors then promote cell cycle progression, leading to mitosis by 48 hours[18]. Proliferation is later arrested by TGF-β and activins via tumour-suppressor gene activation, thus preserving liver size and homeostasis[19,22].

Understanding the regulatory mechanisms of liver regeneration could have profound implications for regenerative medicine. Although genetic and epigenetic drivers have been described[23,24], the role of specialised enhancers in controlling pro-regenerative genes is still unclear. Recent studies have explored histone modifications and DNA methylation post-PHx[21,25–27], chromatin accessibility dynamics after toxicity in a model of hereditary tyrosinemia[28], and epigenetic changes during biliary reprogramming[29]. Single-cell approaches have further revealed the gene regulatory networks of hepatic cells during the later stages of liver regeneration following PHx[30–32].

However, our understanding of how early signals reshape gene expression and chromatin architecture during liver regeneration remains incomplete. While recent evidence suggests that hepatocytes adopt a foetal-like chromatin and transcriptional state[30,31], it is still unclear whether regeneration relies solely on reactivating developmental networks or involves a distinct regeneration-specific programme.

Here, we profiled gene expression and chromatin accessibility during the early stages of liver regeneration in mice. Using an integrative algorithm that combines chromatin state and 3D conformation data, we identified regulatory elements specifically activated after PHx and predicted their target genes. This analysis revealed reduced accessibility at regions associated with liver-specific metabolic genes, alongside increased accessibility at regulatory elements linked to pro-proliferative genes. Additionally, we constructed a gene regulatory network that uncovered a cascade of transcription factor (TF) activation, highlighting key TFs that are upregulated and/or essential for regeneration. Our findings further suggest that liver regeneration involves both regeneration-specific enhancers and reactivated developmental enhancers, each governed by distinct regulatory mechanisms and associated with different biological functions.

RESULTS

Liver regeneration-responsive regulatory elements

To identify regulatory elements involved in early liver regeneration, we performed genome-wide transcriptomics and chromatin accessibility profiling on mouse livers at 6, 24, and 48 h after SHAM (CTRL) or two-thirds (2/3) PHx (REG) surgery (Figure 1A), using the same samples for RNA-seq[33] and ATAC-seq. The time points selected correspond to critical stages in liver regeneration, marking the end of the priming stage (6 h), the entry of hepatocytes into the S phase of the cell cycle (24 h) and their progression into mitosis (48 h). The latter two fall within the proliferation or progression phase of liver regeneration[17,18].

First, we employed correspondence analysis and association plots[34] to cluster the expressed genes (11,512 genes) (Figure S1A-C). This method enabled us to identify the genes that were differentially expressed either in the control livers or at specific time points during regeneration (6, 24, or 48 h post-PHx) (Figure 1B,C), as well as those that were co-expressed across different regeneration time points (Figure S1D,E, Table S1). The cluster corresponding to the initial stage of regeneration (REG 6 h)

showed the highest gene count, with 1,375 genes exhibiting significantly higher expression levels at 6 h compared to the other conditions (Figure 1B,C; Figure S1C). As previously reported[35], we found that the gene expression profile at the initial time point post-PHx resembled that of the corresponding SHAM-operated control, albeit with a tendency towards increased expression levels in regeneration (Figure S1A,B). This similarity is likely due to the disturbance in gene expression caused by surgical stress and anaesthesia. The other gene clusters specific to regeneration encompassed approximately 200 to 400 genes each (Figure 1B,C; Figure S1D,E). Notably, the cluster of genes co-expressed across regeneration (REG 6 - 24 - 48 h) comprised only 227 genes (Figure S1D,E). This suggests a dynamic transcriptomic profile with sequential gene activation and repression.

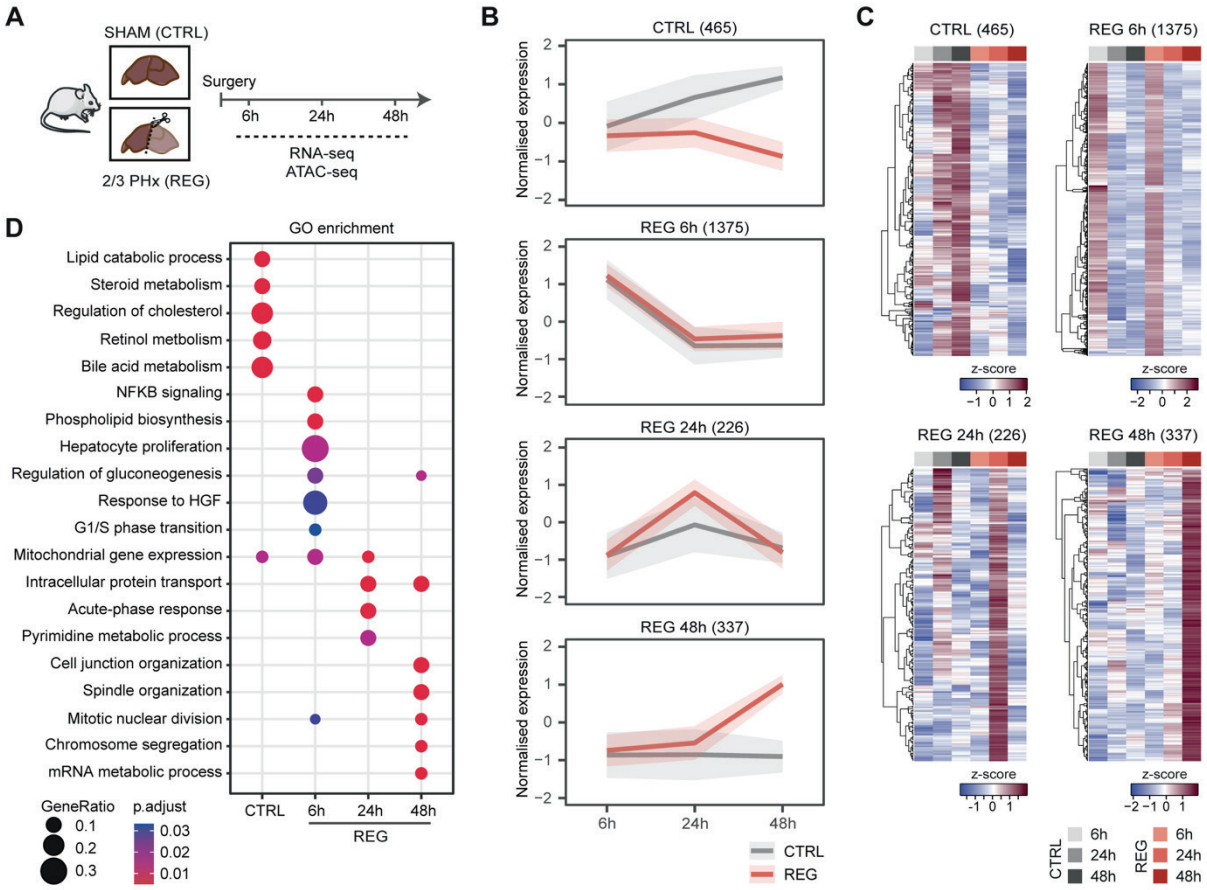

Figure 1. Gene expression profiles of liver regeneration after partial hepatectomy

(A) Experimental design. Male and female mice aged 8–16 weeks underwent either sham surgery (SHAM/CTRL) or 2/3 PHx (REG). Mice were euthanised at 6, 24, or 48 h post-surgery, and liver lobes were snap-frozen. RNA-seq data were obtained from Herranz-Itúrbide et al. (2021)[33] and the same biological samples were used for ATAC-seq. **(B)** Standardised expression profiles of four gene clusters: control, 6 h, 24 h, and 48 h after PHx. Gene expression values are z-score normalised. Mean expression (line) +/- the standard deviation (shade) and gene counts are shown per cluster. **(C)** Heatmaps of expression for each cluster. Columns represent conditions (averaged across replicates), and gene expression is z-score normalised, gene order was established by hierarchical clustering. Gene counts per cluster are shown above. **(D)** GO terms enriched in each gene cluster (one-sided Fisher's exact test p-adjust < 0.05). NFKB = Nuclear factor kappa-light-chain-enhancer of activated B cells; HGF = hepatocyte growth factor. See also Figure S1.

Gene Ontology (GO) analysis revealed that control livers were enriched for lipid-related pathways, including steroid and bile acid metabolism, as well as lipid catabolism (Figure 1D), consistent with known suppression of bile acid synthesis during liver regeneration to prevent cytotoxicity[36]. In contrast, genes associated with cell signalling, cell response, proliferation and mitosis were specifically enriched in particular regeneration clusters, indicating a sequential activation during regeneration (Figure 1D).

For instance, the REG 6 h cluster showed unique enrichment for hepatocyte growth factor (HGF) response and phospholipid biosynthesis, whereas several terms related to the mitotic cell cycle were significantly enriched among the REG 48 h cluster. HGF is among the earliest mitogens detected after PHx in mice and plays a crucial role in liver regeneration[37], while the synthesis of phospholipids is essential for generating new cell membranes and, therefore, for hepatocyte proliferation during regeneration[38]. These transcriptomic changes after PHx accurately reflect known physiological events underlying early liver regeneration[25,35].

Next, we examined the changes in chromatin accessibility that could trigger these transcriptional profiles by mapping open regions by ATAC-seq in livers at 6, 24 and 48 h after SHAM-surgery or 2/3 PHx (Figure S2A,B). We performed pairwise comparisons between control and regeneration at each time point (|FC| > 1.7) and identified over 17,000 differentially accessible chromatin regions in at least one time point, compared to 60,000 that were non-differentially accessible (NDA). Differentially accessible regions were classified into *de novo*, increasing or decreasing peaks: *de novo* peaks were open regions detected exclusively during regeneration; increasing peaks were regions already open in the control but displaying higher accessibility during regeneration; and decreasing peaks were regions with lower accessibility during regeneration (Figure 2A,B). We observed a similar number of decreasing peaks over time, with nearly 4,000 identified at each time point (Figure 2C). In contrast, the number of increasing peaks slightly increased over time (1,717 peaks at 6 h, 2,935 peaks at 24 h, and 2,886 peaks at 48 h after PHx) and *de novo* peaks were more enriched at 6 h and 48 h compared to 24 h: 427, 449 and 255 peaks, respectively (Figure 2C). Differentially accessible peaks from all classes were mostly time point-specific (Figure S2C), indicating that chromatin architecture changes throughout the regenerative process.

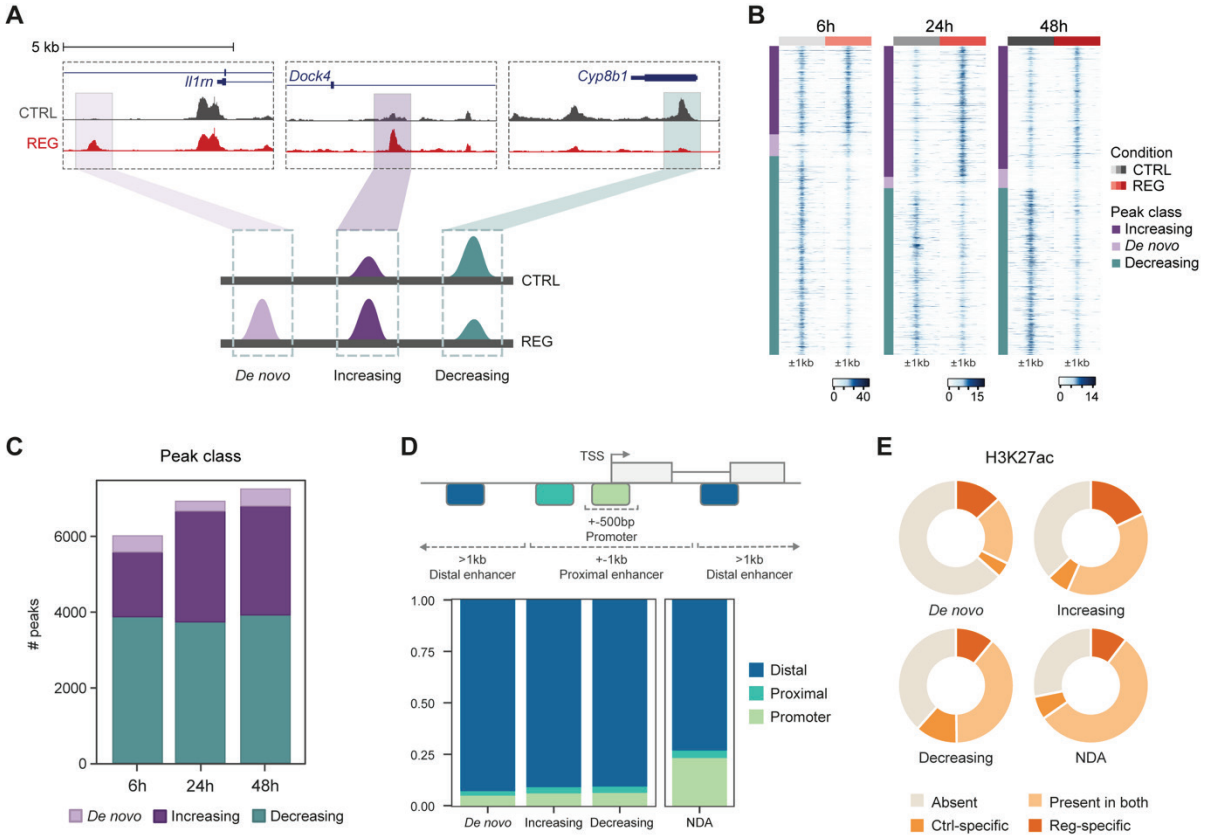

Figure 2. Chromatin accessibility changes during liver regeneration

(A) Genome browser views and schematics of *de novo*, increasing and decreasing peaks. **(B)** Quantile normalised ATAC-seq signals ±1 kb from peak summits, grouped by peak class. **(C)** Number of differentially accessible peaks per class at each time point. **(D)** (Top) genomic annotation of peaks. (Bottom) proportion of promoters, proximal, and distal enhancers per class peaks. NDA= non-differentially accessible. **(E)** H3K27ac presence in control (uninjured) and regeneration (40 h post-PHx) livers in NDA peaks and RREs. See also Figure S2.

We next classified ATAC-seq peaks by distance to the nearest transcription start site (TSS) as promoter (± 500 bp), proximal (<1 kb), or distal (≥1 kb) regions. In comparison to NDA, the de novo, increasing and decreasing peaks tended to be more prevalent in the distal regions (> 90%), primarily within introns and intergenic regions, while less than 7% were in promoters and only 2-3% within proximal regions (Figure 2D; Figure S2D). Indeed, most promoters remained relatively stable during regeneration, comprising nearly 25% of NDA peaks. Given that distal regions are typically associated with enhancers, these findings suggest that the chromatin response to PHx predominantly involves the modulation of enhancer accessibility.

To further characterise regeneration-responsive regulatory elements (RREs), we integrated ATAC-seq data with H3K27ac profiles from undamaged[39] and regenerating livers[40], as this histone mark is linked to active enhancers[41]. First, we observed a highly statistically significant overlap (Fisher's exact test, p = 2.2 e-16) between RREs (extended to 500 bp to incorporate the flanking nucleosomes) and H3K27ac. Approximately 65% of RREs were flanked by H3K27ac enriched regions, further supporting their role as enhancers. We observed that the H3K27ac signature differed for each type of RRE (Figure 2E). Compared to NDA, *de novo* and increasing RREs exhibited a higher proportion of peaks exclusively marked by H3K27ac during regeneration (Reg-specific). In contrast, decreasing peaks tended to be marked both in control and regeneration or only in the control. While certain *de novo* peaks exhibited regeneration-specific H3K27ac, indicating they can gain acetylation after PHx, most of them were unmarked in all conditions. This suggests that the regulation mediated by these elements may occur independently of this histone tail acetylation. As previously proposed, the active enhancer repertoire cannot be fully characterised by H3K27ac alone[42].

Switch in chromatin accessibility from RREs linked to homeostatic lipid metabolism to proliferation-associated RREs

To better understand gene regulation during liver regeneration, we mapped genome-wide functional enhancer-gene pairs. Proximal enhancers were assigned to the nearest gene, while the target genes of distal enhancers were predicted using the activity-by-contact (ABC) model of enhancer-promoter regulation[43]. Briefly, this model is based on the principle that each enhancer regulates gene expression proportionally to its activity, and the frequency of its interaction with the gene's promoter. The ABC model combines chromatin state data, such as accessibility and histone modifications, to assess enhancer activity, and uses chromosome conformation capture (Hi-C) data to infer contact frequency between enhancers and promoters. This model outperforms simpler alternatives such as distance-based and Hi-C contact-based predictions. For input into the ABC model, we used our ATAC-seq data, publicly available H3K27ac ChIP-seq data from regenerating livers[40] and *in situ* Hi-C and promoter-capture Hi-C data from intact livers[44].

The ABC algorithm predicted 15,816 distal enhancer-gene pairs, of which 15,499 (97.9%) were associated with expressed genes in at least one condition (Tables S2 and S3). Unlike conventional methods that assign enhancers solely based on the proximity to the nearest gene, the ABC method allowed us to predict the target genes of distal enhancers even when these were located megabases away. For instance, it identified an interaction between two increasing enhancers and a *de novo* enhancer with the promoter of the *Pnpla8* gene, despite being separated by more than 1.2 Mb in the linear genome (Figure 3A). We next assessed Pearson's correlation coefficient between chromatin accessibility at regeneration-responsive promoters and enhancers and their target gene expression across time points. Promoters showed the highest correlation, followed by proximal and distal enhancers (Figure S3A). Moreover, increasing peaks exhibited significantly stronger correlations than *de novo* or decreasing peaks (Figure S3B). Altogether, these results support the accuracy of ABC-predicted enhancer-gene pairs.

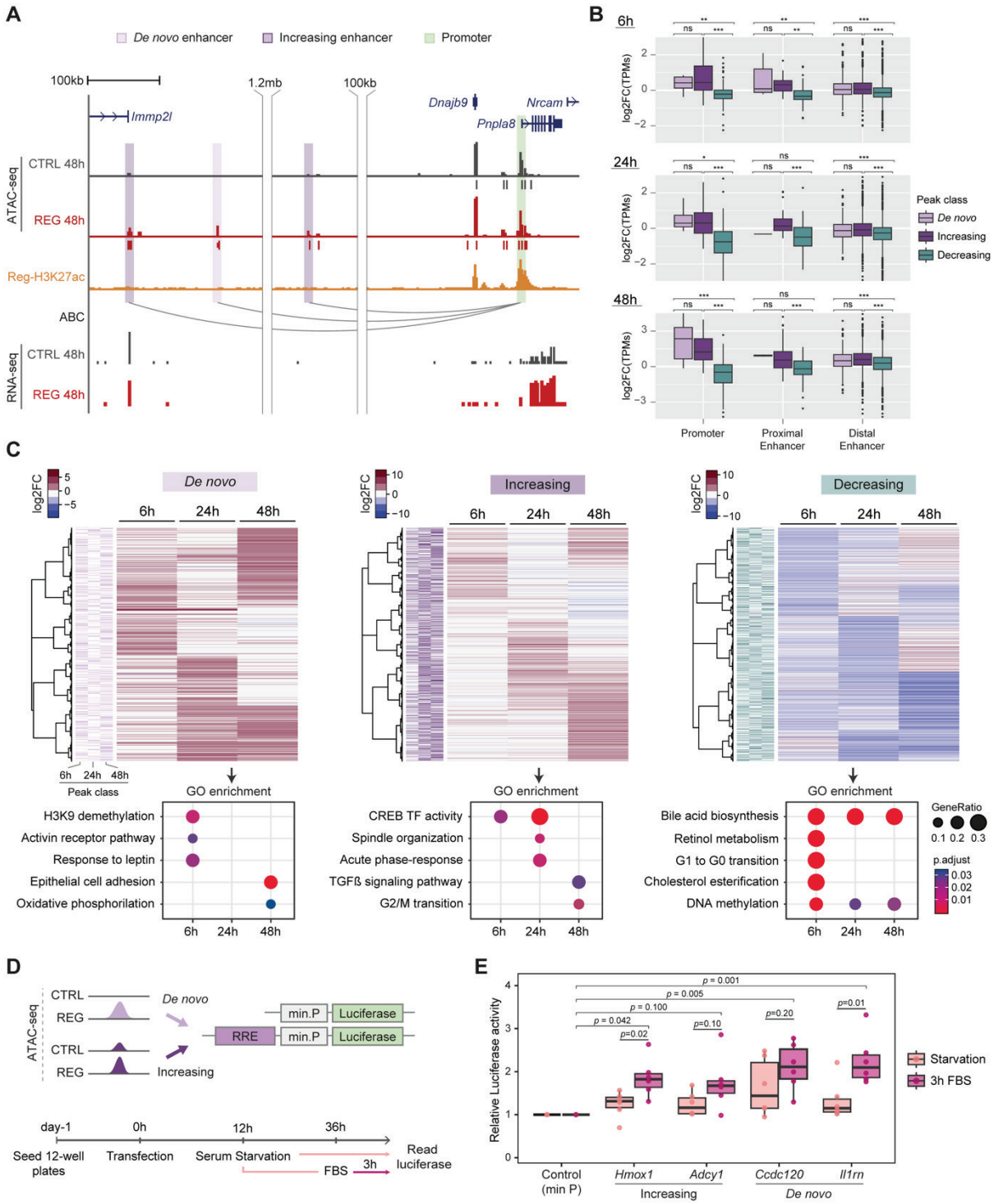

Figure 3. Enhancer-gene predictions using the activity-by-contact algorithm reveal opposite regulation for proliferation and metabolic genes

(A) Genome browser screenshot showing an ABC prediction at 48 h post-PHx. **(B)** Log2FC (TPM) of target genes associated with RREs in REG vs. CTRL samples. Two-way ANOVA followed by Tukey's HSD test was used to assess statistical differences between peak classes (*de novo*, increasing, decreasing) and genomic regions (promoter, proximal, distal) at 6, 24, and 48 h. Significance shown only between peak classes: ns = non-significant, *$p < 0.05$, **$p < 0.01$, ***$p < 0.001$. **(C)** Target gene expression linked to RREs, clustered by log2FC (TPM), ordered by hierarchical clustering. Below: time-specific GO terms. **(D)** Reporter assay design. Candidate *de novo* and increasing RREs were cloned upstream of a luciferase cassette, transfected into hepatocyte cultures, serum-starved for 24 h, then either kept in starvation or treated with 10% FBS for 3 h. The constructs were measured in a total of six biological replicates. **(E)** Relative luciferase activity under starvation or FBS. Two-way ANOVA with Tukey's HSD test to compare constructs vs. minP and between serum conditions ($p < 0.05$). See also Figure S3.

Next, we analysed the expression of predicted target genes during regeneration and found distinct transcriptional patterns across RRE types: genes linked to *de novo* and increasing promoters were largely upregulated, while those associated with decreasing promoters showed consistent downregulation (ANOVA with Tukey's Honestly Significant Difference (HSD) test, p-value <0.05) (Figure 3B). The target genes of *de novo* and increasing enhancers displayed no statistically significant differences between them but differed significantly from those associated with decreasing enhancers across all time points (Figure 3B). Furthermore, the target genes of *de novo* and increasing RREs tended to be upregulated during regeneration, whereas decreasing RREs were found to be mainly associated with downregulated genes (Figure 3C). GO analysis revealed that *de novo* and increasing RRE target genes were significantly enriched in signalling pathways known to play a role in liver regeneration at all three time points, such as the activin/TGF-ß pathway[19], with increasing RREs also associated with genes involved in the cell cycle (Figure 3C). In contrast, decreasing RREs mainly controlled the expression of genes related to liver-specific functions in lipid metabolism, including pathways associated with cholesterol and retinol metabolism, as well as bile acid biosynthesis. These findings align with the enriched biological functions identified in our transcriptomics analysis. Notably, the target genes from *de novo* and increasing RREs were enriched in functions that parallel those of the regeneration-specific transcriptomic gene clusters (Figure 1D), including the acute-phase response at 24 h and the mitosis-related signalling pathways at 48 h post-PHx. On the other hand, the steroids/cholesterol, retinol and bile acid metabolic pathways, specifically enriched for decreasing RRE-target genes, also exhibited enrichment within the cluster of control-specific genes from the RNA-seq analysis (Figure 1D). This suggests that *de novo* and increasing enhancers are activated post-PHx to upregulate genes required for early liver regeneration, whereas decreasing RREs influence gene expression in the intact adult liver but have reduced activity after PHx. Furthermore, our analysis revealed an enrichment of genes associated with the DNA methylation pathway among all decreasing RREs (Figure 3C). The dynamics of DNA methylation during liver regeneration are complex[45], and consistent with this, we identified genes within this group involved in both methylation and demethylation processes.

To validate putative RREs as enhancers capable of driving gene expression, we conducted a transient reporter assay in hepatocyte cell cultures. We cloned candidate RREs upstream of a minimal promoter and a luciferase gene cassette to assess their enhancer activity. Specifically, we tested four candidate sequences: (1) a distal increasing enhancer upstream of *Hmox1*; (2) an increasing enhancer located within the 10th intron of *Adcy1*; (3) a proximal *de novo* enhancer that progressively gains accessibility and is predicted to regulate *Ccdc120*, a gene exhibiting increased expression throughout regeneration; and (4) an intronic *de novo* enhancer predicted by the ABC model to target *Il1rn*, a gene upregulated 6 h post-PHx (Figure S3C). These constructs were transiently transfected into a hepatocyte cell line[46], serum-starved for 24 h to induce quiescence, and then either stimulated with 10% FBS for 3 h or maintained in serum-free conditions (Figure 3D), mimicking the quiescence-to-proliferation transition characteristic of liver regeneration. Serum stimulation significantly increased luciferase activity for the *Hmox1* (increasing) and *Il1rn* (*de novo*) RREs (n=6, ANOVA with Tukey's HSD test, p-value < 0.05), while the other two showed non-significant increases (Figure 3E). Under serum conditions, all four RREs exhibited significantly higher activity than the control, but not under starvation, suggesting that they act as enhancers activated upon cell cycle re-entry.

Cascade of TF activation during early liver regeneration

We next conducted TF footprint analysis within RREs using HINT-ATAC[47] to identify potential transcriptional regulators of the liver response following PHx. We identified differential TF footprints by comparing the ATAC-seq profiles of regenerating and control livers within all RREs at each time point. Only TFs that were expressed in our transcriptomics data and exhibited a significant change in activity (p-value < 0.05) were considered in the analysis.

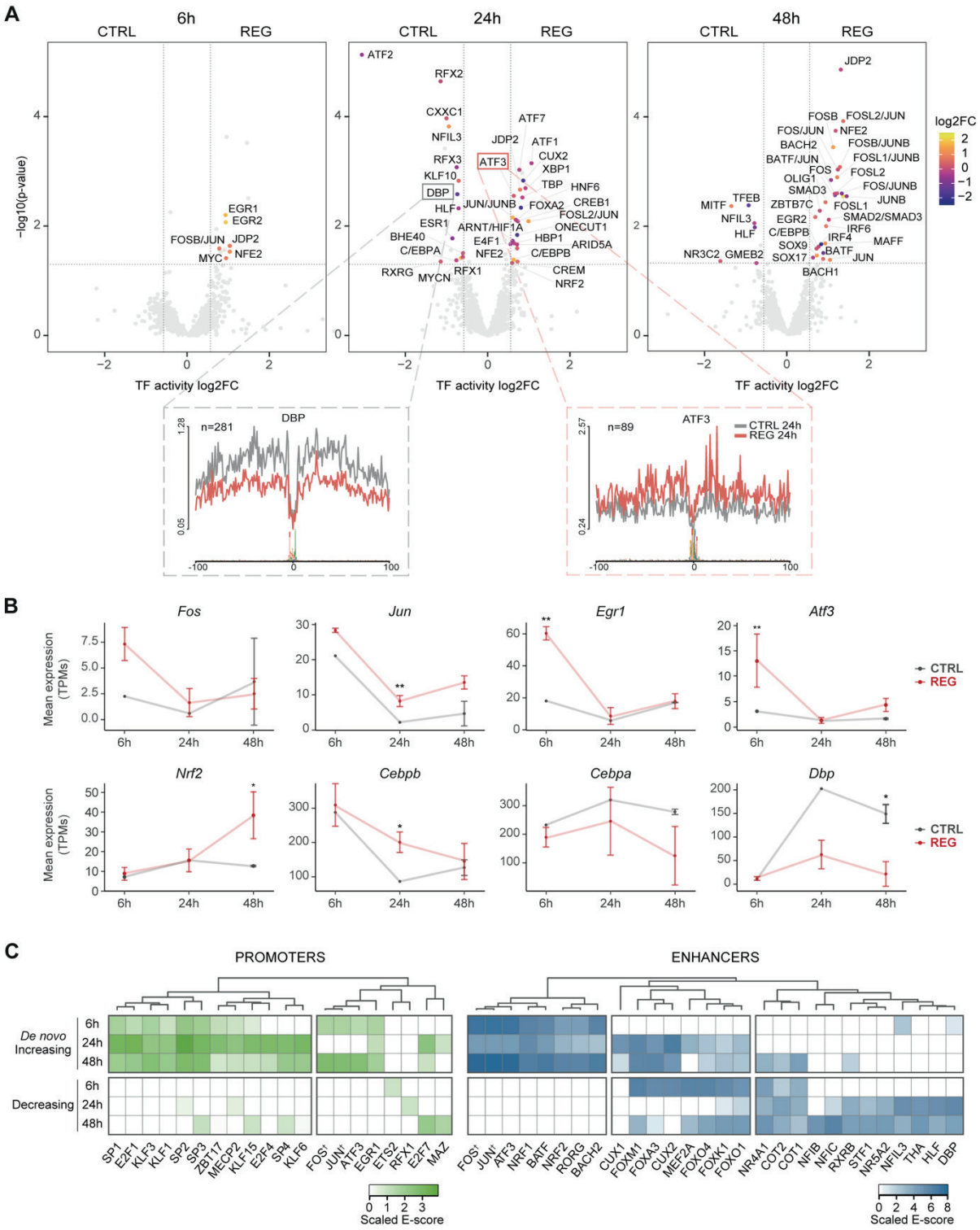

Figure 4. Time point-specific TF motif patterns during liver regeneration

(A) Differential TF binding sites at each time point identified by HINT-ATAC[47] footprinting. Each point represents a TF; and only those with expression >1 TPM in at least one condition and significant change in activity (p-value < 0.05) are labelled. Circle colour reflects log2FC of the TF-encoding gene. Below: ATAC-seq profiles for two example TF footprints at 24 h post-PHx (CTRL vs. REG). **(B)** Expression of *Fos*, *Jun*, *Egr1*, *Atf3*, *Nrf2*, *Cebpb*, *Cebpa*, and *Dbp* over time in CTRL (grey) and REG (red). Significance: ***p-adjust* < 0.01, **p-adjust* < 0.05 (DESeq2, pairwise comparison vs. control, Wald test, assuming negative binomial distribution). **(C)** Top 10 enriched TF motifs in *de novo*, increasing, or decreasing promoters (left) and enhancers (right), identified using AME[49] with the HOCOMOCO v11 database (Mann–Whitney U test, *p-adjust* < 0.05). Scaled enrichment E-scores are shown. † = includes all family members. See also Figure S4.

We observed that predicted TFs footprints within RREs during liver regeneration differed entirely from those in control livers (Figure 4A). Across all regeneration time points, we identified various combinations of the activator protein 1 (AP-1) dimer motif (FOS/JUN) (Figure S4A) and the nuclear factor erythroid 2 (NFE2) binding site. Some motifs were shared between two time points, such as early growth response 2 (EGR2) at 6 and 48 h, and CCAAT/enhancer-binding protein ß (C/EBPß) at 24 and 48 h post-PHx. Others were exclusive to specific time points, including EGR1 and MYC at 6 h; and activating TFs (ATF) 1, 3 and 7, Nfe2-related factor 2 (NRF2), X-box binding protein 1 (XBP1) and Onecut1/hepatocyte nuclear factor 6 (HNF6) at 24 h (Figure 4A; Figure S4B-E). At 48 h, we detected Mothers against decapentaplegic homolog 3 (SMAD3) footprints (Figure 4A), and although not significantly, the NRF2 motif also appeared enriched (Figure S4E). Notably, many of these TFs were upregulated at the transcriptional level, including *Fos*, *Jun*, *Egr1*, *Atf3*, *Nrf2*, and *Cebpß* (Figure 4B). Several of these are well-known regulators of the transcriptional response during liver regeneration. For instance, *Fos* and *Jun* are immediate-early genes induced within the first hours after PHx, playing a key role in promoting hepatocyte proliferation[19]. Similarly, C/EBPß contributes to cytokine-mediated activation pathways and supports both proliferation and metabolic homeostasis in remnant hepatocytes[17], while XBP1 regulates proteostasis and the acute-phase response during liver regeneration[48]. In control livers, we predicted the binding sites for D-box binding PAR bZIP TF (DBP) and C/EBPα (Figure 4A), both of which showed decreased expression at 48 h after PHx (Figure 4B), along with nuclear factor interleukin 3 regulated (NFIL3), among others.

To further investigate putative TFs involved in liver regeneration, we analysed motif enrichment in RREs using AME (MEME Suite)[49]. We compared TF motif enrichment in *de novo* and increasing or decreasing RREs at each time point against all accessible regions (Mann–Whitney U test p-value < 0.05). Since the motifs within enhancer and core-promoter sequences may recruit different *trans*-acting factors[50], we analysed them separately. We selected the top 10 TF motifs per time point and peak class, excluding non-expressed TFs. Our analysis revealed substantial differences between promoters and enhancers, and distinct TF motif patterns in increasing or decreasing regions (Figure 4C). E2F, SP, and Krüppel-like factor motifs were consistently enriched in *de novo* and increasing promoters across all time points, with several encoded by genes co-expressed in the 6 or 6–48 h REG clusters (Table S1). The E2F family is known for its critical role in regulating the cell cycle and apoptosis, with E2F1 specifically binding to the promoter regions of genes involved in the progression to the S phase[51]. FOS and JUN motifs were also among the top hits, enriched in both *de novo* and increasing promoters and enhancers, but absent from decreasing RREs (Figure 4C). These TFs were highly expressed in the liver at 6 h post-PHx (Figure 4B). We also identified the STAT3 motif, a key transcription factor driving hepatocyte proliferation during liver regeneration[52], exclusively enriched in *de novo* and increasing enhancers at both 6 hours (*padj* = 4.23e-04) and 48 hours (*padj* = 2.11e-07) post-PHx (Figure S4F). Although STAT3 was not among the top 10 enriched motifs, its significant enrichment, along with the strong enrichment for the E2F and AP-1 motifs, further supports the robustness of our findings. In addition, the ATF3 motif was enriched in both *de novo* and increasing promoters and enhancers, with NRF1 and NRF2 motifs also exclusively enriched within these enhancers. In contrast, decreasing enhancers showed enrichment for the COUP TFs (COT) 1 and 2, nuclear factors I (NFI) B and C, and DBP motifs (Figure 4C).

Subsequently, we integrated our transcriptomics data, TF binding predictions, and enhancer-gene map to construct a gene regulatory network (GRN). We selected the top 10 most enriched TFs in RREs at each time point (Figure 4C) and computed Pearson's correlation coefficients between the expression of each TF and that of its predicted target genes. We retained only significant interactions (|correlation| ≥ 0.8) and TFs with motifs present in at least 5 RREs. Most TFs showed positive correlations with their targets, suggesting a predominantly activating role via enhancers (Figure 5A; Figure S5A,B). For instance, NRF2 positively correlated with all its targets, especially at later stages, whereas BACH2 showed mixed effects, negatively correlating with 66% of its targets (Figure S5A-C).

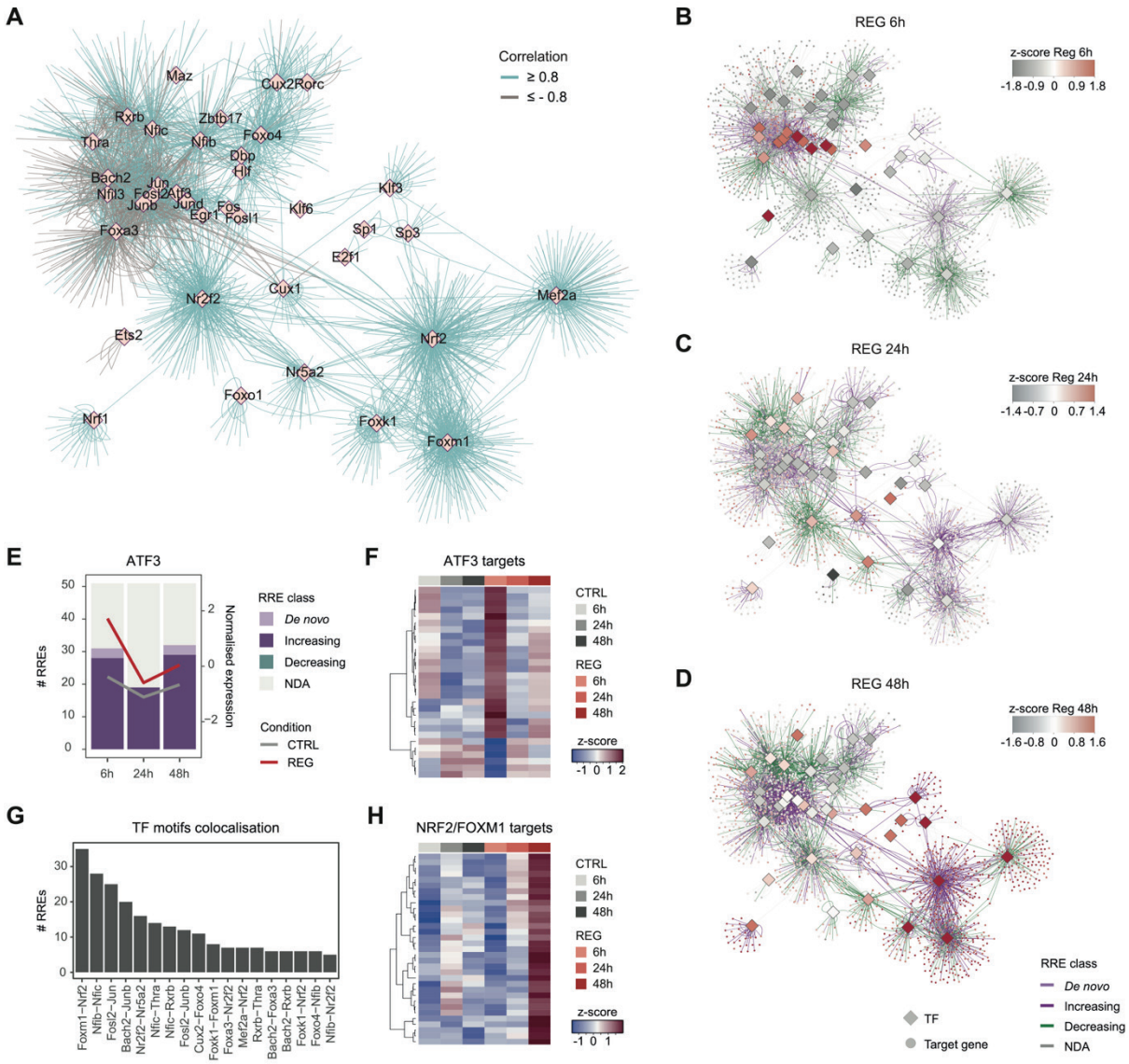

Figure 5. Early regeneration gene regulatory network (GRN)

(A) GRN with edges coloured by TF-target Pearson's correlation coefficient (blue ≥ 0.8, grey ≤ -0.8). While most correlations are positive, negative interactions are predicted for some TFs. **(B)** GRN at 6 h: nodes are coloured by target gene normalised expression, and edges by RRE classification at 6 h. **(C)** GRN at 24 h: same as (B), but for 24 h. **(D)** GRN at 48 h: same as (B), but for 48 h. **(E)** Number and type of RREs with ATF3 motifs (left axis) and *Atf3* expression in z-scores (right axis) (REG in red, CTRL in grey). **(F)** Expression of predicted target genes linked to ATF3 motif-containing RREs. Each column is one condition (average across replicates), gene expression as z-scores. **(G)** Number of RREs containing TF motif pairs. **(H)** Expression of predicted target genes associated with RREs with co-localization of the NRF2 and FOXM1 motifs. Each column is one condition (average across replicates), gene expression as z-scores. See also Figure S5.

We next profiled gene expression over time and categorised edges based on their corresponding RRE behaviour at each time point. The resulting GRN suggested a cascade of TF activation during the early stages of liver regeneration (Figure 5B-D). At 6 h post-PHx, key early-induced TFs, including EGR1, the AP-1 subunits JUN and FOS, and ATF3, were upregulated, likely driving the expression of their target genes via *de novo* and increasing enhancers (Figure 5B,E,F; Figure S5D). As regeneration progressed, additional TFs, such as CUX1, may have contributed to the transcriptional activation of genes at 24 h (Figure 5C). By 48 h after PHx, several TFs including NRF2, FOXM1, MEF2A, NRF1 and FOXK1 emerged as potential central drivers of gene upregulation (Figure 5D, Figure S5D,E). Notably,

we observed co-localisation of NRF2 and FOXM1 motifs at numerous RREs, suggesting potential cooperation in activating their target genes at 48 h post-PHx (Figure 5G,H; Figure S5F). Conversely, some TFs likely mediated the downregulation of their target genes at specific time points. For instance, FOXK1, FOXO4 and FOXM1 motifs were primarily associated with decreasing enhancers and low gene expression at 6 h post-PHx (Figure 5B; Figure S5D). Meanwhile, downregulated regulons at 24 and 48 h included DBP, NFIB and NFIC (Figure 5C,D; Figure S5D,E).

Focusing on ATF3, which was significantly upregulated at 6 h post-PHx (Figure 4B), we performed immunohistochemical analysis and confirmed the presence of ATF3-positive hepatocyte nuclei in regenerating livers at this time point, but not in controls (Figure 6A). Next, we identified a set of putative ATF3 target regions by analysing available ATF3 ChIP-seq datasets in mice and comparing them with *de novo* and increasing RREs. ATF3 peaks were significantly enriched at these RREs, particularly at 6 h post-PHx (Fisher's exact test, *padj* < 0.001) (Figure 6B), supporting the GRN predictions. Further analysis confirmed that ATF3 binds to the promoters and enhancers of over 85% of the GRN-predicted ATF3 target genes. Among these, *Hcar2*, which was upregulated at 6 h, was associated with a *de novo* RRE (Figure 6C), while *Trib1,* previously shown to be regulated by ATF3 in HepG2 cells[53], was linked to three increasing enhancers with ATF3 binding (Figure S6A). Additionally, functional characterisation of predicted ATF3 target genes linked to *de novo* and increasing RREs (Table S4), using the KEGG PATHWAY database, revealed enrichment in regeneration-related pathways. These included glucagon signalling and adherens junctions across all time points, as well as the MAPK, TGFß and Hippo signalling pathways, particularly at later stages (Figure 6D). Furthermore, we analysed *Atf3* expression using a published single-cell RNA-seq dataset from livers collected at different time points post-PHx[31], although no scRNA-seq data were available for 6 hours. *Atf3* was predominantly expressed in a subset of hepatocytes at 24 and 48 h post-PHx (Figure 6E,F), confirming that its expression was mostly restricted to regenerating hepatocytes. Moreover, GRN-predicted ATF3 target genes, validated through ChIP-seq analysis, exhibited higher expression levels in *Atf3*-expressing cells compared to those without *Atf3* expression (Figure S6B). Altogether, these findings support our GRN predictions and highlight the role of ATF3 in transcriptional regulation during liver regeneration.

We next integrated our ATAC-seq dataset with the published NRF2 ChIP-seq profiles from mouse intact livers[54]. NRF2 is a TF that plays a key role in the response to oxidative stress by binding to the antioxidant response elements (ARE) in the promoter regions of cytoprotective genes, such as phase II detoxification enzymes, thus inducing their expression[55]. We focused our analysis on increasing RREs, since these regions were more likely to feature NRF2 in the intact liver. Indeed, we observed a significant overlap between increasing RREs and NRF2 peaks at all time points (Fisher's exact test, *padj* < 0.001), with this overlap becoming more pronounced at the later stages of regeneration (Figure 6G). These results are consistent with the concurrent increase in *Nrf2* expression over time (Figure 4B) and further reinforce the role of NRF2 especially at this later time point. *Hmox1*, a well-established NRF2 target[56], was upregulated 48 h post-PHx and associated with an NRF2-bound increasing RRE (Figure 6H). Similarly, *Aldh1a7*[57], was also upregulated and linked to an NRF2-bound increasing RRE (Figure 6H). Moreover, single-cell analysis of *Nrf2* expression[31] revealed its overexpression in hepatocytes at 24 and 48 hours post-PHx (Figure S6C), with a similar expression pattern observed for its known target genes, *Hmox1* and *Aldh1a7* (Figure S6D,E). Overall, NRF2 target genes, identified by the GRN and validated by ChIP-seq, showed significantly higher expression in *Nrf2*-expressing cells compared to non-expressing ones in the scRNA-seq data (Figure S6B). Functional analysis of NRF2-bound increasing RRE targets revealed enrichment in wound healing, kinase activity, apoptosis, angiogenesis, and epithelial proliferation (Figure S6F; Table S5). As expected, when all target genes were considered, there was enrichment for oxidative stress response (GO:0006979, p-adj = 2.10E-03). This suggests NRF2 may bind both promoters and enhancers of regeneration-related genes under normal conditions, but during regeneration, increased *Nrf2* expression and RRE accessibility likely promote NRF2 binding to RREs, leading to target gene upregulation. In contrast, DBP, which is downregulated during regeneration according to our transcriptomics analysis (Figure 4B) and the

published scRNA-seq[31] (Figure S6G), likely detaches from RREs, contributing to their closure and reduced gene expression.

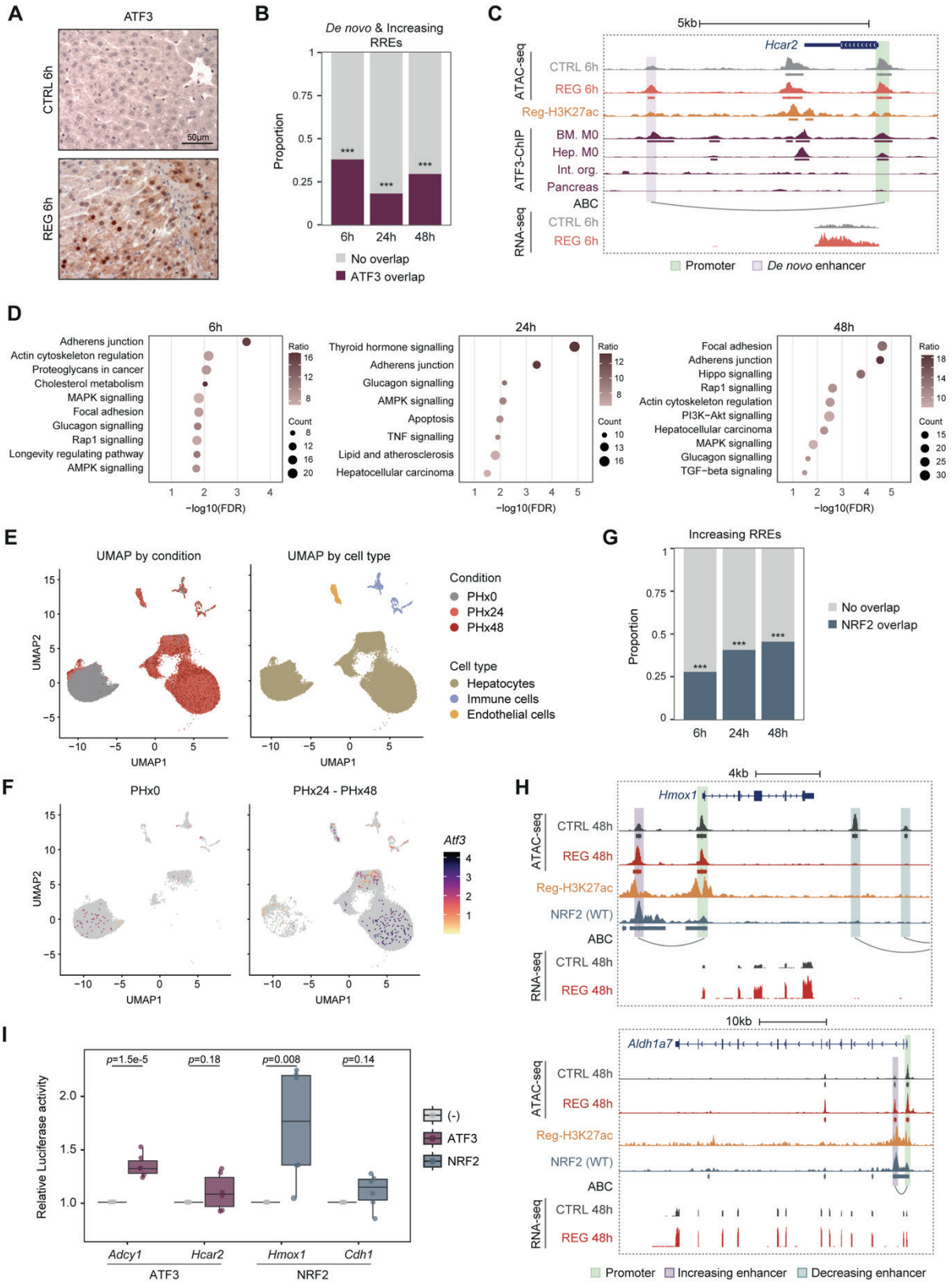

(Legend on next page)

Figure 6. ATF3 and NRF2 bind to *de novo* and increasing RREs to activate the expression of regeneration-associated genes

(A) Representative ATF3 immunostaining images in control and regenerating livers at 6 h post-surgery. No positive nuclei observed in controls. **(B)** Proportion of *de novo* and increasing RREs overlapping ATF3 ChIP-seq peaks at each time point. Fisher's exact test (****padj* < 0.001). **(C)** Genome browser screenshot of the *Hcar2* locus at 6h. Promoter shows ATF3 binding and is linked to an ATF3-bound *de novo* enhancer. **(D)** KEGG Pathway analysis of target genes from ATF3-bound *de novo* and increasing RREs **(E)** UMAP of cells from quiescent (PHx0) and regenerating (PHx24 - PHx48) livers, coloured by condition (left) or annotated cell type (right). **(F)** Feature plot of *Atf3* expression at PHx0 and PHx24 - PHx48. **(G)** Proportion of increasing RREs overlapping NRF2 ChIP-seq peaks at each time point. Fisher's exact test (****padj* < 0.001). **(H)** Genome browser views of *Hmox1* and *Aldh1a7* loci at 48 h. Both promoters show NRF2 binding and are linked to NRF2-bound increasing enhancers. **(I)** Relative luciferase activity of candidate enhancers co-transfected with ATF3 or NRF2 vectors, or alone (-), in hepatocyte cultures. One-way ANOVA with Tukey's HSD ($p < 0.05$). See also Figure S6.

To confirm that ATF3 and NRF2 act as transcriptional activators of liver regeneration through RREs, we cotransfected expression vectors for these TFs with luciferase reporter vectors containing candidate enhancers. For ATF3, we tested RREs associated with *Hcar2* (Figure 6C) and *Adcy1* (Figure S3C), both identified by the GRN as ATF3 targets. As candidate NRF2-regulated enhancers, we selected the *Hmox1*-linked enhancer (Figure 6I) and an intronic enhancer associated with *Cdh1*, a gene upregulated at 48h post-PHx and predicted by the GRN as a potential NRF2 target. Transient cotransfection assays in hepatocyte cultures revealed a significant increase in luciferase expression in ATF3-expressing cells with the *Adcy1*-associated RRE and in NRF2-expressing cells with the *Hmox1* RRE, compared to non-expressing control cells (ANOVA with Tukey's HSD, p-value < 0.05) (Figure 6I). Additionally, the *Hcar2* and *Cdh1* enhancers showed a trend toward increased luciferase activity upon ATF3 and NRF2 overexpression, respectively. These results support ATF3 and NRF2 as transcriptional activators of RREs.

Interplay of regeneration-specific and developmental regulatory elements

While liver regeneration and development share some molecular mechanisms, the two processes differ significantly. For instance, their cellular origins are distinct: liver regeneration following PHx is primarily driven by mature hepatocytes, whereas during embryonic development, hepatocytes originate from hepatoblasts—bipotential precursors that also give rise to biliary epithelial cells[19]. To determine if the gene expression changes observed during liver regeneration rely on the same regulatory mechanisms employed during liver development or involve unique, regeneration-specific regulatory networks, we analysed chromatin accessibility data from mouse liver development, spanning embryonic day 11.5 (E11.5) to postnatal day 0 (P0)[58] (Figure 7A). This period encompasses the stages of accelerated liver bud growth (E10-E13), hepatoblast differentiation into hepatocytes (E14) and hepatocyte maturation (E15-P0), a process that continues after birth[19]. We specifically examined whether *de novo* RREs—regions uniquely accessible in regenerating livers but not in uninjured ones—were also accessible during any stage of liver development. Such overlap would indicate the reuse of developmental enhancers for regeneration. Conversely, regions exclusively accessible during regeneration, with no accessibility during development, would suggest the presence of regeneration-specific enhancers (Figure 7B). Our analysis revealed that 45% of *de novo* RREs were developmental enhancers repurposed for regeneration (Reused), while the remaining 55% were enhancers exclusive to regeneration (Reg-specific) (Figure 7C). Among the Reused enhancers, most were either repurposed from late developmental stages (E16.5 and P0) (Figure 7B-D) or were active throughout all stages of liver development (Figure S7A,B). To further characterise these regulatory elements, we explored their distribution in the genome. While both subtypes of *de novo* RREs were predominantly located in distal regions, consistent with the general distribution of all RREs, their proportions in proximal and promoter regions differed significantly (chi-square p< 2.2e-16). Specifically, Reused RREs were more abundant in proximal (2%) and promoter (6%) regions, compared to Reg-specific regulatory elements (1% and

2%, respectively). These findings suggest that regeneration-specific regulatory mechanisms primarily function through distal enhancers.

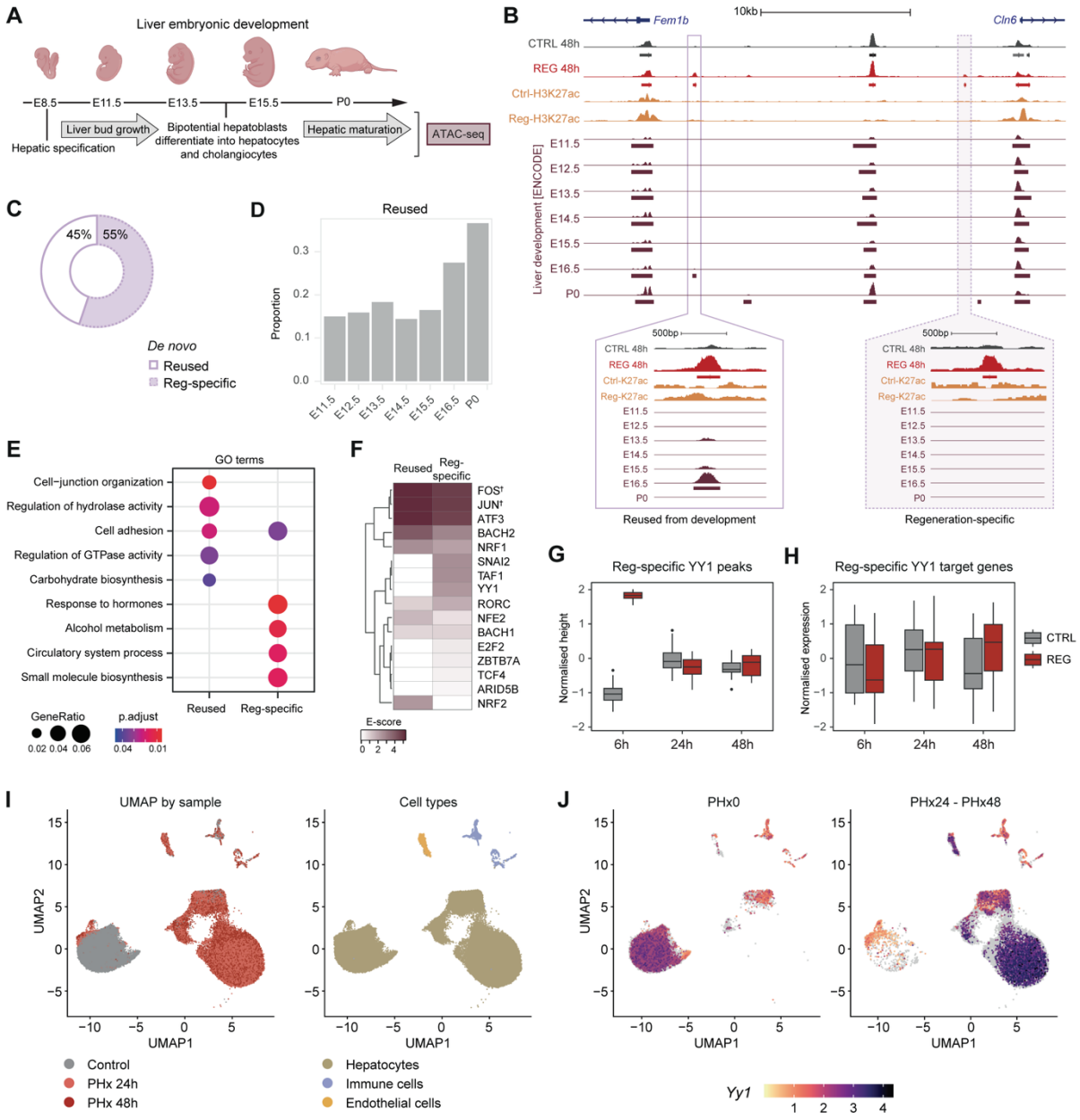

Figure 7. Enhancers from development are repurposed in the adult liver to activate the expression of regeneration genes

(A) Liver developmental stages used for ATAC-seq data in the comparative analysis with *de novo* RREs. **(B)** Genome browser views of a *de novo* enhancer overlapping a developmental enhancer (Reused) and one specific to regeneration (Reg-specific). **(C)** Proportion of *de novo* RREs classified as reused or reg-specific. **(D)** Proportion of *de novo* peaks overlapping developmental enhancers at each developmental stage. **(E)** GO term analysis of target genes from reused vs. reg-specific *de novo* RREs (*padj* < 0.05). **(F)** Heatmap of enriched TF motifs in reused and reg-specific *de novo* RREs. Scaled enrichment E-score shown; † = all family members included. **(G)** Normalised accessibility of reg-specific *de novo* peaks with YY1 motifs. **(H)** Normalised expression of reg-specific YY1 putative target genes. **(I)** UMAP of gene expression from quiescent (PHx0) and regenerating livers (PHx24, PHx48), coloured by condition (left) and annotated cell type (right). **(J)** Feature plot of *Yy1* expression in PHx0 and PHx24-PHx48. See also Figure S7.

GO term enrichment analysis of *de novo* RRE target genes revealed distinct functional categories. Reused RRE genes were enriched in cell-cell interactions and carbohydrate biosynthesis, including gluconeogenesis genes like *Sik1* (Figure 7E; Figure S7C), a process regulated during both regeneration and birth[59]. In contrast, Reg-specific targets were enriched in liver-related functions, such as alcohol metabolism and hormone responses, including insulin, leptin, and growth hormone signalling, such as peroxisome proliferator-activated receptor gamma (*Pparg*) gene (Figure 7E; Figure S7D,E). These pathways act as auxiliary mitogens, delaying but not impairing regeneration when disrupted[18].

Next, we performed TF motif enrichment between Reg-specific and Reused *de novo* RREs (Figure 7F). Although many TFs were shared between these two groups, distinct TF signatures were identified. For instance, NRF2 was exclusively enriched in Reused enhancers, while other TFs, such as the transcriptional repressor YY1, were uniquely enriched in Reg-specific enhancers. We focused on YY1 due to its well-established role in intestinal stem cell renewal[60] and its involvement in hepatic lipid metabolism[61]. YY1 overexpression promotes the growth of immortalized, non-tumorigenic human hepatocytes, whereas its depletion inhibits the growth of hepatocellular carcinoma cells[62]. We observed that the YY1 binding motif was predominantly enriched in Reg-specific *de novo* RREs that became accessible at 6 h after PHx (Figure 7G), while its predicted target genes were generally downregulated at this time point (Figure 7H). Pearson's correlation coefficient analysis between the accessibility of these Reg-specific RREs with YY1 motifs and the expression of their associated target genes revealed that nearly 70% exhibited a negative correlation (Figure S7F). This suggests that these regions might function as Reg-specific silencers rather than enhancers, consistent with the role of YY1 as a transcriptional repressor[63]. To determine which cells express *Yy1* during regeneration, we analysed a published scRNA-seq dataset from livers collected at 0, 24 and 48 h post-PHx[31]. We found that *Yy1* was highly expressed in hepatocytes and endothelial cells during regeneration, with lower levels of expression observed in quiescent hepatocytes and immune cells (Figure 7I,J). Altogether, our results suggest that liver regeneration involves a collaborative interplay between regeneration-specific regulatory elements and developmental enhancers repurposed in adulthood, each governed by distinct regulatory mechanisms and linked to specific biological functions.

DISCUSSION

The mammalian liver possesses an exceptional capacity for compensatory growth following injury or PHx, a process driven by transcriptional reprogramming and epigenetic modifications[21,24]. In quiescent hepatocytes, pro-regenerative genes are maintained in active or permissive chromatin states[27,64], enabling rapid and widespread transcriptional changes in response to injury[65]. During regeneration, some hepatocytes preserve their original chromatin landscape, while others shift toward a foetal-like state[30,31]. Despite significant progress in understanding the epigenetic events of liver regeneration, the mechanisms regulating chromatin architecture, specific enhancers and transcriptional networks that control regenerative programmes remain unclear.

Here, we identify the regulatory elements that are dynamically modulated during early liver regeneration after PHx (RREs) and uncover new TFs potentially regulating their activity. RREs mainly function as enhancers activating the expression of regeneration-associated genes, particularly those involved in key signalling and cell cycle pathways. However, RREs also include regions that become inactive during regeneration, which may lead to a global downregulation of liver-specific homeostatic functions, such as the biosynthesis of bile acids and retinol. This suggests that hepatocytes suppress energy-intensive metabolic programmes characteristic of quiescent hepatocytes to prioritize proliferation. An inverse correlation between hepatocyte proliferation and metabolic function during liver regeneration has been previously proposed[65,66]. A similar shift in chromatin accessibility has been observed in chronic liver injury[28], and spatially resolved transcriptomics during liver regeneration further confirm an initial downregulation of metabolic genes, concurrent with hepatocyte priming and proliferation[32]. Consistently, single-cell studies show that regenerating hepatocytes undergo reprogramming after PHx,

shifting from metabolic to developmental functions[30,31]. However, a subset of hepatocytes retains the chromatin landscape of metabolically active uninjured cells[30,31]. Consequently, changes in RRE accessibility may occur selectively within specific hepatocyte populations.

Hepatocyte metabolic reprogramming in the injured liver is essential for meeting energy demands, supplying anabolic precursors, and regulating signalling pathways that drive tissue repair[67]. Our findings suggest that during regeneration, hepatocytes suppress bile acid biosynthesis and undergo changes in cholesterol metabolism through transcriptional and chromatin regulation. While lipid utilisation increases during regeneration to support the synthesis of phospholipids and cholesterol, both essential for cell membrane formation[68], repression of *Cyp7a1* post-PHx limits bile acid production from cholesterol, despite Cyp7a1 protein levels remaining stable[36,69]. Furthermore, the ubiquitin ligase Uhrf2-mediated suppression of cholesterol biosynthesis genes is essential for regeneration[70], and a hypercholesterolemic diet impairs liver repair[71]. Further studies are warranted to elucidate the relationship between steroid metabolic regulation and hepatic regeneration.

Our study also identifies potential transcriptional regulators orchestrating liver regeneration. The AP-1 complex emerges as a key factor driving the transcriptional response at the chromatin level, especially during the priming phase. In particular, the AP-1 subunit JUN is a critical regulator of hepatocyte proliferation, as studies have shown that liver regeneration is impaired in mice lacking JUN[72]. The role of AP-1 appears to be conserved across various regenerative models[73], including *Drosophila* wing discs[8], zebrafish heart[74], as well as killifish and zebrafish fin regeneration[6], in which AP-1 motifs are essential for the activation of RREs. Consequently, the AP-1 complex may serve as a master regulator, collaborating with tissue-specific TFs, to facilitate the opening of *de novo* RREs as a pioneer factor and activate gene expression during regeneration. Significantly, recent evidence suggests that AP-1 can act as a pioneer factor in hepatocytes, by contributing to global changes in chromatin accessibility following *in vivo* reprogramming by the Yamanaka factors[75]. Furthermore, our findings suggest a cascade of TF activation following PHx, with ATF3, alongside JUN and FOS, driving the transcriptional response during the priming stage of liver regeneration. While the role of ATF3 in liver regeneration is still unclear, it is rapidly induced following PHx in rats[76] and has been implicated in various processes, including hepatic proliferation[77], the inhibition of gluconeogenesis[78], a liver-specific function that is initially downregulated during liver regeneration[79], and the regulation of lipoprotein and bile acid metabolism[80], processes that undergo alterations during liver regeneration, as observed in our study. Here, we propose that ATF3 selectively binds to the promoters and enhancers of genes essential for the initiation of regeneration, while NRF2 and FOXM1 likely mediate gene upregulation during the proliferation stage. Significantly, it has been demonstrated that the absence of NRF2 impairs liver regeneration[81], while its ectopic activation enhances regenerative capacity[82]. Moreover, previous studies have shown that FOXM1 is essential for hepatocyte mitosis by stimulating the expression of cell cycle genes during liver regeneration[83].

A long-standing question in regenerative biology is whether regeneration recapitulates embryonic development. On the one hand, research in animals with a high regenerative potential has shown that the genes involved in development are frequently reactivated after injury and are essential for successful regeneration[84,85]. However, evidence also suggests that the regulatory networks controlling tissue regeneration and proliferation in wounded tissues differ from those involved in developmental growth[1]. In the liver, recent studies indicate that a subset of hepatocytes undergo reversible reprogramming after PHx, activating the same gene expression programmes that are used for physiological growth during the postnatal stage of development[30,31]. At the same time, STAT3 binding to injury-specific enhancers, rather than developmental enhancers, to activate reprogramming-related genes[86] suggests distinct regulatory networks between regeneration and development. Our findings indicate that the regenerating liver is capable of reactivating developmental enhancers, preferentially from the postnatal or late developmental stages, to regulate genes associated with cell junctions and glucose metabolism. Significantly, hepatocytes acquire junctional integrity and polarity and undergo changes in glucose metabolism during the maturation stage of liver development, a process that takes

place around the perinatal period[19]. These changes bear resemblance to those observed during liver regeneration following PHx.

In summary, our study provides a genome-wide atlas of enhancer-gene interactions and highlights key transcriptional regulators in early liver regeneration. These findings could be a valuable resource for researchers aiming to target regulatory elements involved in liver regeneration, with significant implications for regenerative medicine. Potential applications include the ectopic activation of regeneration enhancers to exert temporal and spatial control over the expression of pro-regenerative factors within an injured area, as proposed by Yan et al. (2022)[16]. The addition of regenerative TFs could also be employed to enhance the regenerative potential, particularly in the context of liver failure.

Limitations of the study

While this study provides key insights into liver regeneration, more biological replicates would improve robustness, and additional time points could provide a more comprehensive understanding of the process. *In vivo* transgenic reporter assays could further clarify enhancer function during regeneration. However, compliance with stringent European regulations on animal research limits the inclusion of additional replicates, time points or transgenic models. Future studies could also benefit from experiments such as ChIP-seq for TFs identified in our gene regulatory network. The lack of high-quality antibodies, particularly for TFs with less characterised roles in liver regeneration, has limited our ability to generate ChIP-seq data using liver tissue from hepatectomies. The absence of detectable changes in chromatin accessibility does not necessarily indicate that specific enhancers or regulatory regions are non-functional; therefore, complementary approaches, such as histone modification profiling or Hi-C, are needed to fully understand enhancer dynamics during liver regeneration. Finally, CRISPR/Cas9-mediated enhancer modifications could provide direct evidence of enhancer function in liver regeneration.

RESOURCE AVAILABILITY

Lead contact

Further information and requests for resources and reagents should be directed to and will be fulfilled by the lead contact, Montserrat Corominas (mcorominas@ub.edu).

Materials availability

This study did not generate new unique reagents.

Data and code availability

The RNA-seq and ATAC-seq raw and processed data from this study are available at NCBI Gene Expression Omnibus under the accession numbers GSE181476 [RNA-seq][33] and GSE266402 [ATAC-seq]. This study did not generate any unique code.

A Catalan version of the abstract, highlights and graphical abstract is available at:
https://doi.org/10.5281/zenodo.15267786

ACKNOWLEDGMENTS

We thank A.S. Nacht, T. Quesada-López, and E. Bertran for technical support; R. Corces for guidance on ATAC-seq; J. and P. Nieto for scRNA-seq advice; and the CRG Genomics Unit for assistance. We are also grateful to C. Camilleri-Robles for helpful discussions and manuscript revision. This project was funded by: PID2021-123300NB-100 from MCIN/ AEI / 10.13039/501100011033 / FEDER, UE to

F.S and M.C.; 2021SGR00293 from the Agency for the Management of University and Research Grants (Generalitat de Catalunya) to M.C.; PID2021-122551OB-100 from MCIN/AEI/10.13039/501100011033/ FEDER, UE to I.F.; FPU20/01473 from the Spanish Ministerio de Universidades to P.L.G. We thank R. Guigó for financial support to M.R.R, and R.N. through grant PID2021-128956NB-I00 funded by MCIN/ AEI / 10.13039/501100011033 / FEDER, UE.

AUTHOR CONTRIBUTIONS

PLG, IF and MC conceived and designed the experiments. PLG and MHI performed the experiments. PLG, MRR and RN analysed the data. GPV provided reagents and advice for the ATAC-seq experiments. PLG and MC wrote the manuscript. PLG, MRR, GPV, FS, IF, RN and MC revised the manuscript. FS, IF and MC acquired the funding.

DECLARATION OF INTERESTS

The authors declare no competing interests.

REFERENCES

1. Goldman, J.A., and Poss, K.D. (2020). Gene regulatory programmes of tissue regeneration. Nat. Rev. Genet. *21*, 511–525. https://doi.org/10.1038/s41576-020-0239-7.
2. Rodriguez, A.M., and Kang, J. (2020). Regeneration enhancers: Starting a journey to unravel regulatory events in tissue regeneration. Semin. Cell Dev. Biol. *97*, 47–54. https://doi.org/10.1016/j.semcdb.2019.04.003.
3. Goldman, J.A., Kuzu, G., Lee, N., Karasik, J., Gemberling, M., Foglia, M.J., Karra, R., Dickson, A.L., Sun, F., Tolstorukov, M.Y., et al. (2017). Resolving Heart Regeneration by Replacement Histone Profiling. Dev. Cell *40*, 392-404.e5. https://doi.org/10.1016/j.devcel.2017.01.013.
4. Begeman, I.J., Shin, K., Osorio-Méndez, D., Kurth, A., Lee, N., Chamberlain, T.J., Pelegri, F.J., and Kang, J. (2020). Decoding an Organ Regeneration Switch by Dissecting Cardiac Regeneration Enhancers. Development, dev.194019. https://doi.org/10.1242/dev.194019.
5. Kang, J., Hu, J., Karra, R., Dickson, A.L., Tornini, V.A., Nachtrab, G., Gemberling, M., Goldman, J.A., Black, B.L., and Poss, K.D. (2016). Modulation of tissue repair by regeneration enhancer elements. Nature *532*, 201–206. https://doi.org/10.1038/nature17644.
6. Wang, W., Hu, C.-K., Zeng, A., Alegre, D., Hu, D., Gotting, K., Ortega Granillo, A., Wang, Y., Robb, S., Schnittker, R., et al. (2020). Changes in regeneration-responsive enhancers shape regenerative capacities in vertebrates. Science *369*, eaaz3090. https://doi.org/10.1126/science.aaz3090.
7. Mokalled, M.H., Patra, C., Dickson, A.L., Endo, T., Stainier, D.Y.R., and Poss, K.D. (2016). Injury-induced *ctgfa* directs glial bridging and spinal cord regeneration in zebrafish. Science *354*, 630–634. https://doi.org/10.1126/science.aaf2679.
8. Harris, R.E., Setiawan, L., Saul, J., and Hariharan, I.K. (2016). Localized epigenetic silencing of a damage-activated WNT enhancer limits regeneration in mature Drosophila imaginal discs. eLife *5*, e11588. https://doi.org/10.7554/eLife.11588.
9. Vizcaya-Molina, E., Klein, C.C., Serras, F., Mishra, R.K., Guigó, R., and Corominas, M. (2018). Damage-responsive elements in *Drosophila* regeneration. Genome Res. *28*, 1852–1866. https://doi.org/10.1101/gr.233098.117.
10. Aguilar, C.A., Pop, R., Shcherbina, A., Watts, A., Matheny, R.W., Cacchiarelli, D., Han, W.M., Shin, E., Nakhai, S.A., Jang, Y.C., et al. (2016). Transcriptional and Chromatin Dynamics of Muscle Regeneration after Severe Trauma. Stem Cell Rep. *7*, 983–997. https://doi.org/10.1016/j.stemcr.2016.09.009.
11. Hung, H.A., Sun, G., Keles, S., and Svaren, J. (2015). Dynamic Regulation of Schwann Cell Enhancers after Peripheral Nerve Injury. J. Biol. Chem. *290*, 6937–6950. https://doi.org/10.1074/jbc.M114.622878.
12. Naik, S., Larsen, S.B., Gomez, N.C., Alaverdyan, K., Sendoel, A., Yuan, S., Polak, L., Kulukian, A., Chai, S., and Fuchs, E. (2017). Inflammatory memory sensitizes skin epithelial stem cells to tissue damage. Nature *550*, 475–480. https://doi.org/10.1038/nature24271.
13. Ge, Y., Gomez, N.C., Adam, R.C., Nikolova, M., Yang, H., Verma, A., Lu, C.P.-J., Polak, L., Yuan, S., Elemento, O., et al. (2017). Stem Cell Lineage Infidelity Drives Wound Repair and Cancer. Cell *169*, 636-650.e14. https://doi.org/10.1016/j.cell.2017.03.042.
14. Huang, G.N., Thatcher, J.E., McAnally, J., Kong, Y., Qi, X., Tan, W., DiMaio, J.M., Amatruda, J.F., Gerard,

R.D., Hill, J.A., et al. (2012). C/EBP Transcription Factors Mediate Epicardial Activation During Heart Development and Injury. Science *338*, 1599–1603. https://doi.org/10.1126/science.1229765.
15. Vieira, J.M., Howard, S., Villa Del Campo, C., Bollini, S., Dubé, K.N., Masters, M., Barnette, D.N., Rohling, M., Sun, X., Hankins, L.E., et al. (2017). BRG1-SWI/SNF-dependent regulation of the Wt1 transcriptional landscape mediates epicardial activity during heart development and disease. Nat. Commun. *8*, 16034. https://doi.org/10.1038/ncomms16034.
16. Yan, R., Cigliola, V., Oonk, K.A., Petrover, Z., DeLuca, S., Wolfson, D.W., Vekstein, A., Mendiola, M.A., Devlin, G., Bishawi, M., et al. (2023). An enhancer-based gene-therapy strategy for spatiotemporal control of cargoes during tissue repair. Cell Stem Cell *30*, 96-111.e6. https://doi.org/10.1016/j.stem.2022.11.012.
17. Taub, R. (2004). Liver regeneration: from myth to mechanism. Nat. Rev. Mol. Cell Biol. *5*, 836–847. https://doi.org/10.1038/nrm1489.
18. Michalopoulos, G.K., and Bhushan, B. (2021). Liver regeneration: biological and pathological mechanisms and implications. Nat. Rev. Gastroenterol. Hepatol. *18*, 40–55. https://doi.org/10.1038/s41575-020-0342-4.
19. López-Luque, J., and Fabregat, I. (2018). Revisiting the liver: from development to regeneration - what we ought to know! Int. J. Dev. Biol. *62*, 441–451. https://doi.org/10.1387/ijdb.170264JL.
20. Blake, M.J., and Steer, C.J. (2023). Liver Regeneration in Acute on Chronic Liver Failure. Clin. Liver Dis. *27*, 595–616. https://doi.org/10.1016/j.cld.2023.03.005.
21. Arechederra, M., Berasain, C., Avila, M.A., and Fernández-Barrena, M.G. (2020). Chromatin dynamics during liver regeneration. Semin. Cell Dev. Biol. *97*, 38–46. https://doi.org/10.1016/j.semcdb.2019.03.004.
22. Zhang, C., Sun, C., Zhao, Y., Ye, B., and Yu, G. (2024). Signaling pathways of liver regeneration: Biological mechanisms and implications. iScience *27*, 108683. https://doi.org/10.1016/j.isci.2023.108683.
23. Bangru, S., and Kalsotra, A. (2020). Cellular and molecular basis of liver regeneration. Semin. Cell Dev. Biol. *100*, 74–87. https://doi.org/10.1016/j.semcdb.2019.12.004.
24. Aloia, L. (2021). Epigenetic Regulation of Cell-Fate Changes That Determine Adult Liver Regeneration After Injury. Front. Cell Dev. Biol. *9*, 643055. https://doi.org/10.3389/fcell.2021.643055.
25. Sato, Y., Katoh, Y., Matsumoto, M., Sato, M., Ebina, M., Itoh-Nakadai, A., Funayama, R., Nakayama, K., Unno, M., and Igarashi, K. (2017). Regulatory signatures of liver regeneration distilled by integrative analysis of mRNA, histone methylation, and proteomics. J. Biol. Chem. *292*, 8019–8037. https://doi.org/10.1074/jbc.M116.774547.
26. Wang, S., Zhang, C., Hasson, D., Desai, A., SenBanerjee, S., Magnani, E., Ukomadu, C., Lujambio, A., Bernstein, E., and Sadler, K.C. (2019). Epigenetic Compensation Promotes Liver Regeneration. Dev. Cell *50*, 43-56.e6. https://doi.org/10.1016/j.devcel.2019.05.034.
27. Zhang, C., Macchi, F., Magnani, E., and Sadler, K.C. (2021). Chromatin states shaped by an epigenetic code confer regenerative potential to the mouse liver. Nat. Commun. *12*, 4110. https://doi.org/10.1038/s41467-021-24466-1.
28. Wang, A.W., Wang, Y.J., Zahm, A.M., Morgan, A.R., Wangensteen, K.J., and Kaestner, K.H. (2020). The Dynamic Chromatin Architecture of the Regenerating Liver. Cell. Mol. Gastroenterol. Hepatol. *9*, 121–143. https://doi.org/10.1016/j.jcmgh.2019.09.006.
29. Merrell, A.J., Peng, T., Li, J., Sun, K., Li, B., Katsuda, T., Grompe, M., Tan, K., and Stanger, B.Z. (2021). Dynamic Transcriptional and Epigenetic Changes Drive Cellular Plasticity in the Liver. Hepatology *74*, 444–457. https://doi.org/10.1002/hep.31704.
30. Chen, T., Oh, S., Gregory, S., Shen, X., and Diehl, A.M. (2020). Single-cell omics analysis reveals functional diversification of hepatocytes during liver regeneration. JCI Insight *5*, e141024. https://doi.org/10.1172/jci.insight.141024.
31. Chembazhi, U.V., Bangru, S., Hernaez, M., and Kalsotra, A. (2021). Cellular plasticity balances the metabolic and proliferation dynamics of a regenerating liver. Genome Res. *31*, 576–591. https://doi.org/10.1101/gr.267013.120.
32. Xu, J., Guo, P., Hao, S., Shangguan, S., Shi, Q., Volpe, G., Huang, K., Zuo, J., An, J., Yuan, Y., et al. (2024). A spatiotemporal atlas of mouse liver homeostasis and regeneration. Nat. Genet. https://doi.org/10.1038/s41588-024-01709-7.
33. Herranz-Itúrbide, M., López-Luque, J., Gonzalez-Sanchez, E., Caballero-Díaz, D., Crosas-Molist, E., Martín-Mur, B., Gut, M., Esteve-Codina, A., Jaquet, V., Jiang, J.X., et al. (2021). NADPH oxidase 4 (Nox4) deletion accelerates liver regeneration in mice. Redox Biol. *40*, 101841. https://doi.org/10.1016/j.redox.2020.101841.
34. Gralinska, E., Kohl, C., Sokhandan Fadakar, B., and Vingron, M. (2022). Visualizing Cluster-specific Genes from Single-cell Transcriptomics Data Using Association Plots. J. Mol. Biol. *434*, 167525. https://doi.org/10.1016/j.jmb.2022.167525.
35. Rib, L., Villeneuve, D., Minocha, S., Praz, V., Hernandez, N., Guex, N., and Herr, W. (2018). Cycles of gene expression and genome response during mammalian tissue regeneration. Epigenetics Chromatin *11*, 52.

https://doi.org/10.1186/s13072-018-0222-0.
36. Zhang, L., Huang, X., Meng, Z., Dong, B., Shiah, S., Moore, D.D., and Huang, W. (2009). Significance and Mechanism of CYP7a1 Gene Regulation during the Acute Phase of Liver Regeneration. Mol. Endocrinol. *23*, 137–145. https://doi.org/10.1210/me.2008-0198.
37. Zhao, Y., Ye, W., Wang, Y.-D., and Chen, W.-D. (2022). HGF/c-Met: A Key Promoter in Liver Regeneration. Front. Pharmacol. *13*, 808855. https://doi.org/10.3389/fphar.2022.808855.
38. Xu, C., Lin, F., and Qin, S. (2008). Relevance between lipid metabolism-associated genes and rat liver regeneration. Hepatol. Res. *38*, 825–837. https://doi.org/10.1111/j.1872-034X.2008.00345.x.
39. Chen, Y., Chen, L., Wu, X., Zhao, Y., Wang, Y., Jiang, D., Liu, X., Zhou, T., Li, S., Wei, Y., et al. (2023). Acute liver steatosis translationally controls the epigenetic regulator MIER1 to promote liver regeneration in a study with male mice. Nat. Commun. *14*, 1521. https://doi.org/10.1038/s41467-023-37247-9.
40. Sun, X., Chuang, J.-C., Kanchwala, M., Wu, L., Celen, C., Li, L., Liang, H., Zhang, S., Maples, T., Nguyen, L.H., et al. (2016). Suppression of the SWI/SNF Component Arid1a Promotes Mammalian Regeneration. Cell Stem Cell *18*, 456–466. https://doi.org/10.1016/j.stem.2016.03.001.
41. Shlyueva, D., Stampfel, G., and Stark, A. (2014). Transcriptional enhancers: from properties to genome-wide predictions. Nat. Rev. Genet. *15*, 272–286. https://doi.org/10.1038/nrg3682.
42. Pradeepa, M.M., Grimes, G.R., Kumar, Y., Olley, G., Taylor, G.C.A., Schneider, R., and Bickmore, W.A. (2016). Histone H3 globular domain acetylation identifies a new class of enhancers. Nat. Genet. *48*, 681–686. https://doi.org/10.1038/ng.3550.
43. Fulco, C.P., Nasser, J., Jones, T.R., Munson, G., Bergman, D.T., Subramanian, V., Grossman, S.R., Anyoha, R., Doughty, B.R., Patwardhan, T.A., et al. (2019). Activity-by-contact model of enhancer–promoter regulation from thousands of CRISPR perturbations. Nat. Genet. *51*, 1664–1669. https://doi.org/10.1038/s41588-019-0538-0.
44. Furlan-Magaril, M., Ando-Kuri, M., Arzate-Mejía, R.G., Morf, J., Cairns, J., Román-Figueroa, A., Tenorio-Hernández, L., Poot-Hernández, A.C., Andrews, S., Várnai, C., et al. (2021). The global and promoter-centric 3D genome organization temporally resolved during a circadian cycle. Genome Biol. *22*, 162. https://doi.org/10.1186/s13059-021-02374-3.
45. Falick Michaeli, T., Sabag, O., Azria, B., Fok, R., Abudi, N., Abramovitch, R., Monin, J., Gielchinsky, Y., Cedar, H., and Bergman, Y. (2024). Hepatocyte regeneration is driven by embryo-like DNA methylation reprogramming. Proc. Natl. Acad. Sci. *121*, e2314885121. https://doi.org/10.1073/pnas.2314885121.
46. López-Luque, J., Caballero-Díaz, D., Martinez-Palacián, A., Roncero, C., Moreno-Càceres, J., García-Bravo, M., Grueso, E., Fernández, A., Crosas-Molist, E., García-Álvaro, M., et al. (2016). Dissecting the role of epidermal growth factor receptor catalytic activity during liver regeneration and hepatocarcinogenesis. Hepatology *63*, 604–619. https://doi.org/10.1002/hep.28134.
47. Li, Z., Schulz, M.H., Look, T., Begemann, M., Zenke, M., and Costa, I.G. (2019). Identification of transcription factor binding sites using ATAC-seq. Genome Biol. *20*, 45. https://doi.org/10.1186/s13059-019-1642-2.
48. Argemí, J., Kress, T.R., Chang, H.C.Y., Ferrero, R., Bértolo, C., Moreno, H., González-Aparicio, M., Uriarte, I., Guembe, L., Segura, V., et al. (2017). X-box Binding Protein 1 Regulates Unfolded Protein, Acute-Phase, and DNA Damage Responses During Regeneration of Mouse Liver. Gastroenterology *152*, 1203-1216.e15. https://doi.org/10.1053/j.gastro.2016.12.040.
49. McLeay, R.C., and Bailey, T.L. (2010). Motif Enrichment Analysis: a unified framework and an evaluation on ChIP data. BMC Bioinformatics *11*, 165. https://doi.org/10.1186/1471-2105-11-165.
50. Catarino, R.R., and Stark, A. (2018). Assessing sufficiency and necessity of enhancer activities for gene expression and the mechanisms of transcription activation. Genes Dev. *32*, 202–223. https://doi.org/10.1101/gad.310367.117.
51. Ertosun, M.G., Hapil, F.Z., and Osman Nidai, O. (2016). E2F1 transcription factor and its impact on growth factor and cytokine signaling. Cytokine Growth Factor Rev. *31*, 17–25. https://doi.org/10.1016/j.cytogfr.2016.02.001.
52. Li, W., Liang, X., Kellendonk, C., Poli, V., and Taub, R. (2002). STAT3 Contributes to the Mitogenic Response of Hepatocytes during Liver Regeneration. J. Biol. Chem. *277*, 28411–28417. https://doi.org/10.1074/jbc.M202807200.
53. Soubeyrand, S., Lau, P., and McPherson, R. (2023). Regulation of TRIB1 abundance in hepatocyte models in response to proteasome inhibition. Sci. Rep. *13*, 9320. https://doi.org/10.1038/s41598-023-36512-7.
54. Nault, R., Doskey, C.M., Fader, K.A., Rockwell, C.E., and Zacharewski, T. (2018). Comparison of Hepatic NRF2 and Aryl Hydrocarbon Receptor Binding in 2,3,7,8-Tetrachlorodibenzo- *p* -dioxin–Treated Mice Demonstrates NRF2-Independent PKM2 Induction. Mol. Pharmacol. *94*, 876–884. https://doi.org/10.1124/mol.118.112144.
55. Itoh, K., Chiba, T., Takahashi, S., Ishii, T., Igarashi, K., Katoh, Y., Oyake, T., Hayashi, N., Satoh, K., Hatayama,

I., et al. (1997). An Nrf2/Small Maf Heterodimer Mediates the Induction of Phase II Detoxifying Enzyme Genes through Antioxidant Response Elements. Biochem. Biophys. Res. Commun. *236*, 313–322. https://doi.org/10.1006/bbrc.1997.6943.

56. Ishida, K., Kaji, K., Sato, S., Ogawa, H., Takagi, H., Takaya, H., Kawaratani, H., Moriya, K., Namisaki, T., Akahane, T., et al. (2021). Sulforaphane ameliorates ethanol plus carbon tetrachloride-induced liver fibrosis in mice through the Nrf2-mediated antioxidant response and acetaldehyde metabolization with inhibition of the LPS/TLR4 signaling pathway. J. Nutr. Biochem. *89*, 108573. https://doi.org/10.1016/j.jnutbio.2020.108573.
57. Leonard, M.O., Kieran, N.E., Howell, K., Burne, M.J., Varadarajan, R., Dhakshinamoorthy, S., Porter, A.G., O'Farrelly, C., Rabb, H., and Taylor, C.T. (2006). Reoxygenation-specific activation of the antioxidant transcription factor Nrf2 mediates cytoprotective gene expression in ischemia-reperfusion injury. FASEB J. Off. Publ. Fed. Am. Soc. Exp. Biol. *20*, 2624–2626. https://doi.org/10.1096/fj.06-5097fje.
58. Gorkin, D.U., Barozzi, I., Zhao, Y., Zhang, Y., Huang, H., Lee, A.Y., Li, B., Chiou, J., Wildberg, A., Ding, B., et al. (2020). An atlas of dynamic chromatin landscapes in mouse fetal development. Nature *583*, 744–751. https://doi.org/10.1038/s41586-020-2093-3.
59. Kalhan, S., and Parimi, P. (2000). Gluconeogenesis in the fetus and neonate. Semin. Perinatol. *24*, 94–106. https://doi.org/10.1053/sp.2000.6360.
60. Perekatt, A.O., Valdez, M.J., Davila, M., Hoffman, A., Bonder, E.M., Gao, N., and Verzi, M.P. (2014). YY1 is indispensable for Lgr5+ intestinal stem cell renewal. Proc. Natl. Acad. Sci. U. S. A. *111*, 7695–7700. https://doi.org/10.1073/pnas.1400128111.
61. Pan, G., Diamanti, K., Cavalli, M., Lara Gutiérrez, A., Komorowski, J., and Wadelius, C. (2021). Multifaceted regulation of hepatic lipid metabolism by YY1. Life Sci. Alliance *4*, e202000928. https://doi.org/10.26508/lsa.202000928.
62. Zhang, S., Jiang, T., Feng, L., Sun, J., Lu, H., Wang, Q., Pan, M., Huang, D., Wang, X., Wang, L., et al. (2012). Yin Yang-1 suppresses differentiation of hepatocellular carcinoma cells through the downregulation of CCAAT/enhancer-binding protein alpha. J. Mol. Med. Berl. Ger. *90*, 1069–1077. https://doi.org/10.1007/s00109-012-0879-y.
63. Verheul, T.C.J., Van Hijfte, L., Perenthaler, E., and Barakat, T.S. (2020). The Why of YY1: Mechanisms of Transcriptional Regulation by Yin Yang 1. Front. Cell Dev. Biol. *8*, 592164. https://doi.org/10.3389/fcell.2020.592164.
64. Li, W., Yang, L., He, Q., Hu, C., Zhu, L., Ma, X., Ma, X., Bao, S., Li, L., Chen, Y., et al. (2019). A Homeostatic Arid1a-Dependent Permissive Chromatin State Licenses Hepatocyte Responsiveness to Liver-Injury-Associated YAP Signaling. Cell Stem Cell *25*, 54-68.e5. https://doi.org/10.1016/j.stem.2019.06.008.
65. Walesky, C.M., Kolb, K.E., Winston, C.L., Henderson, J., Kruft, B., Fleming, I., Ko, S., Monga, S.P., Mueller, F., Apte, U., et al. (2020). Functional compensation precedes recovery of tissue mass following acute liver injury. Nat. Commun. *11*, 5785. https://doi.org/10.1038/s41467-020-19558-3.
66. Chen, F., Schönberger, K., and Tchorz, J.S. (2023). Distinct hepatocyte identities in liver homeostasis and regeneration. JHEP Rep. *5*, 100779. https://doi.org/10.1016/j.jhepr.2023.100779.
67. Ma, X., Huang, T., Chen, X., Li, Q., Liao, M., Fu, L., Huang, J., Yuan, K., Wang, Z., and Zeng, Y. (2025). Molecular mechanisms in liver repair and regeneration: from physiology to therapeutics. Signal Transduct. Target. Ther. *10*, 63. https://doi.org/10.1038/s41392-024-02104-8.
68. Solhi, R., Lotfinia, M., Gramignoli, R., Najimi, M., and Vosough, M. (2021). Metabolic hallmarks of liver regeneration. Trends Endocrinol. Metab. *32*, 731–745. https://doi.org/10.1016/j.tem.2021.06.002.
69. Uriarte, I., Santamaria, E., López-Pascual, A., Monte, M.J., Argemí, J., Latasa, M.U., Adán-Villaescusa, E., Irigaray, A., Herranz, J.M., Arechederra, M., et al. (2024). New insights into the regulation of bile acids synthesis during the early stages of liver regeneration: A human and experimental study. Biochim. Biophys. Acta BBA - Mol. Basis Dis. *1870*, 167166. https://doi.org/10.1016/j.bbadis.2024.167166.
70. Slabber, C.F., Bachofner, M., Speicher, T., Kuklin, A., Fearon, A.E., Padrissa-Altés, S., Bogorad, R., Horváth Rudigier, C., Wüst, D., Krautbauer, S., et al. (2023). The ubiquitin ligase Uhrf2 is a master regulator of cholesterol biosynthesis and is essential for liver regeneration. Sci. Signal. *16*, eade8029. https://doi.org/10.1126/scisignal.ade8029.
71. Živný, P., Živná, H., Palička, V., Žaloudková, L., Mocková, P., Cermanová, J., and Mičuda, S. (2018). Modulation of Rat Liver Regeneration after Partial Hepatectomy by Dietary Cholesterol. Acta Medica Hradec Kralove Czech Repub. *61*, 22–28. https://doi.org/10.14712/18059694.2018.19.
72. Behrens, A. (2002). Impaired postnatal hepatocyte proliferation and liver regeneration in mice lacking c-jun in the liver. EMBO J. *21*, 1782–1790. https://doi.org/10.1093/emboj/21.7.1782.
73. Jia, X., Lin, W., and Wang, W. (2023). Regulation of chromatin organization during animal regeneration. Cell Regen. *12*, 19. https://doi.org/10.1186/s13619-023-00162-x.
74. Cao, Y., Xia, Y., Balowski, J.J., Ou, J., Song, L., Safi, A., Curtis, T., Crawford, G.E., Poss, K.D., and Cao, J.

(2022). Identification of enhancer regulatory elements that direct epicardial gene expression during zebrafish heart regeneration. Development *149*, dev200133. https://doi.org/10.1242/dev.200133.
75. Hishida, T., Yamamoto, M., Hishida-Nozaki, Y., Shao, C., Huang, L., Wang, C., Shojima, K., Xue, Y., Hang, Y., Shokhirev, M., et al. (2022). In vivo partial cellular reprogramming enhances liver plasticity and regeneration. Cell Rep. *39*, 110730. https://doi.org/10.1016/j.celrep.2022.110730.
76. Hsu, J.C., Laz, T., Mohn, K.L., and Taub, R. (1991). Identification of LRF-1, a leucine-zipper protein that is rapidly and highly induced in regenerating liver. Proc. Natl. Acad. Sci. *88*, 3511–3515. https://doi.org/10.1073/pnas.88.9.3511.
77. Allan, A.L., Albanese, C., Pestell, R.G., and LaMarre, J. (2001). Activating Transcription Factor 3 Induces DNA Synthesis and Expression of Cyclin D1 in Hepatocytes. J. Biol. Chem. *276*, 27272–27280. https://doi.org/10.1074/jbc.M103196200.
78. Cui, A., Ding, D., and Li, Y. (2021). Regulation of Hepatic Metabolism and Cell Growth by the ATF/CREB Family of Transcription Factors. Diabetes *70*, 653–664. https://doi.org/10.2337/dbi20-0006.
79. Milland, J., and Schreiber, G. (1991). Transcriptional activity of the phosphoenolpyruvate carboxykinase gene decreases in regenerating rat liver. FEBS Lett. *279*, 184–186. https://doi.org/10.1016/0014-5793(91)80144-R.
80. Xu, Y., Li, Y., Jadhav, K., Pan, X., Zhu, Y., Hu, S., Chen, S., Chen, L., Tang, Y., Wang, H.H., et al. (2021). Hepatocyte ATF3 protects against atherosclerosis by regulating HDL and bile acid metabolism. Nat. Metab. *3*, 59–74. https://doi.org/10.1038/s42255-020-00331-1.
81. Beyer, T.A., Xu, W., Teupser, D., Auf Dem Keller, U., Bugnon, P., Hildt, E., Thiery, J., Kan, Y.W., and Werner, S. (2008). Impaired liver regeneration in Nrf2 knockout mice: role of ROS-mediated insulin/IGF-1 resistance. EMBO J. *27*, 212–223. https://doi.org/10.1038/sj.emboj.7601950.
82. Chan, B.K.Y., Elmasry, M., Forootan, S.S., Russomanno, G., Bunday, T.M., Zhang, F., Brillant, N., Starkey Lewis, P.J., Aird, R., Ricci, E., et al. (2021). Pharmacological Activation of Nrf2 Enhances Functional Liver Regeneration. Hepatology *74*, 973–986. https://doi.org/10.1002/hep.31859.
83. Wang, X., Kiyokawa, H., Dennewitz, M.B., and Costa, R.H. (2002). The Forkhead Box m1b transcription factor is essential for hepatocyte DNA replication and mitosis during mouse liver regeneration. Proc. Natl. Acad. Sci. *99*, 16881–16886. https://doi.org/10.1073/pnas.252570299.
84. Suzuki, N., and Ochi, H. (2020). Regeneration enhancers: A clue to reactivation of developmental genes. Dev. Growth Differ. *62*, 343–354. https://doi.org/10.1111/dgd.12654.
85. Harris, R.E. (2022). Regeneration enhancers: a field in development. Am. J. Physiol.-Cell Physiol. *323*, C1548–C1554. https://doi.org/10.1152/ajpcell.00403.2022.
86. Li, L., Cui, L., Lin, P., Liu, Z., Bao, S., Ma, X., Nan, H., Zhu, W., Cen, J., Mao, Y., et al. (2023). Kupffer-cell-derived IL-6 is repurposed for hepatocyte dedifferentiation via activating progenitor genes from injury-specific enhancers. Cell Stem Cell *30*, 283-299.e9. https://doi.org/10.1016/j.stem.2023.01.009.
87. Dobin, A., Davis, C.A., Schlesinger, F., Drenkow, J., Zaleski, C., Jha, S., Batut, P., Chaisson, M., and Gingeras, T.R. (2013). STAR: ultrafast universal RNA-seq aligner. Bioinformatics *29*, 15–21. https://doi.org/10.1093/bioinformatics/bts635.
88. Li, B., and Dewey, C.N. (2011). RSEM: accurate transcript quantification from RNA-Seq data with or without a reference genome. BMC Bioinformatics *12*, 323. https://doi.org/10.1186/1471-2105-12-323.
89. Yu, G., Wang, L.-G., Han, Y., and He, Q.-Y. (2012). clusterProfiler: an R Package for Comparing Biological Themes Among Gene Clusters. OMICS J. Integr. Biol. *16*, 284–287. https://doi.org/10.1089/omi.2011.0118.
90. Love, M.I., Huber, W., and Anders, S. (2014). Moderated estimation of fold change and dispersion for RNA-seq data with DESeq2. Genome Biol. *15*, 550. https://doi.org/10.1186/s13059-014-0550-8.
91. Bolger, A.M., Lohse, M., and Usadel, B. (2014). Trimmomatic: a flexible trimmer for Illumina sequence data. Bioinformatics *30*, 2114–2120. https://doi.org/10.1093/bioinformatics/btu170.
92. Langmead, B., and Salzberg, S.L. (2012). Fast gapped-read alignment with Bowtie 2. Nat. Methods *9*, 357–359. https://doi.org/10.1038/nmeth.1923.
93. Tarasov, A., Vilella, A.J., Cuppen, E., Nijman, I.J., and Prins, P. (2015). Sambamba: fast processing of NGS alignment formats. Bioinforma. Oxf. Engl. *31*, 2032–2034. https://doi.org/10.1093/bioinformatics/btv098.
94. Zhang, Y., Liu, T., Meyer, C.A., Eeckhoute, J., Johnson, D.S., Bernstein, B.E., Nusbaum, C., Myers, R.M., Brown, M., Li, W., et al. (2008). Model-based analysis of ChIP-Seq (MACS). Genome Biol. *9*, R137. https://doi.org/10.1186/gb-2008-9-9-r137.
95. Pohl, A., and Beato, M. (2014). bwtool: a tool for bigWig files. Bioinforma. Oxf. Engl. *30*, 1618–1619. https://doi.org/10.1093/bioinformatics/btu056.
96. Li, H., and Durbin, R. (2009). Fast and accurate short read alignment with Burrows–Wheeler transform. Bioinformatics *25*, 1754–1760. https://doi.org/10.1093/bioinformatics/btp324.
97. Durand, N.C., Shamim, M.S., Machol, I., Rao, S.S.P., Huntley, M.H., Lander, E.S., and Aiden, E.L. (2016).

Juicer Provides a One-Click System for Analyzing Loop-Resolution Hi-C Experiments. Cell Syst. *3*, 95–98. https://doi.org/10.1016/j.cels.2016.07.002.
98. Hao, Y., Stuart, T., Kowalski, M.H., Choudhary, S., Hoffman, P., Hartman, A., Srivastava, A., Molla, G., Madad, S., Fernandez-Granda, C., et al. (2024). Dictionary learning for integrative, multimodal and scalable single-cell analysis. Nat. Biotechnol. *42*, 293–304. https://doi.org/10.1038/s41587-023-01767-y.
99. Korsunsky, I., Millard, N., Fan, J., Slowikowski, K., Zhang, F., Wei, K., Baglaenko, Y., Brenner, M., Loh, P., and Raychaudhuri, S. (2019). Fast, sensitive and accurate integration of single-cell data with Harmony. Nat. Methods *16*, 1289–1296. https://doi.org/10.1038/s41592-019-0619-0.
100. Danecek, P., Bonfield, J.K., Liddle, J., Marshall, J., Ohan, V., Pollard, M.O., Whitwham, A., Keane, T., McCarthy, S.A., Davies, R.M., et al. (2021). Twelve years of SAMtools and BCFtools. GigaScience *10*, giab008. https://doi.org/10.1093/gigascience/giab008.
101. Shannon, P., Markiel, A., Ozier, O., Baliga, N.S., Wang, J.T., Ramage, D., Amin, N., Schwikowski, B., and Ideker, T. (2003). Cytoscape: A Software Environment for Integrated Models of Biomolecular Interaction Networks. Genome Res. *13*, 2498–2504. https://doi.org/10.1101/gr.1239303.
102. Higgins, M and Anderson, R.M (1931). Experimental pathology of liver: restoration of liver of white rat following partial surgical removal. Arch. Pathol. Lab. Med. *12*, 186–202.
103. Corces, M.R., Trevino, A.E., Hamilton, E.G., Greenside, P.G., Sinnott-Armstrong, N.A., Vesuna, S., Satpathy, A.T., Rubin, A.J., Montine, K.S., Wu, B., et al. (2017). An improved ATAC-seq protocol reduces background and enables interrogation of frozen tissues. Nat. Methods *14*, 959–962. https://doi.org/10.1038/nmeth.4396.
104. Buenrostro, J.D., Wu, B., Chang, H.Y., and Greenleaf, W.J. (2015). ATAC-seq: A Method for Assaying Chromatin Accessibility Genome-Wide. Curr. Protoc. Mol. Biol. *109*. https://doi.org/10.1002/0471142727.mb2129s109.
105. Fazio, E.N., Young, C.C., Toma, J., Levy, M., Berger, K.R., Johnson, C.L., Mehmood, R., Swan, P., Chu, A., Cregan, S.P., et al. (2017). Activating transcription factor 3 promotes loss of the acinar cell phenotype in response to cerulein-induced pancreatitis in mice. Mol. Biol. Cell *28*, 2347–2359. https://doi.org/10.1091/mbc.e17-04-0254.
106. Nguyen, H.C.B., Adlanmerini, M., Hauck, A.K., and Lazar, M.A. (2020). Dichotomous engagement of HDAC3 activity governs inflammatory responses. Nature *584*, 286–290. https://doi.org/10.1038/s41586-020-2576-2.
107. Seidman, J.S., Troutman, T.D., Sakai, M., Gola, A., Spann, N.J., Bennett, H., Bruni, C.M., Ouyang, Z., Li, R.Z., Sun, X., et al. (2020). Niche-Specific Reprogramming of Epigenetic Landscapes Drives Myeloid Cell Diversity in Nonalcoholic Steatohepatitis. Immunity *52*, 1057-1074.e7. https://doi.org/10.1016/j.immuni.2020.04.001.
108. Huang, M., Wang, X., Zhang, M., Liu, Y., and Chen, Y.-G. (2024). METTL3 restricts RIPK1-dependent cell death via the ATF3-cFLIP axis in the intestinal epithelium. Cell Regen. *13*, 14. https://doi.org/10.1186/s13619-024-00197-8.

STAR★METHODS

KEY RESOURCES TABLE

REAGENT OR RESOURCE	SOURCE	IDENTIFIER
Antibodies		
Anti-ATF3 antibody [EPR19488]	Abcam	ab207434
Critical commercial assays		
Nano-GLO® Dual-Luciferase Reporter Assay Kit	Promega	N1610
Optiprep Density Gradient Medium	Sigma-Aldrich	D1556
Deposited data		
RNA-seq liver regeneration post-PHx (6h, 24h, 48h)	10.1016/j.redox.2020.101841	GSE181476
ATAC-seq liver regeneration post-PHx (6h, 24h, 48h)	Present study	GSE266402
ChIP-seq H3K27ac in liver pre-PHx (0 h)	10.1038/s41467-023-37247-9	GSE188742
ChIP-seq H3K27ac in liver, post-PHx (40 hours)	10.1016/j.stem.2016.03.001	GSE76935
ChIP-seq Atf3 in Intestinal organoids	10.1186/s13619-024-00197-8	GSE262282

ChIP-seq Atf3 in bone marrow macrophages	10.1038/s41586-020-2576-2	GSE140581
ChIP-seq Atf3 in hepatic macrophages	10.1016/j.immuni.2020.04.001	GSE128336
ChIP-seq Atf3 in pancreatic tissue	10.1091/mbc.e17-04-0254	GSE60250
ChIP-seq Nrf2 in liver	10.1124/mol.118.112144	GSE109865
Hi-C liver	10.1186/s13059-021-02374-3	GSE155158
scRNA-seq liver regeneration post-PHx (0h, 24h, 48h)	10.1101/gr.267013.120	GSE151309
ATAC-seq liver development	10.1038/s41586-020-2093-3	GSE172627
Experimental models: Cell lines		
Immortalised hepatocytes	López-Luque et al., 2016	10.1002/hep.28134
Experimental models: Organisms/strains		
Mouse: C57BL/6J	The Jackson Laboratory	C57BL/6J
Oligonucleotides		
Primer: ATACseqPeak_39376 cloning primer forward: GTAGCTAGCGGAATGGGATGGGGAGACAG	This paper	
Primer: ATACseqPeak_39376 cloning primer reverse: ATGAAGCTTCTCAGCCCAAATTCAGATGG	This paper	
Primer: ATACseqPeak_76443 cloning primer forward: GTAGCTAGCGCTTGCCTGAACCCTTCTCC	This paper	
Primer: ATACseqPeak_76443 cloning primer reverse: ATGAAGCTTCCTAAGCCCGTAACAGGACC	This paper	
Primer: ATACseqPeak_69905 cloning primer forward: GTAGCTAGCCAGCTTTGGACTGTCTGCTC	This paper	
Primer: ATACseqPeak_69905 cloning primer reverse: ATGAAGCTTGTGTGTACCAGTTCGAAGTG	This paper	
Primer: ATACseqPeak_9588 cloning primer forward: GTAGCTAGCCAGGACGAGTACTTCACCAG	This paper	
Primer: ATACseqPeak_9588 cloning primer reverse: ATGAAGCTTCCATGAAGAAGGGCAAGTGC	This paper	
Primer: ATACseqPeak_70885 cloning primer forward: CTGCGGGCTAGCAGTAGAAG	This paper	
Primer: ATACseqPeak_70885 cloning primer reverse: ATGAAGCTTGACCTGACTCCTGGTCTGTC	This paper	
Primer: ATACseqPeak_57343 cloning primer forward: GTAGCTAGCTCCTCTGTGTTGAAGAAGGC	This paper	
Primer: ATACseqPeak_57343 cloning primer reverse: ATGAAGCTTCCAGGCTAGGATGTGATAGC	This paper	
Recombinant DNA		
Plasmid: pGL4.27[luc2P/minP/Hygro]	Promega	E8451
Plasmid: pNL1.1.TK[Nluc/TK] Vector	Promega	N1501
Plasmid: Atf3 (NM_007498) Mouse Tagged ORF Clone	Origene	MR201634
Plasmid: Nfe2l2 (NM_010902) Mouse Tagged ORF Clone	Origene	MR226717
Software and algorithms		
grape-nf	in-house	https://github.com/guigolab/grape-nf
STAR 2.4.0	Dobin et al.[87]	
RSEM	Li et al.[88]	
clusterProfiler	Yu et al.[89]	

heatmap3		https://github.com/slzhao/heatmap3
DESeq2	Love et al.[90]	
Trimmomatic	Bolger et al.[91]	
Bowtie2	Langmead et al.[92]	
Sambamba	Tarasov et al.[93]	
MACS2	Zhang et al.[94]	
bwtool	Pohl et al.[95]	
BWA	Li et al.[96]	
Juicer	Durand et al.[97]	
Activity-by-contact algorithm	Fulco et al.[43]	
Seurat v5.0.3	Hao et al.[98]	
Harmony v1.2.0	Korsunsky et al.[99]	
HINT-ATAC	Li et al.[47]	
SAMtools v.1.16	Danecek et al.[100]	
MEME Suite 5.4.1	McLeay et al.[49]	
Cytoscape Software v3.10.2	Shannon et al.[101]	

EXPERIMENTAL MODEL AND STUDY PARTICIPANT DETAILS

Animal procedures

C57BL/6J wild-type (WT) mice were obtained from Jackson Laboratories and housed at the IDIBELL (Barcelona, Spain). All experiments complied with the EU Directive 2010/63/UE for animal experiments and the institution's guidelines (Ethics Committee for Animal Experimentation of the IDIBELL) and were approved by the General Direction of Environment and Biodiversity, Government of Catalonia (experiments #4589). Animals were 8 to 16-week-old male and female mice, housed under a 12h light/dark cycle with free access to food and water. Partial hepatectomies (PHx) were performed by removing two-thirds of the adult mouse liver, as described by Higgins and Anderson (1931)[102]. The mice that had undergone surgery without liver resection (SHAM-operated) were used as controls. The mice were euthanised 6, 24 and 48 h after surgery, and their liver lobes were immediately frozen in liquid nitrogen and stored at -80 ºC. The same livers used to extract RNA were used to prepare the ATAC-seq libraries. The number of animals used in the study was minimised for ethical reasons. Thus, 2 hepatectomised and 1-2 SHAM-operated animals were used for each time point after surgery.

METHOD DETAILS

ATAC sequencing

ATAC-seq libraries were prepared following the Omni-ATAC protocol[103] with minor modifications. Briefly, 10-20 mg of frozen liver were placed in a pre-chilled Tenbroeck tissue grinder containing 1 ml of the Omni-ATAC homogenisation buffer and let thaw for 5 min. The tissue was homogenised on ice using a glass Tenbroeck grinder and then filtered through a 70µm Flowmi strainer. Nuclei were pelleted for 5 min at 350 g and isolated using iodixanol density gradient centrifugation (OptiPrep™). The nucleus band was transferred to a fresh tube and diluted in ATAC-seq resuspension buffer (ATAC-RSB)-Tween. Nuclei were counted using trypan blue staining and 50,000 nuclei were aliquoted per sample and resuspended in 50 µl of the transposition mixture (25 µl of 2× TD buffer (Illumina, San Francisco, CA), 2.5 µl of transposase (Illumina, San Francisco, CA), 16.5 µl of PBS, 0.5 µl of 1% digitonin, 0.5 µl of 10% Tween-20 and 5 µl of H_2O). Transposition reactions were incubated at 37°C for 30 min in a thermomixer at 1,000 RPM. Reactions were cleaned up with the Qiagen MinElute PCR Purification Kit (Qiagen,

Frederick, MD) and eluted into 10 µl of the elution buffer. Purified DNA was used to prepare the ATAC-seq libraries, as described previously[104]. The quality of the tagmented libraries was visualised with the Agilent Bioanalyzer High Sensitivity DNA Assay (Agilent Technologies, Savage, DE) and sequenced on the HiSeq2500 platform at the Centre for Genomic Regulation (CRG) sequencing facility in Barcelona, Spain. A minimum of 49 million paired-end 50-bp-long reads were obtained per sample.

Immunohistochemistry

Paraffin-embedded tissues were cut into 4-µm-thick sections. Immunohistochemical (IHC) analyses were performed using standard procedures[33]. Sections were incubated overnight at 4ºC with a recombinant anti-ATF3 antibody (1:100; ab207434, Abcam). Binding was developed with the VECTASTAIN ABC HRP Kit (rabbit IgG; PK-4001, Vector Laboratories). Tissues were visualised and imaged under a microscope.

Reporter assays

Candidate RREs were amplified from mouse genomic DNA using the primers listed in Key Resources Table and cloned into the pGL4.27[luc2P/minP/Hygro] plasmid (Promega). NheI and HindIII restriction sites were added to the 5' ends of the forward and reverse primers, respectively, to facilitate directional cloning. The amplified PCR products of RREs and the pGL4.27 plasmid were double digested with NheI-HF and HindIII-HF restriction enzymes (New England Biolabs), followed by dephosphorylation of the 5′ ends of the digested plasmid using calf intestinal alkaline phosphatase (0.01u CIAP/pmol of DNA ends). After digestion, the PCR-amplified inserts and the linearized vector were purified and then ligated at a 1:3 vector-to-insert ratio using T4 DNA ligase (New England Biolabs), following the manufacturer's instructions. The ligation products were transformed into DH5α competent cells (Invitrogen), and successfully transformed Ampicillin-resistant colonies were confirmed by sequencing.

In-house immortalised hepatocyte cell line[46] was grown in Dulbecco's Modified Eagle Medium (DMEM) supplemented with 10% fetal bovine serum (FBS) (Sera Laboratories International Ltd, West Sussex, UK), Penicillin (100 U/mL), Streptomycin (100 µg/mL), Amphotericin (2.5 µg/mL) and L-glutamine (2 mM), and maintained in a humidified atmosphere of 37ºC, 5% CO2. Cells seeded in 12-well plates at a density of 3 x 10^4 cells per well were transiently cotransfected using polyethylenimine (3µl PEI /µg DNA) with 995 ng/mL of DNA reporter of interest per well (recombinant pGL4.24 [luc2P/minP/Hygro]) and 5 ng/mL of NanoLuc® plasmid (N1501, Promega, Madison, WI, USA) in complete media. 16 hours post-transfection, the medium was replaced, and cells were serum-starved for 24 hours. After, cells were either switched to complete medium with 10% FBS or continued serum starvation for an additional 3 hours. Cells were then harvested, lysed, and luciferase activities were measured using the Nano-GLO® Dual-Luciferase Reporter Assay Kit (Promega, Madison, WI, USA) following the manufacturer's instructions. Firefly luciferase signal was divided by the NanoLuc® signal to determine relative luciferase activity. The activity for each luciferase construct was normalised for the activity of the minimal promoter (minP). The constructs were measured in two independent experiments in a total of six biological replicates. Statistical significance was assessed using two-way ANOVA followed by Tukey's Honest Significant Difference (Tukey's HSD) test to compare each construct against minP, and to compare between starvation and FBS-treatment. Normality and homogeneity of variance were assumed. All tests were two-sided. Differences were considered statistically significant when p-value was < 0.05.

Validation of transcriptional activators was performed following the same experimental conditions with minor modifications. Cells were transiently cotransfected with 800 ng/mL of luciferase reporter, 195 ng of mouse ATF3 plasmid (MR201634, Origene) or mouse Nfe2l2 plasmid (MR226717, Origene), and 5 ng/mL of NanoLuc® plasmid (N1501, Promega, Madison, WI, USA) in complete media. 16 hours post-transfection, the medium was replaced and 24 hours later cells were harvested, lysed, and luciferase activities were measured using the Nano-GLO® Dual-Luciferase Reporter Assay Kit (Promega, Madison, WI, USA) following the manufacturer's instructions. The constructs were measured in two independent experiments in a total of six biological replicates. Statistical significance was assessed

using one-way ANOVA followed by Tukey's HSD. Normality and homogeneity of variance were assumed. All tests were two-sided. Differences were considered statistically significant when p-value was < 0.05.

RNA sequencing data analysis

RNA-seq raw data for WT mice at 6, 24 and 48 h after PHx were downloaded from GEO accession number GSE181476[33] and processed using the in-house pipeline grape-nf (available at https://github.com/guigolab/grape-nf). RNA-seq reads were aligned to the *Mus musculus* genome assembly GRCm39 using the STAR 2.4.0 software[87] allowing up to 4 mismatches per paired alignment. We used the mouse genome GENCODE annotation vM27. Only alignments for reads mapping to ten or fewer loci were reported. Genes and transcripts per kilobase million (TPMs) were quantified using RSEM[88]. Tracks were visualised with the UCSC Genome Browser. From the RNA-seq data, the expression values for 55,360 annotated genes were estimated and the gene expression matrix was quantile normalised. Only genes with > 1 TPM in at least one condition were considered for subsequent analyses (11,512 genes). Correspondence analysis and association plots[34] were used to cluster and identify the genes with differential expression profiles during early liver regeneration. Briefly, we used the APL R package, considering 5 dimensions and clusters were defined setting a threshold of Sα score > -0.05. Normalised expression values as z-scores were used to visualise differential expressed genes using line plots or hierarchical clustering from heatmap3 R package. Gene Ontology enrichment analysis of the clusters of interest was performed using the Bioconductor package clusterProfiler[89], one-sided Fisher's exact test was applied and p-adjust < 0.05 was used as cut-off, no assumptions about the underlying distribution of gene expression data was done. Differential gene expression analysis of the TFs from Figure 4 was performed using DESeq2[90] using Wald test, assuming negative binomial distribution.

ATAC sequencing data analysis

Reads were trimmed *in silico* to remove adapter sequences and low-quality reads using Trimmomatic[91] while FastQC was used to check their quality. The reads were aligned to the mouse (mm39) reference genome using Bowtie2[92]. Duplicate reads were removed using Picard (http://broadinstitute.github.io/picard/), and the mitochondrial reads and the reads mapping to the ENCODE blacklisted regions were filtered out using BEDTools2. Sambamba[93] was used to eliminate fragments larger than 400 bp. Peak calling was performed using a MACS2[94] run in the pair-end mode, requesting an p-adjust < 0.01. Read depth-normalised values (pileup) were generated by MACS2 and stored in bigWig files. All the ATAC-seq samples were checked for the library complexity and PCR bottlenecking following ENCODE standards https://www.encodeproject.org/data-standards/terms/#library (Table S6). Each replicate, time point and condition in the ATAC-seq data was processed independently. However, we combined the data, processing together the read alignments from all 6 experiments in the regenerated livers. The peaks that had at least 50% overlap in each replicate in at least one condition were retained, while the peaks with an overlap smaller than 25 nucleotides were discarded. The maximum heights of all the peaks were then quantified for each sample using bwtool[95]. These values were quantile-normalised among the samples and the peak heights were averaged between replicates (Table S7). Differentially accessible regions were identified using an absolute fold-change larger than 1.7 as the cut-off between regeneration and control at each time point. These regions were classified into *de novo* (open regions detected exclusively in REG), increasing (both in CTRL and REG, and at least 1.7-fold higher in REG) or decreasing peaks (1.7-fold lower in REG). Finally, the peaks were classified into promoters (+-500 bp around the TSS), proximal enhancers (+-500 bp away from promoters) or distal enhancers (> 1 kb from the TSS), considering all possible protein-coding and non-coding isoforms from the GENCODE mouse annotation vM27.

ChIP sequencing data analysis

ChIP-seq raw read data corresponding to H3K27ac histone modification pre-PHx[39] and post-PHx[40] as well as NRF2 binding in intact liver[54] and ATF3 binding in different tissues[105–108] were obtained from NCBI GEO. Reads were aligned to the *Mus musculus* genome assembly GRCm39 with BWA[96]. Peak calling was performed using MACS2[94], applying a cut-off of 0.05 for the FDR. Fold changes in relation to input control data were calculated and converted into the BigWig format. All the ChIP-seq samples were checked for the library complexity and PCR bottlenecking following ENCODE standards https://www.encodeproject.org/data-standards/terms/#library (Table S6). The presence of H3K27ac around RREs was analysed by extending the ATAC-seq peaks to 500 bp to incorporate the flanking nucleosomes and using BEDTools2 intersectBed with default conditions. The overlap between ATAC-seq peaks and NRF2 and ATF3 ChIP-seq peaks was analysed using BEDTools intersectBed with default conditions. The statistical significance of this overlap between the ATF3 peaks and the *de novo* and increasing peaks, and between the NRF2 peaks and the increasing peaks was calculated using BEDTools2 Fisher's exact test.

Hi-C data analysis

Raw read sequences for *in situ* and promoter-capture Hi-C from intact livers[44] were downloaded from NCBI GEO under the accession number GSE155161. The Juicer pipeline[97] was used to process these data. In brief, paired-end reads were mapped to the *Mus musculus* genome assembly GRCm39 with BWA[96], keeping the most 5' alignment block. The custom-made Juicer script "chimeric_blacklist.awk" was used to select the proper pair alignments. These alignments in turn were sorted and duplicates were removed. Hi-C matrices were generated with the Juicer Pre command, using standard resolutions of up to 5 kb and the SCALE normalisation method. To calculate the contact probability of the promoter and enhancer regions, these regions were projected onto particular 5-kb genomic intervals and before calculating the probability as a fraction of the normalised read counts supporting the interaction of the promoter and enhancer intervals (n-th diagonal) divided by the normalised read counts supporting the interaction of the promoter with itself (zero-diagonal). The generated Hi-C contact matrices were also used to calculate the background contact probabilities by averaging contact probabilities genome-wide across contacting regions at the same distance and using these average values to impute contact probabilities to the regions that are absent in the Hi-C matrices due to their low mappability.

Enhancer-gene pair association

Proximal peaks were classified as proximal enhancers and associated with the nearby promoters directly. For distal peaks, the activity-by-contact (ABC) algorithm[43] was implemented. The activity of the corresponding regions was calculated as a geometric mean of the ATAC-seq and H3K27ac signals. The maximum pileup signal across all the regeneration samples combined (see above) was used as a source of the ATAC-seq data. The maximum fold-change from the regenerated livers (GSE76935)[40] was used as a source of H3K27ac data. H3K27ac was determined in nucleosomes adjusted to the open chromatin regions, extending these regions by 250 bp in both directions. All enhancers lying closer than 2 Mb up- or downstream of the corresponding promoter were considered candidate regulatory elements. The maximum value from the *in situ* Hi-C, promoter-capture Hi-C or the same distance background control was used to calculate the contact probabilities of the promoter and enhancer regions. The activity of the promoter was included in the prediction model, assuming the contact probability of the promoter with itself to be equal to one. ABC scores were calculated for the promoter and each candidate enhancer by multiplying the activity value with the contact probability. Finally, the ABC scores were normalised for each enhancer by the sum of the ABC scores for all the enhancers and promoter. For each enhancer, the interaction with the highest ABC score was selected, filtering for expressed genes only (> 1 TPM in at least one condition) (Tables S2 and S3). Gene Ontology Biological Process enrichment for the annotated genes was performed using the Bioconductor package clusterProfiler[89], one-sided Fisher's exact test was applied with a p-adjust < 0.05 as a cut-off, no assumptions about the underlying distribution of gene expression data was done. Pearson's correlation

coefficient was determined between the enhancer profile and the gene expression profile. Statistical differences were calculated using one-way analysis of variance (ANOVA) with Tukey's HSD for multiple comparisons (p-value < 0.05). To identify gene expression differences between the *de novo*, increasing and decreasing RRE-associated candidate target genes, two-way ANOVA with Tukey's HSD test for multiple comparisons was performed for each type of element (promoter, proximal and distal) (p-value < 0.05).

Single-cell RNA sequencing analysis

The single-cell RNA-seq dataset generated from mouse livers collected at 0, 24 and 48 h post-PHx was retrieved from GSE151309[31]. The standard 10X Genomics Cell Ranger output was downloaded and imported using the Read10X function in Seurat v5.0.3[98]. The genes detected in 10 or fewer cells were filtered out. Cells with unique gene counts exceeding 500 for PHx0, 300 for PHx24, and 200 for PHx48 were retained, while cells with total gene counts above 4,000 or a mitochondrial gene percentage greater than 30% were filtered out. Seurat objects were then normalised and scaled to remove unwanted sources of variation, enhancing comparability among the samples. The top 2,000 variable genes were identified using the FindVariableFeatures function in Seurat for subsequent principal component analysis (PCA). To address potential batch effects, the RunHarmony function of Harmony v1.2.0[99] was applied to integrate the merged Seurat object. The clustering of cells was performed using the FindNeighbors and FindClusters functions in Seurat with a resolution parameter set to 0.4. Dimensionality reduction was achieved through Uniform Manifold Approximation and Projection (UMAP). Cell clusters were annotated based on the expression of marker genes in accordance with Chembazhi et al. (2021)[31]. Visualisation plots were generated using scCustomize v2.1.2 to facilitate interpretation and analysis.

Transcription factor motif enrichment analysis

TF differential binding analysis was performed with HINT-ATAC[47], a computational footprinting tool tailored for ATAC-seq data. As input, BAMs of biological replicate samples were merged with SAMtools v.1.16[100] and differentially accessible peaks were used as input regions for each time point. The resulting footprints were searched for motif enrichment using the HOCOMOCO v11 database. The analysis focused exclusively on the TFs expressed in the RNA-seq data (> 1 TPM). Only the TF motifs with a HINT-ATAC absolute fold change activity value greater than 1.5 and an associated p-value < 0.05 were considered significant (visualised by volcano plots). TF footprints were also visualised as lineplots, showing the mean of the ATAC-seq signal (adjusted for Tn5 cutting-bias) in the 200 bp window centred at each occupied motif.

For TF motif analysis, the Analysis of Motif Enrichment (AME) tool from the MEME suite v5.4.1[49] was used, using the HOCOMOCO v11 database and default parameters. To check for differential TF binding between the promoter and enhancer regulatory elements, the peaks located within 500 bp upstream or downstream of the transcriptional start site were considered promoter peaks and the rest were considered putative enhancer peaks. Only the TFs that were significantly enriched (Mann–Whitney U test, p-adjust < 0.05) and expressed in the RNA-seq data (> 1 TPM) were considered a hit, with the redundant hits removed. Only the top 10 TF motifs for each time point and peak class were represented in the heatmaps from Figure 4c.

Gene coexpression regulatory network

To construct the early regeneration gene coexpression regulatory network (GRN), we computed the correlation of expression across all samples between target genes linked to RREs (RRE-linked targets) and potential regulatory TFs, based on the presence of their motifs within these RREs. The GRN was generated using the expression values of 1,805 RRE-linked targets and 37 TFs. Only TF-target gene pairs containing the TF motif present in the RRE and those with absolute values of Pearson's correlation coefficient equal to or higher than 0.8 were considered as reliable. The resulting GRN included 1,829 nodes, of which 37 were source nodes (selected TFs), interconnected by 3,794 edges representing *de novo*, increasing and decreasing regulatory interactions. Network visualisation was performed using

Cytoscape Software v3.10.2[101]. Nodes were displayed according to Edge-weighted Spring-Embedded Layout analysis of TF-target correlation of expression (Pearson's correlation coefficient between TF and target expression). Node size was adjusted to denote TFs and coloured by normalised expression values calculated as z-scores for each time point. Edges were coloured depending on TF-target correlation of expression (negative or positive) or based on RREs classification at each time point. Edge transparency was adjusted depending on RRE classification at each time point for visualisation purposes (Non-differentially accessible peaks were made more transparent).

Developmental analysis

To determine if the regeneration enhancers were repurposed from development, ATAC-seq data from mouse livers at different embryonic stages were obtained from the ENCODE development series ENCSR326DKM[58]. The ATAC-seq postnatal dataset was obtained from the reference epigenome ENCSR687SNT[58]. Peak coordinates were converted from mm10 to mm39 using the liftOver tool from the UCSC Genome Browser. *De novo* peaks overlapping open regions in the foetal or postnatal day 0 livers were considered to be reused. This overlap was calculated using BEDTools2 intersectBed.

QUANTIFICATION AND STATISTICAL ANALYSIS

The quantitative and statistical analyses are described in the relevant sections of the method details or in the figure legends.

SUPPLEMENTAL INFORMATION

Document S1: Figures S1-S7, Table S6
Table S1: Clusters of coexpressed genes identified by correspondence analysis and association plots, related to Figure 1.
Table S2: Prediction by the activity-by-contact (ABC) algorithm correlating each ATAC-seq peak with its corresponding target gene, related to STAR Methods.
Table S3: RREs and associated target genes, related to Figure 3.
Table S4: ATF3-bound RREs and associated target genes, related to Figure 6.
Table S5: NRF2-bound RREs and associated target genes, related to Figure 6.
Table S7: Quantification of ATAC-seq peak heights (average maximum height between replicates), related to STAR Methods.

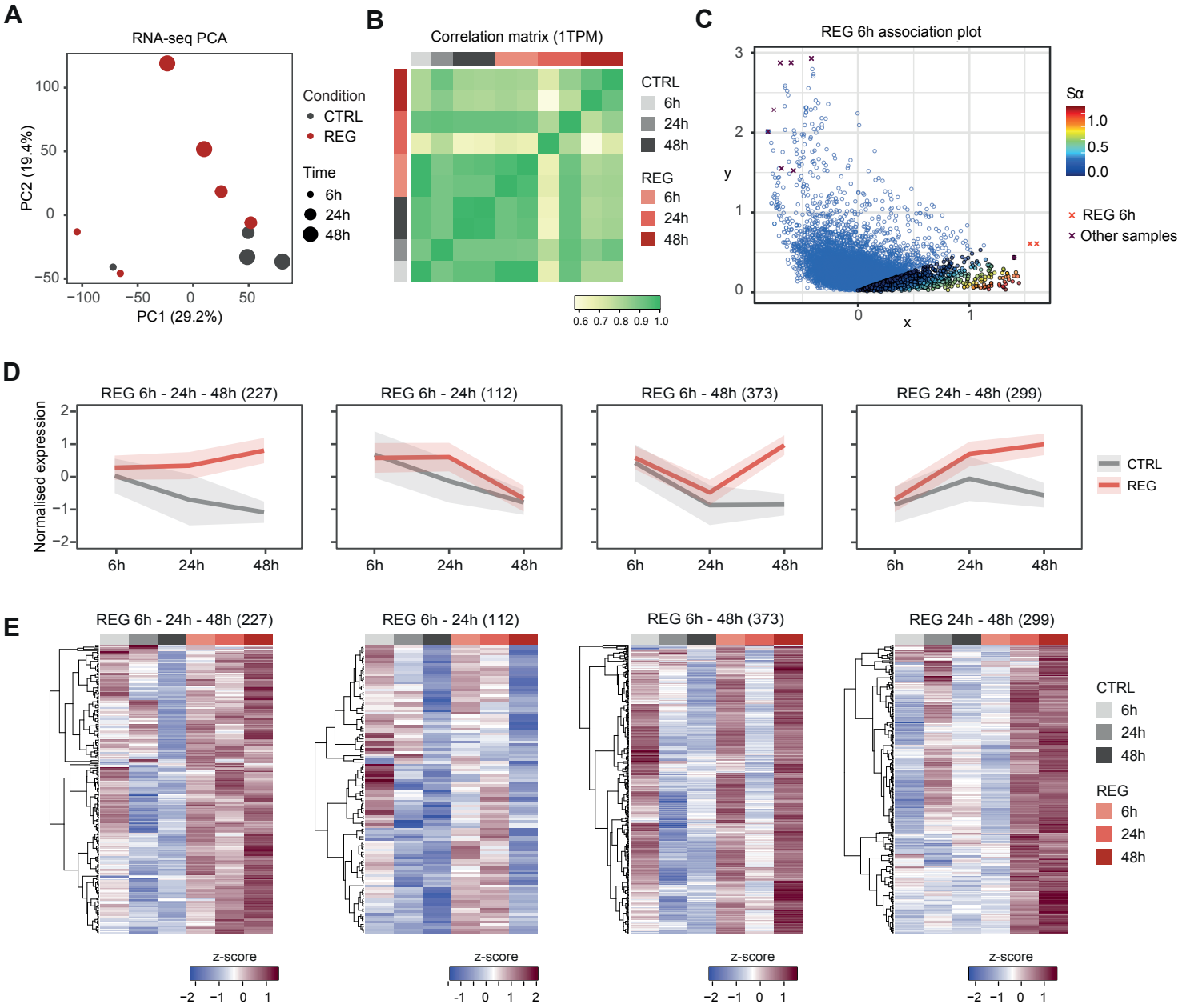

Figure S1. Correspondence analysis and association plots to visualise cluster-specific genes, related to Figure 1.
(A) Principal Component Analysis (PCA) on the normalised TPM values of expressed genes (>1TPM). Two biological replicates were includ-ed for each time point after hepatectomy, as well as for the 48 h time point following SHAM surgery, with single samples for the CTRL at 6 and 24 h. **(B)** Pearson's correlation coefficient matrix of RNA-seq samples (correlation between replicates > 0.8). **(C)** Association plot generated for the 6 h post-PHx cluster. Each circle represents one gene from the input data. Genes with a positive Sα score are highlighted in colour according to the key colour scale. The higher the Sα score, the higher the cluster-specificity of a gene. **(D)** Standardised gene expression profile of specific clusters of coexpressed genes: regeneration (REG 6 - 24 - 48 h), 6 - 24 h post-PHx, 6 - 48 h post-PHx, and 24 - 48 h post-PHx. Gene expression values are normalised to z-score values. The mean expression profile (line) +/- the standard deviation (shadow) is presented for each cluster and the number of genes belonging to each cluster is depicted above the plots. **(E)** Heatmaps of RNA-seq data showing the expression signals of the four clusters of coexpressed genes: regenera-tion (REG 6 - 24 - 48 h), 6 - 24 h post-PHx, 6 - 48 h post-PHx, and 24 - 48 h post-PHx. Gene expression values are normalised to z-score values. Each column represents one condition, calculated as the average value among the replicates and the number of genes belonging to each cluster is depicted above the plots, gene order is established by hierarchical clustering using heatmap3 R package.

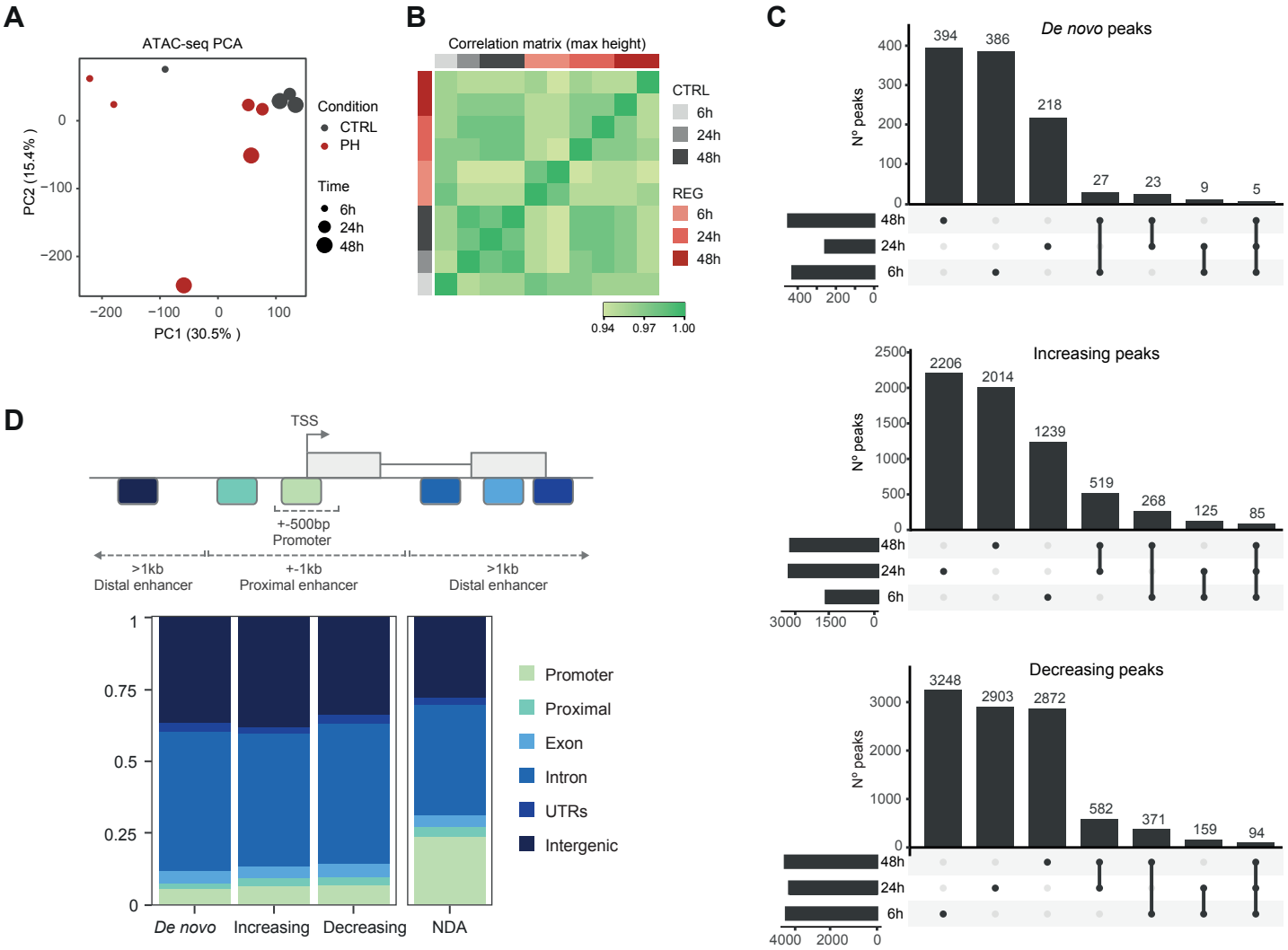

Figure S2. Characterisation of differentially accessible peaks over time, related to Figure 2.
(A) Principal Component Analysis (PCA) on the normalised peak height of ATAC-seq data, using peaks present in at least one condition. The same livers were used for both RNA and ATAC-seq experiments: two biological replicates for each time point after hepatectomy and for the 48 h time point following SHAM surgery, with single samples for the CTRL at 6 and 24 h. **(B)** Pearson's correlation coefficient matrix of ATAC-seq samples (correlation between replicates > 0.94). **(C)** Intersection of differentially accessible peaks over time. **(D)** Genomic distribution of peaks in promoters, proximal enhancers, exons, introns, UTRs and intergenic regions for each class of peaks: *de novo*, increasing, decreasing or non-differentially accessible (NDA).

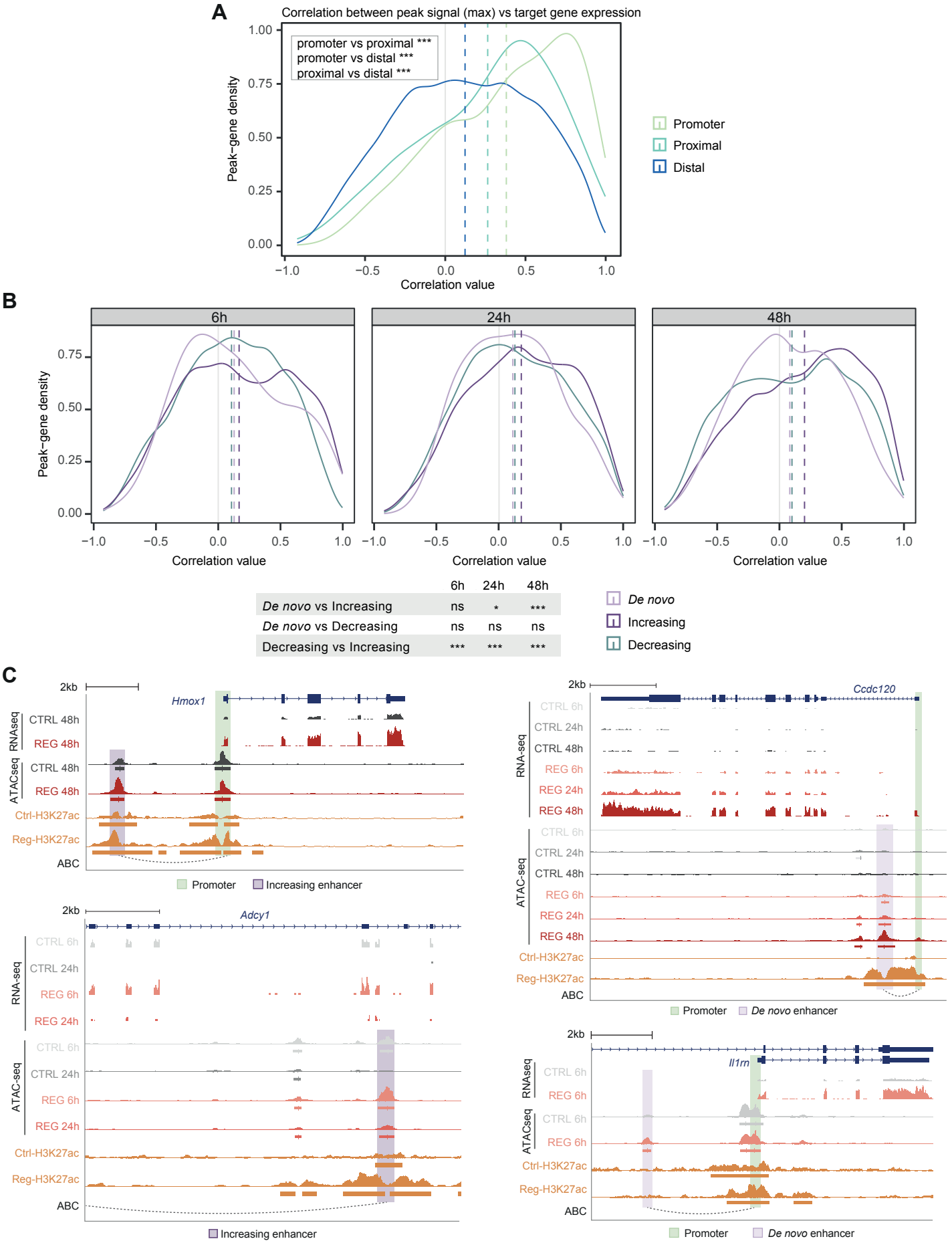

Figure S3. Correlation between RRE accessibility and target gene expression, related to Figure 3.
(A) Density plots showing the Pearson's correlation coefficient values between the RRE maximum peak signal and their target gene expression, separated by promoters, proximal enhancers and distal enhancers. Statistical differences were assessed using a one-way ANOVA, followed by Tukey's HSD test for multiple comparisons. Ns = non-significant, *p-adjust < 0.05, **p-adjust < 0.01, ***p-adjust < 0.001. **(B)** Density plots showing the Pearson's correlation coefficient values between the RRE peak signal and their target gene expression at each time point (6, 24, or 48 hours post-surgery), separated by *de novo*, increasing and decreasing class. Groups were compared using one-way ANOVA followed by Tukey's HSD test for multiple comparisons. Ns = non-significant, *p-adjust < 0.05, **p-adjust < 0.01, ***p-adjust < 0.001. **(C)** Genome browser screen-shot depicting the genomic loci of *Hmox1*, *Adcy1*, *Ccdc120* and *Il1rn* genes. *Hmox1* and *Adcy1* are predicted by the Activity-By-Contact (ABC) algorithm to be targeted by increasing enhancers, while *Ccdc120* and *Il1rn* by *de novo* enhancers.

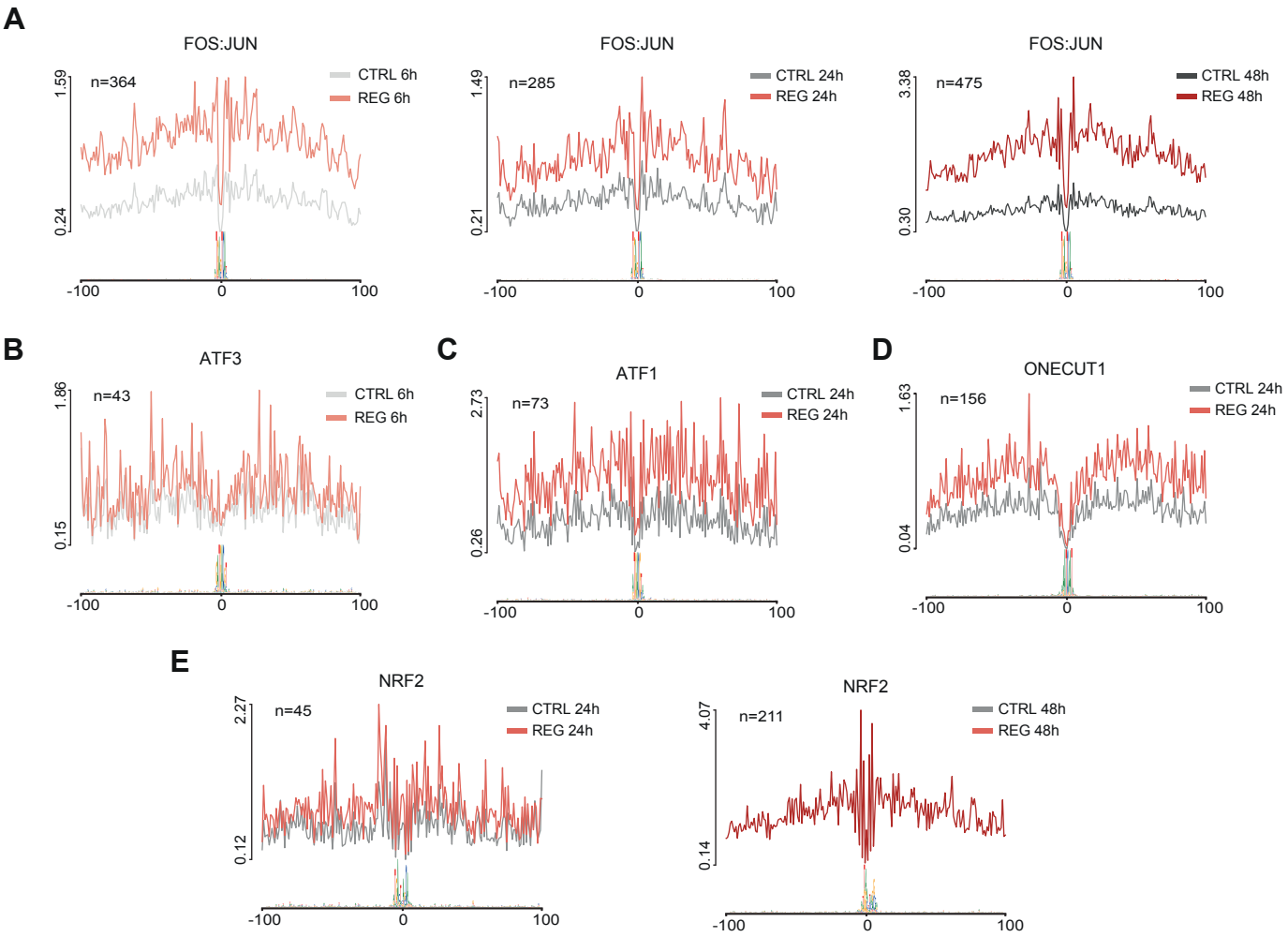

F

STAT3 motif enrichment in *de novo* and increasing RREs

TF	Motif	6h		24h		48h	
		adj p-value	E-value	adj p-value	E-value	adj p-value	E-value
STAT3		4.32e-4	1.55e-1	NA	NA	2.11e-7	7.56e-5

Figure S4. Footprints of TFs enriched in regeneration, related to Figure 4.
(A-E) ATAC-seq profiles showing various TF footprints at 6, 24 or 48 h after SHAM surgery (CTRL) or PHx (REG) generated with HINT-ATAC[47]. **(A)** FOS:JUN footprint at 6, 24 and 48 h; **(B)** ATF3 footprint at 6 h; **(C)** ATF1 footprint at 24 h; **(D)** ONECUT1 footprint at 24 h; **(E)** NRF2 footprint at 24 and 48 h. **(F)** STAT3 motif enrichment (Mann–Whitney U test, p-adjust < 0.05) in *de novo* and increasing RREs at 6, 24 and 48 h after PHx. Analysis of Motif Enrichment (AME) tool from the MEME suite v5.4.1[49] was used for motif enrichment analysis, using the HOCOMOCO v11 database and default parameters.

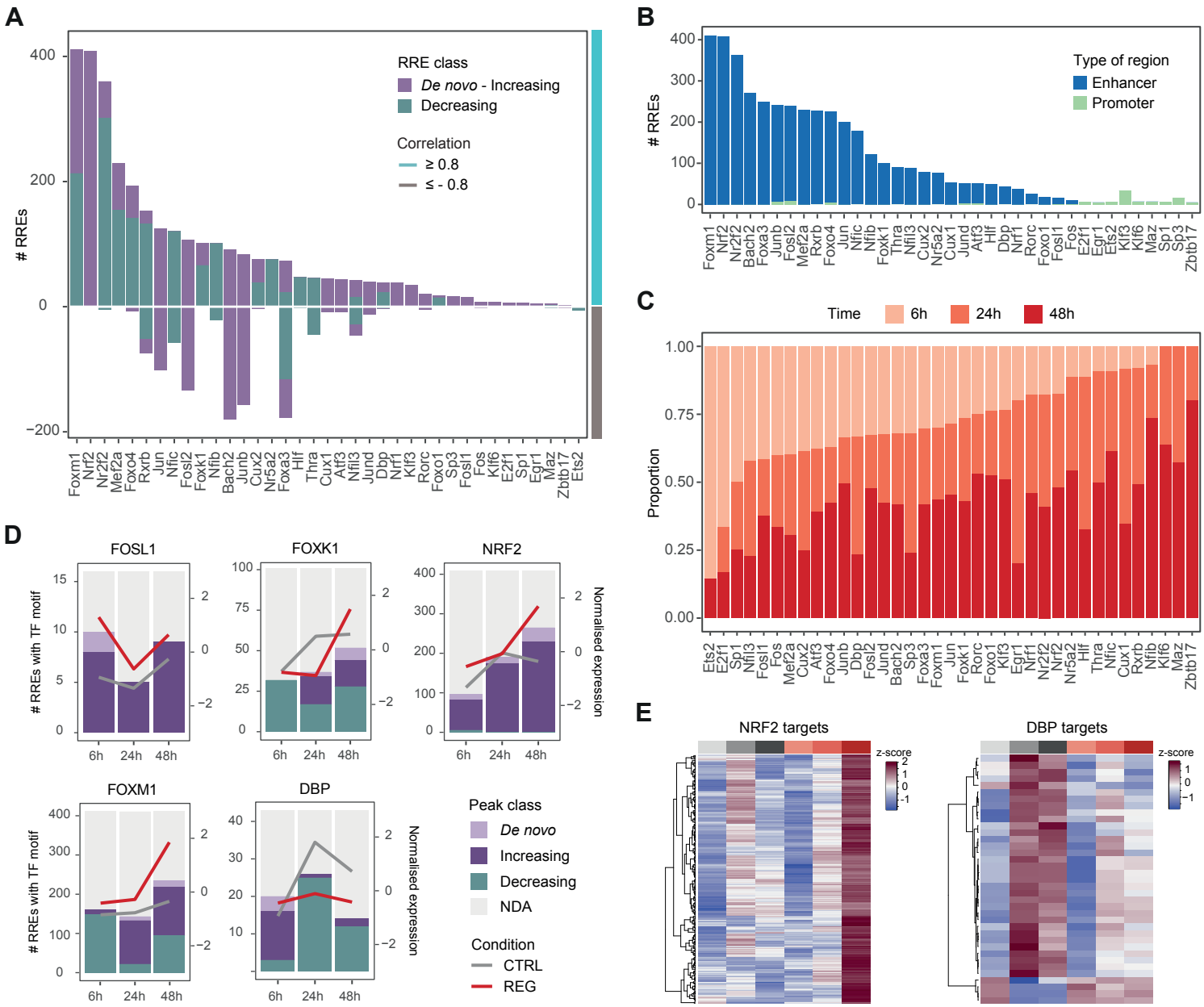
A
RREs
RRE class
De novo - Increasing
Decreasing
Correlation
≥ 0.8
≤ - 0.8
Foxm1 Nrf2 Nr2f2 Mef2a Foxo4 Rxrb Jun Nfic Fosl2 Foxk1 Nfib Bach2 Junb Cux2 Nr5a2 Foxa3 Hlf Thra Cux1 Atf3 Nfil3 Jund Dbp Nrf1 Klf3 Rorc Foxo1 Sp3 Fosl1 Fos Klf6 E2f1 Sp1 Egr1 Maz Zbtb17 Ets2
B
RREs
Type of region
Enhancer
Promoter
Foxm1 Nrf2 Nr2f2 Bach2 Foxa3 Junb Fosl2 Mef2a Rxrb Foxo4 Jun Nfic Nfib Foxk1 Thra Nfil3 Cux2 Nr5a2 Cux1 Jund Atf3 Hlf Dbp Nrf1 Rorc Foxo1 Fosl1 Fos E2f1 Egr1 Ets2 Klf3 Klf6 Maz Sp1 Sp3 Zbtb17
C
Time
6h
24h
48h
Proportion
Ets2 E2f1 Sp1 Nfil3 Fosl1 Fos Mef2a Cux2 Atf3 Foxo4 Junb Dbp Fosl2 Jund Bach2 Sp3 Foxa3 Foxm1 Jun Foxk1 Rorc Foxo1 Klf3 Egr1 Nrf1 Nr2f2 Nrf2 Nr5a2 Hlf Thra Nfic Cux1 Rxrb Nfib Klf6 Maz Zbtb17
D
FOSL1
FOXK1
NRF2
FOXM1
DBP
RREs with TF motif
Normalised expression
6h 24h 48h
Peak class
De novo
Increasing
Decreasing
NDA
Condition
CTRL
REG
E
NRF2 targets
DBP targets
z-score

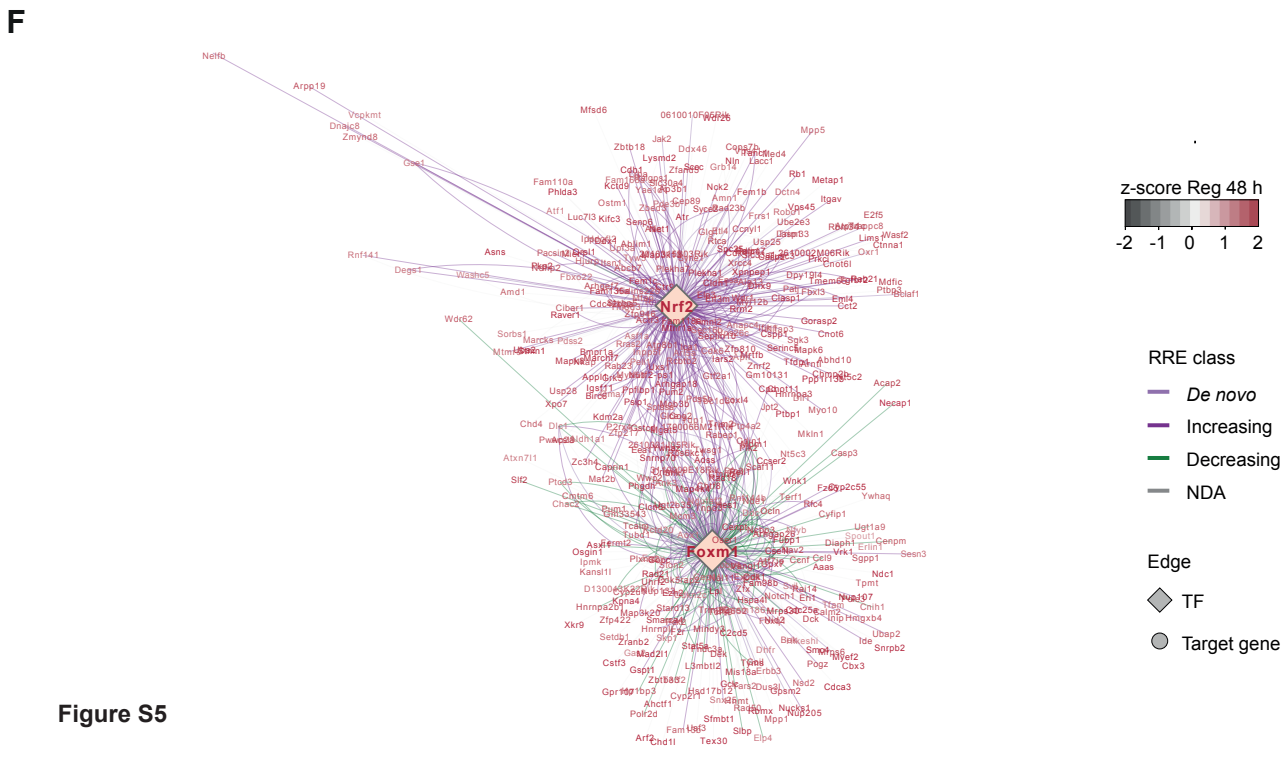
F
Nrf2
Foxm1
z-score Reg 48 h
-2 -1 0 1 2
RRE class
De novo
Increasing
Decreasing
NDA
Edge
TF
Target gene

Figure S5

Figure S5. Gene coexpression regulatory network analysis and NRF2/FOXM1 subnetwork, related to Figure 5. (A) Barplot showing number of RREs with the predicted binding site for each TF, colour-coded by RRE class (*de novo* or increasing in purple, decreasing in green) and arranged on the y-axis based on correlation values (positive correlation above 0 or negative correlation below 0). **(B)** Number of RREs with each TF motif, colour-coded by type of region (enhancer or promoter). **(C)** Proportion of RREs with each TF motif at each time point. **(D)** Barplots and lineplots showing number and classification of RREs with FOSL1, FOXK1, NRF2, FOXM1 or DBP binding sites at each time point (left axis) and TF normalised expression values (z-scores) across all samples (regeneration in red and control in grey) (right axis). **(E)** Expression signals of predicted target genes associated with RREs containing the NRF2 or DBP motifs. Genes are sorted using a hierarchical clustering function from heatmap3 R package. Each column of the heatmap represents one condition, calculated as the average value among the replicates, and gene expression values are normalised to z-scores. **(F)** Subnetwork of the GRN featuring interactions exclusively involving NRF2 and FOXM1 at 48 h. Nodes are coloured according to target gene normalised expression values (z-score values) at 48 h after PHx and edges are coloured depending on RRE classification at 48 h of regeneration.

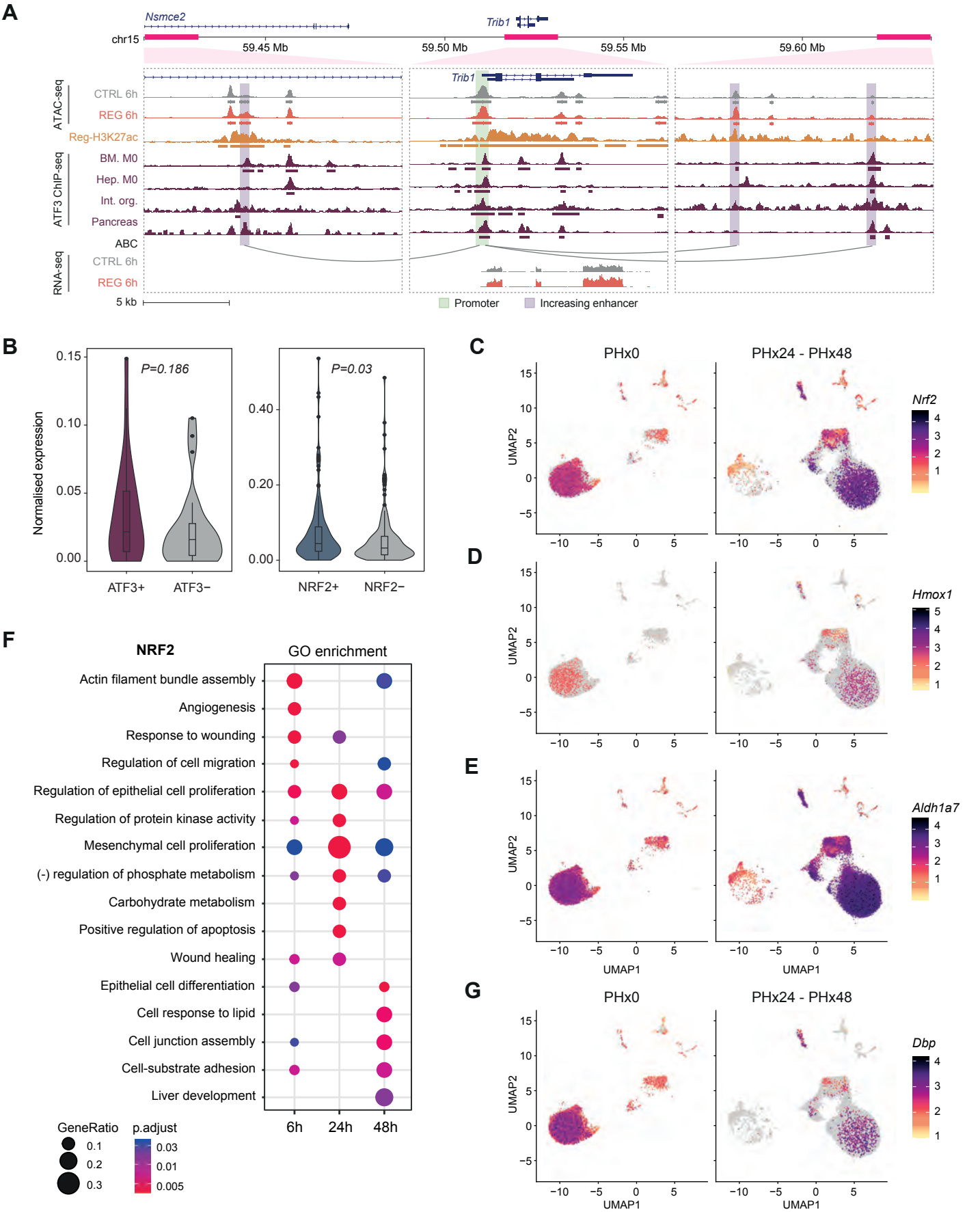

Figure S6. ATF3 and NRF2 target genes are associated with the injury response, related to Figure 6.
(A) Genome browser screenshot illustrating the genomic region of the *Trib1* at 6 h post-surgery. The promoter bound by ATF3 is linked to three increasing enhancers with ATF3 binding. Only one replicate is shown for simplicity. **(B)** Violin plots of scRNA-seq collapsed and normalised expression values (z-score values). Left: expression of ATF3 target genes in *Atf3*-expressing cells versus non-expressing cells. Right: expression of NRF2 target gene in *Nrf2*-expressing cells versus non-expressing cells. Statistical significance was assessed using the Wilcoxon rank-sum two-sided test with continuity correction. **(C-E)** Feature plots showing *Nrf2* **(C)** expression and its target genes, *Hmox1* **(D)** and *Aldh1a7* **(E)**, in quiescent livers (PHx0) and at 24 and 48 h after PHx (PHx24 - PHx48). **(F)** Functional analysis (GO terms) of the target genes of the increasing RREs with NRF2-binding. GO enrichment analysis was performed using the Bioconductor package clusterProfiler[89], with a padj< 0.05. **(G)** Feature plot of *Dbp* expression in quiescent livers (PHx0) and at 24 and 48 h after PHx (PHx24 - PHx48).

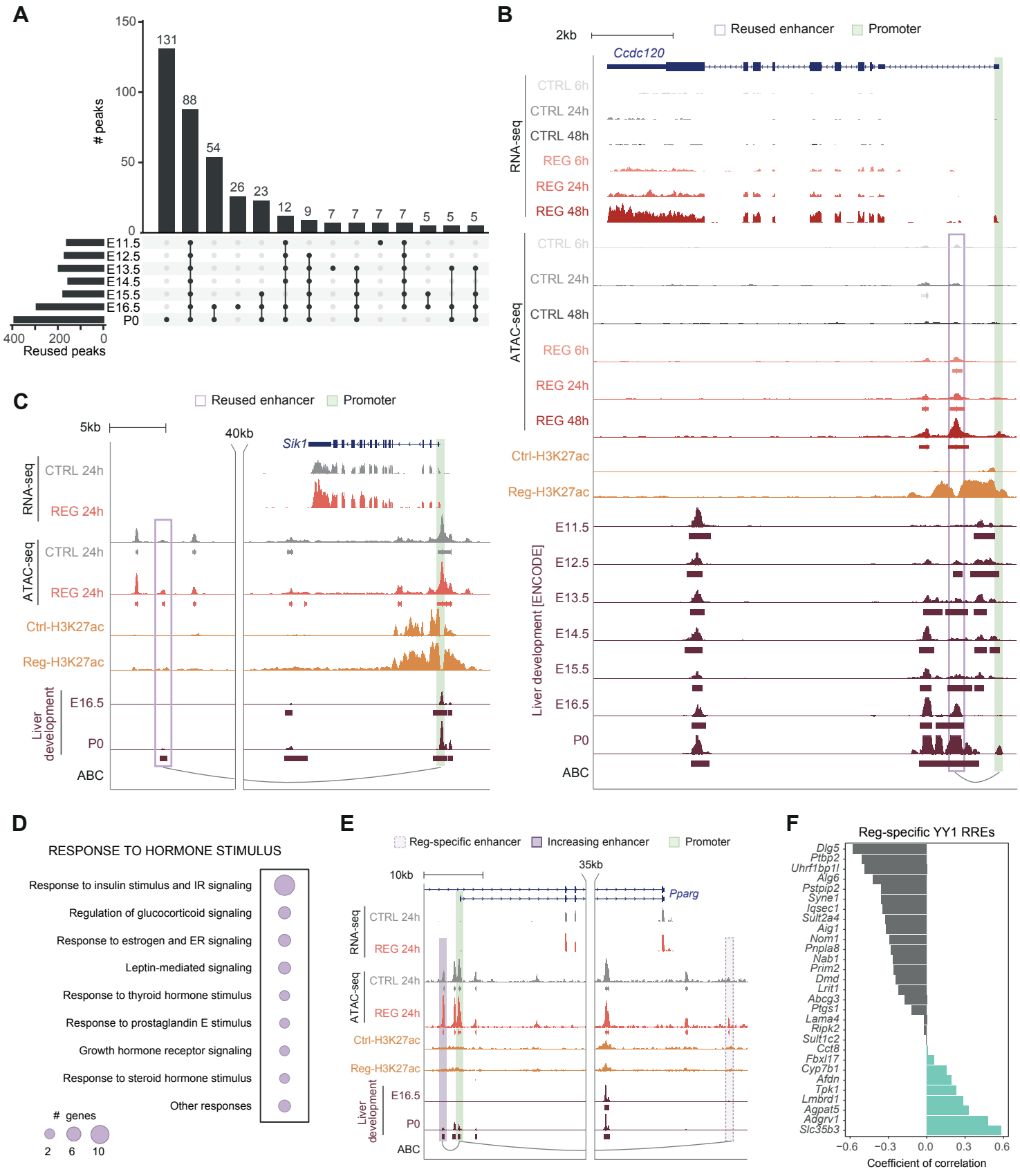

Figure S7. *De novo* enhancers include enhancers reused from development and regeneration-specific enhancers, related to Figure 7. (A) Overlap between the *de novo* peaks and the ATAC-seq peaks from liver embryonic development. The highest overlap is observed with postnatal peaks or peaks that persist throughout all stages of liver development. Only combinations with at least 5 peaks are shown. **(B)** Genome browser screenshot depicting the genomic locus of the *Ccdc120* gene. *Ccdc120* is targeted by a *de novo* reused enhancer with sustained activity throughout regeneration (highlighted in light purple). The enhancer exhibits progressively increased accessibility both during regeneration and development, consistent with the upregulation of the *Ccdc120* gene over time after PHx. Only one replicate is shown for simplicity. **(C)** Genome browser screenshot illustrating the genomic region of the *Sik1* gene. *Sik1* is targeted by a *de novo* enhancer 24 h after PHx, which is reused from postnatal day 0 of liver development. **(D)** Response to hormones (GO term) associated with Reg-specific enhancers, divided into subcategories. The size of the circle denotes the number of genes in each term. **(E)** Genome browser screenshot depicting the genomic locus of the *Pparg* gene. *Pparg* is targeted by a *de novo* reg-specific enhancer and a proximal increasing enhancer 24 h after PHx. **(F)** Bar plot showing Pearson's correlation coefficient between the acces-sibility of regeneration-specific RREs containing YY1 motifs and the expression of their associated target genes.

Table S6. Quality control of ATAC-seq and ChIP-seq experiments, related to STAR Methods.

GEO accession	Experiment	Type of Data	NRF	PBC1	PBC2
GSE262282	ChIP-Seq	Atf3 in Intestinal organoids	0.2586	0.3520	1.7639
GSE140581	ChIP-Seq	Atf3 in bone marrow macrophages	0.5871	0.6366	2.7900
GSE128336	ChIP-Seq	Atf3 in hepatic macrophages	0.6859	0.7147	3.5912
GSE60250	ChIP-Seq	Atf3 in pancreatic tissue	0.8802	0.9510	21.7648
GSE188742	ChIP-Seq	H3K27ac in liver, prePHx (0 hours)	0.8855	0.8926	9.2248
GSE76935	ChIP-Seq	H3K27ac in liver, postPHx (40 hours)	0.8465	0.8588	7.0418
GSE109865	ChIP-Seq	Nrf2 in liver	0.4808	0.4636	1.8114
GSM8246425	ATAC-seq	Liver, post-PHx 6h, rep1	0.8437	0.8757	8.3968
GSM8246426	ATAC-seq	Liver, post-PHx 6h, rep 2	0.9377	0.9594	27.4230
GSM8246427	ATAC-seq	Liver, post-PHx 24h, rep1	0.7899	0.8272	6.0137
GSM8246428	ATAC-seq	Liver, post-PHx 24h, rep 2	0.8786	0.9131	12.2968
GSM8246429	ATAC-seq	Liver, post-PHx 48h, rep1	0.9027	0.9460	21.3726
GSM8246430	ATAC-seq	Liver, post-PHx 48h, rep2	0.8502	0.9021	11.3583
GSM8246431	ATAC-seq	Liver, control L6h, rep1	0.7681	0.8321	6.2932
GSM8246432	ATAC-seq	Liver, control 24h, rep1	0.7245	0.7302	3.5697
GSM8246433	ATAC-seq	Liver, control 48h, rep1	0.8502	0.8804	8.7782
GSM8246434	ATAC-seq	Liver, control 48h, rep2	0.7800	0.7915	4.7270

CHAPTER II.
Three-dimensional genome architecture in wing disc regeneration

3D genome organization in tissue regeneration: functional requirement of long-range loops

Palmira Llorens-Giralt[1], Carlos Camilleri-Robles[1], Maria Marti-Marimon[2,3], Florenci Serras[1], Maria Cristina Gambetta[4], Marc A Marti-Renom[2,3,5], Montserrat Corominas[1*].

[1]Department of Genetics, Microbiology and Statistics, School of Biology, Institute of Biomedicine (IBUB), University of Barcelona, Barcelona, Catalonia, Spain.
[2]National Center for Genomic Analysis (CNAG), Barcelona, Catalonia, Spain.
[3]Center for Genomic Regulation (CRG), The Barcelona Institute for Science and Technology (BIST), Barcelona, Catalonia, Spain.
[4]Center for Integrative Genomics, University of Lausanne, 1015 Lausanne, Switzerland
[5]Catalan Institution for Research and Advanced Studies (ICREA), Barcelona, Catalonia, Spain.
**Corresponding author. Email: mcorominas@ub.edu*

ABSTRACT

The three-dimensional (3D) organization of the genome plays a fundamental role in gene regulation. However, little is known about how transcriptional responses are influenced by changes in genome architecture during tissue regeneration. Here, we used Hi-C to profile genome organization during *Drosophila* wing imaginal disc regeneration. We found that, although compartments and topologically associating domains (TADs) are largely maintained, regeneration is accompanied by reduced compartmentalization and increased boundary insulation. Notably, we identified three long-range chromatin loops with increased contact frequency during regeneration. Precise deletion of their anchors demonstrated that these loops are essential for proper disc regeneration but dispensable for normal wing development. These findings provide functional evidence that 3D genome architecture actively contributes to the regenerative process.

INTRODUCTION

The spatial organization of the genome is increasingly recognized as a crucial regulator of gene expression during cellular differentiation and development (*1–3*). High-resolution chromosome conformation capture technologies have revealed that the genome folds into functional domains, facilitating regulatory interactions between enhancers and promoters (*4–6*). Chromosomes are organized into active (A) and inactive (B) compartments, corresponding to gene-rich, transcriptionally active open euchromatin, and gene-poor, heterochromatic regions, respectively (*7*). Within these compartments, smaller structures known as topologically associating domains (TADs) are defined by frequent internal interactions and sharp boundaries that insulate them from the neighboring regions (*5*, *8*). In *Drosophila*, TADs correspond to physical units that correlate well with distinct chromatin states, such as Polycomb-repressed, heterochromatic, or active regions (*9–13*). Unlike in mammals, where TAD boundaries are often enriched for CCCTC-binding factor (CTCF) (*6*, *14*), most *Drosophila* TAD borders are associated with active promoters or small domains containing expressed genes (*9*, *15*). Alternatively, non-promoter TAD boundaries in flies largely require the presence of the architectural protein Centrosomal protein 190 kDa (Cp190) (*16*). Recent studies have also identified long-range chromatin loops, high-frequency interactions spanning hundreds of kilobases to a few megabases, whose anchors often overlap with TAD boundaries and are likely stabilized by architectural proteins (*17*). These loops contribute to transcriptional regulation by enabling the precise spatiotemporal control of neuronal gene expression in the central nervous system (*18*, *19*) and supporting the cross-regulation of paralogous genes during embryogenesis (*20*, *21*). Other long-range loops are established by

Polycomb complexes, and can facilitate either activation or repression of developmental genes (*22–24*).

Evidence from different species and injury contexts suggests that regenerative potential is closely linked to chromatin state dynamics and enhancer activation (*25*, *26*). Following tissue damage, neighboring cells integrate signals from the wound, triggering transcriptional reprogramming and widespread chromatin remodeling to enable effective tissue repair (*27*, *28*). However, whether this reprogramming involves higher-order chromatin reorganization, such as changes in TADs or chromatin loops, remains unclear. *Drosophila* imaginal discs, epithelial tissues capable of compensatory regeneration, offer a powerful model to address this question. Their cellular plasticity, combined with an extensive genetic toolkit, has enabled the identification of key signaling and epigenetic factors involved in tissue repair (*29–31*). The early stages of wing disc regeneration are characterized by a reduction in repressive histone marks, increased chromatin accessibility and transcriptional activation (*27*). These regenerative gene programs are driven by damage-responsive regulatory elements (DRREs), enhancers that are preferentially or specifically activated by injury (*27*, *32*). Despite these advances, little is known about the contribution of three-dimensional chromatin architecture in regulating injury-induced gene expression. Understanding how 3D genome topology changes in response to damage could reveal new principles of gene regulation during tissue regeneration.

Here, we investigate the 3D regulatory landscape of wing disc regeneration by generating Hi-C interaction maps in control and genetically ablated discs. We find that while global genome organization is largely preserved following injury, chromatin compartmentalization is notably weakened. In addition, we identify three long-range chromatin loops that exhibit significantly increased interaction frequency during regeneration. Deletion of the intergenic anchors of each loop impairs regeneration but does not affect normal development, demonstrating their specific requirement for tissue repair. These loops are anchored by Cp190, which may be recruited at these sites by the insulator-binding factors Ibf1/2. Together, our findings identify a previously unknown role for genome architecture in tissue repair, revealing an additional regulatory layer of gene expression during regeneration.

RESULTS

Global changes in 3D chromatin architecture during regeneration

To study whether chromatin changes during wing disc regeneration are associated with a reorganization of genome topology, we performed Hi-C to map the 3D genome architecture of wing discs after genetic ablation. Cell death was induced for 16 hours by expressing the proapoptotic gene *reaper* (*rpr*) in the spalt (*sal*$^{E/Pv}$) domain of the wing pouch in third-instar larvae (*33*, *34*). Wing discs were collected immediately after *rpr* expression was switched off, and two biological replicates were processed for *in situ* Hi-C (Fig. 1A). The high correlation between replicates allowed us to merge them into a single dataset per condition (Fig. S1A).

We first identified A/B compartments in control (CTRL) and regenerating (REG) discs at a 10 kb resolution. This analysis revealed a strong correlation between the two conditions, with 56% and 57% of compartments classified as A, and 44% and 43% classified as B in CTRL and REG samples, respectively (Fig. 1B, Fig. S1B). Compartmental switches during regeneration were infrequent, with 3.05% of the genome changing from A to B, and 2.55% switching from B to A (Fig. 1C). To further characterize the A/B compartments, we integrated our previously published ATAC-seq, H3K27ac ChIP-seq, and RNA-seq datasets from regenerating wing discs (*27*, *35*). As expected, A compartments were enriched for accessible chromatin, H3K27ac, and actively expressed genes, whereas B compartments predominantly contained inactive chromatin and non-expressed genes (Fig. 1D-E). In addition, B compartments exhibited greater differences between conditions than A compartments (Fig. S1C). Notably, we observed weakened compartment strength following damage (Fig. 1F, Fig. S1D).

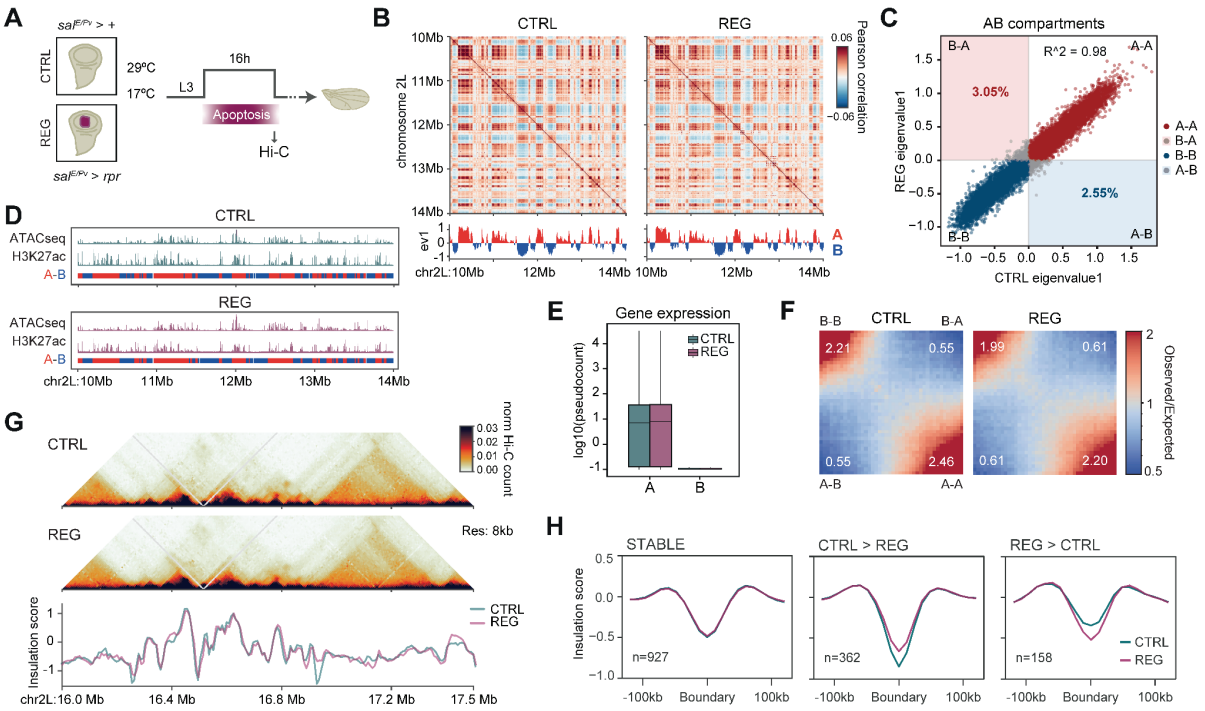

Figure 1. AB compartment strength and boundary insulation is mildly reduced during regeneration.
(A) Experimental design. Flies were raised at 17°C until 192 hours after egg laying (corresponding to the third-instar larval stage, L3) then shifted to 29ºC for 16 hours to induce cell death via *rpr* expression in the *sal*$^{E/Pv}$ domain of the wing pouch (purple region). Wing discs were dissected immediately after treatment and processed for Hi-C. Controls without *rpr* expression were treated in parallel. **(B)** A/B compartment analysis showing Pearson correlation matrices and eigenvectors for chromosome 2L in control (CTRL) and regeneration (REG). **(C)** Scatter plot comparing pairwise compartment eigenvectors between control and regeneration. **(D)** Genome browser tracks displaying ATAC-seq and H3K27ac ChIP-seq signals intensities (*27*), alongside compartment classifications: A (red) and B (blue). **(E)** Gene expression levels of genes located in A or B compartments in control and regeneration (*35*). **(F)** Saddle plots showing genome-wide compartmentalization strength. A–A and B–B interactions are stronger in control than in regeneration. **(G)** Hi-C contact maps with insulation scores for control and regeneration, including an example of a boundary with significantly increased insulation in control. **(H)** Pairwise comparison of insulation scores across boundaries categorized as stable, increased in control, or increased in regeneration.

To assess changes at the level of domains, we calculated insulation scores to identify TAD boundaries at 8 kb resolution (Fig. 1G). Pairwise comparison between CTRL and REG discs showed that insulation at border regions remained largely stable (Fig. 1H). However, 36% of boundaries exhibited significant changes in insulation, with a greater proportion showing increased insulation in the control (70%) compared to regeneration (30%). Among boundaries with increased insulation during regeneration, half reflected increases in insulation (quantitative), while the other half corresponded to newly formed (*de novo*) TAD boundaries (Fig. S1E). In contrast, two-thirds of boundaries with increased insulation in the control were quantitative, with the remaining third being *de novo*. Together, these results suggest that while overall genome organization is largely preserved after injury, regeneration is accompanied by a general reduction in compartmentalization and boundary insulation.

Enrichment of specific long-range chromatin loops during regeneration

Chromatin loops appear as interaction hotspots in high-resolution Hi-C maps, reflecting frequent physical contacts between distant genomic loci (*36*). To identify regeneration-specific loops, we applied an automated loop-calling algorithm (*18*) in both control and regeneration Hi-C datasets. Following

manual validation, we identified 28 curated long-range loops (> 1 Mb) in the wing disc (Table S1). Among these, only two loops showed significant enrichment in regeneration: **L1**, spanning loop anchors **A1** to **A4** (chr2L:6,357,000-9,464,000), and **L3**, between **A2** and **A5** (chr2L:6,411,000-9,486,000) (Fig. 2A). Anchor A2 was also involved in a third loop, **L2**, connecting **A2** and **A3** (chr2L:6,411,000–9,083,000), but did not exhibit significant enrichment. These three loops were previously characterized as meta-loops, high-frequency interactions between meta-TADs, which are defined as TAD pairs separated by megabases that preferentially interact in the central nervous system (*18*). Visual inspection of the REG/CTRL fold change Hi-C matrix confirmed an interaction hotspot spanning more than 3 Mb on chromosome 2L (Fig. 2B), and specific inspection of the individual Hi-C maps validated the specific enrichment of loops L1 and L3 during regeneration (Fig. 2C). Virtual 4C analysis further confirmed these findings, showing a strong enrichment of L1 and L3 during regeneration, but not of L2 (Fig. 2D). To precisely map the meta-loop anchors, we used previously published ATAC-seq data (*27*), assigning each anchor to an open chromatin region (Fig. S2A). Except for A2, which is located at the *Dip-epsilon* promoter, all anchors mapped to intergenic regions: A1 near the 3' end of *CG9500*, A3 upstream of *Toll-4*, A4 near the 3' end of *numb*, and A5 downstream of *Gdi* (Fig. 2E, Fig. S2A).

Given the regeneration-specific enrichment of L1 and L3, we next assessed their spatial proximity and cell-to-cell variability by measuring physical distances between meta-loop anchors in control and regenerating wing discs using DNA fluorescence *in situ* hybridization (DNA-FISH). We designed probes targeting the two anchors of each loop and quantified the distance between A1 and A4 (L1), and between A2 and A5 (L3) within individual nuclei, considering distances below 250 nm as indicative of a physical interaction (*37*). This analysis revealed a significant increase in the proportion of nuclei with physically close anchors during regeneration compared to controls: 29.6% vs. 9.2% for L1, and 33.6% vs. 9.9% for L3 (Fig. 2F-G). These results are consistent with our Hi-C data, indicating that although these loops are present in a minority of cells in control discs, their interaction frequency increases during regeneration. As a control, we performed DNA-FISH of a previously characterized meta-loop connecting the *nolo* promoter with an intergenic region 1.6 Mb away on chromosome 2L, detected in both wing discs and the central nervous system of third-instar larvae (*18*). This loop was also observed in our control and regeneration Hi-C maps (Fig. S2B), and was identified by the meta-loop calling algorithm (Table S1). Quantitative analysis of the DNA-FISH results confirmed the reliability of our approach in detecting physical chromatin interactions (Fig. S2C).

To determine whether the increased interaction frequency of L1 and L3 during regeneration is associated with transcriptional changes, we analyzed the expression of genes located at loop anchors or within the corresponding TADs using transcriptomic data from regenerating wing discs (*35*). For L1, we found that *CG9500* was not expressed, while *numb* was highly expressed in both control and regenerating wing discs, with no significant change (Fig. S2D). At the L3 anchors, *Dip-epsilon* showed a trend toward upregulation, while *Gdi* remained highly expressed in both conditions. *Toll4*, located near A3, was not expressed in either condition. Among genes within the meta-TADs, only *Tig* was significantly upregulated, while the others showed no significant differential expression (Fig. S2D).

Regeneration-enriched meta-loops are required for wing disc regeneration

To investigate the functional relevance of L1 and L3 in wing discs, we first disrupted their anchor sites using chromosomal deficiencies. Specifically, we used *Df(2L)BSC186* (chr2L:6,253,005-6,363,074), which encompasses anchor A1 (L1), and *Df(2L)Exel6022* (chr2L:9,447,643-9,560,489), which includes both A4 (L1) and A5 (L3), hereafter referred to as *Df(a)* and *Df(b)*, respectively (Fig. 3A). Both deficiencies are homozygous lethal, so their effects were examined in heterozygosity. Trans-heterozygous flies harboring each deficiency in one chromosome were used to assess the effects of meta-loop disruption. We reasoned that heterozygous removal of both anchor sites would impair meta-loop formation while maintaining gene expression of the hemizygous genes.

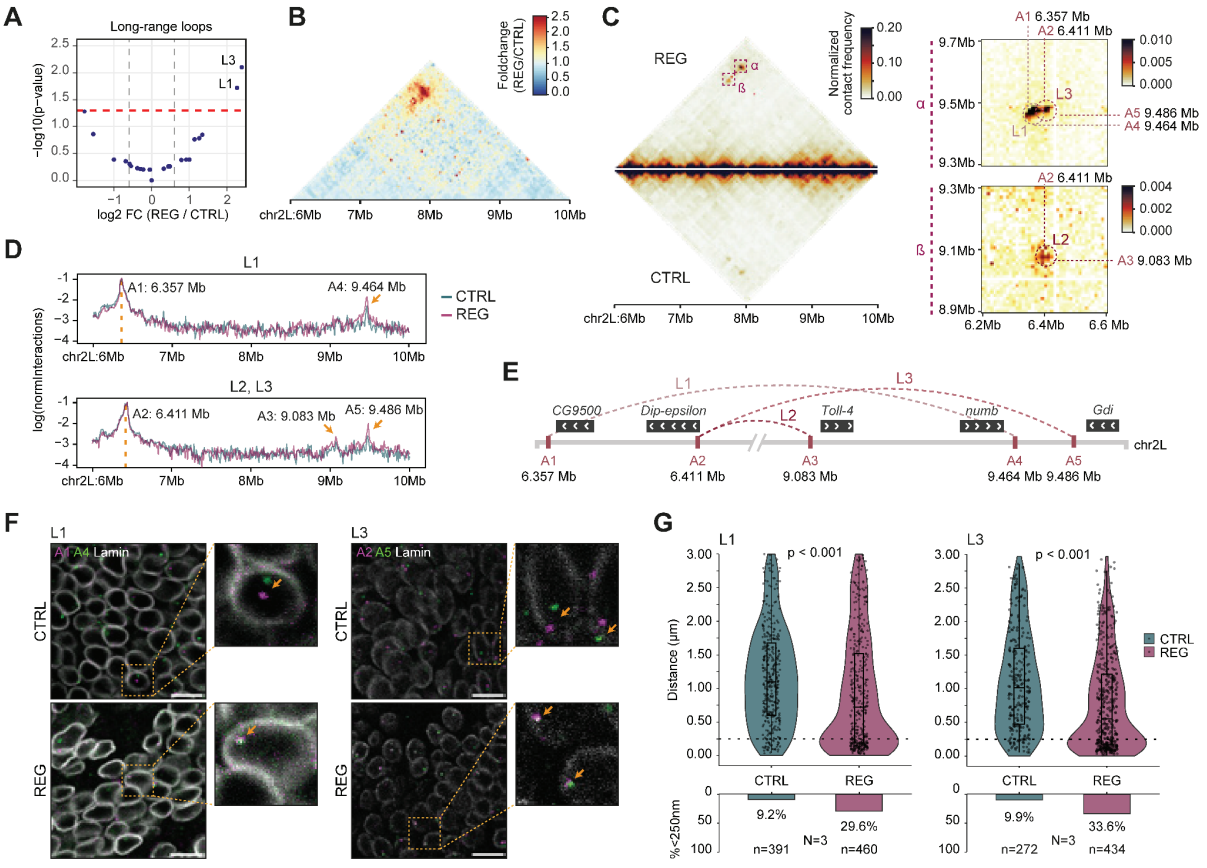

Figure 2. Specific long-range chromatin loops are enriched during regeneration.
(A) Differential analysis of strengths of meta-loops in control versus regenerating wing discs. Labeled loops were significantly stronger (fold change > 1.5 and *p*-value < 0.05) during regeneration. **(B)** Hi-C fold change map (Regeneration/Control) showing differential contacts across chromosome 2L: 6-10Mb. **(C)** Left: Mirror plot of normalized Hi-C contact maps for regeneration (top) and control (bottom), with two regeneration-enriched regions highlighted. Right: Zoom-in views of the alpha (α) and beta (ß) regions from the regeneration map, showing loops L1, L2 and L3. Coordinates of each loop anchor are indicated. **(D)** Virtual 4C plots generated from Hi-C data using A1 as bait to visualize loop L1 (top) and A2 to detect loops L2 and L3 (bottom) in regeneration and control conditions. **(E)** Schematic representation of loops L1–L3, their corresponding anchors A1–A5, and the nearest gene associated with each anchor. **(F)** Representative DNA-FISH images of wing discs labeled with probes targeting A1 (magenta) and A4 (green) for loop L1 (left), and A2 (magenta) and A5 (green) for loop L3 (right). Lamin staining (white) marks the nuclear lamina. **(G)** Quantification of DNA-FISH distances (in µm) for L1 (left) and L3 (right) anchors. Violin plots show the distribution of measured distances and the percentage of nuclei with distances <250 nm is indicated below. *n* denotes the number of nuclei analyzed; *N* indicates the number of biological replicates.

Heterozygous and trans-heterozygous deficiency flies developed normally, with no observable defects in adult wing size or morphology (Fig. S3A). To investigate whether the absence of L1 and L3 impaired the regeneration capacity, we activated *rpr* in the wing pouch as previously described (Fig. 1A), in combination with either *Df(a)*, *Df(b)*, or both deficiencies in heterozygosity (*Df(a)/Df(b)*). Following cell death induction, we observed a significant reduction in wing regeneration among flies carrying a deficiency, compared to the control (Fig. 3B). *Df(a)* flies exhibited a higher proportion of regenerated wings (81.3%) than *Df(b)* (49.1%). These single-deficiency flies mainly showed mild phenotypes, such as missing or extra crossveins, in 15.6% of *Df(a)* and 23.6% of *Df(b)*. In contrast, *Df(a)/Df(b)* flies exhibited a further decrease in regenerated wings (37.7%) and a higher proportion of severe phenotypes (43.7%), including complete vein loss or multiple defects in veins and crossveins (Fig. 3B). These findings suggest that the formation of L1 and possibly L3 is essential for wing disc regeneration but dispensable for normal development. The more severe defects observed in *Df(b)* compared to *Df(a)*

flies may indicate that both meta-loops contribute to regeneration, as *Df(b)* lacks anchors for both L1 and L3, while *Df(a)* only disrupts L1. However, since these deficiencies encompass multiple genes, we cannot exclude the possibility that impaired regeneration results from haploinsufficiency of one or more genes, rather than loss of meta-loop formation.

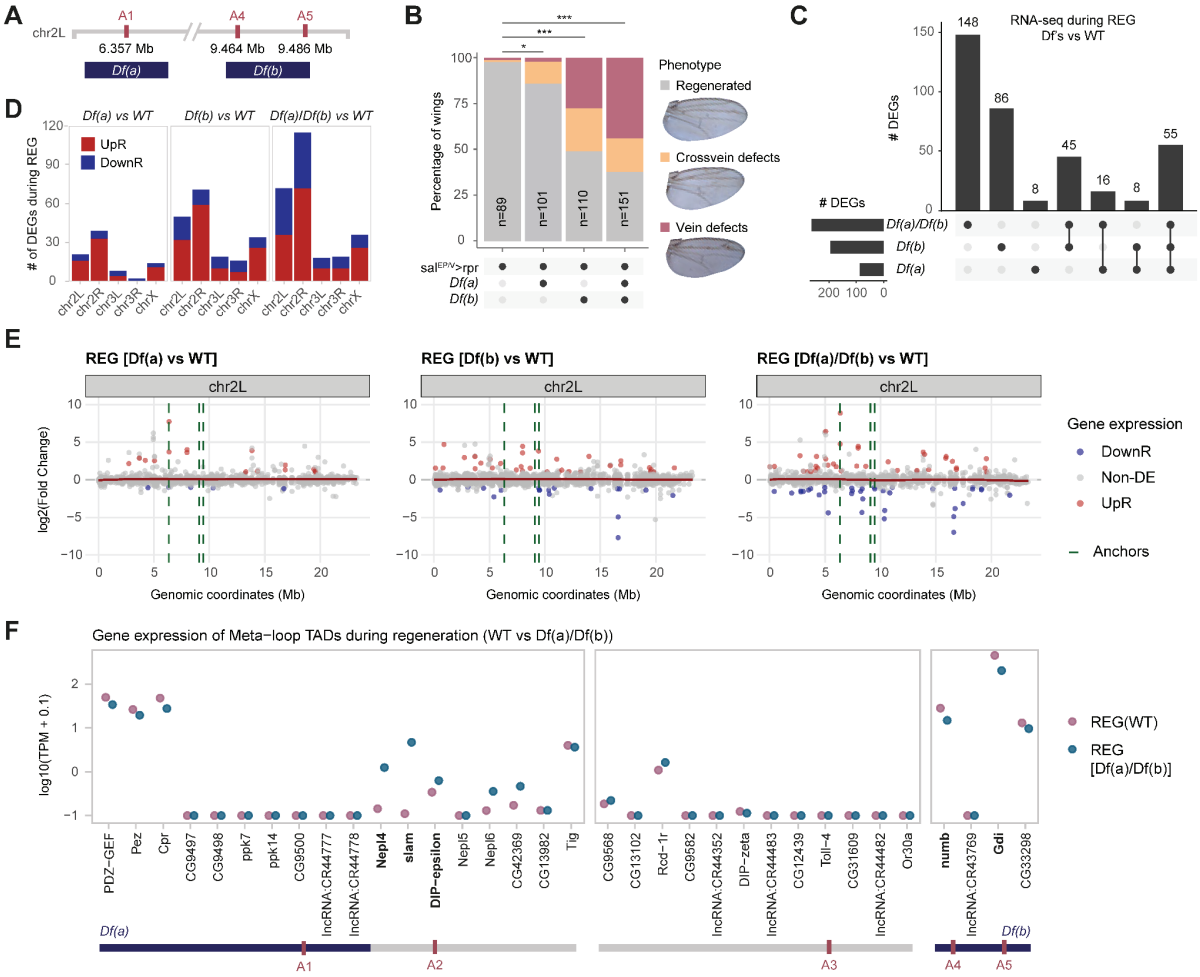

Figure 3. Disrupting meta-loop anchors using chromosomal deficiencies impairs regeneration.
(A) Schematic representation of chromosomal deficiencies *Df(a)* and *Df(b)*, showing their overlap with specific loop anchor regions. **(B)** Proportion of adult wing phenotypes across genotypes: fully regenerated wings (grey), crossvein defects (yellow), and other vein abnormalities (rose). Representative images of each phenotype are shown to the right. *p*-values are indicated above: $*p < 0.05$, $***p < 0.001$. **(C)** Upset plot showing differentially expressed genes (DEGs) during regeneration in heterozygous flies carrying either single deficiencies or both deficiencies in trans, compared to wild-type controls. Intersections of DEGs across comparisons are shown. **(D)** Total number of DEGs per genotype (as in panel C), grouped by chromosome. **(E)** Scatter plot of gene expression changes on chromosome 2L for each mutant compared to wild type during regeneration. Log_2(fold change) is plotted for all genes; upregulated genes are shown in red, downregulated in blue, and loop anchor positions are marked in green. **(F)** Gene expression levels (log_{10}[TPM + 0.1]) for genes located within meta-TADs in wild-type and *Df(a)/Df(b)* trans-heterozygous flies during regeneration. DEGs are in bold. A schematic below indicates meta-TAD boundaries, loop anchors, and the positions of each deficiency.

Next, we performed RNA-seq on regenerating flies harboring single deficiencies and flies carrying both deficiencies in trans-heterozygosis, using wild-type regenerating wing discs as controls. Principal component analysis (PCA) revealed that, despite differences in regeneration phenotypes, samples from single-deficiency flies clustered together, whereas trans-heterozygous samples formed a distinct group (Fig. S3B-C). Consistent with the phenotypic observations, *Df(a)/Df(b)* flies showed the highest number of differentially expressed genes (DEGs) compared to controls (264 genes), followed by *Df(b)* (194

genes), and *Df(a)* (87 genes) (Fig. 3C). In both single deficiency flies, most DEGs were upregulated (77% and 71%, respectively) and preferentially located on chr2L (where the meta-loops are located) and chr2R (Fig. 3D). In *Df(a)/Df(b)* trans-heterozygous flies, upregulated genes remained predominant (59%) and showed preferential localization to chromosome 2 (Fig. 3C-D). We visually inspected the localization of DEGs along all chromosomes, searching for differential expression clusters (Fig. 3E, Fig. S3D). Though a few genes within or near the deficiencies showed differential expression, no particular region harbored a large number of dysregulated genes. The A1-associated gene *CG9500*, located within *Df(a)*, and *Dip-epsilon*, linked to A2, were not expressed in any condition (Fig. 3F, Fig. S4A-B). Additionally, none of the genes within *Df(a)* were differentially expressed. However, *Nepl4* and *slam*, located between A1 and A2 but not deleted by *Df(a)*, were upregulated both in *Df(a)* and *Df(a)/Df(b)* flies. In contrast, genes near A4 and A5—*numb* and *Gdi*, both encompassed by *Df(b)*—were downregulated in *Df(a)/Df(b)* flies, with *numb* also downregulated in *Df(b)* flies. No other genes within *Df(b)* showed differential expression in *Df(a)/Df(b)* flies (Fig. 3F). These results suggest a potential role for L1 and L3 meta-loops in transcriptional regulation.

To determine whether precise deletion of an L3 anchor was sufficient to affect nearby gene expression, we used CRISPR-Cas9 to delete the ATAC-seq peak corresponding to the A5 anchor. We specifically targeted the intergenic anchor, rather than the anchor encompassing the *Dip-epsilon* promoter (A2), to avoid disrupting coding sequences. Because A2 is shared between L2 and L3, we also generated CRISPR knockout (KO) flies for the intergenic anchor A3, which is specific to L2. We crossed independent CRISPR alleles to generate trans-heterozygous flies for each loop anchor deletion, hereafter $L2^{\Delta A3}$ and $L3^{\Delta A5}$. We extracted total RNA of wing discs from third-instar larvae and compared the expression of anchor genes in $L2^{\Delta A3}$ and $L3^{\Delta A5}$ mutants versus controls by reverse transcription-quantitative (RT-qPCR). While *Toll-4*, *numb* and *Gdi* expression remained similar to the control, we observed a tendency towards upregulation for *DIP-epsilon* (fold change = 1.5 in $L3^{\Delta A5}$) and *CG9500* (fold change = 1.57 and 1.84 in $L2^{\Delta A3}$ and $L3^{\Delta A5}$, respectively) (Fig. 4A-B). Although statistically not significant, these results suggest that deleting the anchor region of a given chromatin loop does not necessarily affect the expression of the nearby genes. Instead, the disruption of the chromatin loop may affect the expression of the genes closer to the undeleted anchor region, which in this case is located ~ 3 Mb upstream.

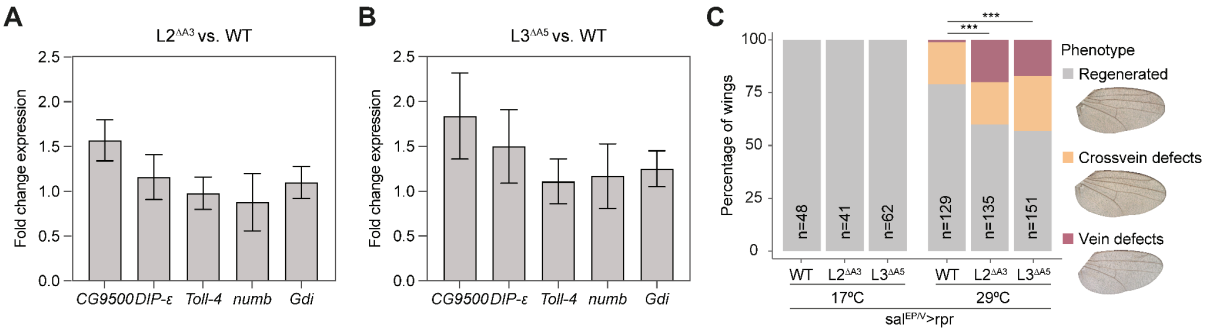

Figure 4. Meta-loops L2 and L3 are required for regeneration.
(A) Gene expression changes measured by qPCR in homozygous $L2^{\Delta A3}$ compared to wild-type wing discs in developmental conditions. The expression fold change relative to the wild type is represented. Error bars indicate the standard error of the mean. **(B)** Same as (A) but $L3^{\Delta A5}$. **(C)** Proportion of adult wing phenotypes across genotypes (WT, $L2^{\Delta A3}$ and $L3^{\Delta A5}$) and conditions (development, 17ºC or regeneration, 29ºC): fully regenerated wings (grey), crossvein defects (yellow), and other vein abnormalities (rose). Representative images of each phenotype are shown to the right. *p*-values are indicated above: ***$p < 0.001$.

We next asked whether these deletions would also impair regeneration, as observed in L1 trans-heterozygous deficient flies. Both $L2^{\Delta A3}$ and $L3^{\Delta A5}$ developed normally, with no observable defects in adult wing size or morphology (Fig. 4C). However, upon *rpr* activation in the wing pouch, these mutants

exhibited impaired regenerative capacity. Only up to 60% of wings regenerated normally, while 20% of $L2^{\Delta A3}$ and 16% of $L3^{\Delta A5}$ wings showed severe defects, including complete loss of a vein or multiple abnormalities in veins and crossveins. In contrast, fewer than 1% of control regenerating wings displayed severe aberrant phenotypes (Fig. 4C). These results demonstrate that these meta-loops are required for proper regeneration and further support the functional importance of chromatin organization in tissue repair.

Architectural proteins mediating regeneration-associated meta-loops

Meta-loops are thought to arise from interactions between structural elements, rather than from enhancer-promoter looping, and be stabilized by dedicated transcription factors and architectural proteins (*18*, *19*). To identify the factors involved in L1-L3 meta-loop formation, we examined ChIP-seq profiles from various *Drosophila* tissues for Cp190, CTCF (*16*), and GAGA-associated factor (GAF) (*38*), all previously shown to be required for establishing long-range regulatory interactions (*18*, *19*, *38*, *39*). We also analyzed profiles for additional architectural proteins, including Insulator binding factors 1 and 2 (Ibf1/Ibf2) (*40*), Suppressor of Hairy wing [Su(Hw)], Boundary element-associated factor of 32kD (BEAF-32), and Motif 1 Binding Protein (M1BP) (*41*), which primarily facilitate looping by recruiting Cp190 to chromatin (*39*, *40*, *42–44*). This analysis revealed binding of Cp190, CTCF, Ibf1, and Ibf2 at L1 anchors regions A1 and A4 (Fig. 5A). In contrast, the anchors for L2 and L3 (A2, A3, and A5) were not bound by any of these factors. No binding of GAF, BEAF-32, or M1BP was observed at any of the L1-L3 anchors, and Su(Hw) binding was only detected adjacent to A4.

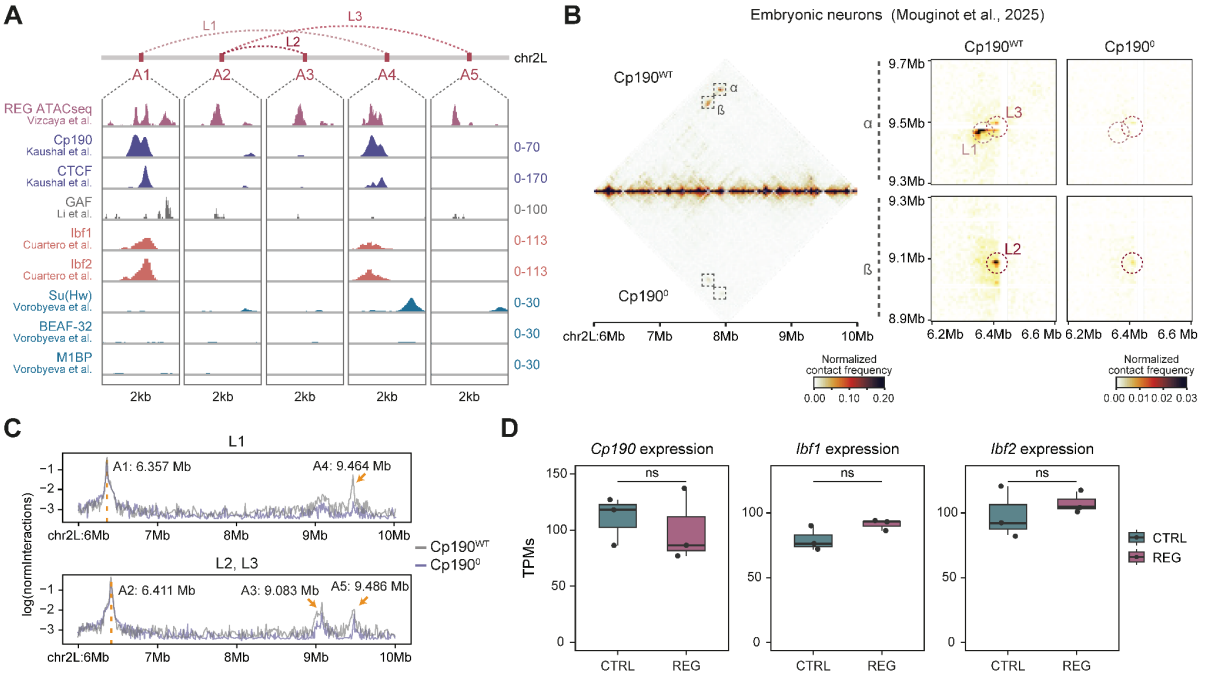

Figure 5. Cp190 is required for meta-loop formation.
(A) Genome browser tracks of published ATAC-seq data from regenerating wing discs and ChIP-seq profiles of indicated insulator proteins across a 2 kb window containing anchors A1-A5. Above, schematic overview of meta-loops L1–L3 and their corresponding anchors A1–A5. The ATAC-seq profile is scaled to view for each anchor. **(B)** Micro-C contact map analysis in wild-type and Cp190-deficient embryonic neurons (maternal depletion and knockout, Cp190⁰) (*19*). Left*:* Mirror plot of normalized Micro-C contact maps for chromosome 2L (6–10 Mb). Right*:* Zoom-in views of the α and β regions containing loops L1 and L2, and L3, respectively. **(C)** Virtual 4C plots with A1 as bait to visualize loop L1 (top) and A2 to detect loops L2 and L3 (bottom). Loop anchor coordinates are indicated. **(D)** Expression levels (TPM) of *Cp190*, *Ibf1*, and *Ibf2* in control and regenerating wing discs (*35*).

To determine whether Cp190 or CTCF are required for the formation of these meta-loops, we analyzed publicly available Micro-C data from embryos lacking maternal and zygotic Cp190 (*Cp190^{0}*) (*19*) and CTCF knock-out (*CTCF^{KO}*) larval neurons (*45*). Consistent with Cp190 occupancy at L1 anchors, the L1 meta-loop was lost in *Cp190^{0}* embryos (Fig. 5B-C). Notably, L2 and L3 were also strongly disrupted in these mutants (Fig. 5B-C), suggesting that they either directly depend on Cp190 or require the formation of L1 to establish themselves. In contrast, contact frequencies across L1-L3 were preserved in *CTCF^{KO}* larvae (Fig. S5A). Similarly, meta-loop architecture remained intact in wing discs from *GAF* mutant flies (*38*) and in pupal heads from *BEAF-32* mutants lacking both maternal and zygotic contributions (*46*) (Fig. S5B-C).

Cp190 was not differentially expressed during wing disc regeneration, based on RNA-seq data (*35*) (Fig. 5D), and other previously identified Cp190-dependent loops (*19*) were not enriched in the regeneration Hi-C matrix (Fig. 2A). This suggests that the increased interaction frequencies of L1, L2 and L3 during regeneration may be driven by a specific, context-dependent mechanism, rather than a general increase in Cp190 activity. Ibf1 and Ibf2, which may be responsible for Cp190 recruitment to L1 anchors based on their ChIP-seq profiles (Fig. 5A), were also not differentially expressed during regeneration (Fig. 5D).

Altogether, these findings indicate that Cp190 is required for the formation of the L1 meta-loop, potentially recruited to its anchors by the insulator-binding factors Ibf1/2. Although the depletion of Cp190 also disrupts the assembly of L2 and L3, it likely acts through an indirect mechanism.

DISCUSSION

In this study, we investigated how genome architecture and long-range chromatin loops contribute to tissue regeneration. Following damage to the wing disc, we observed weakened A/B compartmentalization and reduced insulation at certain TAD boundaries, likely facilitating increased interactions between neighboring TADs. Despite these localized changes, global genome organization remained largely stable, with no substantial compartment switching. This is consistent with previous findings in both human and *Drosophila* cells, where TADs and compartments remain mostly unaltered after stress such as heat shock, except for a general reduction in TAD boundary strength (*47–49*).

Furthermore, we identified three long-range chromatin loops with increased contact frequency after damage and demonstrated their requirement for successful wing disc regeneration. Disruption of these meta-loops, using trans-heterozygous deficiencies encompassing L1 anchors and CRISPR-mediated deletion of L2 and L3 intergenic anchors, resulted in severe wing regeneration defects. Notably, these mutants displayed no obvious developmental abnormalities or defects in adult wing morphology in the absence of injury, despite the presence of these loops during embryogenesis (*21*) and in larval neurons (*18*), which suggests a regeneration-specific function. To explain this context-specific requirement, we propose two models: (1) meta-loops mediate regulatory interactions that remain latent during development but are specifically activated in response to damage; or (2) meta-loops play redundant roles during development, where regulatory networks are robust to minor perturbations, but become essential during regeneration, when precise transcriptional control is critical and there is less tolerance for alterations.

Supporting the first model, it has been previously described that sequences lacking intrinsic enhancer activity, termed distal tethering elements (DTEs), may form focal contacts with promoters prior to transcriptional activation (*50*). These loops facilitate enhancer–promoter interactions and prime genes for rapid activation, enabling temporal precision in gene expression. Although deletion of DTEs disrupts these loops and delays gene activation, overall transcriptional output remains largely unaffected. Similarly, Polycomb complexes can form long-range contacts that enable regulatory interactions

between enhancers and genes in a silenced but poised state (*24*). Recent studies suggest that meta-loops do not directly establish enhancer–promoter interactions but instead facilitate the regulatory crosstalk between distant TADs by sharing regulatory elements and transcription factors, as their intergenic anchors also generally lack enhancer activity (*18*, *19*). In line with this, transcriptomic analysis of regenerating wing discs from L1-deficient flies, with an intergenic-to-intergenic meta-loop disrupted, revealed changes in gene expression extending beyond the anchor-associated genes. Notably, genes located near opposite anchors were affected in opposite directions: *Nepl4* and *slam* (near A1) were upregulated, while *numb* and *Gdi* (near A4) were downregulated, suggesting potential negative cross-regulation between these loci. A similar pattern of inverse regulation via long-range loops was previously found between paralogous genes during embryogenesis (*21*), though whether this type of antagonistic regulation also occurs between non-paralogous genes remains an open question. Disruption of L2 and L3 only showed non-significant upregulation of anchor-associated genes *CG9500* and *Dip-epsilon*. It is worth noting that none of the anchor-associated genes affected by the L1–L3 disruptions have known functions in wing disc regeneration. Thus, the functional requirement of these loops during regeneration may reflect an architectural function or subtle regulatory effects that are not captured in bulk transcriptomic assays. High-resolution methods such as single-molecule RNA-FISH or quantitative single-cell live imaging (*18*–*20*) may be necessary to fully elucidate how meta-loops contribute to gene expression during regeneration.

Consistent with its known role in stabilizing long-range chromatin contacts (*19*), Cp190 was found to be required for the formation of all three regeneration-associated meta-loops. Considering that Cp190 binding is detected at L1 but not at L2 and L3, we suggest a hierarchical assembly model in which the Cp190-mediated L1 loop is established first and facilitates the subsequent formation of L2 and L3. This model aligns with previous findings showing that intergenic–intergenic loops often precede intergenic–promoter interactions during meta-loop assembly within the same domain (*18*, *19*). Although we have not directly addressed which factors localize Cp190 at L1 anchor sites, available Hi-C data from CTCF, BEAF-32, and GAF mutants suggest that these factors are likely not required for Cp190 recruitment. Instead, we hypothesize that Ibf1 and/or Ibf2 may bind to the L1 anchors and promote Cp190-dependent loop formation, subsequently enabling the assembly of L2 and L3 meta-loops.

In conclusion, our study provides the first direct evidence that changes in 3D genome architecture are essential for successful regeneration. Future studies across different regenerative contexts and species will be key to determine whether reduced chromatin compartmentalization is a conserved feature of injury responses, how changes in genome structure drive transcriptional reprogramming toward regenerative gene expression programs, and the specific contribution of architectural proteins in coordinating tissue repair. Furthermore, advances in single-cell resolution Hi-C technologies will help unravel the dynamics of genome organization across different cell types, and even at the single cell level, within the context of tissue repair.

MATERIALS AND METHODS

Drosophila strains

The following *Drosophila melanogaster* strains were used: w^{1118} (RRID:BDSC_5905), *UAS-rpr* (*51*), *LexO-rpr* and $sal^{E/Pv}$*-LHG* (*52*), $sal^{E/Pv}$*-Gal4* (*33*), and *tub-Gal80*^{TS} (RRID:BDSC_7017), *Df(2L)BSC186* (RRID:BDSC_9614), and *Df(2L)Exel6022* (RRID:BDSC_7506) from the Bloomington Drosophila Stock Center.

Genetic Ablation and Dual Gal4/LexA Transactivation System

Cell death was induced as previously described (*33*, *34*). For Hi-C and DNA-FISH experiments, expression of the proapoptotic gene *reaper* (*rpr*) was driven using $sal^{E/Pv}$*-Gal4* in combination with the

thermosensitive repressor *tub-Gal80^{TS}*. For deficiencies and CRISPR experiments, genetic ablation was induced using *sal$^{E/Pv}$-LHG*, *LexO-rpr* and *tub-Gal80^{TS}* strains. For wing regeneration assays, embryos were maintained at 17 °C until 180 h after egg laying (AEL) to prevent *rpr* expression. They were then shifted to 29 °C for 11 h to induce cell death, and then back to 17 °C until adulthood to check for regenerated wings. To collect wing discs, embryos were kept at 17 °C until the 192 h AEL, then moved to 29 °C for 16 h to induce *rpr*, and wing discs were immediately collected afterwards for processing. Control samples without *rpr* expression were always treated in parallel.

Test for Adult Wing Phenotypes

Adult female flies were fixed in a 1:2 glycerol:ethanol solution for 24 hours. After fixation, wings were dissected in water and subsequently washed with ethanol. The wings were then mounted in 6:5 lactic acid:ethanol and imaged under a Leica DMLB optical microscope. Aberrant wings were classified based on vein defects: strong aberrations were defined as missing veins or multiple defects, while mild aberrations were characterized by missing or extra crossveins. The frequency of regenerated vs non-regenerated wings for each genotype was statistically compared using Fisher's exact test.

CRISPR/Cas9-mediated intergenic anchor deletions

Loop anchors were precisely deleted by CRISPR-Cas9-mediated genome editing using small guide RNAs (sgRNAs) flanking the regions chosen for deletion: *L2$^{\Delta A3}$* and *L3$^{\Delta A5}$*, as previously published (*18*). Males and females harboring independently isolated CRISPR knockout alleles were first crossed to flies carrying either *LexO-rpr* or *sal$^{E/Pv}$-LHG*, *tub-Gal80^{TS}*. The resulting flies were crossed to obtain trans-heterozygous flies, which were analyzed by RT-qPCR or assessed for wing phenotypes.

Hi-C library preparation and sequencing

Hi-C experiments from wing discs were performed in duplicate as previously described (*23*, *53*). Briefly, ~ 200 wing discs for each replicate were quickly dissected (<1 hour) from wandering larvae at room temperature (RT) in Schneider's insect medium before being directly processed. Wing discs were washed twice in PBS and resuspended in A1 Buffer (60 mM KCl, 15 mM NaCl, 4 mM $MgCl_2$, 15 mM HEPES, 0.5% Triton-X-100, 0.5 mM DTT, 1x Protease Inhibitor Cocktail (Sigma-Aldrich), H_2O). Then, formaldehyde was added to reach a 1.8% final concentration and transferred on a rotating wheel for 10 minutes at RT. Formaldehyde was quenched with 1.25 M glycine and samples were washed twice with ice-cold A1 Buffer. Supernatant was discarded and fixed wing discs were air dried and then snapped frozen in liquid nitrogen to process all samples in parallel. For all samples, wing discs were thawed on ice and resuspended in ice-cold A1 Buffer. The samples were homogenized on ice using a tight Tenbroeck, centrifuged and resuspended in 0.5% SDS for 10 min at 62°C to permeabilize nuclei. SDS was quenched by adding Triton-X-100 and incubated for 15 min at 37°C with rotation. Next, samples were resuspended in lysis buffer for a 30 min incubation on ice and nuclei were subjected to Mbo I treatment O/N at 37°C in NEB2.1 buffer. The next day, restriction sites were end-repaired and biotinylated using Klenow [New England BioLabs (NEB), catalog no. M0210] and biotin-14-dATP (Life Technologies, catalog no. 19524-016) before being re-ligated using T4 DNA ligase (NEB, catalog no. M0202) O/N at 16 ºC. Next day, samples were treated with RNAse A for 15 min at 37ºC and then incubated with proteinase K and reverse crosslinked for 6 h at 65°C. Subsequently, DNA was purified using AMPure XP beads (Beckman Coulter^{TM}, catalog no. A63880) and then sheared to obtain fragments of an average size of 300–400 bp using the Bioruptor Pico (Diagenode; 1µg of DNA in 100µl; 6 cycles; 20'' ON, 60'' OFF). For library preparation, biotinylated DNA was pulled down by adding an equal volume of Dynabeads MyOne Streptavidin T1 beads (Life Technologies, catalog no. 65602). Biotin was removed from unligated ends, and pulled-down DNA fragments were end-repaired and A-tailed with NEBNext A-tailing module (E6053L). Illumina adaptors were ligated, and libraries were amplified by eight cycles of PCR using NEBNext High-Fidelity 2X PCR Master Mix (catalog no. M0541S). DNA was size selected using AMPure XP beads (Beckman Coulter^{TM}, catalog no. A63880)

at a ratio of beads to library of 0.9:1 to isolate 300- to 800-bp fragments. Lastly, the quality of the libraries was visualized with the Agilent Bioanalyzer High Sensitivity DNA Assay (Agilent Technologies, Savage, DE) and checked by low sequencing depth on a NextSeq 500 prior to higher sequencing depth on NovaSeq6000 platform at the Centre for Genomic Regulation (CRG) sequencing facility in Barcelona, Spain. A minimum of 500 million paired-end 150-bp-long reads were obtained per sample.

DNA-fluorescent in situ hybridization

DNA-fluorescent in situ hybridization (FISH) was performed as previously described with minor modifications (*18*). Probes were prepared by nick translation. First, 5 kb PCRs from genomic DNA were cloned into a plasmid. Next, 2 µg of miniprep plasmid DNA was nick-translated (Abbott Molecular 07J100-001) following the manufacturer's protocol in the presence of 10 mM aminoallyl-dUTP-XX-ATTO-488 (Jena Bioscience NU-803-XX-488-S) or aminoallyl-dUTP-ATTO-550 (Jena Bioscience NU-803-550-S) at 15ºC for 5 hours, and stored at -20ºC. Prior to DNA-FISH, both probes per two-color DNA-FISH experiment were precipitated separately in the presence of salmon sperm DNA, and resuspended in 100% formamide. Samples were prepared by dissecting L3 larval cuticles in ice-cold PBS 1x and subsequently fixing in 4% formaldehyde for 30 min at RT, washing 3 x PBT, 1 x PBT:MeOH (1:1) and 1 x MeOH, and then were stored in 100% MeOH at -20ºC. Samples were rehydrated in 2xSSCT (30 mM sodium citrate dihydrate pH 7.4, 300 mM NaCl, 0.1% Tween20), treated with RNase A for 30 minutes at RT, washed in 2xSSCT, and permeabilized with PBS-0.5% Triton for 15 min at RT. Next, samples were washed in 2xSSCT, incubated in freshly prepared 0.2 N HCl, washed in 2xSCCT, and incubated for 2 hours in 50% formamide/2xSSCT at 37ºC. DNA-FISH probes in 80% formamide and larval cuticles in 50% formamide/2xSSCT were pre-denatured by incubating 10 min at 80ºC and immediately cooled on ice. Then, probes were mixed with the larval cuticles in 25 µl total of 2xSSC, 10% (w/v) dextran sulfate, 0.1% Tween20, 50% formamide, heated to 80ºC for 10 min, then incubated at 37ºC overnight in the dark. Larval cuticles were then washed in 50% formamide in 2xSSCT (2 x 30 min at 37ºC), 20% formamide in 2xSSCT (20 min at 37ºC), 2xSSCT (2 x 5 min at 37ºC), and 2xSCTT (5 min at RT). Samples were then incubated in PBS, 0.1% Tween20, 1x Western blocking reagent (Sigma 1921673) (BBT buffer) for 30 min at RT and immunostained with anti-lamin (mouse monoclonal clone ADL67.10, Developmental Studies Hybridoma Bank) diluted 1:10 in BBT O/N at 4ºC. Next day, samples were washed in BBT, and then incubated for 1 hour at RT with Alexa 647 anti-mouse IgG (Thermo Fisher A21235) diluted 1:200 in BBT. Samples were washed in PBS with 0.1% Tween-20 (3 x 10 min), and finally mounted with DAPI to stain DNA. Images were acquired on a Leica DMi8 inverted fluorescence microscope using a 63x oil objective and visualized with Fiji software v2.1.0/1.53c. Three independent biological replicates were analyzed for each condition. To quantify the distance between anchors, nuclei were 3D segmented using the lamin channel using Cellpose cyto3 model (*54*). Image preprocessing and detection of individual FISH spots was performed using IMARIS as previously described (Mouginot et al., 2025). Nuclei with only one spot for each channel were selected, and the shortest distance between the center of each DNA-FISH spot (each anchor) was 3D measured, considering <250 nm as interacting loci (*37*). Statistical analysis was performed in R using the Shapiro-Wilk test to assess normality, followed by a Mann-Whitney U test to compare between control and regeneration.

Hi-C data analysis

Hi-C data production, from raw FASTQ files through to interaction matrices, was conducted using the TADbit pipeline (*55*). The workflow began with quality control checks on the raw FASTQ data. Sequencing reads were then mapped using the GEM mapper (*56*) to the *Drosophila melanogaster* reference genome (dm6). Mapping was done using an iterative alignment strategy (*57*). Following mapping, reads were subjected to a series of filters to eliminate artifacts, such as non-specific ligations, sequencing errors, and other experimental anomalies. Specifically, TADbit's default filtering applied nine distinct criteria: self-circles, dangling ends, errors, extra dangling ends, over-represented fragments, overly short or long fragments, duplicates, and random breaks. Next, the data were

normalized using the ICE (Iterative Correction and Eigenvector decomposition) balancing method (*57*). The resulting valid read pairs were binned at multiple resolutions (2kb, 4kb, 5kb, 8kb, 10kb, 20kb, 25kb, 50kb, 100kb, 500kb, 1Mb), with normalization biases and decay corrections incorporated to construct interaction matrices. Table S2 summarizes the number of valid read pairs, and the quantity of reads filtered out per replicate. Replicate datasets were compared and merged using TADbit's merging function, which incorporates the HiCRep similarity score (*58*).

A/B compartment analysis

A/B compartments were identified as previously proposed (*4*) in 10 kb normalized hi-c matrices using cooltools (*59*) and cooler (*60*). Each individual chromosome arm was analyzed separately and bins around centromeres were excluded (*45*) (chr2L:1-22,170,000; chr2R: 5,650,000-25,286,936; chr3L:0-22,900,000; chr3L: 4,200,000-32,080,000; chrX:0-23,542,271). The first eigenvector of the correlation matrix was obtained by principal component analysis of the observed-over-expected matrix. Bins with positive eigenvector values were assigned to A and bins with negative values to B compartments. The saddle plots were generated using cooltools and show the interaction frequency of intra- or inter-compartments, representing the compartment strength or level of compartmentalization for each condition.

Insulation analysis

Insulation scores were calculated in the 8 kb normalized, merged matrices using FAN-C (*61*) (parameters: window size 80 kb, threshold 0.4). Bins around centromeres were excluded (*45*). Bedtools intersect function was used to assess which boundaries were present or absent in control and regeneration.

Meta-loop analysis

Meta-loops were called by applying the loop calling algorithm from the meta-loops-22 repository (available at https://github.com/gambettalab/meta-loops-2022/) (*18*). As the input, we used the balanced Hi-C interaction matrix for REG and CTRL conditions in .mcool format, and set the following parameters: *resolution=2000*, *score-tresh=35*, *clustering-distance=3*. Then, we intersected the called meta-loops in each condition to get a single matrix containing the coordinates of all identified meta-loops. After manual curation, we filtered out meta-loops shorter than 1 Mb. The final list of identified meta-loops is shown in Table S1.

For differential loop strength analysis, we used a non-parametric, bootstrapping-based approach. We generated 10,000 randomly shifted loops preserving the same loop sizes of the original identified meta-loops. For each condition, the strength of both real and random loops was calculated as the total number of Hi-C contacts (raw counts) of the 12 kb window centered on the 2 kb bin containing the summit of both meta-loop anchors. For each loop, we computed the $\log_2$ fold change (log2FC) of contact strength between conditions (REG/CTRL), using a pseudo-count of 1. We used the log2FC distribution of random loops to construct the empirical null distribution. Then, we calculated the empirical two-sided *p*-values for each real loop by comparing its absolute log2FC to the null distribution.

RNA-seq library preparation and sequencing

Embryos of the appropriate genotypes were maintained at 17 °C until 192 h AEL. They were then shifted to 29 °C for 16 h to induce *rpr* expression. Third-instar larvae (L3) from the following genotypes were selected: (1) *w⁻; +; sal$^{E/Pv}$-LHG:tub-Gal80^{TS}/lexO-rpr*, (2) *w⁻; Df(2L)BSC186/+*; *sal$^{E/Pv}$-LHG:tub-Gal80^{TS}/lexO-rpr*, (3) *w⁻; Df(2L)Exel6022/+*; *sal$^{E/Pv}$-LHG:tub-Gal80^{TS}/lexO-rpr*, and (4) *w⁻; Df(2L)BSC186/Df(2L)Exel6022*; *sal$^{E/Pv}$-LHG:tub-Gal80^{TS}/lexO-rpr*. 40 wing discs per sample were dissected in cold Schneider's medium. The Quick-RNA Microprep kit (Zymo Research) was used following manufacturer's instructions, including a 15-minute DNase incubation, to isolate the RNA. The

purity and concentration of the resulting RNA were assessed using Nanodrop (Thermo Fisher Scientific) and Bioanalyzer (Agilent Technologies).

For the library preparation, 500 ng of total RNA were used for reverse transcription. Ribosomal RNA (rRNA) was depleted by using poly-A selection. All libraries were sequenced on an Illumina NextSeq2000 sequencer, using 50-bp paired-end reads. Library preparation and sequencing were performed at the Genomics Unit of the Center for Genomic Regulation (CRG).

RNA-seq data analysis

Reads were aligned to the *Drosophila melanogaster* dm6 genome using STAR v2.7.10b (*62*), with up to 4 mismatches per alignment, using the FlyBase genome annotation version r6.62. Reads mapping to more than 10 loci were discarded. Gene expression was quantified in the number of counts using the featureCounts function from the Rsubread package v2.22.1 (*63*) in R. Genes whose sum of counts in all replicates was lower than 10 were discarded. The principal component analysis (PCA) and the Pearson correlation coefficient matrix of each replicate is shown in Fig. S3A-B.

Differential gene expression was analyzed using DESeq2 package v1.40.2 (*64*) in R. Only genes with at least 1 transcript per million (TPM) in at least one sample were selected for the differential expression analysis. A generalized linear model was fitted with the design formula ~ condition, where condition is a factor with 4 levels corresponding to each genotype. The control genotype (*w^-; +; sal$^{E/Pv}$-LHG:tub-Gal80^{TS}/lexO-rpr*) was used as the reference level, and differential expression was assessed by comparing each of the other genotypes to the reference. The Benjamini-Hochberg method was used to adjust *p*-values for multiple testing. All genes with an absolute fold change > 2 and an adjusted *p*-value < 0.05 were considered differentially expressed.

RT-qPCR on wing discs

RNA extraction and purification for quantitative PCR (qPCR) analysis was performed following the same protocol previously described for the RNA-seq. A total of 1 µg of RNA was used as a template for cDNA synthesis using the Moloney Murine Leukemia Virus reverse transcriptase (M-MLV RT) (Invitrogen).

Reactions containing FastStart Universal SYBR Green Master (Rox) (Roche) and the appropriate cDNA and primers were run in a 7500 Real-Time PCR System (Applied Biosystems). Gene expression was normalized to the levels of *sply*, and fold changes were calculated using the ddCt method. Statistical significance was assessed using Student's *t*-tests, with *p*-values adjusted for multiple comparisons via the False Discovery Rate (FDR) approach. For each reaction, three technical replicates were used, and three independent biological replicates were collected for each experiment. The designed primer sequences are shown in Table S3.

REFERENCES

1. Y. B. Schwartz, G. Cavalli, Three-Dimensional Genome Organization and Function in *Drosophila*. *Genetics* **205**, 5–24 (2017).
2. B. van Steensel, E. E. M. Furlong, The role of transcription in shaping the spatial organization of the genome. *Nat. Rev. Mol. Cell Biol.* **20**, 327–337 (2019).
3. T. Misteli, The Self-Organizing Genome: Principles of Genome Architecture and Function. *Cell* **183**, 28–45 (2020).
4. E. Lieberman-Aiden, N. L. Van Berkum, L. Williams, M. Imakaev, T. Ragoczy, A. Telling, I. Amit, B. R. Lajoie, P. J. Sabo, M. O. Dorschner, R. Sandstrom, B. Bernstein, M. A. Bender, M. Groudine, A. Gnirke, J. Stamatoyannopoulos, L. A. Mirny, E. S. Lander, J. Dekker, Comprehensive Mapping of Long-Range Interactions Reveals Folding Principles of the Human Genome. *Science* **326**, 289–293 (2009).

5. T. Sexton, E. Yaffe, E. Kenigsberg, F. Bantignies, B. Leblanc, M. Hoichman, H. Parrinello, A. Tanay, G. Cavalli, Three-Dimensional Folding and Functional Organization Principles of the Drosophila Genome. *Cell* **148**, 458–472 (2012).

6. S. S. P. Rao, M. H. Huntley, N. C. Durand, E. K. Stamenova, I. D. Bochkov, J. T. Robinson, A. L. Sanborn, I. Machol, A. D. Omer, E. S. Lander, E. L. Aiden, A 3D Map of the Human Genome at Kilobase Resolution Reveals Principles of Chromatin Looping. *Cell* **159**, 1665–1680 (2014).

7. B. Bonev, G. Cavalli, Organization and function of the 3D genome. *Nat. Rev. Genet.* **17**, 661–678 (2016).

8. E. P. Nora, B. R. Lajoie, E. G. Schulz, L. Giorgetti, I. Okamoto, N. Servant, T. Piolot, N. L. Van Berkum, J. Meisig, J. Sedat, J. Gribnau, E. Barillot, N. Blüthgen, J. Dekker, E. Heard, Spatial partitioning of the regulatory landscape of the X-inactivation centre. *Nature* **485**, 381–385 (2012).

9. M. J. Rowley, M. H. Nichols, X. Lyu, M. Ando-Kuri, I. S. M. Rivera, K. Hermetz, P. Wang, Y. Ruan, V. G. Corces, Evolutionarily Conserved Principles Predict 3D Chromatin Organization. *Mol. Cell* **67**, 837-852.e7 (2017).

10. Q. Szabo, D. Jost, J.-M. Chang, D. I. Cattoni, G. L. Papadopoulos, B. Bonev, T. Sexton, J. Gurgo, C. Jacquier, M. Nollmann, F. Bantignies, G. Cavalli, TADs are 3D structural units of higher-order chromosome organization in *Drosophila*. *Sci. Adv.* **4**, eaar8082 (2018).

11. S. V. Ulianov, V. V. Zakharova, A. A. Galitsyna, P. I. Kos, K. E. Polovnikov, I. M. Flyamer, E. A. Mikhaleva, E. E. Khrameeva, D. Germini, M. D. Logacheva, A. A. Gavrilov, A. S. Gorsky, S. K. Nechaev, M. S. Gelfand, Y. S. Vassetzky, A. V. Chertovich, Y. Y. Shevelyov, S. V. Razin, Order and stochasticity in the folding of individual Drosophila genomes. *Nat. Commun.* **12**, 41 (2021).

12. P. Llorens-Giralt, C. Camilleri-Robles, M. Corominas, P. Climent-Cantó, Chromatin Organization and Function in Drosophila. *Cells* **10**, 2362 (2021).

13. S. Denaud, G. Sabarís, M. Di Stefano, G.-L. Papadopoulos, B. Schuettengruber, G. Cavalli, Determining the functional relationship between epigenetic and physical chromatin domains in Drosophila. *Genome Biol.* **26**, 116 (2025).

14. A. L. Sanborn, S. S. P. Rao, S.-C. Huang, N. C. Durand, M. H. Huntley, A. I. Jewett, I. D. Bochkov, D. Chinnappan, A. Cutkosky, J. Li, K. P. Geeting, A. Gnirke, A. Melnikov, D. McKenna, E. K. Stamenova, E. S. Lander, E. L. Aiden, Chromatin extrusion explains key features of loop and domain formation in wild-type and engineered genomes. *Proc. Natl. Acad. Sci.* **112** (2015).

15. F. Ramírez, V. Bhardwaj, L. Arrigoni, K. C. Lam, B. A. Grüning, J. Villaveces, B. Habermann, A. Akhtar, T. Manke, High-resolution TADs reveal DNA sequences underlying genome organization in flies. *Nat. Commun.* **9**, 189 (2018).

16. A. Kaushal, J. Dorier, B. Wang, G. Mohana, M. Taschner, P. Cousin, P. Waridel, C. Iseli, A. Semenova, S. Restrepo, N. Guex, E. L. Aiden, M. C. Gambetta, Essential role of Cp190 in physical and regulatory boundary formation. *Sci. Adv.* **8**, eabl8834 (2022).

17. S. Zunjarrao, M. C. Gambetta, Principles of long-range gene regulation. *Curr. Opin. Genet. Dev.* **91**, 102323 (2025).

18. G. Mohana, J. Dorier, X. Li, M. Mouginot, R. C. Smith, H. Malek, M. Leleu, D. Rodriguez, J. Khadka, P. Rosa, P. Cousin, C. Iseli, S. Restrepo, N. Guex, B. D. McCabe, A. Jankowski, M. S. Levine, M. C. Gambetta, Chromosome-level organization of the regulatory genome in the Drosophila nervous system. *Cell* **186**, 3826-3844.e26 (2023).

19. M. Mouginot, S. Hani, P. Cousin, J. Dorier, A. Ravera, M. C. Gambetta, A boundary-defining protein facilitates megabase-scale regulatory chromosomal loop formation in *Drosophila* neurons. *Genes Dev.*, genesdev;gad.352646.125v1 (2025).

20. M. Levo, J. Raimundo, X. Y. Bing, Z. Sisco, P. J. Batut, S. Ryabichko, T. Gregor, M. S. Levine, Transcriptional coupling of distant regulatory genes in living embryos. *Nature* **605**, 754–760 (2022).

21. T. Pollex, R. Marco-Ferreres, L. Ciglar, Y. Ghavi-Helm, A. Rabinowitz, R. R. Viales, C. Schaub, A. Jankowski, C. Girardot, E. E. M. Furlong, Chromatin gene-gene loops support the cross-regulation of genes with related function. *Mol. Cell* **84**, 822-838.e8 (2024).

22. Y. Ogiyama, B. Schuettengruber, G. L. Papadopoulos, J.-M. Chang, G. Cavalli, Polycomb-Dependent Chromatin Looping Contributes to Gene Silencing during Drosophila Development. *Mol. Cell* **71**, 73-88.e5 (2018).

23. V. Loubiere, G. L. Papadopoulos, Q. Szabo, A.-M. Martinez, G. Cavalli, Widespread activation of developmental gene expression characterized by PRC1-dependent chromatin looping. *Sci. Adv.* **6**, eaax4001 (2020).

24. F. Paldi, G. Cavalli, 3D genome folding in epigenetic regulation and cellular memory. *Trends Cell Biol.*,

S0962892425000650 (2025).

25. J. A. Goldman, K. D. Poss, Gene regulatory programmes of tissue regeneration. *Nat. Rev. Genet.* **21**, 511–525 (2020).

26. X. Jia, W. Lin, W. Wang, Regulation of chromatin organization during animal regeneration. *Cell Regen.* **12**, 19 (2023).

27. E. Vizcaya-Molina, C. C. Klein, F. Serras, R. K. Mishra, R. Guigó, M. Corominas, Damage-responsive elements in *Drosophila* regeneration. *Genome Res.* **28**, 1852–1866 (2018).

28. E. Vizcaya-Molina, C. C. Klein, F. Serras, M. Corominas, Chromatin dynamics in regeneration epithelia: Lessons from Drosophila imaginal discs. *Semin. Cell Dev. Biol.* **97**, 55–62 (2020).

29. I. K. Hariharan, F. Serras, Imaginal disc regeneration takes flight. *Curr. Opin. Cell Biol.* **48**, 10–16 (2017).

30. R. Martín, G. Morata, Regenerative response of different regions of Drosophila imaginal discs. *Int. J. Dev. Biol.* **62**, 507–512 (2018).

31. B. K. Tripathi, K. D. Irvine, The wing imaginal disc. *Genetics* **220**, iyac020 (2022).

32. R. E. Harris, M. J. Stinchfield, S. L. Nystrom, D. J. McKay, I. K. Hariharan, Damage-responsive, maturity-silenced enhancers regulate multiple genes that direct regeneration in Drosophila. *eLife* **9**, e58305 (2020).

33. C. Bergantiños, M. Corominas, F. Serras, Cell death-induced regeneration in wing imaginal discs requires JNK signalling. *Development* **137**, 1169–1179 (2010).

34. A. Repiso, C. Bergantiños, F. Serras, Cell fate respecification and cell division orientation drive intercalary regeneration in *Drosophila* wing discs. *Development* **140**, 3541–3551 (2013).

35. C. Camilleri-Robles, R. Amador, M. Tiebe, A. A. Teleman, F. Serras, R. Guigó, M. Corominas, Long non-coding RNAs involved in *Drosophila* development and regeneration. *NAR Genomics Bioinforma.* **6**, lqae091 (2024).

36. K. P. Eagen, Principles of Chromosome Architecture Revealed by Hi-C. *Trends Biochem. Sci.* **43**, 469–478 (2018).

37. E. H. Finn, G. Pegoraro, H. B. Brandão, A.-L. Valton, M. E. Oomen, J. Dekker, L. Mirny, T. Misteli, Extensive Heterogeneity and Intrinsic Variation in Spatial Genome Organization. *Cell* **176**, 1502-1515.e10 (2019).

38. X. Li, X. Tang, X. Bing, C. Catalano, T. Li, G. Dolsten, C. Wu, M. Levine, GAGA-associated factor fosters loop formation in the Drosophila genome. *Mol. Cell* **83**, 1519-1526.e4 (2023).

39. K. T. Chathoth, L. A. Mikheeva, G. Crevel, J. C. Wolfe, I. Hunter, S. Beckett-Doyle, S. Cotterill, H. Dai, A. Harrison, N. R. Zabet, The role of insulators and transcription in 3D chromatin organization of flies. *Genome Res.* **32**, 682–698 (2022).

40. S. Cuartero, U. Fresan, O. Reina, E. Planet, M. L. Espinas, Ibf1 and Ibf2 are novel CP190-interacting proteins required for insulator function. *EMBO J.* **33**, 637–647 (2014).

41. N. E. Vorobyeva, A. N. Krasnov, M. Erokhin, D. Chetverina, M. Mazina, Su(Hw) interacts with Combgap to establish long-range chromatin contacts. *Epigenetics Chromatin* **17**, 17 (2024).

42. C.-Y. Pai, E. P. Lei, D. Ghosh, V. G. Corces, The Centrosomal Protein CP190 Is a Component of the gypsy Chromatin Insulator. *Mol. Cell* **16**, 737–748 (2004).

43. C. Cubeñas-Potts, M. J. Rowley, X. Lyu, G. Li, E. P. Lei, V. G. Corces, Different enhancer classes in Drosophila bind distinct architectural proteins and mediate unique chromatin interactions and 3D architecture. *Nucleic Acids Res.* **45**, 1714–1730 (2017).

44. I. Bag, S. Chen, L. F. Rosin, Y. Chen, C.-Y. Liu, G.-Y. Yu, E. P. Lei, M1BP cooperates with CP190 to activate transcription at TAD borders and promote chromatin insulator activity. *Nat. Commun.* **12**, 4170 (2021).

45. A. Kaushal, G. Mohana, J. Dorier, I. Özdemir, A. Omer, P. Cousin, A. Semenova, M. Taschner, O. Dergai, F. Marzetta, C. Iseli, Y. Eliaz, D. Weisz, M. S. Shamim, N. Guex, E. Lieberman Aiden, M. C. Gambetta, CTCF loss has limited effects on global genome architecture in Drosophila despite critical regulatory functions. *Nat. Commun.* **12**, 1011 (2021).

46. A. Tonelli, P. Cousin, A. Jankowski, B. Wang, J. Dorier, J. Barraud, S. Zunjarrao, M. C. Gambetta, Systematic screening of enhancer-blocking insulators in Drosophila identifies their DNA sequence determinants. *Dev. Cell* **60**, 630-645.e9 (2025).

47. L. Li, X. Lyu, C. Hou, N. Takenaka, H. Q. Nguyen, C.-T. Ong, C. Cubeñas-Potts, M. Hu, E. P. Lei, G. Bosco, Z. S. Qin, V. G. Corces, Widespread Rearrangement of 3D Chromatin Organization Underlies Polycomb-Mediated Stress-Induced Silencing. *Mol. Cell* **58**, 216–231 (2015).

48. R. Amat, R. Böttcher, F. Le Dily, E. Vidal, J. Quilez, Y. Cuartero, M. Beato, E. de Nadal, F. Posas, Rapid reversible changes in compartments and local chromatin organization revealed by hyperosmotic shock. *Genome Res.* **29**, 18–28 (2019).

49. J. Ray, P. R. Munn, A. Vihervaara, J. J. Lewis, A. Ozer, C. G. Danko, J. T. Lis, Chromatin conformation remains stable upon extensive transcriptional changes driven by heat shock. *Proc. Natl. Acad. Sci.* **116**, 19431–19439 (2019).

50. P. J. Batut, X. Y. Bing, Z. Sisco, J. Raimundo, M. Levo, M. S. Levine, Genome organization controls transcriptional dynamics during development. *Science* **375**, 566–570 (2022).

51. J. P. Wing, L. Zhou, L. M. Schwartz, J. R. Nambu, Distinct cell killing properties of the Drosophila reaper, head involution defective, and grim genes. *Cell Death Differ.* **5**, 930–939 (1998).

52. P. Santabárbara-Ruiz, M. López-Santillán, I. Martínez-Rodríguez, A. Binagui-Casas, L. Pérez, M. Milán, M. Corominas, F. Serras, ROS-Induced JNK and p38 Signaling Is Required for Unpaired Cytokine Activation during Drosophila Regeneration. *PLOS Genet.* **11**, e1005595 (2015).

53. K. Viets, M. E. G. Sauria, C. Chernoff, R. Rodriguez Viales, M. Echterling, C. Anderson, S. Tran, A. Dove, R. Goyal, L. Voortman, A. Gordus, E. E. M. Furlong, J. Taylor, R. J. Johnston, Characterization of Button Loci that Promote Homologous Chromosome Pairing and Cell-Type-Specific Interchromosomal Gene Regulation. *Dev. Cell* **51**, 341-356.e7 (2019).

54. C. Stringer, T. Wang, M. Michaelos, M. Pachitariu, Cellpose: a generalist algorithm for cellular segmentation. *Nat. Methods* **18**, 100–106 (2021).

55. F. Serra, D. Baù, M. Goodstadt, D. Castillo, G. J. Filion, M. A. Marti-Renom, Automatic analysis and 3D-modelling of Hi-C data using TADbit reveals structural features of the fly chromatin colors. *PLoS Comput. Biol.* **13**, e1005665 (2017).

56. S. Marco-Sola, M. Sammeth, R. Guigó, P. Ribeca, The GEM mapper: fast, accurate and versatile alignment by filtration. *Nat. Methods* **9**, 1185–1188 (2012).

57. M. Imakaev, G. Fudenberg, R. P. McCord, N. Naumova, A. Goloborodko, B. R. Lajoie, J. Dekker, L. A. Mirny, Iterative correction of Hi-C data reveals hallmarks of chromosome organization. *Nat. Methods* **9**, 999–1003 (2012).

58. T. Yang, F. Zhang, G. G. Yardımcı, F. Song, R. C. Hardison, W. S. Noble, F. Yue, Q. Li, HiCRep: assessing the reproducibility of Hi-C data using a stratum-adjusted correlation coefficient. *Genome Res.* **27**, 1939–1949 (2017).

59. Open2C, N. Abdennur, S. Abraham, G. Fudenberg, I. M. Flyamer, A. A. Galitsyna, A. Goloborodko, M. Imakaev, B. A. Oksuz, S. V. Venev, Y. Xiao, Cooltools: Enabling high-resolution Hi-C analysis in Python. *PLOS Comput. Biol.* **20**, e1012067 (2024).

60. N. Abdennur, L. A. Mirny, Cooler: scalable storage for Hi-C data and other genomically labeled arrays. *Bioinformatics* **36**, 311–316 (2020).

61. K. Kruse, C. B. Hug, J. M. Vaquerizas, FAN-C: a feature-rich framework for the analysis and visualisation of chromosome conformation capture data. *Genome Biol.* **21**, 303 (2020).

62. A. Dobin, C. A. Davis, F. Schlesinger, J. Drenkow, C. Zaleski, S. Jha, P. Batut, M. Chaisson, T. R. Gingeras, STAR: ultrafast universal RNA-seq aligner. *Bioinformatics* **29**, 15–21 (2013).

63. Y. Liao, G. K. Smyth, W. Shi, The R package Rsubread is easier, faster, cheaper and better for alignment and quantification of RNA sequencing reads. *Nucleic Acids Res.* **47**, e47–e47 (2019).

64. M. I. Love, W. Huber, S. Anders, Moderated estimation of fold change and dispersion for RNA-seq data with DESeq2. *Genome Biol.* **15**, 550 (2014).

Acknowledgements

We thank A. Crespo, J. Khadka and S. Hani for experimental help and the CRG Genomics Unit for assistance with sequencing.

Funding

PID2021-123300NB-100 from MCIN/ AEI / 10.13039/501100011033 / FEDER, UE (FS, MC.). 2021SGR00293 from the Agency for the Management of University and Research Grants (Generalitat de Catalunya) (MC). FPU20/01473 from the Spanish Ministerio de Universidades (PLG). PID2023-151484NB-I00 from MCIN/AEI (MAM-R). 2021SGR01127 from the Agency for the Management of University and Research Grants (Generalitat de Catalunya) (MAM-R).

Author contributions
PLG, CCR, MAM-R and MC conceived and designed the experiments. PLG, MMM and CCR performed the experiments. PLG, CCR, and MAM-R analysed the data. PLG, CCR and MC wrote the manuscript. PLG, CCR, FS, MAM-R and MC revised the manuscript. FS, MAM-R, and MC acquired the funding.

Competing interests
The authors declare no competing interests.

Data and materials availability
The Hi-C and RNA-seq raw and processed data from this study will be available at NCBI Gene Expression Omnibus. Other datasets and their accession numbers are available in Table S4.

SUPPLEMENTARY MATERIALS

Figures S1 to S5
Tables S1 to S4

SUPPLEMENTARY MATERIALS

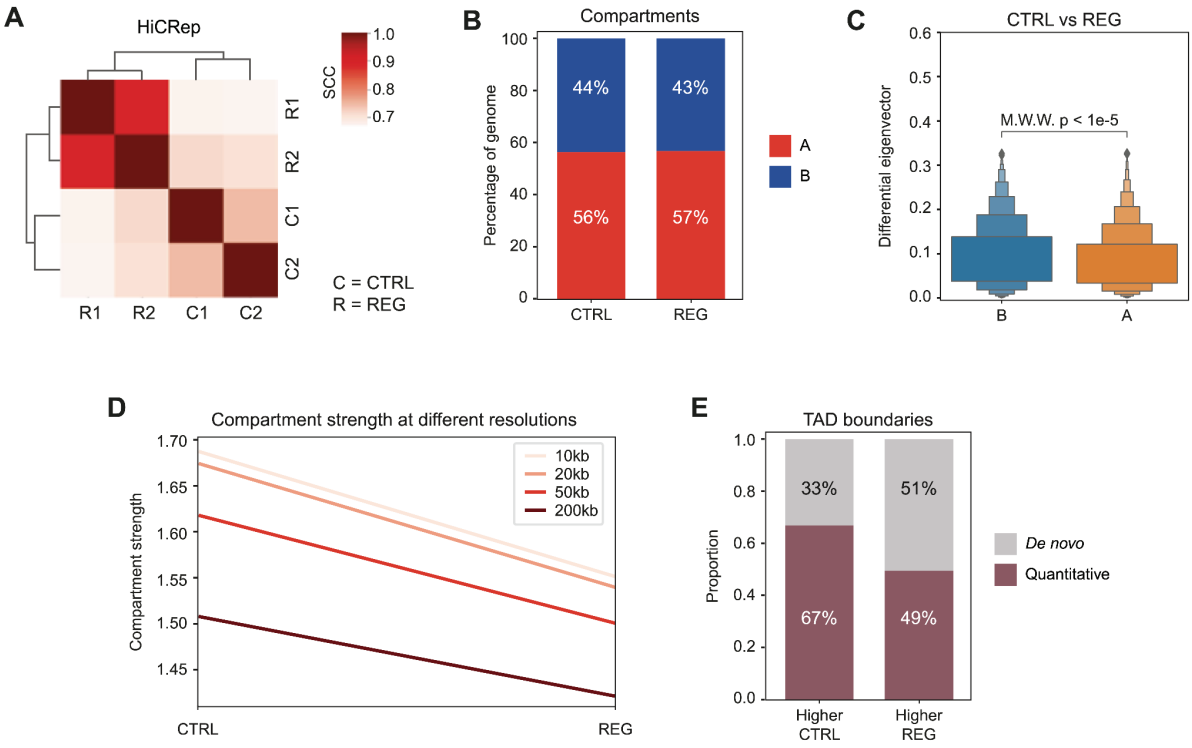

Figure S1. Genome-wide AB compartment and boundary insulation analysis.
(A) Sample correlation analysis using HiCRep. Stratum-adjusted correlation coefficients (SCC) are shown for each pairwise Hi-C comparison. **(B)** Genome-wide proportions of A and B compartments in control and regenerating discs. **(C)** Differential eigenvector values (control vs. regeneration) for regions assigned to A or B compartments. **(D)** Compartment strength measured at multiple resolutions in control and regeneration conditions. **(E)** Proportion of topologically associating domain (TAD) boundaries classified as either *de novo* or quantitative, showing increased insulation in control (Higher CTRL) or in regeneration (Higher REG).

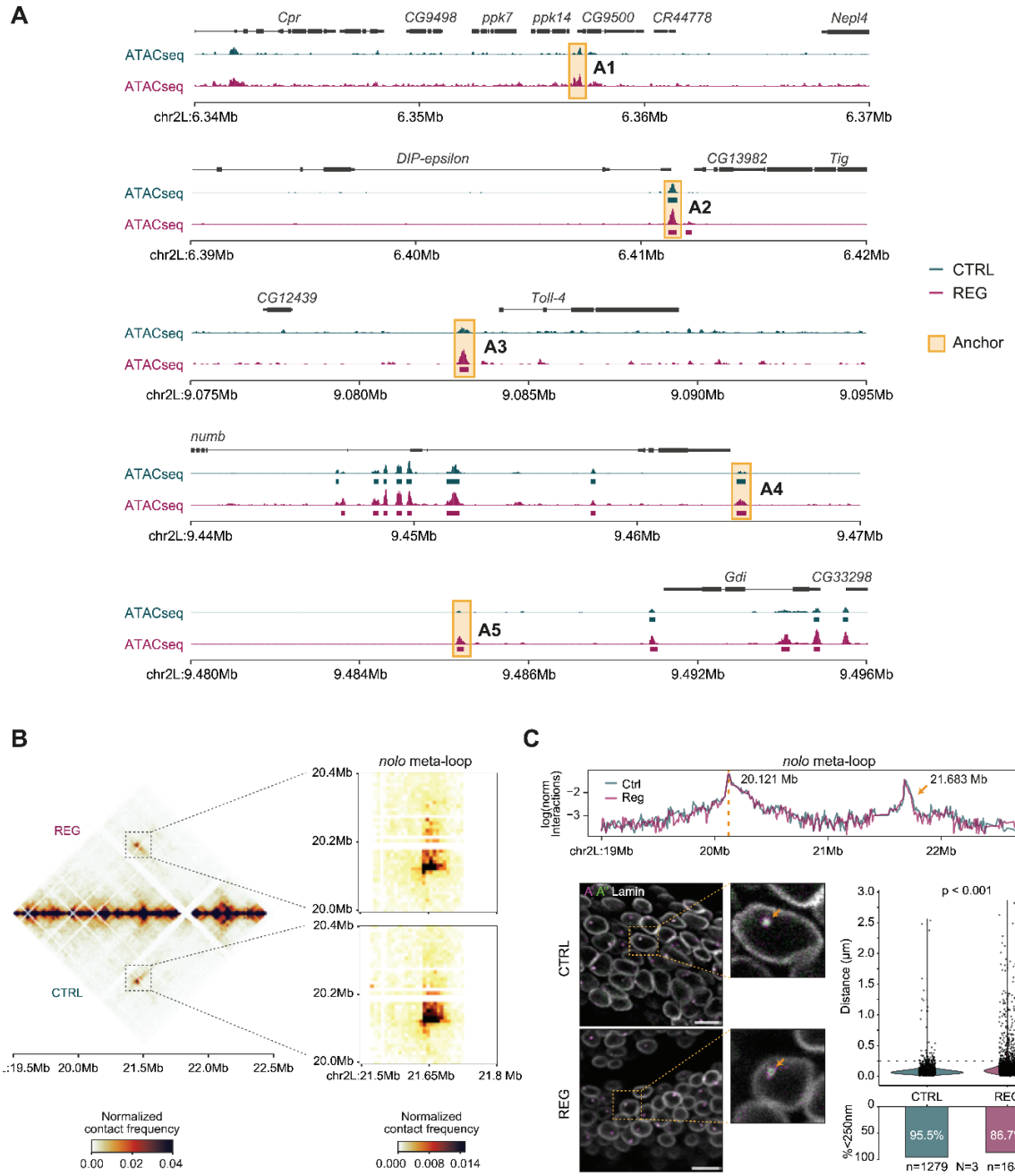

(legend on next page)

Figure S2. Mapping of meta-loop anchors and *nolo* meta-loop.
(A) Genome browser tracks showing gene annotations and ATAC-seq signal intensities in control and regenerating wing discs (*27*) at each meta-loop anchor region. The ATAC-seq peak assigned as the loop anchor is highlighted in yellow. **(B)** Mirror plot of normalized Hi-C contact maps for regeneration (top) and control (bottom), centered on the *nolo* meta-loop region. **(C)** Top: Virtual 4C plots using Hi-C data from regeneration and control samples, with the intergenic anchor (chr2L: 20.121Mb) as the bait to detect the loop with the *nolo* promoter (chr2L: 21.683Mb). Bottom left: Representative DNA-FISH images of wing discs labeled with probes targeting each *nolo* loop anchor. Lamin staining (white) marks the nuclear lamina. Bottom right: Quantification of DNA-FISH distances (in μm) for the *nolo* loop is shown as violin plots. The percentage of nuclei with distances <250 nm is indicated below. *n* denotes the number of nuclei analyzed; *N* indicates the number of biological replicates. **(D)** Gene expression levels ($\log_{10}$[TPM + 0.1]) for genes located within meta-TADs in control and regenerating wing discs. Differentially expressed genes are shown in bold. The schematic below indicates meta-TAD boundaries and anchor positions.

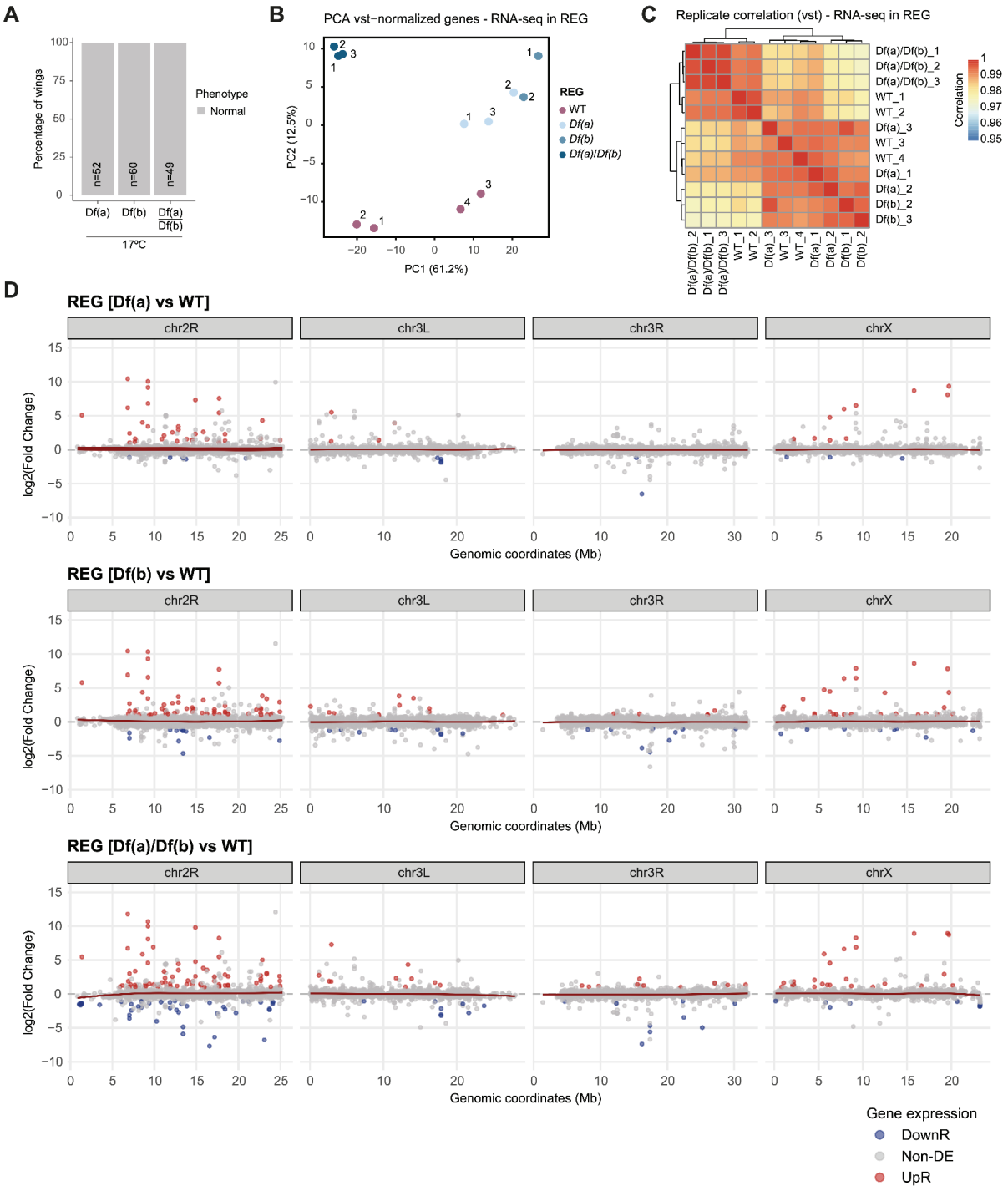

Figure S3. Transcriptomic effects of meta-loop anchor disruption during regeneration.
(A) Proportion of adult wings in heterozygous and trans-heterozygous deficiency flies under normal conditions (17ºC). A representative image is shown to the right. **(B)** Principal Component Analysis (PCA) on the vst-normalized gene expression values during regeneration in wild-type (WT) or heterozygous flies carrying either single deficiencies or both deficiencies in trans. **(C)** Pearson correlation coefficient matrix of RNA-seq samples. **(D)** Scatter plots of gene expression changes log_2(fold change) for each mutant compared to wild-type during regeneration, separated by chromosome. Upregulated genes are shown in red, downregulated in blue.

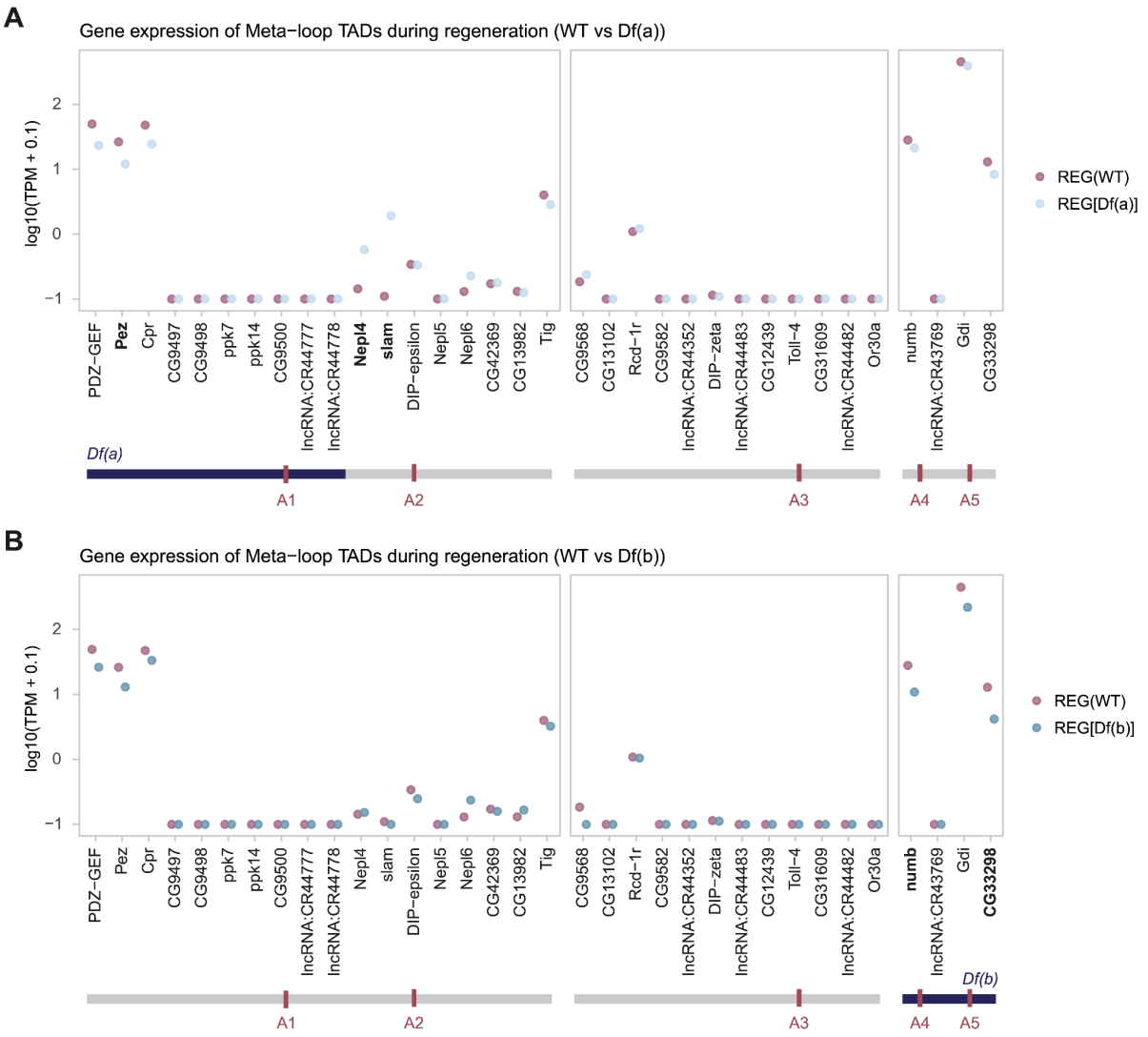

Figure S4. Gene expression during regeneration within meta-TADs in single deficiency flies.
(A) Gene expression levels (log_{10}[TPM + 0.1]) for genes located within meta-TADs in wild-type and *Df(a)* heterozygous flies during regeneration. Differentially expressed genes are in bold. Schematic below indicates meta-TAD boundaries, loop anchors, and the location of *Df(a)*. **(B)** Same as (A) for *Df(b)* heterozygous flies.

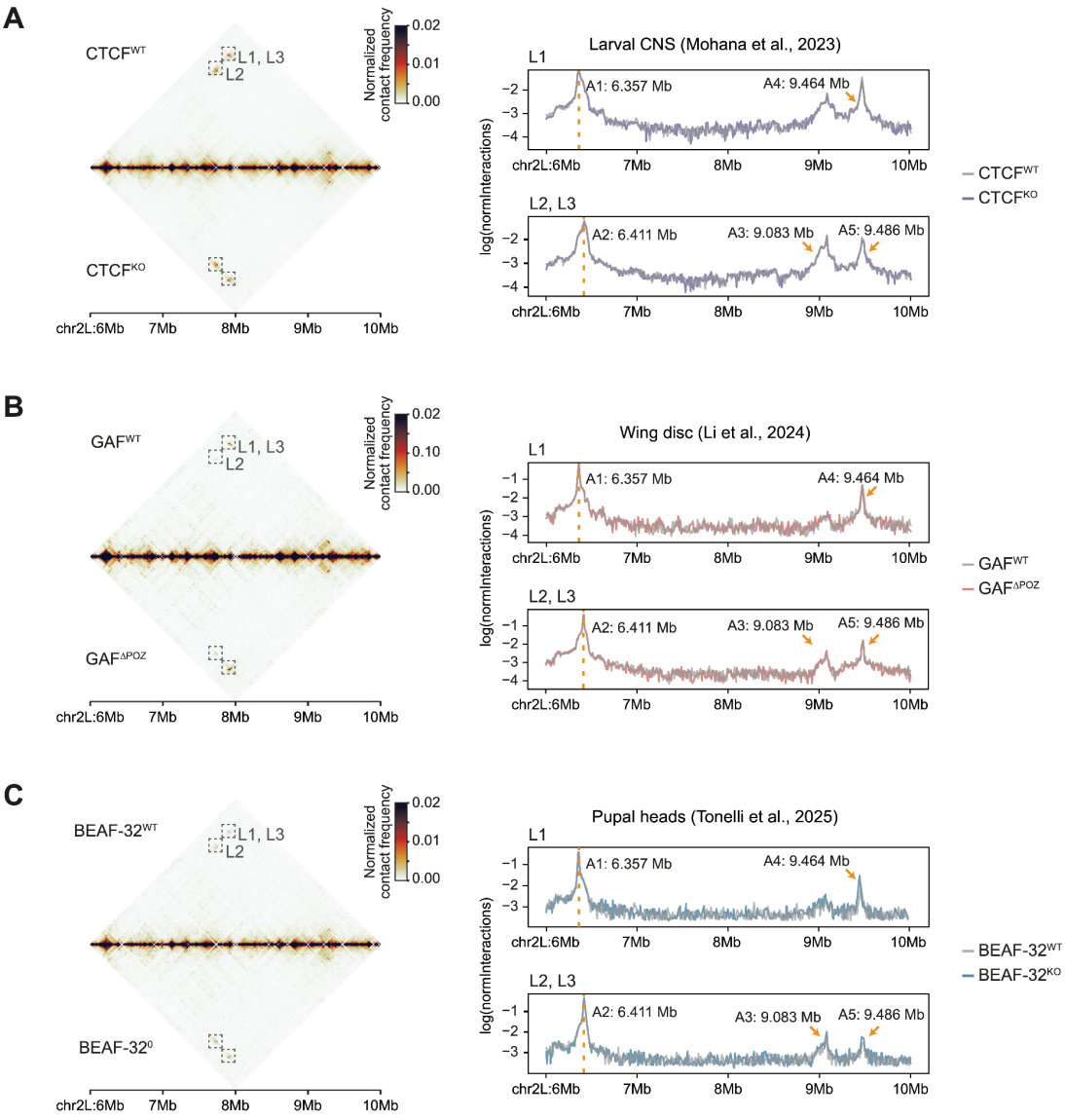

Figure S5. CTCF and GAF are not required for meta-loop formation.
(A) Hi-C contact map analysis of larval central nervous system tissue from wild-type (top) and *CTCF*^{KO} (bottom) flies (*18*). Left*:* Mirror plot of normalized Hi-C contact maps for chromosome 2L (6–10 Mb). Right*:* Virtual 4C plots using A1 as bait to visualize loop L1 (top) and A2 to detect loops L2 and L3 (bottom). Loop anchor coordinates are indicated. **(B)** Same as (A) but comparing wild-type (top) and *GAF* mutant (bottom) wing discs (*38*). **(C)** Same as (A) but comparing wild-type (top) and BEAF-32-deficient (maternal depletion and knockout, *BEAF-32*^{0}) (bottom) pupal heads (*46*).

Table S1. Meta-loops identified in the wing discs using the loop calling algorithm from Mohana *et al*. 2023. Strength differences between control and regeneration (log2FC) and the associated *p*-values are shown.

Loop ID	chr1	start1	end1	chr2	start2	end2	log2FC	p-val
L1	chr2L	6354000	6356000	chr2L	9464000	9466000	2.265	0.019
L2	chr2L	6398000	6400000	chr2L	9082000	9084000	0.918	0.413
L3	chr2L	6410000	6412000	chr2L	9484000	9486000	2.392	0.008
L4	chr2L	13346000	13348000	chr2L	20242000	20244000	-1.000	0.413
L5	chr2L	20122000	20124000	chr2L	21684000	21686000	-0.046	0.636
L6	chr2L	20218000	20220000	chr2L	21708000	21710000	0.000	1.000
L7	chr2L	20238000	20240000	chr2L	21702000	21704000	1.000	0.413
L8	chr2R	36000	38000	chr2R	5280000	5282000	-1.000	0.413
L9	chr2R	2000000	2002000	chr2R	3594000	3596000	1.344	0.142
L10	chr2R	8796000	8798000	chr2R	15054000	15056000	0.474	0.554
L11	chr2R	8848000	8850000	chr2R	15070000	15072000	0.000	1.000
L12	chr3L	7646000	7648000	chr3L	17248000	17250000	0.322	0.611
L13	chr3L	12858000	12860000	chr3L	18720000	18722000	-0.379	0.598
L14	chr3L	23148000	23150000	chr3L	27156000	27158000	1.138	0.173
L15	chr3L	23324000	23326000	chr3L	27150000	27152000	0.788	0.421
L16	chr3L	24630000	24632000	chr3L	27070000	27072000	1.263	0.166
L17	chr3R	3056000	3058000	chr3R	11918000	11920000	-1.547	0.138
L18	chr3R	4078000	4080000	chr3R	7778000	7780000	0.441	0.554
L19	chr3R	4290000	4292000	chr3R	7648000	7650000	-0.585	0.493
L20	chr3R	8036000	8038000	chr3R	21732000	21734000	-0.051	0.636
L21	chr3R	8048000	8050000	chr3R	21736000	21738000	-0.044	0.636
L22	chr3R	12886000	12888000	chr3R	14954000	14956000	0.000	1.000
L23	chr3R	24502000	24504000	chr3R	28936000	28938000	-0.222	0.631
L24	chrX	948000	950000	chrX	16058000	16060000	-1.778	0.053
L25	chrX	1006000	1008000	chrX	16064000	16066000	-0.687	0.443
L26	chrX	11198000	11200000	chrX	21736000	21738000	-0.293	0.619
L27	chrX	13362000	13364000	chrX	19348000	19350000	-0.550	0.547
L28	chrX	21508000	21510000	chrX	22666000	22668000	0.485	0.554

Table S2. Hi-C mapping results

ID	Reads	Intersect	%	Valid interactions	%	CIS%	Dangling	%
CTRL_1	570,869,344	559,409,126	98.0%	295,967,093	51.8%	72.0%	33,664,060	6%
CTRL_2	580,056,454	570,516,966	98.4%	313,422,371	54.0%	73.0%	33,846,233	6%
REG_1	461,920,910	453,990,777	98.3%	273,564,949	59.2%	69.0%	23,382,502	5%
REG_2	563,556,925	550,153,826	98.6%	331,416,207	58.8%	68.0%	28,693,391	5%

ID	Extra DE	%	Duplicates	%	R. Breaks	%	Error	%	Self circle	%
CTRL_1	100,437,826	18%	146,411,350	26%	1,940,749	0%	45,146,122	8%	395,628	0%
CTRL_2	100,437,826	17%	134,975,570	23%	1,698,931	0%	43,223,663	7%	421,745	0%
REG_1	73,685,374	16%	77,345,636	17%	1,001,857	0%	27,256,413	6%	296,082	0%
REG_2	89,468,603	16%	96,649,021	17%	1,231,786	0%	33,214,971	6%	336,868	0%

Table S3. Primer sequences

Assay	Target gene	Forward sequence (5' → 3')	Reverse sequence (5' → 3')
qPCR	*sply*	CTTTCCCGATTCCCGTA	TGACGGGCTTAAGGCAATC
qPCR	*CG9500*	CCAAGAATGCCAGACGATGCC	CGAGGAGTATGTGGGTGCTTGG
qPCR	*Dip-epsilon*	GCAGCATTACAGTATATTCCGGCTC	CCTGCCGACATCTGACGC
qPCR	*Toll-4*	GATGCTCGAAATCTGAACAGC	CGTTTTCGCCAAGTTCATCC
qPCR	*numb*	TCTGGGATGTGTCGAGGTCT	CGTCTCCGCTGACATGAAGT
qPCR	*Gdi*	TCGAGGGCAGCTACGTTTAC	GCGACGCTTCTCGAACATAC

Table S4. NCBI GEO Accession Numbers

GEO accession	Experiment	Type of Data	doi
Pending	Hi-C	Wing discs (CTRL, REG)	Present study
Pending	RNA-seq	Wing discs REG (WT, Df(a), Df(b),Df(a,b))	Present study
GSE223411	RNA-seq	Wing discs (CTRL, REG)	10.1093/nargab/lqae091
GSE102841	ATAC-seq	Wing discs (CTRL, REG)	10.1101/gr.233098.117
GSE102841	ChIP-seq	H3K27ac in wing discs (CTRL, REG)	10.1101/gr.233098.117
GSE180376	ChIP-seq	Cp190 in embryos	10.1126/sciadv.abl8834
GSE180376	ChIP-seq	CTCF in embryos	10.1126/sciadv.abl8834
GSE218168	ChIP-seq	GAF in wing discs	10.1016/j.molcel.2023.03.011
GSE47559	ChIP-seq	Ibf1 in S2	10.1002/embj.201386001
GSE47559	ChIP-seq	Ibf2 in S2	10.1002/embj.201386001
GSE168894	ChIP-seq	Su(Hw) in ovaries	10.1038/s41598-021-96488-0
GSE231576	ChIP-seq	BEAF-32 in ovaries	10.1186/s13072-024-00541-x
GSE231576	ChIP-seq	M1BP in ovaries	10.1186/s13072-024-00541-x
GSE286361	Hi-C	Embryonic neurons (WT, Cp190[0])	10.1101/gad.352646.125
GSE146752	Hi-C	Larval CNS (WT, CTCF[K0])	10.1038/s41467-021-21366-2
GSE218168	Hi-C	Larval CNS (WT, GAF[POZ])	10.1016/j.molcel.2023.03.011
GSE253140	Hi-C	Pupal heads (WT, BEAF-32[0])	10.1016/j.devcel.2024.10.017

GENERAL DISCUSSION

This work sheds light on the role of chromatin organization and genome activity during regeneration in two epithelial tissues that rely on compensatory proliferation. In both contexts, regeneration occurs independently of stem cells and instead involves the reprogramming of pre-existing differentiated cells. As shown here and discussed in recent reviews (Jia *et al*., 2023; Poss and Tanaka, 2024), this reprogramming is orchestrated through changes in chromatin accessibility, histone modifications, genome architecture, and transcription factor binding, which together reshape the transcriptional profiles of regeneration-competent cells to support proliferation, differentiation, and tissue patterning. In the liver, we show that regeneration after PHx involves the activation of regeneration-responsive enhancers that drive the expression of priming and proliferation genes, while enhancers linked to energy-intensive functions of quiescent hepatocytes become repressed. These regulatory elements are governed by a cascade of transcription factors that modulate gene expression in a time-specific manner. Similarly, in *Drosophila* wing imaginal discs, our group previously identified damage-responsive regulatory elements as enhancers activated upon injury to induce the transcriptional programs of regeneration (Vizcaya *et al*., 2018). We now uncover that, beyond changes in chromatin accessibility, genome architecture in regenerating wing disc cells also undergoes subtle but significant reorganization, characterized by reduced compartmentalization and increased contact frequency across three long-range chromatin loops. Significantly, we demonstrate that these loops are required for proper regeneration, yet dispensable during normal development. Together, the results of this thesis highlight the significance of chromatin states and higher-order genome architecture in orchestrating regenerative responses, and suggest conserved regulatory principles underlying tissue repair.

THE CHROMATIN REGULATORY LANDSCAPE OF LIVER REGENERATION

The mammalian liver is one of the few organs that retains its capacity for regeneration in adulthood, largely due to the inherent plasticity of hepatocytes. Unlike many other differentiated cells, hepatocytes can re-enter the cell cycle, rapidly proliferate in response to acute injury and even dedifferentiate and transdifferentiate into cholangiocytes under chronic injury conditions (recently reviewed in Chen *et al*., 2023a). This injury-induced plasticity has been thoroughly investigated in rodent models, such as the partial hepatectomy model employed here and toxin-induced injury models involving acetaminophen or CCl_4. With increasing focus on the transcriptional and epigenetic regulators that enable hepatocyte reprogramming (reviewed in Monga and Sadler, 2020; Aloia, 2021), these systems have offered important insights into the cellular and molecular basis of liver regeneration.

An atlas of enhancer-promoter interactions during liver regeneration

To better understand the regulatory mechanisms underlying liver regeneration, we profiled gene expression and chromatin accessibility in hepatocytes at 6, 24, and 48 hours post-PHx. This analysis uncovered widespread transcriptional and chromatin remodeling, primarily driven by changes in enhancer accessibility. By constructing a regulatory map of enhancer-gene interactions, we found a strong correlation between chromatin dynamics and

gene expression: genes linked to *de novo* or increasing RREs were mostly upregulated and enriched in cell cycle and signaling pathways, whereas genes associated with decreasing RREs were downregulated and mainly involved in energy-intensive metabolic processes. These findings point to an inverse correlation between metabolic and proliferative gene programs, with lipid metabolism in particular being transiently suppressed to prioritize hepatocyte priming and division. Previous single-cell transcriptomic studies after PHx (Chen *et al*., 2020; Chembazhi *et al*., 2021; Xu *et al*., 2024) and chromatin profiling in liver injury models (Wang *et al*., 2020b) have also reported a similar trade-off between metabolic and regenerative functions.

Notably, single-cell studies have revealed functional heterogeneity among hepatocytes, suggesting a division-of-labor model during both homeostasis (Halpern *et al*., 2017) and regeneration (Chen *et al*., 2020). Following PHx, most hepatocytes adopt a fetal-like transcriptional state with reduced metabolic and biosynthetic activities, while a subset retains chromatin landscapes characteristic of quiescent hepatocytes (Chen *et al*., 2020). Some cells may even acquire a hypermetabolic state during regeneration, which could compensate for the transient loss of liver function (Chembazhi *et al*., 2021). Given this cellular diversity, it is possible that changes in RRE activity may also be spatially and temporally restricted to specific hepatocyte subpopulations. This is supported by the comparatively lower signal seen for *de novo* enhancers, which suggests that these regeneration-specific elements may be activated only in a subset of cells. Investigating RRE dynamics at single-cell resolution could help better understand the cellular and spatial specificity of the regulatory mechanisms involved in liver regeneration.

The functional zonation of hepatocytes along the porto-central axis of the liver lobule is another layer of complexity to liver regeneration that was not directly addressed in this study. Whether and how this metabolic zonation influences regenerative capacity remains unclear. Findings from injury models suggest that hepatocytes from different zones exhibit distinct plasticities. For instance, periportal hepatocytes, but not centrilobular ones, can undergo transdifferentiation into biliary epithelial cells following injury (Yanger *et al*., 2013). In addition, zone 2 hepatocytes have been shown to preferentially repopulate the lobule during both homeostasis and after liver injury, indicating spatial differences in proliferative potential (Wei *et al*., 2021). In the context of PHx, studies using lineage tracing and cumulative EdU labeling have also revealed zonal differences in proliferation dynamics: hepatocyte division initiates in the midlobular zone, peaking there around 48 hours post-surgery, whereas periportal and pericentral hepatocytes largely remain non-proliferative and metabolically active during this period (He *et al*., 2021; Chembazhi *et al*., 2021; Xu *et al*., 2024) (Fig. 10). Spatial transcriptomics data further support zone-specific changes during regeneration, including strong activation of IL-6 and NF-κB signaling specifically in periportal and pericentral regions, respectively (Fig. 10) (Xu *et al*., 2024). In summary, these findings highlight spatial heterogeneity in the regenerative response and suggest a relationship between metabolic zonation and proliferative activity. However, much is still unknown. In particular, whether such zonation-dependent differences are also reflected at the level of chromatin accessibility remains an open and intriguing question.

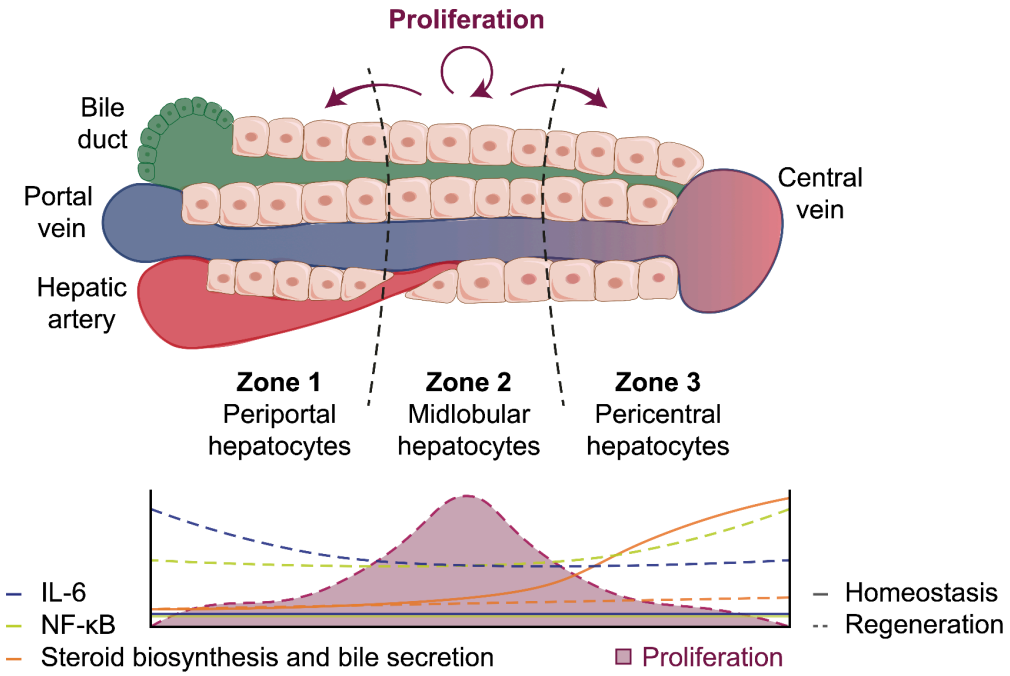

Figure 10. Model for zonated differences in hepatocyte proliferation and transcriptomic responses during liver regeneration. Illustration of spatial heterogeneity in the regenerative response of hepatocytes. Zone 2 hepatocytes predominantly proliferate, while periportal hepatocytes upregulate IL-6 signaling genes, and pericentral hepatocytes induce NF-κB signaling genes and downregulate genes involved in body homeostasis. *Drawing adapted from Itoh (2021); proliferation results from He et al. (2021); transcriptomic results from Xu et al. (2024)*.

The dual logic of liver regeneration: intrinsic plasticity and environmental cues

Hepatocyte proliferation after PHx is generally believed to occur through self-renewal without changes in cell identity (Li *et al.*, 2020). In contrast, hepatocytes during development arise from hepatoblasts, which are bipotent progenitors that also give rise to biliary epithelial cells (López-Luque and Fabregat, 2018). This fundamental difference has led to the prevailing view that liver regeneration relies on injury-specific regulatory programs, rather than shared mechanisms from embryonic development. Supporting this idea, Li *et al.* (2023) showed that regenerating hepatocytes activate reprogramming genes through STAT3, a transcription factor that is not required for hepatocyte specification during development. After periportal injury, STAT3, which is activated by IL-6 secreted by Kupffer cells, induces progenitor-associated genes via injury-specific enhancers, rather than enhancers reused from embryogenesis. In line with this, we identified a set of enhancers that are activated exclusively during regeneration (*de novo*) and remain inaccessible throughout development, suggesting the existence of *bona fide* regeneration-specific regulatory elements.

Our results, however, also indicate that liver regeneration is not entirely independent of developmental programs. We found that another subset of *de novo* RREs actually correspond to enhancers repurposed from embryonic stages, particularly the perinatal period. This suggests a partial reactivation of developmental regulatory mechanisms,

consistent with recent single-cell and epigenomic studies. For instance, Falick Michaeli *et al*. (2024) showed that liver regeneration involves dynamic, reversible changes in DNA methylation that transiently recapitulate the methylation landscape of late-stage hepatoblasts (E16.5), indicating an epigenetic reversion to a more plastic, fetal-like state. Similarly, single-cell transcriptomic analyses have shown that regenerating hepatocytes temporarily adopt progenitor-like states by reactivating gene regulatory networks characteristic of fetal and early postnatal development (Chen *et al*., 2020; Chembazhi *et al*., 2021).

Taken together, these findings suggest that while adult liver regeneration does not fully recapitulate embryonic development, it may selectively co-opt specific developmental enhancers and epigenetic states to facilitate expression of pro-regenerative genes and restore tissue after injury or resection. This raises a fundamental question: is regeneration driven by intrinsic plasticity within hepatocytes, enabling the reactivation of developmental regulatory programs, or is it orchestrated by the adult hepatic microenvironment, which provides the necessary cues to unlock these latent capacities?

Emerging evidence suggests that quiescent hepatocytes retain a latent regenerative potential that is encoded at the epigenomic level. Significantly, many genes induced during regeneration are found in a bivalent chromatin state in quiescent hepatocytes, marked by both activating (H3K4me3) and repressive (H3K27me3) histone modifications, as well as accessible chromatin (Zhang *et al*., 2021). This epigenetic signature maintains them transcriptionally silent yet poised for rapid activation. Following PHx, decreased levels of H3K27me3 at these genes enables their expression and helps initiate the regenerative response. Further support for an epigenetic control of regenerative capacity comes from studies manipulating key chromatin regulators. For example, deletion of *Arid1a*, a component of the SWI/SNF chromatin remodeling complex, was shown to enhance hepatocyte proliferation (Sun *et al*., 2016). Similarly, hepatocyte-specific deficiency of *Uhrf1*, a critical factor in DNA methylation maintenance, improved regeneration via an epigenetic compensation mechanism in which DNA hypomethylation led to redistribution of H3K27me3, reducing its presence at promoters of pro-regenerative genes (Wang *et al*., 2019).

Beyond chromatin-level regulation, hepatocyte plasticity is also evident at the cellular level, particularly in their ability to dedifferentiate and transdifferentiate in response to injury. Whether the liver harbors stem cells that contribute to injury-induced regeneration has long been debated, with evidence suggesting that oval cells, located in the canal of Hering, may function as bipotent progenitors capable of giving rise to both hepatocytes and cholangiocytes under severe injury. However, direct *in vivo* evidence remains limited (reviewed in Itoh, 2016; Miyajima *et al*., 2014; Li *et al*., 2020). In contrast, numerous studies have shown that, particularly during chronic injury, mature hepatocytes can dedifferentiate to replenish the hepatocyte pool and, in some cases, transdifferentiate into biliary epithelial cells, highlighting their exceptional plasticity (Michalopoulos *et al*., 2005; Schaub *et al*., 2018).

At the same time, the hepatic microenvironment is critical in shaping the regenerative response. Among the various cell types that produce pro-regenerative signals, immune cells are critical regulators of successful regeneration following injury. Tissue-resident macrophages, in contrast to circulating ones, have been shown to favor regeneration in models such as neonatal mouse heart injury and zebrafish skeletal muscle (reviewed Poss and Tanaka, 2024). A similar function has been described in the liver, where activation of

Kupffer cells supports tissue repair through the secretion of cytokines like IL-6 (reviewed in Li and Hua, 2017). However, in the context of chronic liver disease, macrophages can also contribute to fibrosis by stimulating hepatic stellate cells, which suggests a dual and context-dependent role of the immune system in tissue regeneration (reviewed in Abnave and Ghigo, 2019). While non-parenchymal cells have been extensively implicated in liver regeneration, their regulatory landscape remains poorly characterized. It would be of particular interest to profile the chromatin landscape of immune cells, especially resident macrophages and infiltrating regulatory T cells, not only in liver regeneration but also in other injury contexts. This would determine if RREs are also activated in these cells, and if so, whether there are tissue-specific differences that could determine a tissues' ability to regenerate or not.

Together, these findings underscore the remarkable plasticity of hepatocytes to adapt and reprogram in response to injury, and highlight the therapeutic potential of targeting epigenetic regulators to enhance the endogenous regenerative capacity of the liver. More broadly, they suggest that successful liver regeneration relies on a dynamic interplay between this intrinsic plasticity and extrinsic signals from the microenvironment, an interaction that is still not fully understood and thus warrants further investigation.

THE SPATIAL ORGANIZATION OF THE GENOME AS AN ACTIVE REGULATOR OF REGENERATION

Increasing evidence suggests that transcriptional regulation is shaped not only by chromatin states and local *cis*-regulatory interactions between enhancers and promoters, but also by the higher-order organization of the genome. To investigate whether changes in genome architecture contribute to transcriptional regulation during regeneration, we used the *Drosophila* wing imaginal disc as a model system. We found that, although global genome organization remains largely stable following tissue damage, both compartment strength and TAD insulation are notably reduced, indicating a weakening of chromatin compartmentalization and likely reflecting a more permissive and dynamic genome architecture during regeneration. We further identified three long-range chromatin loops with increased interaction frequency following damage, and demonstrated that these loops are required for proper wing disc regeneration but are dispensable for normal wing development. Our findings are significant for several reasons. To our knowledge, this is the first evidence that: (1) genome architecture plays an active role in tissue regeneration; (2) long-range chromatin loops formed between intergenic regions contribute to transcriptional regulation within a specific biological context; and (3) disruption of meta-loops results in a clear morphological defect (impaired wing disc regeneration). Therefore, these findings advance our understanding not only of the mechanisms underlying tissue regeneration but also of broader principles of gene regulation through 3D genome organization.

Function and mechanisms of meta-loop formation

Chromatin loops have recently been identified as an ancestral feature of genome architecture, present in non-bilaterian animals such as cnidarians but absent in their closest

unicellular relatives. While chromatin compartments defined by transcriptional activity exist in unicellular organisms, sequence-driven chromatin looping appears to have emerged with multicellularity, adding an additional layer of regulatory complexity to cell type-specific gene expression (Kim *et al*., 2025). These loops can be short-range, often linking enhancers to promoters, or span several megabases, where they may contribute to genome folding or enable precise transcriptional control (recently reviewed in Dekker and Mirny, 2024; Paldi and Cavalli, 2025).

The regulatory functions of long-range loops have been increasingly well-characterized in *Drosophila*, where recent studies suggests that they are particularly important in the central nervous system, enabling specialized neuronal gene expression, though their functional requirement remains unresolved (Mohana *et al*., 2023; Mouginot *et al*., 2025). Other long-range loops are established by Polycomb complexes and can mediate either activation or repression of developmental genes, depending on their interactions with specific transcription factors or other Polycomb components (Ogiyama *et al*., 2018; Loubiere *et al*., 2020; Paldi and Cavalli, 2025). These loops often serve as architectural platforms, maintaining genes and enhancers in a silenced yet poised state. Moreover, many long-range interactions have been shown to form constitutive loops during development but regulate transcription in a context-dependent manner (Pollex *et al*., 2024). Altogether, these findings suggest that chromatin loops may provide regulatory advantages in specific cell types or biological processes. In many cases, loops appear to fine-tune gene expression or facilitate co-transcription, rather than being strictly required for full transcriptional activation or repression (Levo *et al*., 2022; Mouginot *et al*., 2025). These subtle regulatory effects have only been detectable using high-resolution methods such as single-molecule RNA-FISH (Mohana *et al*., 2023; Mouginot *et al*., 2025) or quantitative single-cell live imaging (Levo *et al*., 2022). Therefore, the bulk RNA-seq used in our study may not be sensitive enough to fully resolve the transcriptional coupling between loop anchors and target genes. We anticipate that integrating single-cell technologies with live imaging will enable spatial and temporal analysis of transcriptional dynamics and help better explain the regeneration defects observed in flies lacking specific meta-loop anchors.

Our findings indicate that Cp190 is responsible for the formation of the L1 meta-loop and is also required for establishing L2 and L3, potentially through an indirect mechanism. Several questions remain open: (1) Which DNA-binding factor recruits Cp190 to the L1 anchors? (2) Does a hierarchical relationship exist among the loops, with L1 forming first and facilitating L2 and L3, or are there additional proteins specifically required for the formation of L2 and L3? (3) Why are these meta-loops specifically enriched and required during regeneration? Future experiments could help address these questions. For example, precise deletion of the A1 or A4 anchors (associated with L1) followed by regeneration assays and DNA-FISH targeting L2 and L3 anchors, or even Hi-C, would determine whether L1 is required for regeneration and for the subsequent formation of L2 and L3. Additional experiments could involve targeted depletion of candidate architectural proteins, combined with regeneration assays and DNA-FISH or Hi-C, to assess both their roles in meta-loop formation and their regeneration-specific function. Ibf1 and Ibf2 are particularly interesting candidates, given their reported role in Cp190 recruitment (Cuartero *et al.*, 2014) and their binding at L1 anchors observed in our analyses.

Genome folding and architectural proteins in regeneration, reprogramming and disease

While numerous studies have used Hi-C to investigate how 3D genome organization contributes to cell reprogramming or gene dysregulation in disease (reviewed in Zhong *et al*., 2023), its relationship to regenerative competence remains largely unexplored. In humans, several developmental disorders have been linked to structural variants that disrupt TAD architecture and lead to aberrant gene expression. These alterations include TAD fusions caused by deletions, neo-TADs generated by duplications or translocations, and boundary disruptions that lead to new enhancer-gene interactions, often referred to as “enhancer hijacking” (reviewed in Lupiáñez *et al*., 2016; Boltsis *et al*., 2021). A well-known example is the deletion of the TAD boundary within the *EPHA4* locus, which results in the fusion of adjacent TADs, gene misexpression, and defects in limb development (Lupiáñez *et al*., 2015). Beyond structural variants, other studies have used Hi-C to link GWAS susceptibility loci, such as type I diabetes risk-conferring variants, to altered chromatin architecture, potentially leading to gene dysregulation and disease pathogenesis (reviewed in Ramos-Rodríguez *et al*., 2021). In addition, mutations in genes encoding architectural proteins, such as CTCF and components of the cohesin complex, have been frequently associated with neurodevelopmental disorders, likely due to their impact on chromatin organization (reviewed in Zhong *et al*., 2023).

Furthermore, both chromatin structure and architectural proteins have been implicated in cell reprogramming. For instance, genome reorganization has been shown to precede transcriptional changes during B cell reprogramming, suggesting that genome topology may play an instructive role in regulating gene expression during cell fate transitions (Stadhouders *et al*., 2018). Moreover, although CTCF degradation has little effect on gene expression in several contexts (Schwartz *et al*., 2012; Nora *et al*., 2017; Kaushal *et al*., 2021; Hsieh *et al*., 2022), it is critical for 3D genome organization during reprogramming, acting both as an insulator to silence somatic expression and as a chromatin remodeler to maintain the accessibility of pluripotency genes (Song *et al*., 2022). Together with our findings, this supports a functional role for higher-order chromatin architecture in regulating tissue regeneration and suggests that architectural proteins like CTCF may serve as key regulators of regenerative potential. Notably, although CTCF is not differentially expressed during wing disc regeneration based on bulk transcriptomic data (Camilleri-Robles *et al*., 2024) (Fig. 11), and regeneration-associated meta-loops form independently of CTCF (Chapter II), its depletion severely impaired regeneration without affecting normal wing development (Fig. 11). This points to a regeneration-specific requirement for CTCF, although we cannot rule out the possibility that its role is transcriptional rather than architectural. Whether CTCF and other architectural proteins are similarly required in other regenerative contexts remains an open question, but emerging evidence suggests that this may be the case. For instance, CTCF binding increases at promoters of proliferation-related genes in hepatocytes after liver injury (Wang *et al*., 2020b), and conditional deletion of CTCF impairs nerve regeneration (Palmisano *et al*., 2019).

All in all, future experiments are needed to better understand the relationship between higher-order genome organization and regenerative potential, and to address key unanswered questions including: (1) whether reduced TAD insulation and increased long-range interactions are general features of injury responses, (2) how changes in genome

structure correlate with transcriptional reprogramming during regeneration, and (3) the specific contributions of architectural proteins to tissue repair.

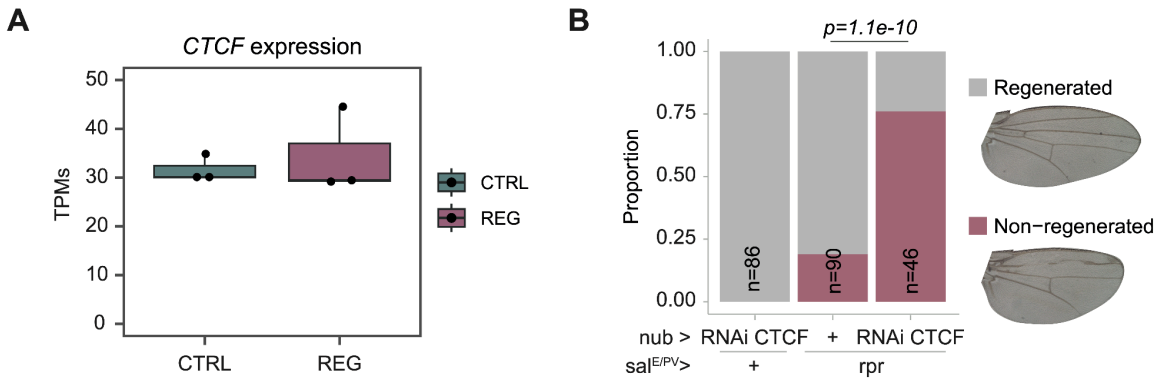

Figure 11. CTCF is required for wing imaginal disc regeneration. (A) Expression levels (TPMs) of *CTCF* in control and regenerating wing discs, based on RNA-seq data from Camilleri-Robles *et al.* (2024). **(B)** Proportion of regenerated versus non-regenerated adult wings after expression of *CTCF RNAi*, *rpr*, or both, in the wing imaginal disc. Gene expression was driven using a dual transactivation system: LexA/LexO-induced *rpr* expression in the $sal^{EP/V}$ domain, and Gal4/UAS-driven RNAi in the nubbin domain, with $Gal80^{ts}$ repressing both drivers at 17°C. Statistical significance (*p*-value) is indicated above the bars. Representative adult wing phenotypes are shown to the right.

CONSERVED REGULATORY PRINCIPLES OF TISSUE REGENERATION

The findings presented here, together with regeneration studies across a wide range of species, from invertebrates like *Drosophila* and planarians to vertebrates such as axolotls, zebrafish, and rodents, indicate that many core principles of tissue regeneration are conserved throughout evolution. These include shared molecular pathways, transcriptional regulators, and epigenetic mechanisms (reviewed in Poss and Tanaka, 2024).

Shared transcriptional regulators of regeneration-responsive enhancers

A conserved feature of regenerative responses across species is the substantial chromatin remodeling that occurs following injury. This reorganization primes the genome for changes in gene expression, either by promoting the release of pro-regenerative signals or by enhancing the competence of cells to respond to such cues (reviewed in Poss and Tanaka, 2024). The specificity of this transcriptional response is directed, at least in part, by *cis*-regulatory DNA elements. Numerous studies, including ours, have identified enhancers that are preferentially or specifically activated after injury and during regeneration (reviewed in Chen and Poss, 2017). These elements have been described using different names, such as tissue regeneration enhancer elements (TREEs) (Kang *et al.*, 2016; Goldman *et al.* 2017), damage-responsive regulatory elements (DRREs) (Vizcaya *et al.*, 2018), and regeneration-responsive regulatory elements or enhancers (RREs) (Wang *et al.*, 2020a; Llorens-Giralt *et al.*, 2025), but they share key functional characteristics: they are typically associated with increased chromatin accessibility in regenerating tissues and, in some

cases, with active histone modifications such as H3K27ac. When combined with a permissive promoter, they can drive transient, regeneration-specific gene expression, which can be validated using *in vitro* or *in vivo* transgenic assays (reviewed in Yang and Kang, 2019) (see Fig. 8D). For example, in our study we validated putative RREs as functional enhancers by performing transient reporter assays in hepatocyte cell cultures. Interestingly, Kang *et al.* (2016) showed that an enhancer linked to the *leptin b* gene (LEN), an RRE identified during zebrafish heart and fin regeneration, was capable of inducing injury-specific gene expression in regenerating mouse hearts and amputated digit tips. Although LEN is not conserved at the sequence level in the mammalian genome, its conserved activity in mammals suggests that the regulatory environment, and, particularly, the transcriptional networks required to activate such enhancers, have been conserved. This raises the possibility that the evolutionary loss of specific enhancer sequences, rather than the loss of the underlying regulatory machinery, may have contributed to the poor regenerative capacity observed in mammals.

Supporting this hypothesis, one of the most striking examples of evolutionary conservation in tissue repair is the involvement of orthologous transcription factors across diverse injury contexts. Many of the factors that activate RREs are shared between different species, despite large phylogenetic distances. Among them, the AP-1 dimer (JUN/FOS) has emerged as a potential master regulator of regeneration (reviewed in Harris, 2022; Jia *et al*., 2023). Its binding motif is a prevalent feature of RREs in multiple species and tissues, including the murine liver (Llorens-Giralt *et al*., 2025), *Drosophila* wing discs (Harris *et al*., 2016), the zebrafish heart (Begeman *et al*., 2020), and fins in both killifish and zebrafish (Wang *et al*., 2020a). In many of these contexts, AP-1 is not only required for proper regeneration, but the presence of its motif within RREs is essential for their activity (Harris *et al*., 2016; Begeman *et al*., 2020; Wang *et al*., 2020a).

We propose that ATF3 and NRF2 may also serve as conserved regulators of regenerative transcriptional programs via RREs. In our study, we found that *Atf3* and *Nfe2l2* (encoding NRF2) were upregulated during liver regeneration and capable of activating transcription through *de novo* and increasing RREs. Supporting a functional role, previous work has shown that liver repair is impaired in mice lacking NRF2 (Beyer *et al*., 2008), although the requirement for ATF3 remains unresolved. Beyond the mammalian liver, motifs for both ATF3 and NRF2 are among the most enriched in RREs during zebrafish heart regeneration (Cao *et al*., 2022). In *Drosophila*, scRNA-seq data show that *Atf3* expression is also induced in regenerating wing discs (Worley *et al*., 2022) (Fig. 12A), and preliminary results indicate that Atf3 is essential for regeneration but dispensable for wing development (Fig. 12B). Similarly, a previous study demonstrated that *Cap'n'Collar* (*cnc*), the *Drosophila* homolog of *Nfe2l2*, is also required for wing disc regeneration (Brock *et al*., 2017).

Our findings also suggest that Yin Yang 1 (YY1) may contribute to the regulation of regeneration-specific RREs. Significantly, these elements could function as silencers rather than enhancers, as their predicted target genes were generally repressed. Silencer elements have recently been implicated in zebrafish fin regeneration, where a larval screen identified tissue regeneration silencer elements (TRSEs) that downregulate unnecessary or regeneration-inhibitory genes after damage (Ando *et al*., 2024). While injury-activated enhancers have been extensively characterized across species, the conservation and functional relevance of TRSEs remains largely unexplored. Other regenerative systems have

revealed functional involvement of YY1, including a requirement for intestinal stem cell renewal (Perekatt *et al*., 2014) and for the metabolic reprogramming of satellite cells during skeletal muscle regeneration (Chen *et al*., 2019). Beyond its transcriptional roles, YY1 contributes to genome organization by facilitating long-range enhancer-promoter interactions in mammalian cells (Weintraub *et al*., 2017; Beagan *et al*., 2017). However, recent studies using acute YY1 degradation have reported contrasting results, with some showing minimal effects (Hsieh *et al*., 2022), while others demonstrate a requirement for YY1 in chromatin looping and transcriptional regulation (Lam *et al*., 2024). Although growing evidence links YY1 to oncogenesis (reviewed in Agarwal and Theodorescu, 2017), its involvement in tissue regeneration is still unclear. Further research will be needed to determine whether YY1 acts primarily as a transcriptional activator, repressor, or structural factor during regeneration, and whether this function is conserved across species.

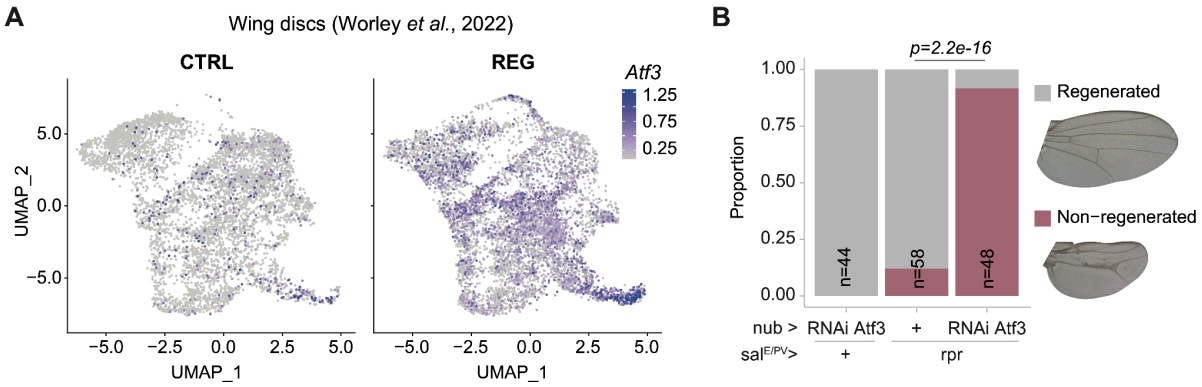

Figure 12. Atf3 is required for wing imaginal disc regeneration. (A) UMAP plots of single-cell RNA sequencing data showing *Atf3* expression in control (left) and regenerating (right) wing discs (Worley *et al*., 2022). Color intensity corresponds to normalized *Atf3* expression levels per cell. Data were processed using Seurat v5.0.3 (Hao *et al*., 2024), with batch correction and integration performed using Harmony v1.2.0 (Korsunsky *et al*., 2019). **(B)** Proportion of regenerated versus non-regenerated adult wings after expression of *Atf3 RNAi*, *rpr*, or both in the wing imaginal disc using the dual transactivation system. Statistical significance (*p*-value) is indicated above the bars. Representative adult wing phenotypes are shown to the right.

Altogether, these findings support a conserved role for ATF3, NRF2, and possibly YY1 in injury-induced gene regulation, highlighting them as potential key components of a core regeneration program. Drawing a parallel to the Yamanaka factors that reprogram somatic cells into induced pluripotent stem cells (Takahashi and Yamanaka, 2006), it is tempting to speculate that a defined combination of transcription factors, including those proposed here, may be sufficient to unlock regenerative potential in tissues with limited repair capacity. While investigating the combinatorial action of multiple TFs in regeneration presents challenges, particularly due to the limitations of cell culture models and the need for tissue- and organ-level studies, it would be interesting to explore whether such TF cocktail exists and whether the underlying transcriptional program is conserved, particularly in human tissues. Notably, RREs could help drive the expression of these TFs specifically to injured areas, thereby enhancing regeneration without the risk of potential tumorigenic effects.

Reactivation of embryonic regulatory programs in tissue regeneration

Another conserved feature of tissue repair across species is that regeneration-competent cells often undergo a transient reversion to a fetal-like state, primarily through the reactivation of developmental transcriptional programs. For instance, enrichment of fetal-like transcriptional signatures during regeneration has been observed in several murine injury models, including the epidermis after wounding (Miao *et al*., 2019), intestinal crypts in multiple injury contexts (recently reviewed in Viragova *et al*., 2024), and the liver after PHx (Chen *et al*., 2020). In non-mammalian models, regeneration also proceeds via developmental reprogramming, such as in axolotl limb regeneration (Gerber *et al*., 2018) and zebrafish heart repair (Kikuchi *et al*., 2010). Indeed, most regenerative processes reuse pathways essential for embryogenesis, including JAK/STAT, Hippo/YAP, and Wnt/β-catenin signaling (reviewed in Sun and Irvine, 2014), and only a few genes have been identified as essential for regeneration but dispensable during normal development. One example is the transcription factor Ets21C, which orchestrates a pro-regenerative transcriptional program during *Drosophila* wing disc regeneration, but is not required during fly development (Worley *et al*., 2022).

At the level of chromatin regulation, regeneration appears to involve both an epigenetic reprogramming toward an embryonic-like state and the activation of regeneration-specific mechanisms. As discussed earlier, regenerating hepatocytes not only re-express fetal gene programs but also adopt chromatin accessibility landscapes and DNA methylation patterns characteristic of immature hepatocytes, while simultaneously activating enhancers specific to the regenerative response. Similarly, RREs identified in *Drosophila* wing disc and zebrafish heart regeneration include both enhancers co-opted from embryonic stages and enhancers that are exclusively activated upon injury (Vizcaya *et al*., 2018; Huang *et al*., 2012; Kang *et al*., 2016). Recent findings in the acoel *Hofstenia miamia*, a model for whole-body regeneration, further support this dual mechanism, suggesting that regeneration-induced genes are regulated by developmental enhancers, but through distinct transcription factor binding sites compared to those used during embryogenesis (Loubet-Senear and Srivastava, 2024).

Moreover, changes in chromatin structure and mechanisms of epigenetic repression during development actively contribute to the loss of regenerative capacity in certain tissues. For instance, localized epigenetic silencing of damage-responsive enhancers in *Drosophila* wing disc cells allows for normal development while preventing regeneration after injury as larvae mature (Harris *et al*., 2016; Harris *et al*., 2020). In adult mouse cardiomyocytes, failure to reactivate neonatal proliferative networks following infarction has been associated with a loss of chromatin accessibility around cell cycle genes during postnatal maturation (Quaife-Ryan *et al*., 2017). On the other hand, studies in the intestinal epithelium show that embryonic developmental genes lose active histone marks without gaining repressive marks or DNA methylation-mediated silencing, suggesting that the adult epithelium remains relatively permissive to reactivation of embryonic programs, thus enabling regeneration after injury (Kazakevych *et al*., 2017). Similarly, neonatal mice can regenerate the inner ear by transdifferentiation of supporting cells into hair cells, as genes and enhancers related to hair cell differentiation remain primed (marked by H3K4me3 and H3K4me1, respectively) but silenced (by H3K27me3). However, this regenerative ability is rapidly lost with maturation, coinciding with the loss of the H3K4me1 priming state in supporting cells (Tao *et al*., 2021).

Taken together, these observations suggest that while regenerative programs frequently repurpose genes and regulatory elements from embryonic development, they also rely on regeneration-specific enhancers and distinct epigenetic mechanisms. We propose a model in which highly regenerative tissues, such as the liver and intestine, possess intrinsic cellular plasticity that enables them to revert to fetal-like epigenetic states (Fig. 13). This regenerative potential is encoded at the epigenomic level, where developmental regulatory elements exist in poised (bivalent chromatin) or permissive (lacking repressive histone marks) states under homeostatic conditions. Following injury, tissue-intrinsic cues and immune-related signals activate regeneration-specific enhancers, potentially reactivating developmental regulatory elements and inducing embryonic gene expression. In contrast, adult tissues with limited regenerative ability may actively repress this potential through stable epigenetic silencing of developmental and regeneration enhancers (Fig. 13), as observed in the maturing *Drosophila* wing disc (Harris *et al*., 2020).

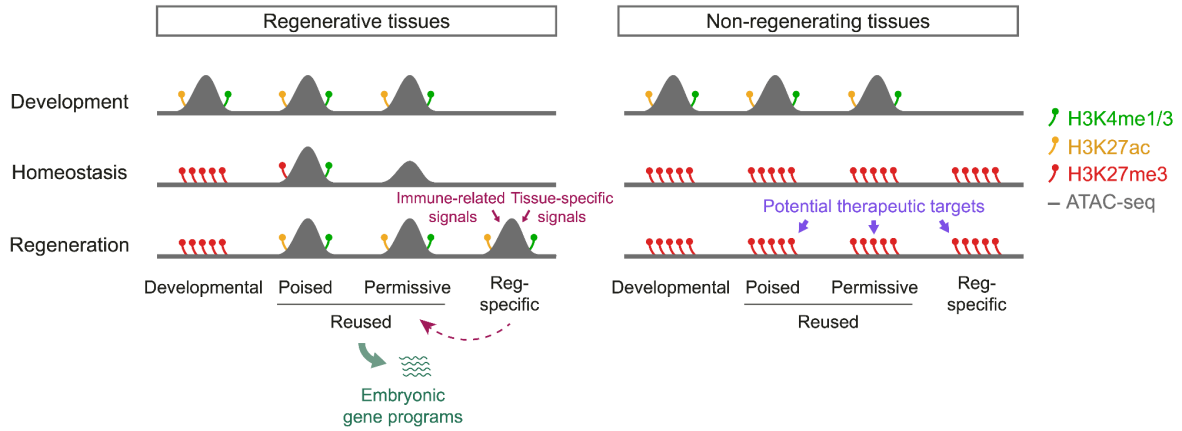

Figure 13. Chromatin states of regulatory elements in regenerating versus non-regenerating tissues. In regenerative tissues, regeneration-specific regulatory elements are activated by tissue-intrinsic or immune-related signals. These elements can, in turn, reactivate developmental enhancers that are either poised (accessible and marked by H3K4me1/3 and H3K27me3) or found in a permissive state (lacking repressive modifications but with unknown chromatin accessibility). Together, these regulatory elements drive regeneration programs, which substantially overlap with embryonic gene expression profiles. In contrast, non-regenerating tissues may repress this potential through stable developmental epigenetic silencing. Therapeutically reactivating regeneration-specific or developmental enhancers in these tissues could restore regenerative competence.

Overall, this model suggests that successful regeneration requires not only access to developmental gene programs, but also a permissive chromatin landscape and regeneration-specific activation cues. This points to new therapeutic strategies aimed at reprogramming pre-existing cells and reactivating silenced enhancers, rather than relying solely on stem cell-based therapies. Indeed, proof-of-concept studies in animal models have already shown that this is possible. For instance, forced, reversible reprogramming of adult cardiomyocytes to a fetal-like state improved cardiac function after myocardial infarction, enabling heart regeneration while avoiding tumor formation (Chen *et al*., 2021a). Similarly, treatment of intestinal organoids with TGFB1 induced fetal-like reprogramming and improved engraftment in a mouse model of intestinal injury (Chen *et al*., 2023b), and inhibition of H3K4me1 demethylation in supporting cells of the inner ear extended their regenerative

capacity (Tao *et al*., 2021). Collectively, these findings underscore the potential of targeting epigenetic plasticity and promoting transient fetal-like reversion to unlock regenerative capacity in otherwise non-regenerating tissues.

Nevertheless, these therapeutic strategies could increase the risk of tumor formation. To minimize this, developmental reprogramming or delivery of pro-regenerative factors should ideally be spatially and temporally restricted to injury sites. One promising approach involves the use of context-dependent regulatory elements. Recent studies have validated RREs in transgenic animals as enhancers that remain inactive under homeostatic conditions, become activated upon injury, and are subsequently silenced once tissue repair is complete. (Kang *et al*., 2016; Chen *et al*., 2021b; Cigliola *et al*., 2023). More recently, zebrafish RREs were incorporated into recombinant adeno-associated viruses (AAVs) as gene therapy modules, and shown to direct gene expression specifically to injured mammalian tissues (Yan *et al*., 2023). When administered systemically after cardiac injury, these RRE-AAV constructs successfully induced expression of pro-regenerative genes in murine and porcine hearts, promoting cardiomyocyte proliferation and improving cardiac function. These findings provide proof-of-principle evidence for the use of RREs as a targeted gene therapy strategy in regenerative medicine.

Future perspectives

This study identifies two levels of chromatin regulation during the regenerative response: enhancer modulation and genome reorganization. It offers a genomic perspective on liver regeneration, a process well characterized at the molecular and cellular levels but less understood from the perspective of chromatin dynamics, and provides, to our knowledge, the first evidence that chromatin architecture actively contributes to tissue regeneration. We anticipate that future research will explore genome folding as a regulatory factor in other injury contexts and will address fundamental questions that remain unanswered, including: (1) Is genome reorganization essential for regenerative competency? (2) What are the key factors driving changes in chromatin architecture and genome function during tissue repair? (3) Are there differences in chromatin structure between species with high regenerative capacity and those with limited capacity, as well as between different developmental stages in animals that lose regenerative potential as they mature? (4) Are silencer elements a conserved regulatory layer in tissue regeneration, and what is their role in transcriptional regulation and regenerative potential? (5) How can we translate insights on chromatin regulation into strategies for improving regeneration in tissues with poor regenerative capabilities? Throughout this thesis, we have discussed several potential therapeutic applications, such as targeting epigenetic regulators and core regenerative TFs, promoting fetal-like reprogramming, and using RREs as pro-regenerative expression drivers. Whether these strategies will ultimately translate into *bona fide* regenerative therapies remains to be seen, but the findings and perspectives presented here offer exciting directions for future research.

CONCLUSIONS

CONCLUSIONS

1. The transcriptional response during liver regeneration is dynamically modulated by regeneration-responsive regulatory elements, including *de novo* enhancers that are specifically activated after PHx, and increasing enhancers that exhibit higher activity during regeneration.

2. An inverse relationship between hepatocyte proliferation and lipid metabolic function is evident at the level of enhancer activation and gene expression during liver regeneration.

3. The transcription factors ATF3 and NRF2 promote liver regeneration by activating gene expression through RREs.

4. Hepatocytes reactivate developmental enhancers, preferentially from the postnatal or late embryonic stages, to regulate genes involved in cell junctional organization and glucose metabolism.

5. Genome compartmentalization is reduced during *Drosophila* wing disc regeneration, both in compartment strength and TAD boundary insulation, likely promoting increased chromatin interactions.

6. Specific long-range chromatin loops on chromosome 2L exhibit increased contact frequency during wing disc regeneration, facilitating coordinated regulation of gene expression across distant loci.

7. Meta-loops L1, L2, and L3 are required for wing disc regeneration, but dispensable during normal wing development, indicating a regeneration-specific architectural or regulatory function.

8. The architectural protein Cp190 is required for the formation of these regeneration-associated meta-loops, although its precise role in regeneration remains to be elucidated.

9. The activity of the transcription factors AP-1, ATF3, and NRF2; the reprogramming of regenerative cells toward a fetal-like chromatin state; and the reorganization of genome architecture, potentially mediated by architectural proteins, may be conserved features of the regenerative response across species.

BIBLIOGRAPHY

BIBLIOGRAPHY

Abnave P and Ghigo E (2019) Role of the immune system in regeneration and its dynamic interplay with adult stem cells. *Seminars in Cell & Developmental Biology* 87: 160–168.

Abu Rmilah A, Zhou W, Nelson E, et al. (2019) Understanding the marvels behind liver regeneration. *WIREs Developmental Biology* 8(3): e340.

Agarwal N and Theodorescu D (2017) The Role of Transcription Factor YY1 in the Biology of Cancer. *Critical Reviews in Oncogenesis* 22(1–2): 13–21.

Aguilar CA, Pop R, Shcherbina A, et al. (2016) Transcriptional and Chromatin Dynamics of Muscle Regeneration after Severe Trauma. *Stem Cell Reports* 7(5): 983–997.

Aldaz S and Escudero LM (2010) Imaginal discs. *Current Biology* 20(10): R429–R431.

Aloia L (2021) Epigenetic Regulation of Cell-Fate Changes That Determine Adult Liver Regeneration After Injury. *Frontiers in Cell and Developmental Biology* 9: 643055.

Alvarado AS (2000) Regeneration in the metazoans: why does it happen? *BioEssays* 22(6): 578–590.

Alvarado AS and Tsonis PA (2006) Bridging the regeneration gap: genetic insights from diverse animal models. *Nature Reviews Genetics* 7(11): 873–884.

Ando K, Ou J, Thompson JD, et al. (2024) A screen for regeneration-associated silencer regulatory elements in zebrafish. *Developmental Cell* 59(5): 676-691.e5.

Arias IM, Alter HJ, Boyer JL, et al. (eds) (2020) *The Liver: Biology and Pathobiology*. 1st ed. Wiley.

Bangru S and Kalsotra A (2020) Cellular and molecular basis of liver regeneration. *Seminars in Cell & Developmental Biology* 100: 74–87.

Beagan JA, Duong MT, Titus KR, et al. (2017) YY1 and CTCF orchestrate a 3D chromatin looping switch during early neural lineage commitment. *Genome Research* 27(7): 1139–1152.

Begeman IJ, Shin K, Osorio-Méndez D, et al. (2020) Decoding an Organ Regeneration Switch by Dissecting Cardiac Regeneration Enhancers. *Development*: dev.194019.

Beira JV and Paro R (2016) The legacy of Drosophila imaginal discs. *Chromosoma* 125(4): 573–592.

Bely AE and Nyberg KG (2010) Evolution of animal regeneration: re-emergence of a field. *Trends in Ecology & Evolution* 25(3): 161–170.

Bergantiños C, Vilana X, Corominas M, et al. (2010a) Imaginal discs: Renaissance of a model for regenerative biology. *BioEssays* 32(3): 207–217.

Bergantiños C, Corominas M and Serras F (2010b) Cell death-induced regeneration in wing imaginal discs requires JNK signalling. *Development* 137(7): 1169–1179.

Beyer TA, Xu W, Teupser D, et al. (2008) Impaired liver regeneration in Nrf2 knockout mice: role of ROS-mediated insulin/IGF-1 resistance. *The EMBO Journal* 27(1): 212–223.

Bideau L, Kerner P, Hui J, et al. (2021) Animal regeneration in the era of transcriptomics. *Cellular and Molecular Life Sciences* 78(8): 3941–3956.

Blake MJ and Steer CJ (2023) Liver Regeneration in Acute on Chronic Liver Failure. *Clinics in Liver Disease* 27(3): 595–616.

Boettiger AN, Bintu B, Moffitt JR, et al. (2016) Super-resolution imaging reveals distinct chromatin folding for different epigenetic states. *Nature* 529(7586): 418–422.

Boltsis I, Grosveld F, Giraud G, et al. (2021) Chromatin Conformation in Development and Disease. *Frontiers in Cell and Developmental Biology* 9: 723859.

Bonev B and Cavalli G (2016) Organization and function of the 3D genome. *Nature Reviews Genetics* 17(11): 661–678.

Bosch M, Serras F, Martín-Blanco E, et al. (2005) JNK signaling pathway required for wound healing in regenerating Drosophila wing imaginal discs. *Developmental Biology* 280(1): 73–86.

Brock AR, Seto M and Smith-Bolton RK (2017) Cap-n-Collar Promotes Tissue Regeneration by Regulating ROS and JNK Signaling in the Drosophila melanogaster Wing Imaginal Disc. *Genetics* 206(3): 1505–1520.

Bryant PJ (1971) Regeneration and duplication following operations in situ on the imaginal discs of Drosophila melanogaster. *Developmental Biology* 26(4): 637–651.

Caldez MJ, Van Hul N, Koh HWL, et al. (2018) Metabolic Remodeling during Liver Regeneration. *Developmental Cell* 47(4): 425-438.e5.

Camilleri-Robles C, Amador R, Tiebe M, et al. (2024) Long non-coding RNAs involved in *Drosophila* development and regeneration. *NAR Genomics and Bioinformatics* 6(3): lqae091.

Cao Y, Xia Y, Balowski JJ, et al. (2022) Identification of enhancer regulatory elements that direct epicardial gene expression during zebrafish heart regeneration. *Development* 149(4): dev200133.

Catarino RR and Stark A (2018) Assessing sufficiency and necessity of enhancer activities for gene expression and the mechanisms of transcription activation. *Genes & Development* 32(3–4): 202–223.

Cattoni DI, Cardozo Gizzi AM, Georgieva M, et al. (2017) Single-cell absolute contact probability detection reveals chromosomes are organized by multiple low-frequency yet specific interactions. *Nature Communications* 8(1): 1753.

Chembazhi UV, Bangru S, Hernaez M, et al. (2021) Cellular plasticity balances the metabolic and proliferation dynamics of a regenerating liver. *Genome Research* 31(4): 576–591.

Chen C-H and Poss KD (2017) Regeneration Genetics. *Annual Review of Genetics* 51(1): 63–82.

Chen F, Zhou J, Li Y, et al. (2019) YY1 regulates skeletal muscle regeneration through controlling metabolic reprogramming of satellite cells. *The EMBO journal* 38(10): e99727.

Chen T, Oh S, Gregory S, et al. (2020) Single-cell omics analysis reveals functional diversification of hepatocytes during liver regeneration. *JCI Insight* 5(22): e141024.

Chen Y, Lüttmann FF, Schoger E, et al. (2021a) Reversible reprogramming of cardiomyocytes to a fetal state drives heart regeneration in mice. *Science (New York, N.Y.)* 373(6562): 1537–1540.

Chen A, Han Y and Poss KD (2021b) Regulation of zebrafish fin regeneration by vitamin D signaling. *Developmental Dynamics* 250(9): 1330–1339.

Chen F, Schönberger K and Tchorz JS (2023a) Distinct hepatocyte identities in liver homeostasis and regeneration. *JHEP Reports* 5(8): 100779.

Chen L, Qiu X, Dupre A, et al. (2023b) TGFB1 induces fetal reprogramming and enhances intestinal regeneration. *Cell Stem Cell* 30(11): 1520-1537.e8.

Cigliola V, Shoffner A, Lee N, et al. (2023) Spinal cord repair is modulated by the neurogenic factor Hb-egf under direction of a regeneration-associated enhancer. *Nature Communications* 14(1): 4857.

Cohen SM (1993) Imaginal disc development. In: Bate M and Martinez Arias A (eds) *The Development of Drosophila Melanogaster*. Plainview, N.Y: Cold Spring Harbor Laboratory Press.

Colombani J, Andersen DS and Léopold P (2012) Secreted Peptide Dilp8 Coordinates *Drosophila* Tissue Growth with Developmental Timing. *Science* 336(6081): 582–585.

Cremer T and Cremer C (2001) Chromosome territories, nuclear architecture and gene regulation in mammalian cells. *Nature Reviews Genetics* 2(4): 292–301.

Csanaky IL, Aleksunes LM, Tanaka Y, et al. (2009) Role of hepatic transporters in prevention of bile acid toxicity after partial hepatectomy in mice. *American Journal of Physiology. Gastrointestinal and Liver Physiology* 297(3): G419-433.

Cuartero S, Fresan U, Reina O, et al. (2014) Ibf1 and Ibf2 are novel CP190-interacting proteins required for insulator function. *The EMBO Journal* 33(6): 637–647.

Dekker J, Rippe K, Dekker M, et al. (2002) Capturing Chromosome Conformation. 295.

Dekker J, Marti-Renom MA and Mirny LA (2013) Exploring the three-dimensional organization of genomes: interpreting chromatin interaction data. *Nature Reviews Genetics* 14(6): 390–403.

Dekker J and Misteli T (2015) Long-Range Chromatin Interactions. *Cold Spring Harbor Perspectives in Biology* 7(10): a019356.

Dekker J and Mirny L (2016) The 3D Genome as Moderator of Chromosomal Communication. *Cell* 164(6): 1110–1121.

Dekker J and Mirny LA (2024) The chromosome folding problem and how cells solve it. *Cell* 187(23): 6424–6450.

Denaud S, Sabarís G, Di Stefano M, et al. (2025) Determining the functional relationship between epigenetic and physical chromatin domains in Drosophila. *Genome Biology* 26(1): 116.

de Wit E, Vos ESM, Holwerda SJB, et al. (2015) CTCF Binding Polarity Determines Chromatin Looping. *Molecular Cell* 60(4): 676–684.

Dixon JR, Selvaraj S, Yue F, et al. (2012) Topological domains in mammalian genomes identified by analysis of chromatin interactions. *Nature* 485(7398): 376–380.

Eagen KP (2018) Principles of Chromosome Architecture Revealed by Hi-C. *Trends in Biochemical Sciences* 43(6): 469–478.

Esteban-Collado J, Corominas M and Serras F (2021) Nutrition and PI3K/Akt signaling are required for p38-dependent regeneration. *Development* 148(8): dev197087.

Esteban-Collado J, Fernández-Mañas M, Fernández-Moreno M, et al. (2024) Reactive oxygen species activate the Drosophila TNF receptor Wengen for damage-induced regeneration. *The EMBO Journal* 43(17): 3604–3626.

Falick Michaeli T, Sabag O, Azria B, et al. (2024) Hepatocyte regeneration is driven by embryo-like DNA methylation reprogramming. *Proceedings of the National Academy of Sciences* 121(16): e2314885121.

Fan M, Wang X, Xu G, et al. (2015) Bile acid signaling and liver regeneration. *Biochimica Et Biophysica Acta* 1849(2): 196–200.

Field A and Adelman K (2020) Evaluating Enhancer Function and Transcription. *Annual Review of Biochemistry* 89(1): 213–234.

Flyamer IM, Gassler J, Imakaev M, et al. (2017) Single-nucleus Hi-C reveals unique chromatin reorganization at oocyte-to-zygote transition. *Nature* 544(7648): 110–114.

Forbes SJ and Newsome PN (2016) Liver regeneration — mechanisms and models to clinical application. *Nature Reviews Gastroenterology & Hepatology* 13(8): 473–485.

Fox DT, Cohen E and Smith-Bolton R (2020) Model systems for regeneration: *Drosophila*. *Development* 147(7): dev173781.

Fristrom D and Fristrom JW (1993) The metamorphic development of the adult epidermis. In: Bate M and Martinez Arias A (eds) *The Development of Drosophila Melanogaster*. Plainview, NY: Cold Spring Harbor Laboratory Press.

Fudenberg G, Imakaev M, Lu C, et al. (2016) Formation of Chromosomal Domains by Loop Extrusion. *Cell Reports* 15(9): 2038–2049.

Fulco CP, Nasser J, Jones TR, et al. (2019) Activity-by-contact model of enhancer–promoter regulation from thousands of CRISPR perturbations. *Nature Genetics* 51(12): 1664–1669.

Galliot B (2012) Hydra, a fruitful model system for 270 years. *The International Journal of Developmental Biology* 56(6-7–8): 411–423.

Garcia-Bellido A, Ripoll P and Morata G (1973) Developmental Compartmentalisation of the Wing Disk of Drosophila. *Nature New Biology* 245(147): 251–253.

Garelli A, Gontijo AM, Miguela V, et al. (2012) Imaginal Discs Secrete Insulin-Like Peptide 8 to Mediate Plasticity of Growth and Maturation. *Science* 336(6081): 579–582.

Ge Y, Gomez NC, Adam RC, et al. (2017) Stem Cell Lineage Infidelity Drives Wound Repair and Cancer. *Cell* 169(4): 636-650.e14.

Gerber T, Murawala P, Knapp D, et al. (2018) Single-cell analysis uncovers convergence of cell identities during axolotl limb regeneration. *Science* 362(6413): eaaq0681.

Ghavi-Helm Y, Jankowski A, Meiers S, et al. (2019) Highly rearranged chromosomes reveal uncoupling between genome topology and gene expression. *Nature Genetics* 51(8): 1272–1282.

Goldman JA, Kuzu G, Lee N, et al. (2017) Resolving Heart Regeneration by Replacement Histone Profiling. *Developmental Cell* 40(4): 392-404.e5.

Goldman JA and Poss KD (2020) Gene regulatory programmes of tissue regeneration. *Nature Reviews Genetics* 21(9): 511–525.

Goss RJ (1991) The natural history (and mystery) of regeneration. In: Dinsmore CE (ed.) *A History of Regeneration Research: Milestones in the Evolution of a Science.* Cambridge: Cambridge Univ. Press, pp. 7–23.

Grompe M (2014) Liver Stem Cells, Where Art Thou? *Cell Stem Cell* 15(3): 257–258.

Hadorn E (1965) Problems of determination and transdetermination. *Brookhaven Symposia in Biology*: 148–161.

Hadorn E, Hürlimann R, Mindek G, et al. (1968) [Developmental capacity of embryonal blastema in Drosophila following cultivation in an adult host]. *Revue Suisse De Zoologie; Annales De La Societe Zoologique Suisse Et Du Museum D'histoire Naturelle De Geneve* 75(3): 557–569.

Hadorn E (1978) Transdetermination. In: Ashburner M and Wright TRF (eds) *The Genetics and Biology of Drosophila*. New York: Academic Press.

Halpern KB, Shenhav R, Matcovitch-Natan O, et al. (2017) Single-cell spatial reconstruction reveals global division of labour in the mammalian liver. *Nature* 542(7641): 352–356.

Hanssen LLP, Kassouf MT, Oudelaar AM, et al. (2017) Tissue-specific CTCF–cohesin-mediated chromatin architecture delimits enhancer interactions and function in vivo. *Nature Cell Biology* 19(8): 952–961.

Hao Y, Stuart T, Kowalski MH, et al. (2024) Dictionary learning for integrative, multimodal and scalable single-cell analysis. *Nature Biotechnology* 42(2): 293–304.

Hariharan IK and Serras F (2017) Imaginal disc regeneration takes flight. *Current Opinion in Cell Biology* 48: 10–16.

Harris RE, Setiawan L, Saul J, et al. (2016) Localized epigenetic silencing of a damage-activated WNT enhancer limits regeneration in mature Drosophila imaginal discs. *eLife* 5: e11588.

Harris RE, Stinchfield MJ, Nystrom SL, et al. (2020) Damage-responsive, maturity-silenced enhancers regulate multiple genes that direct regeneration in Drosophila. *eLife* 9: e58305.

Harris RE (2022) Regeneration enhancers: a field in development. *American Journal of Physiology-Cell Physiology* 323(5): C1548–C1554.

Haynie JL and Bryant PJ (1977) The effects of X-rays on the proliferation dynamics of cells in the imaginal wing disc ofDrosophila melanogaster. *Wilhelm Roux's Archives of Developmental Biology* 183(2): 85–100.

Haynie JL and Bryant PJ (1986) Development of the eye-antenna imaginal disc and morphogenesis of the adult head in *Drosophila melanogaster*. *Journal of Experimental Zoology* 237(3): 293–308.

He L, Pu W, Liu X, et al. (2021) Proliferation tracing reveals regional hepatocyte generation in liver homeostasis and repair. *Science* 371(6532): eabc4346.

Herrera SC and Morata G (2014) Transgressions of compartment boundaries and cell reprogramming during regeneration in Drosophila. *eLife* 3: e01831.

Higgins, M and Anderson, R.M (1931) Experimental pathology of liver: restoration of liver of white rat following partial surgical removal. *Archives of Pathology & Laboratory Medicine* 12: 186–202.

Hijmans BS, Grefhorst A, Oosterveer MH, et al. (2014) Zonation of glucose and fatty acid metabolism in the liver: Mechanism and metabolic consequences. *Biochimie* 96: 121–129.

Hou C, Li L, Qin ZS, et al. (2012) Gene Density, Transcription, and Insulators Contribute to the Partition of the Drosophila Genome into Physical Domains. *Molecular Cell* 48(3): 471–484.

Hsieh T-HS, Cattoglio C, Slobodyanyuk E, et al. (2022) Enhancer–promoter interactions and transcription are largely maintained upon acute loss of CTCF, cohesin, WAPL or YY1. *Nature Genetics* 54(12): 1919–1932.

Huang GN, Thatcher JE, McAnally J, et al. (2012) C/EBP Transcription Factors Mediate Epicardial Activation During Heart Development and Injury. *Science* 338(6114): 1599–1603.

Huang J and Rudnick DA (2014) Elucidating the Metabolic Regulation of Liver Regeneration. *The American Journal of Pathology* 184(2): 309–321.

Huch M, Dorrell C, Boj SF, et al. (2013) In vitro expansion of single Lgr5+ liver stem cells induced by Wnt-driven regeneration. *Nature* 494(7436): 247–250.

Iismaa SE, Kaidonis X, Nicks AM, et al. (2018) Comparative regenerative mechanisms across different mammalian tissues. *npj Regenerative Medicine* 3(1): 6.

Ing-Simmons E, Vaid R, Bing XY, et al. (2021) Independence of chromatin conformation and gene regulation during Drosophila dorsoventral patterning. *Nature Genetics* 53(4): 487–499.

Itoh T (2016) Stem/progenitor cells in liver regeneration. *Hepatology* 64(2): 663–668.

Itoh T (2021) The truth lies somewhere in the middle: the cells responsible for liver tissue maintenance finally identified. *Cell Regeneration* 10(1): 28.

Jerkovic´ I and Cavalli G (2021) Understanding 3D genome organization by multidisciplinary methods. *Nature Reviews Molecular Cell Biology* 22(8): 511–528.

Jia X, Lin W and Wang W (2023) Regulation of chromatin organization during animal regeneration. *Cell Regeneration* 12(1): 19.

Kaestner KH (2009) In the Zone: How a Hepatocyte Knows Where It Is. *Gastroenterology* 137(2): 425–427.

Kang J, Hu J, Karra R, et al. (2016) Modulation of tissue repair by regeneration enhancer elements. *Nature* 532(7598): 201–206.

Karpen GH and Schubiger G (1981) Extensive regulatory capabilities of a Drosophila imaginal disk blastema. *Nature* 294(5843): 744–747.

Katsuyama T, Comoglio F, Seimiya M, et al. (2015) During *Drosophila* disc regeneration, JAK/STAT coordinates cell proliferation with Dilp8-mediated developmental delay. *Proceedings of the National Academy of Sciences* 112(18).

Kaushal A, Mohana G, Dorier J, et al. (2021) CTCF loss has limited effects on global genome architecture in Drosophila despite critical regulatory functions. *Nature Communications* 12(1): 1011.

Kawasaki K and Fukaya T (2024) Regulatory landscape of enhancer-mediated transcriptional activation. *Trends in Cell Biology* 34(10): 826–837.

Kazakevych J, Sayols S, Messner B, et al. (2017) Dynamic changes in chromatin states during specification and differentiation of adult intestinal stem cells. *Nucleic Acids Research* 45(10): 5770–5784.

Kikuchi K, Holdway JE, Werdich AA, et al. (2010) Primary contribution to zebrafish heart regeneration by gata4+ cardiomyocytes. *Nature* 464(7288): 601–605.

Kim IV, Navarrete C, Grau-Bové X, et al. (2025) Chromatin loops are an ancestral hallmark of the animal regulatory genome. *Nature*. Epub ahead of print 7 May 2025. DOI: 10.1038/s41586-025-08960-w.

Korsunsky I, Millard N, Fan J, et al. (2019) Fast, sensitive and accurate integration of single-cell data with Harmony. *Nature Methods* 16(12): 1289–1296.

La Fortezza M, Schenk M, Cosolo A, et al. (2016) JAK/STAT signalling mediates cell survival in response to tissue stress. *Development* 143(16): 2907–2919.

Lajoie BR, Dekker J and Kaplan N (2015) The Hitchhiker's guide to Hi-C analysis: Practical guidelines. *Methods* 72: 65–75.

Lam JC, Aboreden NG, Midla SC, et al. (2024) YY1-controlled regulatory connectivity and transcription are influenced by the cell cycle. *Nature Genetics* 56(9): 1938–1952.

Lázaro CA, Rhim JA, Yamada Y, et al. (1998) Generation of hepatocytes from oval cell precursors in culture. *Cancer Research* 58(23): 5514–5522.

Lee N, Maurange C, Ringrose L, et al. (2005) Suppression of Polycomb group proteins by JNK signalling induces transdetermination in Drosophila imaginal discs. *Nature* 438(7065): 234–237.

Leung W and Nagano T (2022) High-Throughput Preparation of Improved Single-Cell Hi-C Libraries Using an Automated Liquid Handling System. *Methods in Molecular Biology (Clifton, N.J.)* 2532: 201–214.

Levo M, Raimundo J, Bing XY, et al. (2022) Transcriptional coupling of distant regulatory genes in living embryos. *Nature* 605(7911): 754–760.

Li N and Hua J (2017) Immune cells in liver regeneration. *Oncotarget* 8(2): 3628–3639.

Li W, Li L and Hui L (2020) Cell Plasticity in Liver Regeneration. *Trends in Cell Biology* 30(4): 329–338.

Li L, Cui L, Lin P, et al. (2023) Kupffer-cell-derived IL-6 is repurposed for hepatocyte dedifferentiation via activating progenitor genes from injury-specific enhancers. *Cell Stem Cell* 30(3): 283-299.e9.

Lieberman-Aiden E, Van Berkum NL, Williams L, et al. (2009) Comprehensive Mapping of Long-Range Interactions Reveals Folding Principles of the Human Genome. *Science* 326(5950): 289–293.

Lizana L and Schwartz YB (2024) The scales, mechanisms, and dynamics of the genome architecture. *Science Advances* 10(15): eadm8167.

Llorens-Giralt P, Camilleri-Robles C, Corominas M, et al. (2021) Chromatin Organization and Function in Drosophila. *Cells* 10(9): 2362.

Llorens-Giralt P, Ruiz-Romero M, Nurtdinov R, et al. (2025) Sequential activation of transcription factors promotes liver regeneration through specific and developmental enhancers. *Cell Genomics*: 100887.

López-Luque J and Fabregat I (2018) Revisiting the liver: from development to regeneration - what we ought to know! *The International Journal of Developmental Biology* 62(6-7–8): 441–451.

Loubet-Senear K and Srivastava M (2024) Regeneration recapitulates many embryonic processes, including reuse of developmental regulatory regions. *bioRxiv: The Preprint Server for Biology*: 2024.07.04.601589.

Loubiere V, Papadopoulos GL, Szabo Q, et al. (2020) Widespread activation of developmental gene expression characterized by PRC1-dependent chromatin looping. *Science Advances* 6(2): eaax4001.

Lu W-Y, Bird TG, Boulter L, et al. (2015) Hepatic progenitor cells of biliary origin with liver repopulation capacity. *Nature Cell Biology* 17(8): 971–983.

Lupiáñez DG, Kraft K, Heinrich V, et al. (2015) Disruptions of Topological Chromatin Domains Cause Pathogenic Rewiring of Gene-Enhancer Interactions. *Cell* 161(5): 1012–1025.

Lupiáñez DG, Spielmann M and Mundlos S (2016) Breaking TADs: How Alterations of Chromatin Domains Result in Disease. *Trends in Genetics* 32(4): 225–237.

Ma X, Huang T, Chen X, et al. (2025) Molecular mechanisms in liver repair and regeneration: from physiology to therapeutics. *Signal Transduction and Targeted Therapy* 10(1): 63.

Maden M (2018) The evolution of regeneration – where does that leave mammals? *The International Journal of Developmental Biology* 62(6-7–8): 369–372.

Mattila J, Omelyanchuk L, Kyttala S, et al. (2005) Role of Jun N-terminal Kinase (JNK) signaling in the wound healing and regeneration of a Drosophila melanogaster wing imaginal disc. *The International Journal of Developmental Biology* 49(4): 391–399.

Maves L and Schubiger G (1995) *wingless* induces transdetermination in developing *Drosophila* imaginal discs. *Development* 121(5): 1263–1272.

Mehta AS and Singh A (2019) Insights into regeneration tool box: An animal model approach. *Developmental Biology* 453(2): 111–129.

Miao Q, Hill MC, Chen F, et al. (2019) SOX11 and SOX4 drive the reactivation of an embryonic gene program during murine wound repair. *Nature Communications* 10(1): 4042.

Michalopoulos GK, Barua L and Bowen WC (2005) Transdifferentiation of rat hepatocytes into biliary cells after bile duct ligation and toxic biliary injury†. *Hepatology* 41(3): 535–544.

Michalopoulos GK (2020) Liver Regeneration. In: Arias IM, Alter HJ, Boyer JL, et al. (eds) *The Liver*. 1st ed. Wiley, pp. 566–584.

Michalopoulos GK and Bhushan B (2021) Liver regeneration: biological and pathological mechanisms and implications. *Nature Reviews Gastroenterology & Hepatology* 18(1): 40–55.

Misteli T (2020) The Self-Organizing Genome: Principles of Genome Architecture and Function. *Cell* 183(1): 28–45.

Miyajima A, Tanaka M and Itoh T (2014) Stem/Progenitor Cells in Liver Development, Homeostasis, Regeneration, and Reprogramming. *Cell Stem Cell* 14(5): 561–574.

Mohana G, Dorier J, Li X, et al. (2023) Chromosome-level organization of the regulatory genome in the Drosophila nervous system. *Cell* 186(18): 3826-3844.e26.

Mokalled MH, Patra C, Dickson AL, et al. (2016) Injury-induced *ctgfa* directs glial bridging and spinal cord regeneration in zebrafish. *Science* 354(6312): 630–634.

Monga SP and Sadler KC (2020) An epigenetic perspective on liver regeneration. *Epigenomics* 12(5): 381–384.

Morata G and Lawrence P (2022) An exciting period of Drosophila developmental biology: Of imaginal discs, clones, compartments, parasegments and homeotic genes. *Developmental Biology* 484: 12–21.

Mouginot M, Hani S, Cousin P, et al. (2025) A boundary-defining protein facilitates megabase-scale regulatory chromosomal loop formation in *Drosophila* neurons. *Genes & Development*: genesdev;gad.352646.125v1.

Nora EP, Lajoie BR, Schulz EG, et al. (2012) Spatial partitioning of the regulatory landscape of the X-inactivation centre. *Nature* 485(7398): 381–385.

Nora EP, Goloborodko A, Valton A-L, et al. (2017) Targeted Degradation of CTCF Decouples Local Insulation of Chromosome Domains from Genomic Compartmentalization. *Cell* 169(5): 930-944.e22.

Ogiyama Y, Schuettengruber B, Papadopoulos GL, et al. (2018) Polycomb-Dependent Chromatin Looping Contributes to Gene Silencing during Drosophila Development. *Molecular Cell* 71(1): 73-88.e5.

Ozaki M (2020) Cellular and molecular mechanisms of liver regeneration: Proliferation, growth, death and protection of hepatocytes. *Seminars in Cell & Developmental Biology* 100: 62–73.

Paldi F and Cavalli G (2025) 3D genome folding in epigenetic regulation and cellular memory. *Trends in Cell Biology*: S0962892425000650.

Palmisano I, Danzi MC, Hutson TH, et al. (2019) Epigenomic signatures underpin the axonal regenerative ability of dorsal root ganglia sensory neurons. *Nature Neuroscience* 22(11): 1913–1924.

Perekatt AO, Valdez MJ, Davila M, et al. (2014) YY1 is indispensable for Lgr5+ intestinal stem cell renewal. *Proceedings of the National Academy of Sciences of the United States of America* 111(21): 7695–7700.

Pollex T, Marco-Ferreres R, Ciglar L, et al. (2024) Chromatin gene-gene loops support the cross-regulation of genes with related function. *Molecular Cell* 84(5): 822-838.e8.

Poss KD and Tanaka EM (2024) Hallmarks of regeneration. *Cell Stem Cell* 31(9): 1244–1261.

Pundhir S, Poirazi P and Gorodkin J (2015) Emerging applications of read profiles towards the functional annotation of the genome. *Frontiers in Genetics* 6.

Quaife-Ryan GA, Sim CB, Ziemann M, et al. (2017) Multicellular Transcriptional Analysis of Mammalian Heart Regeneration. *Circulation* 136(12): 1123–1139.

Ramírez F, Bhardwaj V, Arrigoni L, et al. (2018) High-resolution TADs reveal DNA sequences underlying genome organization in flies. *Nature Communications* 9(1): 189.

Ramos-Rodríguez M, Pérez-González B and Pasquali L (2021) The β-Cell Genomic Landscape in T1D: Implications for Disease Pathogenesis. *Current Diabetes Reports* 21(1): 1.

Rao SSP, Huang S-C, Glenn St Hilaire B, et al. (2017) Cohesin Loss Eliminates All Loop Domains. *Cell* 171(2): 305-320.e24.

Repiso A, Bergantiños C, Corominas M, et al. (2011) Tissue repair and regeneration in Drosophila imaginal discs: Regeneration in Drosophila. *Development, Growth & Differentiation* 53(2): 177–185.

Repiso A, Bergantiños C and Serras F (2013) Cell fate respecification and cell division orientation drive intercalary regeneration in *Drosophila* wing discs. *Development* 140(17): 3541–3551.

Restrepo S and Basler K (2016) Drosophila wing imaginal discs respond to mechanical injury via slow InsP3R-mediated intercellular calcium waves. *Nature Communications* 7(1): 12450.

Rodriguez AM and Kang J (2020) Regeneration enhancers: Starting a journey to unravel regulatory events in tissue regeneration. *Seminars in Cell & Developmental Biology* 97: 47–54.

Rowley MJ, Nichols MH, Lyu X, et al. (2017) Evolutionarily Conserved Principles Predict 3D Chromatin Organization. *Molecular Cell* 67(5): 837-852.e7.

Rowley MJ and Corces VG (2018) Organizational principles of 3D genome architecture. *Nature Reviews Genetics* 19(12): 789–800.

Rui L (2014) Energy metabolism in the liver. *Comprehensive Physiology* 4(1): 177–197.

Santabárbara-Ruiz P, López-Santillán M, Martínez-Rodríguez I, et al. (2015) ROS-Induced JNK and p38 Signaling Is Required for Unpaired Cytokine Activation during Drosophila Regeneration. *PLOS Genetics* Copenhaver GP (ed.) 11(10): e1005595.

Santabárbara-Ruiz P, Esteban-Collado J, Pérez L, et al. (2019) Ask1 and Akt act synergistically to promote ROS-dependent regeneration in Drosophila. *PLOS Genetics* Copenhaver GP (ed.) 15(1): e1007926.

Schaub JR, Huppert KA, Kurial SNT, et al. (2018) De novo formation of the biliary system by TGFβ-mediated hepatocyte transdifferentiation. *Nature* 557(7704): 247–251.

Schubiger G (1971) Regeneration, duplication and transdetermination in fragments of the leg disc of Drosophila melanogaster. *Developmental Biology* 26(2): 277–295.

Schwartz YB, Linder-Basso D, Kharchenko PV, et al. (2012) Nature and function of insulator protein binding sites in the *Drosophila* genome. *Genome Research* 22(11): 2188–2198.

Sexton T, Yaffe E, Kenigsberg E, et al. (2012) Three-Dimensional Folding and Functional Organization Principles of the Drosophila Genome. *Cell* 148(3): 458–472.

Shlyueva D, Stampfel G and Stark A (2014) Transcriptional enhancers: from properties to genome-wide predictions. *Nature Reviews Genetics* 15(4): 272–286.

Shteyer E, Liao Y, Muglia LJ, et al. (2004) Disruption of Hepatic Adipogenesis Is Associated With Impaired Liver Regeneration in Mice. *Hepatology* 40(6): 1322–1332.

Si-Tayeb K, Lemaigre FP and Duncan SA (2010) Organogenesis and Development of the Liver. *Developmental Cell* 18(2): 175–189.

Slack JM (2017) Animal regeneration: ancestral character or evolutionary novelty? *EMBO reports* 18(9): 1497–1508.

Smith-Bolton RK, Worley MI, Kanda H, et al. (2009) Regenerative Growth in Drosophila Imaginal Discs Is Regulated by Wingless and Myc. *Developmental Cell* 16(6): 797–809.

Solhi R, Lotfinia M, Gramignoli R, et al. (2021) Metabolic hallmarks of liver regeneration. *Trends in Endocrinology & Metabolism* 32(9): 731–745.

Song Y, Liang Z, Zhang J, et al. (2022) CTCF functions as an insulator for somatic genes and a chromatin remodeler for pluripotency genes during reprogramming. *Cell Reports* 39(1): 110626.

Stadhouders R, Vidal E, Serra F, et al. (2018) Transcription factors orchestrate dynamic interplay between genome topology and gene regulation during cell reprogramming. *Nature Genetics* 50(2): 238–249.

Stanger BZ (2015) Cellular Homeostasis and Repair in the Mammalian Liver. *Annual Review of Physiology* 77(1): 179–200.

Sun G and Irvine KD (2011) Regulation of Hippo signaling by Jun kinase signaling during compensatory cell proliferation and regeneration, and in neoplastic tumors. *Developmental Biology* 350(1): 139–151.

Sun X, Chuang J-C, Kanchwala M, et al. (2016) Suppression of the SWI/SNF Component Arid1a Promotes Mammalian Regeneration. *Cell Stem Cell* 18(4): 456–466.

Sunderland ME (2010) Regeneration: Thomas Hunt Morgan's Window into Development. *Journal of the History of Biology* 43(2): 325–361.

Suzuki N and Ochi H (2020) Regeneration enhancers: A clue to reactivation of developmental genes. *Development, Growth & Differentiation* 62(5): 343–354.

Szabo Q, Jost D, Chang J-M, et al. (2018) TADs are 3D structural units of higher-order chromosome organization in *Drosophila*. *Science Advances* 4(2): eaar8082.

Takahashi K and Yamanaka S (2006) Induction of Pluripotent Stem Cells from Mouse Embryonic and Adult Fibroblast Cultures by Defined Factors. *Cell* 126(4): 663–676.

Tanaka EM and Reddien PW (2011) The Cellular Basis for Animal Regeneration. *Developmental Cell* 21(1): 172–185.

Tao L, Yu HV, Llamas J, et al. (2021) Enhancer decommissioning imposes an epigenetic barrier to sensory hair cell regeneration. *Developmental Cell* 56(17): 2471-2485.e5.

Taub R (1996) Transcriptional control of liver regeneration. *The FASEB Journal* 10(4): 413–427.

Taub R (2004) Liver regeneration: from myth to mechanism. *Nature Reviews Molecular Cell Biology* 5(10): 836–847.

Thomas HF and Buecker C (2023) What is an enhancer? *BioEssays* 45(10): 2300044.

Trefts E, Gannon M and Wasserman DH (2017) The liver. *Current biology: CB* 27(21): R1147–R1151.

Ulianov SV, Zakharova VV, Galitsyna AA, et al. (2021) Order and stochasticity in the folding of individual Drosophila genomes. *Nature Communications* 12(1): 41.

van Steensel B and Furlong EEM (2019) The role of transcription in shaping the spatial organization of the genome. *Nature Reviews. Molecular Cell Biology* 20(6): 327–337.

Verghese S and Su TT (2016) Drosophila Wnt and STAT Define Apoptosis-Resistant Epithelial Cells for Tissue Regeneration after Irradiation. *PLOS Biology* Edgar BA (ed.) 14(9): e1002536.

Vieira JM, Howard S, Villa Del Campo C, et al. (2017) BRG1-SWI/SNF-dependent regulation of the Wt1 transcriptional landscape mediates epicardial activity during heart development and disease. *Nature Communications* 8(1): 16034.

Viragova S, Li D and Klein OD (2024) Activation of fetal-like molecular programs during regeneration in the intestine and beyond. *Cell Stem Cell* 31(7): 949–960.

Vizcaya-Molina E, Klein CC, Serras F, et al. (2018) Damage-responsive elements in *Drosophila* regeneration. *Genome Research* 28(12): 1852–1866.

Vizcaya-Molina E, Klein CC, Serras F, et al. (2020) Chromatin dynamics in regeneration epithelia: Lessons from Drosophila imaginal discs. *Seminars in Cell & Developmental Biology* 97: 55–62.

Wang X, Foster M, Al-Dhalimy M, et al. (2003) The origin and liver repopulating capacity of murine oval cells. *Proceedings of the National Academy of Sciences of the United States of America* 100 Suppl 1(Suppl 1): 11881–11888.

Wang S, Zhang C, Hasson D, et al. (2019) Epigenetic Compensation Promotes Liver Regeneration. *Developmental Cell* 50(1): 43-56.e6.

Wang W, Hu C-K, Zeng A, et al. (2020a) Changes in regeneration-responsive enhancers shape regenerative capacities in vertebrates. *Science* 369(6508): eaaz3090.

Wang AW, Wang YJ, Zahm AM, et al. (2020b) The Dynamic Chromatin Architecture of the Regenerating Liver. *Cellular and Molecular Gastroenterology and Hepatology* 9(1): 121–143.

Wei Y, Wang YG, Jia Y, et al. (2021) Liver homeostasis is maintained by midlobular zone 2 hepatocytes. *Science* 371(6532): eabb1625.

Weintraub AS, Li CH, Zamudio AV, et al. (2017) YY1 Is a Structural Regulator of Enhancer-Promoter Loops. *Cell* 171(7): 1573-1588.e28.

Worley MI, Setiawan L and Hariharan IK (2012) Regeneration and Transdetermination in *Drosophila* Imaginal Discs. *Annual Review of Genetics* 46(1): 289–310.

Worley MI, Everetts NJ, Yasutomi R, et al. (2022) Ets21C sustains a pro-regenerative transcriptional program in blastema cells of Drosophila imaginal discs. *Current biology: CB* 32(15): 3350-3364.e6.

Wutz G, Várnai C, Nagasaka K, et al. (2017) Topologically associating domains and chromatin loops depend on cohesin and are regulated by CTCF, WAPL, and PDS5 proteins. *The EMBO Journal* 36(24): 3573–3599.

Xu J, Guo P, Hao S, et al. (2024) A spatiotemporal atlas of mouse liver homeostasis and regeneration. *Nature Genetics* 56(5): 953–969.

Yan R, Cigliola V, Oonk KA, et al. (2023) An enhancer-based gene-therapy strategy for spatiotemporal control of cargoes during tissue repair. *Cell Stem Cell* 30(1): 96-111.e6.

Yang K and Kang J (2019) Tissue Regeneration Enhancer Elements: A Way to Unlock Endogenous Healing Power. *Developmental Dynamics* 248(1): 34–42.

Yanger K, Zong Y, Maggs LR, et al. (2013) Robust cellular reprogramming occurs spontaneously during liver regeneration. *Genes & Development* 27(7): 719–724.

Zhang L, Huang X, Meng Z, et al. (2009) Significance and Mechanism of CYP7a1 Gene Regulation during the Acute Phase of Liver Regeneration. *Molecular Endocrinology* 23(2): 137–145.

Zhang C, Macchi F, Magnani E, et al. (2021) Chromatin states shaped by an epigenetic code confer regenerative potential to the mouse liver. *Nature Communications* 12(1): 4110.

Zhong H, Zhang J, Lu Y, et al. (2023) 3D genome perspective on cell fate determination, organ regeneration, and diseases. *Cell Proliferation* 56(5): e13482.

Zunjarrao S and Gambetta MC (2025) Principles of long-range gene regulation. *Current Opinion in Genetics & Development* 91: 102323.

APPENDICES

APPENDIX I

Publication (Llorens-Giralt *et al*., 2025)

Cell Genomics

Article

Sequential activation of transcription factors promotes liver regeneration through specific and developmental enhancers

Graphical abstract

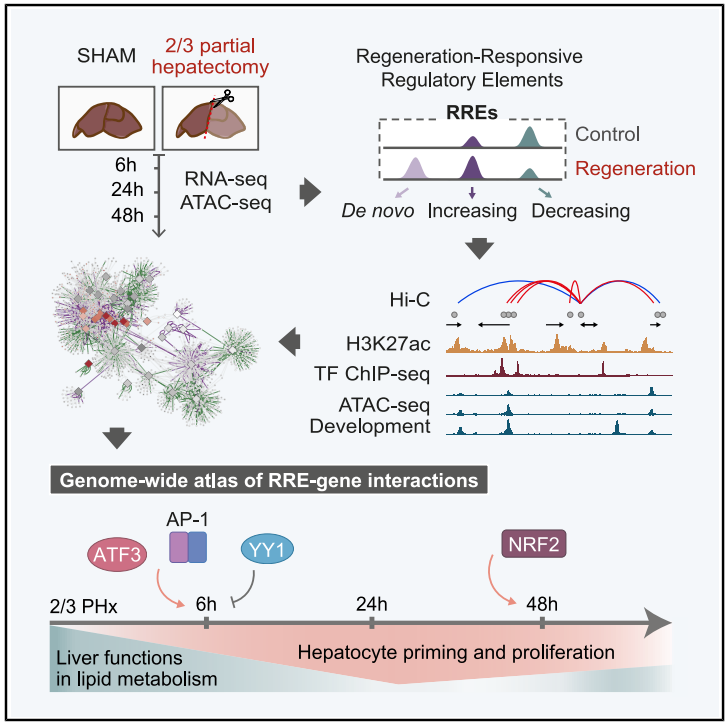

Highlights

- Regeneration-responsive regulatory elements (RREs) were identified in early liver regeneration
- RRE-gene interaction atlas reveals shift from lipid metabolism to proliferative programs
- RREs comprise both regeneration-specific and reactivated developmental enhancers
- Integrative genomic analysis generates GRN with a transcription-factor-activation cascade

Authors

Palmira Llorens-Giralt, Marina Ruiz-Romero, Ramil Nurtdinov, ..., Florenci Serras, Isabel Fabregat, Montserrat Corominas

Correspondence

mcorominas@ub.edu

In brief

Llorens-Giralt et al. study how liver cells respond to partial hepatectomy by examining changes in gene activity and chromatin accessibility. They create a functional regulatory map of early liver regeneration and identify key elements controlling specific gene programs essential for liver repair and growth.

Llorens-Giralt et al., 2025, Cell Genomics 5, 100887
July 9, 2025
https://doi.org/10.1016/j.xgen.2025.100887

CellPress

Please cite this article in press as: Llorens-Giralt et al., Sequential activation of transcription factors promotes liver regeneration through specific and developmental enhancers, Cell Genomics (2025), https://doi.org/10.1016/j.xgen.2025.100887

Cell Genomics

CellPress
OPEN ACCESS

Article

Sequential activation of transcription factors promotes liver regeneration through specific and developmental enhancers

Palmira Llorens-Giralt,[1,6] Marina Ruiz-Romero,[2,6] Ramil Nurtdinov,[2] Macarena Herranz-Itúrbide,[3,4] Guillermo P. Vicent,[5] Florenci Serras,[1] Isabel Fabregat,[3,4] and Montserrat Corominas[1,7,*]

[1]Department of Genetics, Microbiology and Statistics, Faculty of Biology and Institute of Biomedicine (IBUB), University of Barcelona, Diagonal 643, 08028 Barcelona, Catalonia, Spain
[2]Centre for Genomic Regulation (CRG), The Barcelona Institute for Science and Technology (BIST), Dr. Aiguader 88, Barcelona 08003, Spain
[3]TGF-beta and Cancer Group, Oncobell Program, Bellvitge Biomedical Research Institute (IDIBELL), Av. Granvia de l'Hospitalet 199, 08908 L'Hospitalet de Llobregat, Barcelona, Spain
[4]Oncology Program, National Biomedical Research Institute on Liver and Gastrointestinal Diseases (CIBEREHD), Instituto de Salud Carlos III, Madrid, Spain
[5]Molecular Biology Institute of Barcelona, Consejo Superior de Investigaciones Científicas (IBMB-CSIC), Baldiri Reixac 4-8, 08028 Barcelona, Spain
[6]These authors contributed equally
[7]Lead contact
*Correspondence: mcorominas@ub.edu
https://doi.org/10.1016/j.xgen.2025.100887

SUMMARY

The mammalian liver exhibits remarkable regenerative capabilities after injury or resection. Central to this process is the precise modulation of gene expression, driven by changes in chromatin structure and the temporal activation of distal regulatory elements. In this study, we integrated chromatin accessibility and transcriptomic data after partial hepatectomy in mice. We show that the expression of crucial regeneration genes is orchestrated by a diverse array of *cis*-regulatory elements, including regeneration-specific enhancers and enhancers repurposed from various developmental stages. These enhancers collaborate to activate the transcriptional programs required for hepatocyte priming and proliferation, with their activity initially regulated by the activator protein-1 (AP-1) complex and ATF3, and subsequently by nuclear factor erythroid 2 (NFE2)-related factor 2 (NRF2) during proliferation. Our results also indicate that hepatic regeneration involves the repression of enhancers regulating liver-specific metabolic functions, particularly those involved in lipid metabolism. This study provides a genome-wide atlas of enhancer-gene interactions, offering new insights into the regulatory mechanisms underlying liver regeneration.

INTRODUCTION

Regenerative capacity varies greatly, not only across species but also between tissues, organs, and developmental stages within the same species. The evolutionary conservation of regeneration-associated genes suggests that variations in regenerative ability arise from differences in how these genes are regulated after injury, rather than simply whether they are present.[1,2] Genome-wide chromatin profiling has identified *cis*-regulatory elements activated by injury that orchestrate regenerative transcriptional programs. These regeneration-responsive elements have been characterized in regenerating zebrafish heart,[3,4] fins,[5,6] and spinal cord,[7] as well as *Drosophila* wing imaginal discs.[8,9] In mice, similar enhancer activity has been observed in skeletal muscle,[10] Schwann cells,[11] skin stem cells,[12,13] and heart.[14,15] Recent studies show that regeneration-responsive enhancers can be engineered to drive pro-regenerative gene expression specifically in damaged tissues via transgenic models or viral vectors.[5,16] These elements are transiently activated after injury and deactivate once repair is complete, minimizing potential tumorigenic risk.

In vertebrates, the liver has remarkable regenerative capacity, fully restoring mass and function after injury or partial hepatectomy (PHx).[17,18] Under normal conditions, hepatocytes are quiescent, but within 4 h after PHx, approximately 95% re-enter the cell cycle.[19,20] This is triggered by a cytokine-driven priming phase, which induces proliferation genes and represses liver-specific differentiation genes.[21] Growth factors then promote cell-cycle progression, leading to mitosis by 48 h.[18] Proliferation is later arrested by transforming growth factor (TGF)-β and activins via tumor-suppressor gene activation, thus preserving liver size and homeostasis.[19,22]

Understanding the regulatory mechanisms of liver regeneration could have profound implications for regenerative medicine.

Please cite this article in press as: Llorens-Giralt et al., Sequential activation of transcription factors promotes liver regeneration through specific and developmental enhancers, Cell Genomics (2025), https://doi.org/10.1016/j.xgen.2025.100887

Although genetic and epigenetic drivers have been described,[23,24] the role of specialized enhancers in controlling pro-regenerative genes remains unclear. Recent studies have explored histone modifications and DNA methylation after PHx,[21,25–27] chromatin accessibility dynamics after toxicity in a model of hereditary tyrosinemia,[28] and epigenetic changes during biliary reprogramming.[29] Single-cell approaches have further revealed the gene regulatory networks (GRNs) of hepatic cells during the later stages of liver regeneration after PHx.[30–32]

However, our understanding of how early signals reshape gene expression and chromatin architecture during liver regeneration remains incomplete. Although recent evidence suggests that hepatocytes adopt a fetal-like chromatin and transcriptional state,[30,31] it remains unclear whether regeneration relies solely on reactivating developmental networks or involves a distinct regeneration-specific program.

Here, we profiled gene expression and chromatin accessibility during the early stages of liver regeneration in mice. Using an integrative algorithm that combines chromatin state and 3D conformation data, we identified regulatory elements specifically activated after PHx and predicted their target genes. This analysis revealed reduced accessibility at regions associated with liver-specific metabolic genes, alongside increased accessibility at regulatory elements linked to pro-proliferative genes. Additionally, we constructed a GRN that uncovered a cascade of transcription factor (TF) activation, highlighting key TFs that are upregulated and/or essential for regeneration. Our findings further suggest that liver regeneration involves both regeneration-specific enhancers and reactivated developmental enhancers, each governed by distinct regulatory mechanisms and associated with different biological functions.

RESULTS

Liver regeneration-responsive regulatory elements

To identify regulatory elements involved in early liver regeneration, we performed genome-wide transcriptomics and chromatin accessibility profiling on mouse livers at 6, 24, and 48 h after sham (control) or two-thirds (2/3) PHx (REG) surgery (Figure 1A), using the same samples for RNA sequencing (RNA-seq)[33] and assay for transposase-accessible chromatin using sequencing (ATAC-seq). The time points selected correspond with critical stages in liver regeneration, marking the end of the priming stage (6 h), the entry of hepatocytes into the S phase of the cell cycle (24 h), and their progression into mitosis (48 h). The latter two fall within the proliferation or progression phase of liver regeneration.[17,18]

First, we used correspondence analysis and association plots[34] to cluster the expressed genes (11,512 genes) (Figures S1A–S1C). This method enabled us to identify the genes that were differentially expressed either in the control livers or at specific time points during regeneration (6, 24, or 48 h post PHx) (Figures 1B and 1C), as well as those that were co-expressed across different regeneration time points (Figures S1D and S1E; Table S1). The cluster corresponding to the initial stage of regeneration (REG 6 h) showed the highest gene count, with 1,375 genes exhibiting significantly higher expression levels at 6 h compared with the other conditions (Figures 1B, 1C, and S1C). As previously reported,[35] we found that the gene expression profile at the initial time point post-PHx resembled that of the corresponding sham-operated control, albeit with a tendency toward increased expression levels in regeneration (Figures S1A and S1B). This similarity is likely due to the disturbance in gene expression caused by surgical stress and anesthesia. The other gene clusters specific to regeneration encompassed approximately 200–400 genes each (Figures 1B, 1C, S1D, and S1E). Notably, the cluster of genes co-expressed across regeneration (REG 6-24-48 h) comprised only 227 genes (Figures S1D and S1E). This suggests a dynamic transcriptomic profile with sequential gene activation and repression.

Gene Ontology (GO) analysis revealed that control livers were enriched for lipid-related pathways, including steroid and bile acid metabolism, as well as lipid catabolism (Figure 1D), consistent with known suppression of bile acid synthesis during liver regeneration to prevent cytotoxicity.[36] In contrast, genes associated with cell signaling, cell response, proliferation, and mitosis were specifically enriched in particular regeneration clusters, indicating a sequential activation during regeneration (Figure 1D). For instance, the REG 6 h cluster showed unique enrichment for hepatocyte growth factor (HGF) response and phospholipid biosynthesis, whereas several terms related to the mitotic cell cycle were significantly enriched among the REG 48 h cluster. HGF is among the earliest mitogens detected after PHx in mice and plays a crucial role in liver regeneration,[37] while the synthesis of phospholipids is essential for generating new cell membranes and, therefore, for hepatocyte proliferation during regeneration.[38] These transcriptomic changes after PHx accurately reflect known physiological events underlying early liver regeneration.[25,35]

Next, we examined the changes in chromatin accessibility that could trigger these transcriptional profiles by mapping open regions by ATAC-seq in livers at 6, 24 and 48 h after sham surgery or 2/3 PHx (Figures S2A and S2B). We performed pairwise comparisons between control and regeneration at each time point ($|FC| > 1.7$) and identified more than 17,000 differentially accessible chromatin regions in at least one time point, compared with 60,000 that were non-differentially accessible (NDA). Differentially accessible regions were classified into *de novo*, increasing or decreasing peaks: *de novo* peaks were open regions detected exclusively during regeneration; increasing peaks were regions already open in the control but displaying higher accessibility during regeneration; and decreasing peaks were regions with lower accessibility during regeneration (Figures 2A and 2B). We observed a similar number of decreasing peaks over time, with nearly 4,000 identified at each time point (Figure 2C). In contrast, the number of increasing peaks slightly increased over time (1,717 peaks at 6 h, 2,935 peaks at 24 h, and 2,886 peaks at 48 h after PHx) and *de novo* peaks were more enriched at 6 h and 48 h compared with 24 h: 427, 449, and 255 peaks, respectively (Figure 2C). Differentially accessible peaks from all classes were mostly time point specific (Figure S2C), indicating that chromatin architecture changes throughout the regenerative process.

We next classified ATAC-seq peaks by distance to the nearest transcription start site as promoter (±500 bp), proximal (<1 kb), or distal (≥1 kb) regions. In comparison with NDA, the *de novo*,

Please cite this article in press as: Llorens-Giralt et al., Sequential activation of transcription factors promotes liver regeneration through specific and developmental enhancers, Cell Genomics (2025), https://doi.org/10.1016/j.xgen.2025.100887

CellPress
OPEN ACCESS

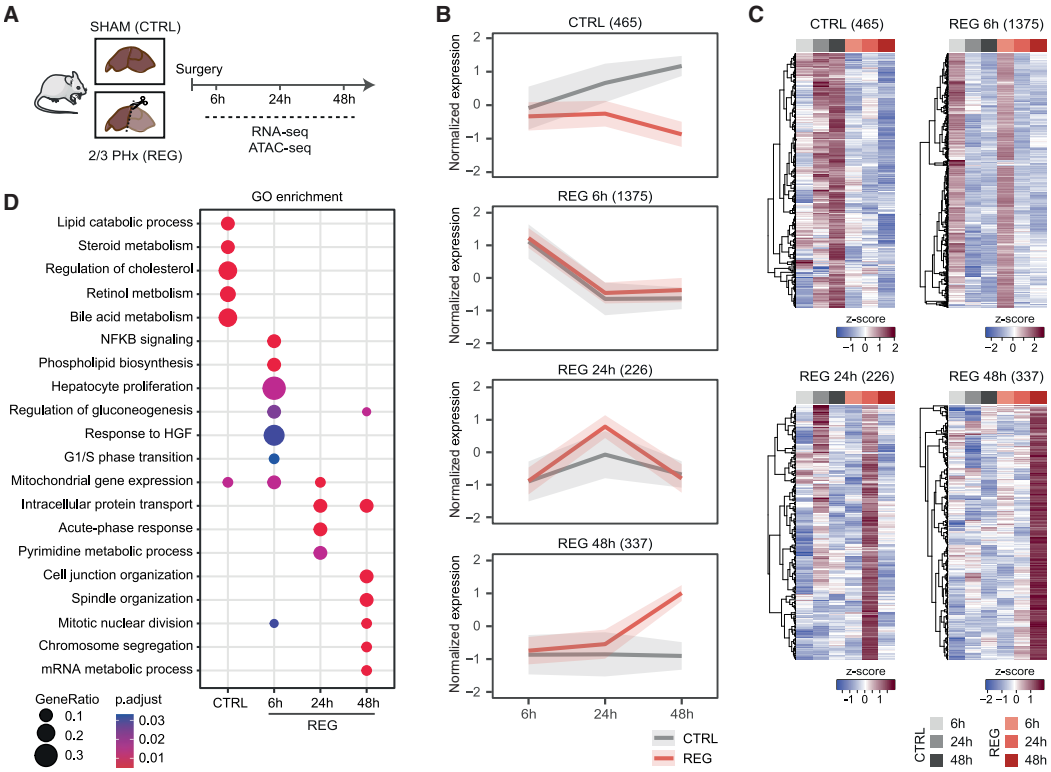

Figure 1. Gene expression profiles of liver regeneration after PHx

(A) Experimental design. Male and female mice aged 8–16 weeks underwent either sham surgery (SHAM/CTRL) or 2/3 PHx/REG. Mice were euthanized at 6, 24, or 48 h post surgery, and liver lobes were snap-frozen. RNA-seq data were obtained from Herranz-Itúrbide et al.[33] and the same biological samples were used for ATAC-seq.

(B) Standardized expression profiles of four gene clusters: control, 6 h, 24 h, and 48 h after PHx. Gene expression values are *Z*- score normalized. Mean expression (line) ± standard deviation (shade) and gene counts are shown per cluster.

(C) Heatmaps of expression for each cluster. Columns represent conditions (averaged across replicates), and gene expression is *Z*- score normalized, gene order was established by hierarchical clustering. Gene counts per cluster are shown above.

(D) GO terms enriched in each gene cluster (one-sided Fisher's exact test $p_{adjusted} < 0.05$). NFKB, nuclear factor κ-light-chain-enhancer of activated B cells. See also Figure S1.

increasing, and decreasing peaks tended to be more prevalent in the distal regions (>90%), primarily within introns and intergenic regions, while less than 7% were in promoters and only 2%–3% within proximal regions (Figures 2D and S2D). Indeed, most promoters remained relatively stable during regeneration, comprising nearly 25% of NDA peaks. Given that distal regions are typically associated with enhancers, these findings suggest that the chromatin response to PHx predominantly involves the modulation of enhancer accessibility.

To further characterize regeneration-responsive regulatory elements (RREs), we integrated ATAC-seq data with H3K27ac profiles from undamaged[39] and regenerating livers,[40] as this histone mark is linked to active enhancers.[41] First, we observed a highly statistically significant overlap (Fisher's exact test, $p = 2.2e^{-16}$) between RREs (extended to 500 bp to incorporate the flanking nucleosomes) and H3K27ac. Approximately 65% of RREs were flanked by H3K27ac enriched regions, further supporting their role as enhancers. We observed that the H3K27ac signature differed for each type of RRE (Figure 2E). Compared with NDA, *de novo* and increasing RREs exhibited a higher proportion of peaks exclusively marked by H3K27ac during regeneration (REG specific). In contrast, decreasing peaks tended to be marked both in control and regeneration or only in the control. While certain *de novo* peaks exhibited regeneration-specific H3K27ac, indicating they can gain acetylation after PHx, most of them were unmarked in all conditions. This suggests that the regulation mediated by these elements may occur independent of this histone tail acetylation. As previously proposed, the active enhancer repertoire cannot be fully characterized by H3K27ac alone.[42]

Switch in chromatin accessibility from RREs linked to homeostatic lipid metabolism to proliferation-associated RREs

To better understand gene regulation during liver regeneration, we mapped genome-wide functional enhancer-gene pairs.

Please cite this article in press as: Llorens-Giralt et al., Sequential activation of transcription factors promotes liver regeneration through specific and developmental enhancers, Cell Genomics (2025), https://doi.org/10.1016/j.xgen.2025.100887

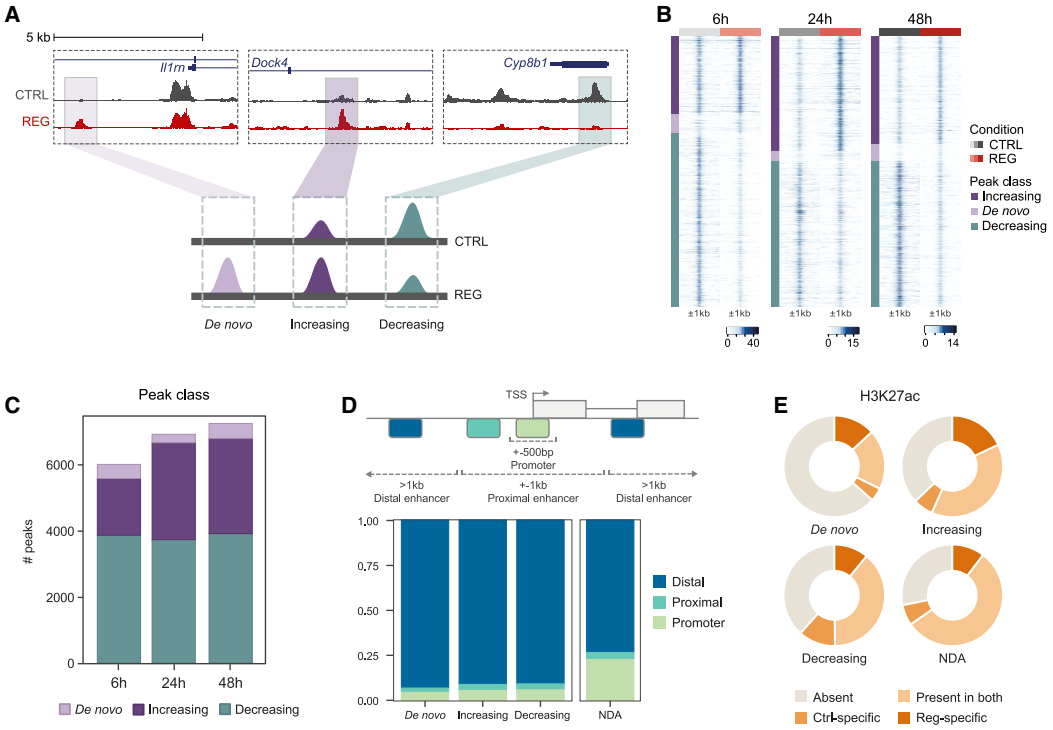

Figure 2. Chromatin accessibility changes during liver regeneration

(A) Genome browser views and schematics of *de novo*, increasing and decreasing peaks.

(B) Quantile normalized ATAC-seq signals ±1 kb from peak summits, grouped by peak class.

(C) Number of differentially accessible peaks per class at each time point.

(D) (Top) Genomic annotation of peaks. (Bottom) Proportion of promoters, proximal, and distal enhancers per class peaks.

(E) H3K27ac presence in control (uninjured) and regeneration (40 h post PHx) livers in NDA peaks and RREs. See also Figure S2.

Proximal enhancers were assigned to the nearest gene, while the target genes of distal enhancers were predicted using the activity-by-contact (ABC) model of enhancer-promoter regulation.[43] Briefly, this model is based on the principle that each enhancer regulates gene expression proportionally to its activity, and the frequency of its interaction with the gene's promoter. The ABC model combines chromatin state data, such as accessibility and histone modifications, to assess enhancer activity, and uses chromosome conformation capture (Hi-C) data to infer contact frequency between enhancers and promoters. This model outperforms simpler alternatives such as distance-based and Hi-C contact-based predictions. For input into the ABC model, we used our ATAC-seq data, publicly available H3K27ac chromatin immunoprecipitation sequencing (ChIP-seq) data from regenerating livers[40] and *in situ* Hi-C and promoter-capture Hi-C data from intact livers.[44]

The ABC algorithm predicted 15,816 distal enhancer-gene pairs, of which 15,499 (97.9%) were associated with expressed genes in at least one condition (Tables S2 and S3). Unlike conventional methods that assign enhancers solely based on the proximity to the nearest gene, the ABC method allowed us to predict the target genes of distal enhancers even when these were located megabases away. For instance, it identified an interaction between two increasing enhancers and a *de novo* enhancer with the promoter of the *Pnpla8* gene, despite being separated by more than 1.2 Mb in the linear genome (Figure 3A). We next assessed the Pearson's correlation coefficient between chromatin accessibility at regeneration-responsive promoters and enhancers and their target gene expression across time points. Promoters showed the highest correlation, followed by proximal and distal enhancers (Figure S3A). Moreover, increasing peaks exhibited significantly stronger correlations than *de novo* or decreasing peaks (Figure S3B). Altogether, these results support the accuracy of ABC-predicted enhancer-gene pairs.

Next, we analyzed the expression of predicted target genes during regeneration and found distinct transcriptional patterns across RRE types: genes linked to *de novo* and increasing promoters were largely upregulated, while those associated with decreasing promoters showed consistent downregulation (ANOVA with Tukey's honestly significant difference [HSD] test, $p < 0.05$) (Figure 3B). The target genes of *de novo* and increasing enhancers displayed no statistically significant differences between them, but differed significantly from those associated with decreasing enhancers across all time points (Figure 3B). Furthermore, the target genes of *de novo* and increasing RREs

Please cite this article in press as: Llorens-Giralt et al., Sequential activation of transcription factors promotes liver regeneration through specific and developmental enhancers, Cell Genomics (2025), https://doi.org/10.1016/j.xgen.2025.100887

CellPress
OPEN ACCESS

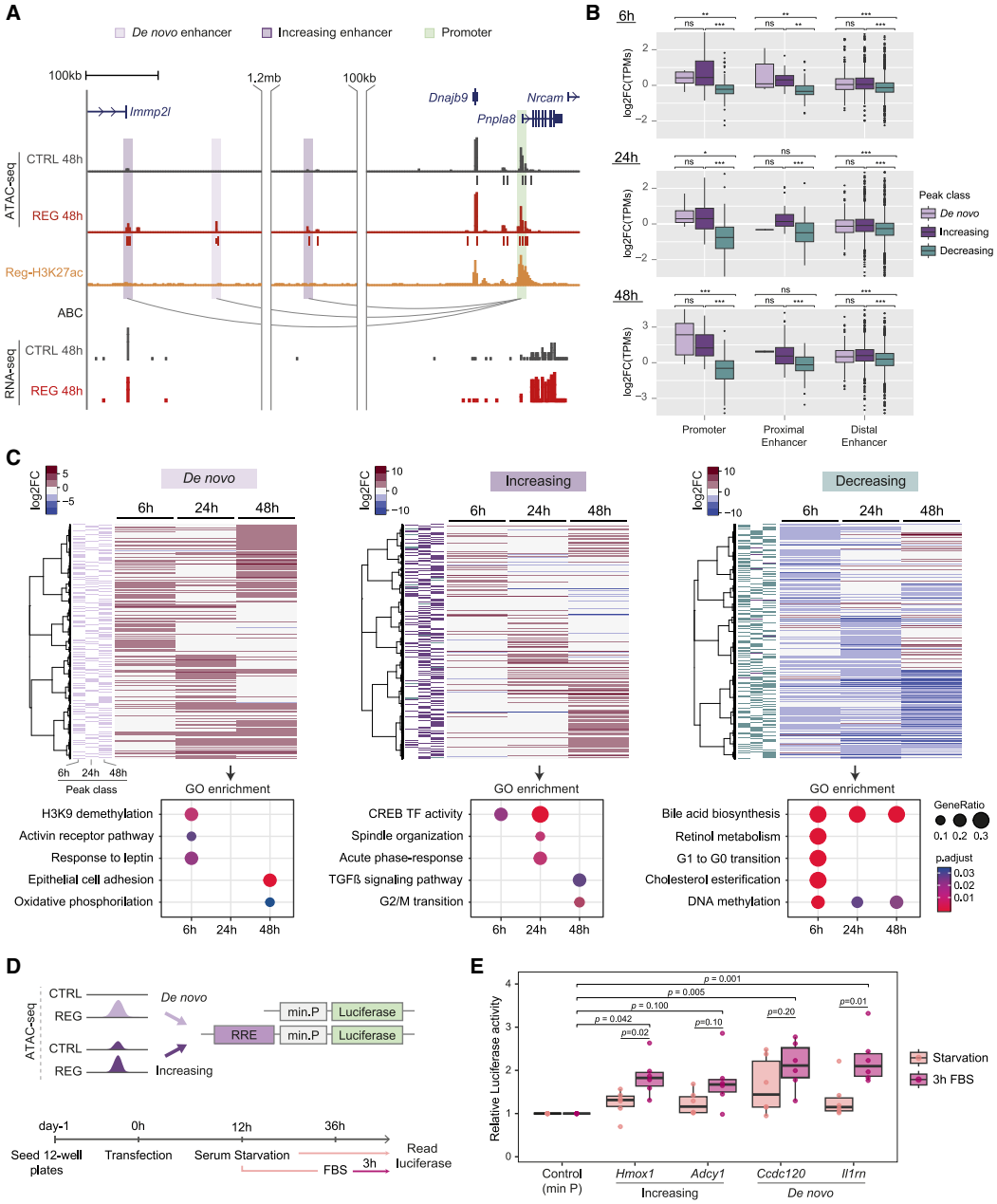

Figure 3. Enhancer-gene predictions using the ABC algorithm reveal opposite regulation for proliferation and metabolic genes

(A) Genome browser screenshot showing an ABC algorithm prediction at 48 h post-PHx. One *de novo* and two increasing enhancers (light and dark purple) are linked to the upregulated gene *Pnpla8*, located kilobases away. One replicate is shown for simplicity.

(B) Log2FC (TPM) of target genes associated with RREs in REG vs. CTRL samples. Two-way ANOVA followed by Tukey's HSD test was used to assess statistical differences between peak classes (*de novo*, increasing, and decreasing) and genomic regions (promoter, proximal, distal) at 6, 24, and 48 h. Significance shown only between peak classes: ns, non-significant; $^{*}p_{adjusted} < 0.05$, $^{**}p_{adjusted} < 0.01$, $^{***}p_{adjusted} < 0.001$.

(C) Expression of target genes linked to *de novo*, increasing, and decreasing RREs, clustered by log2FC (TPM), gene order was established by hierarchical clustering. (Below) Time-specific GO terms enriched in each RRE class (one-sided Fisher's exact test $p_{adjusted} < 0.05$).

(legend continued on next page)

Please cite this article in press as: Llorens-Giralt et al., Sequential activation of transcription factors promotes liver regeneration through specific and developmental enhancers, Cell Genomics (2025), https://doi.org/10.1016/j.xgen.2025.100887

tended to be upregulated during regeneration, whereas decreasing RREs were found to be mainly associated with downregulated genes (Figure 3C). GO analysis revealed that *de novo* and increasing RRE target genes were significantly enriched in signaling pathways known to play a role in liver regeneration at all three time points, such as the activin/TGF-β pathway,[19] with increasing RREs also associated with genes involved in the cell cycle (Figure 3C). In contrast, decreasing RREs mainly controlled the expression of genes related to liver-specific functions in lipid metabolism, including pathways associated with cholesterol and retinol metabolism, as well as bile acid biosynthesis. These findings align with the enriched biological functions identified in our transcriptomics analysis. Notably, the target genes from *de novo* and increasing RREs were enriched in functions that parallel those of the REG-specific transcriptomic gene clusters (Figure 1D), including the acute-phase response at 24 h and the mitosis-related signaling pathways at 48 h post PHx. In contrast, the steroids/cholesterol, retinol and bile acid metabolic pathways, specifically enriched for decreasing RRE-target genes, also exhibited enrichment within the cluster of control-specific genes from the RNA-seq analysis (Figure 1D). This suggests that *de novo* and increasing enhancers are activated post PHx to upregulate genes required for early liver regeneration, whereas decreasing RREs influence gene expression in the intact adult liver but have reduced activity after PHx. Furthermore, our analysis revealed an enrichment of genes associated with the DNA methylation pathway among all decreasing RREs (Figure 3C). The dynamics of DNA methylation during liver regeneration are complex,[45] and consistent with this, we identified genes within this group involved in both methylation and demethylation processes.

To validate putative RREs as enhancers capable of driving gene expression, we conducted a transient reporter assay in hepatocyte cell cultures. We cloned candidate RREs upstream of a minimal promoter and a luciferase gene cassette to assess their enhancer activity. Specifically, we tested four candidate sequences: (1) a distal increasing enhancer upstream of *Hmox1*; (2) an increasing enhancer located within the 10th intron of *Adcy1*; (3) a proximal *de novo* enhancer that progressively gains accessibility and is predicted to regulate *Ccdc120*, a gene exhibiting increased expression throughout regeneration; and (4) an intronic *de novo* enhancer predicted by the ABC model to target *Il1rn*, a gene upregulated 6 h post PHx (Figure S3C). These constructs were transiently transfected into a hepatocyte cell line,[46] serum starved for 24 h to induce quiescence, and then either stimulated with 10% fetal bovine serum for 3 h or maintained in serum-free conditions (Figure 3D), mimicking the quiescence-to-proliferation transition characteristic of liver regeneration. Serum stimulation significantly increased luciferase activity for the *Hmox1* (increasing) and *Il1rn* (*de novo*) RREs ($n = 6$, ANOVA with Tukey's HSD test, $p < 0.05$), while the other two showed non-significant increases (Figure 3E). Under serum conditions, all four RREs exhibited significantly higher activity than the control, but not under starvation, suggesting that they act as enhancers activated upon cell cycle re-entry.

Cascade of TF activation during early liver regeneration

We next conducted a TF footprint analysis within RREs using HINT-ATAC[47] to identify potential transcriptional regulators of the liver response after PHx. We identified differential TF footprints by comparing the ATAC-seq profiles of regenerating and control livers within all RREs at each time point. Only TFs that were expressed in our transcriptomics data and exhibited a significant change in activity ($p < 0.05$) were considered in the analysis.

We observed that predicted TFs footprints within RREs during liver regeneration differed entirely from those in control livers (Figure 4A). Across all regeneration time points, we identified various combinations of the activator protein-1 (AP-1) dimer motif (FOS/JUN) (Figure S4A) and the nuclear factor erythroid 2 (NFE2) binding site. Some motifs were shared between two time points, such as early growth response 2 (EGR2) at 6 and 48 h, and CCAAT/enhancer-binding protein β (C/EBPβ) at 24 and 48 h post PHx. Others were exclusive to specific time points, including EGR1 and MYC at 6 h; and activating TFs (ATFs) 1, 3 and 7, NFE2-related factor 2 (NRF2), X-box binding protein 1 (XBP1), and One-cut1/hepatocyte nuclear factor 6 at 24 h (Figures 4A and S4B–S4E). At 48 h, we detected Mothers against decapentaplegic homolog 3 (SMAD3) footprints (Figure 4A), and although not significantly, the NRF2 motif also seemed to be enriched (Figure S4E). Notably, many of these TFs were upregulated at the transcriptional level, including *Fos*, *Jun*, *Egr1*, *Atf3*, *Nrf2*, and *Cebpβ* (Figure 4B). Several of these are well-known regulators of the transcriptional response during liver regeneration. For instance, *Fos* and *Jun* are immediate-early genes induced within the first hours after PHx, playing a key role in promoting hepatocyte proliferation.[19] Similarly, C/EBPβ contributes to cytokine-mediated activation pathways and supports both proliferation and metabolic homeostasis in remnant hepatocytes,[17] while XBP1 regulates proteostasis and the acute-phase response during liver regeneration.[48] In control livers, we predicted the binding sites for D-box binding PAR bZIP TF (DBP) and C/EBPα (Figure 4A), both of which showed decreased expression at 48 h after PHx (Figure 4B), along with nuclear factor interleukin 3 regulated (NFIL3), among others.

To further investigate putative TFs involved in liver regeneration, we analyzed motif enrichment in RREs using AME (MEME Suite).[49] We compared TF motif enrichment in *de novo* and increasing or decreasing RREs at each time point against all accessible regions (Mann-Whitney U test $p < .05$). Since the motifs within enhancer and core-promoter sequences may recruit different *trans*-acting factors,[50] we analyzed them separately. We selected the top 10 TF motifs per time point and peak class,

(D) Reporter assay design. Candidate *de novo* and increasing RREs were cloned upstream of a luciferase cassette, transfected into hepatocyte cultures, serum-starved for 24 h, then either kept in starvation or treated with 10% fetal bovine serum (FBS) for 3 h. The constructs were measured in two independent experiments in a total of six biological replicates.

(E) Relative luciferase activity under starvation or FBS treatment. Two-way ANOVA with Tukey's HSD test was used to compare constructs vs. minP and between serum conditions ($p < 0.05$). See also Figure S3.

Please cite this article in press as: Llorens-Giralt et al., Sequential activation of transcription factors promotes liver regeneration through specific and developmental enhancers, Cell Genomics (2025), https://doi.org/10.1016/j.xgen.2025.100887

CellPress
OPEN ACCESS

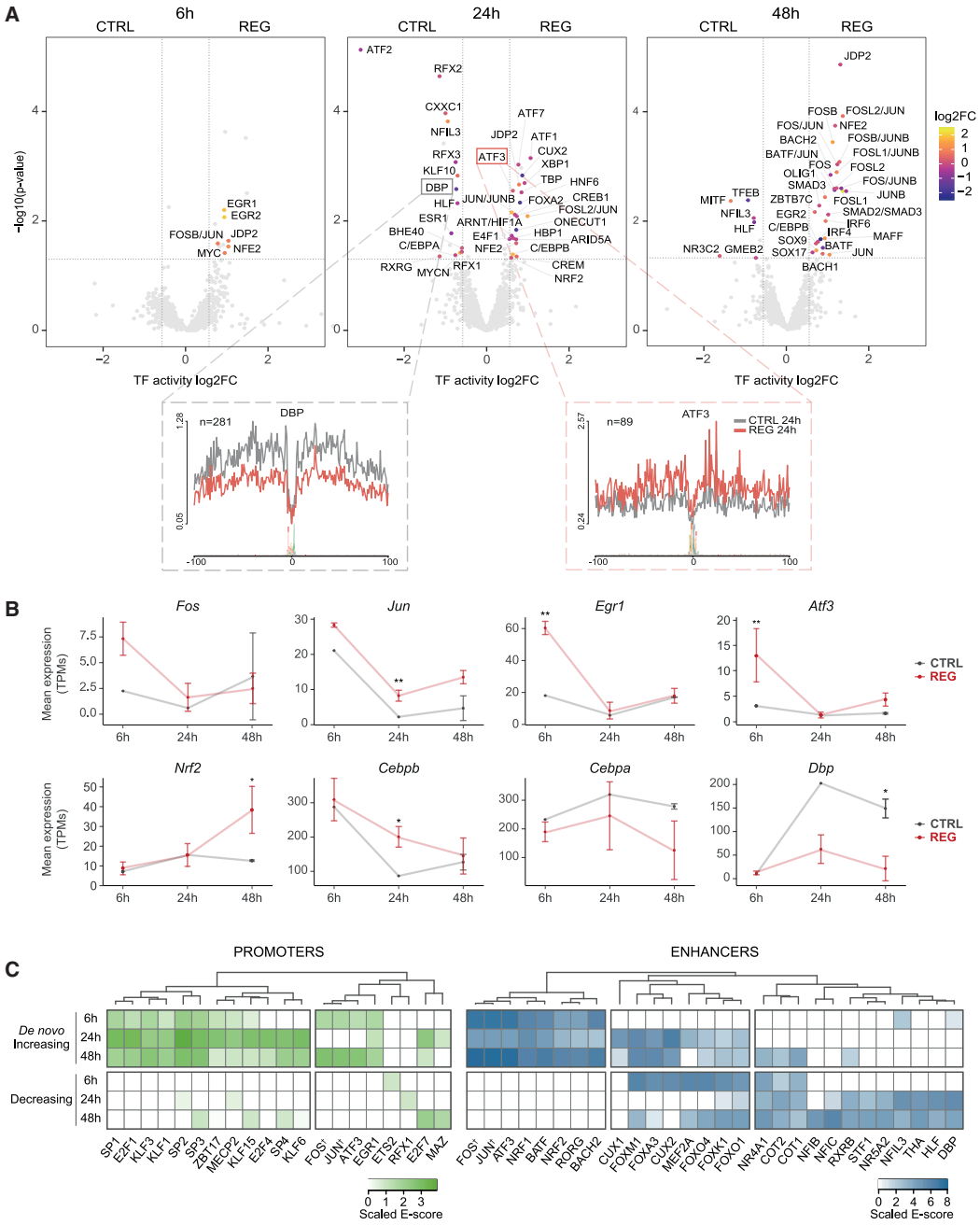

Figure 4. Time point-specific TF motif patterns during liver regeneration

(A) Differential TF binding sites at each time point identified by HINT-ATAC[47] footprinting. Each point represents a TF; only those with expression >1 TPM in at least one condition and significant change in activity ($p < 0.05$) are labeled. Circle color reflects log2FC of the TF-encoding gene. (Below) ATAC-seq profiles for two example TF footprints at 24 h post PHx (CTRL vs. REG).

(B) Expression of *Fos*, *Jun*, *Egr1*, *Atf3*, *Nrf2*, *Cebpb*, *Cebpa*, and *Dbp* over time in CTRL (gray) and REG (red). Significance: $^{**}p_{adjusted} < 0.01$, $^{*}p_{adjusted} < 0.05$ (DESeq2, pairwise comparison vs. control, Wald test, assuming negative binomial distribution).

(C) Top 10 enriched TF motifs in *de novo*, increasing, or decreasing promoters (left) and enhancers (right), identified using AME[49] with the HOCOMOCO v11 database (Mann-Whitney U test, $p_{adjusted} < 0.05$). Scaled enrichment E-scores are shown. †Includes all family members. See also Figure S4.

Please cite this article in press as: Llorens-Giralt et al., Sequential activation of transcription factors promotes liver regeneration through specific and developmental enhancers, Cell Genomics (2025), https://doi.org/10.1016/j.xgen.2025.100887

excluding non-expressed TFs. Our analysis revealed substantial differences between promoters and enhancers, and distinct TF motif patterns in increasing or decreasing regions (Figure 4C). E2F, SP, and Krüppel-like factor motifs were consistently enriched in *de novo* and increasing promoters across all time points, with several encoded by genes co-expressed in the 6 or 6–48 h REG clusters (Table S1). The E2F family is known for its critical role in regulating the cell cycle and apoptosis, with E2F1 specifically binding to the promoter regions of genes involved in the progression to the S phase.[51] FOS and JUN motifs were also among the top hits, enriched in both *de novo* and increasing promoters and enhancers, but absent from decreasing RREs (Figure 4C). These TFs were highly expressed in the liver at 6 h post PHx (Figure 4B). We also identified the STAT3 motif, a key TF driving hepatocyte proliferation during liver regeneration,[52] exclusively enriched in *de novo* and increasing enhancers at both 6 h ($p_{adjusted} = 4.23e^{-04}$) and 48 h ($p_{adjusted} = 2.11e^{-07}$) post PHx (Figure S4F). Although STAT3 was not among the top 10 enriched motifs, its significant enrichment, along with the strong enrichment for the E2F and AP-1 motifs, further supports the robustness of our findings. In addition, the ATF3 motif was enriched in both *de novo* and increasing promoters and enhancers, with NRF1 and NRF2 motifs also exclusively enriched within these enhancers. In contrast, decreasing enhancers showed enrichment for the COUP TFs 1 and 2, nuclear factors I (NFI) B and C, and DBP motifs (Figure 4C).

Subsequently, we integrated our transcriptomics data, TF binding predictions, and enhancer-gene map to construct a GRN. We selected the top 10 most enriched TFs in RREs at each time point (Figure 4C) and computed Pearson's correlation coefficients between the expression of each TF and that of its predicted target genes. We retained only significant interactions ($|correlation| \geq 0.8$) and TFs with motifs present in at least five RREs. Most TFs showed positive correlations with their targets, suggesting a predominantly activating role via enhancers (Figures 5A, S5A, and S5B). For instance, NRF2 positively correlated with all its targets, especially at later stages, whereas BACH2 showed mixed effects, negatively correlating with 66% of its targets (Figures S5A–S5C).

We next profiled gene expression over time and categorized edges based on their corresponding RRE behavior at each time point. The resulting GRN suggested a cascade of TF activation during the early stages of liver regeneration (Figures 5B–5D). At 6 h post PHx, key early induced TFs, including EGR1, the AP-1 subunits JUN and FOS, and ATF3, were upregulated, likely driving the expression of their target genes via *de novo* and increasing enhancers (Figures 5B–5F and S5D). As regeneration progressed, additional TFs, such as CUX1, may have contributed to the transcriptional activation of genes at 24 h (Figure 5C). By 48 h after PHx, several TFs including NRF2, FOXM1, MEF2A, NRF1, and FOXK1 emerged as potential central drivers of gene upregulation (Figures 5D, S5D, and S5E). Notably, we observed co-localization of NRF2 and FOXM1 motifs at numerous RREs, suggesting potential cooperation in activating their target genes at 48 h post PHx (Figures 5G, 5H, and S5F). Conversely, some TFs likely mediated the downregulation of their target genes at specific time points. For instance, FOXK1, FOXO4, and FOXM1 motifs were primarily associated with decreasing enhancers and low gene expression at 6 h post PHx (Figures 5B and S5D). Meanwhile, downregulated regulons at 24 and 48 h included DBP, NFIB, and NFIC (Figures 5C, 5D, S5D, and S5E).

Focusing on ATF3, which was significantly upregulated at 6 h post PHx (Figure 4B), we performed immunohistochemical analysis and confirmed the presence of ATF3-positive hepatocyte nuclei in regenerating livers at this time point, but not in controls (Figure 6A). Next, we identified a set of putative ATF3 target regions by analyzing available ATF3 ChIP-seq datasets in mice and comparing them with *de novo* and increasing RREs. ATF3 peaks were significantly enriched at these RREs, particularly at 6 h post PHx (Fisher's exact test, $p_{adjusted} < 0.001$) (Figure 6B), supporting the GRN predictions. Further analysis confirmed that ATF3 binds to the promoters and enhancers of over 85% of the GRN-predicted ATF3 target genes. Among these, *Hcar2*, which was upregulated at 6 h, was associated with a *de novo* RRE (Figure 6C), while *Trib1,* previously shown to be regulated by ATF3 in HepG2 cells,[53] was linked to three increasing enhancers with ATF3 binding (Figure S6A). Additionally, functional characterisation of predicted ATF3 target genes linked to *de novo* and increasing RREs (Table S4), using the Kyoto Encyclopedia of Genes and Genomes Pathway database, revealed enrichment in regeneration-related pathways. These included glucagon signaling and adherens junctions across all time points, as well as the MAPK, TGF-β, and Hippo signaling pathways, particularly at later stages (Figure 6D). Furthermore, we analyzed *Atf3* expression using a published single-cell RNA-seq dataset from livers collected at different time points post PHx,[31] although no scRNA-seq data were available for 6 h. *Atf3* was predominantly expressed in a subset of hepatocytes at 24 and 48 h post PHx (Figures 6E and 6F), confirming that its expression was mostly restricted to regenerating hepatocytes. Moreover, GRN-predicted ATF3 target genes, validated through ChIP-seq analysis, exhibited higher expression levels in *Atf3*-expressing cells compared with those without *Atf3* expression (Figure S6B). Altogether, these findings support our GRN predictions and highlight the role of ATF3 in transcriptional regulation during liver regeneration.

We next integrated our ATAC-seq dataset with the published NRF2 ChIP-seq profiles from mouse intact livers.[54] NRF2 is a TF that plays a key role in the response to oxidative stress by binding to the antioxidant response elements in the promoter regions of cytoprotective genes, such as phase II detoxification enzymes, thus inducing their expression.[55] We focused our analysis on increasing RREs, since these regions were more likely to feature NRF2 in the intact liver. Indeed, we observed a significant overlap between increasing RREs and NRF2 peaks at all time points (Fisher's exact test, $p_{adjusted} < 0.001$), with this overlap becoming more pronounced at the later stages of regeneration (Figure 6G). These results are consistent with the concurrent increase in *Nrf2* expression over time (Figure 4B) and further reinforce the role of NRF2 especially at this later time point. *Hmox1*, a well-established NRF2 target,[56] was upregulated 48 h post PHx and associated with an NRF2-bound increasing RRE (Figure 6H). Similarly, *Aldh1a7*[57] was also upregulated and linked to an NRF2-bound increasing RRE (Figure 6H). Moreover, single-cell analysis of *Nrf2* expression[31] revealed its overexpression in

Please cite this article in press as: Llorens-Giralt et al., Sequential activation of transcription factors promotes liver regeneration through specific and developmental enhancers, Cell Genomics (2025), https://doi.org/10.1016/j.xgen.2025.100887

CellPress
OPEN ACCESS

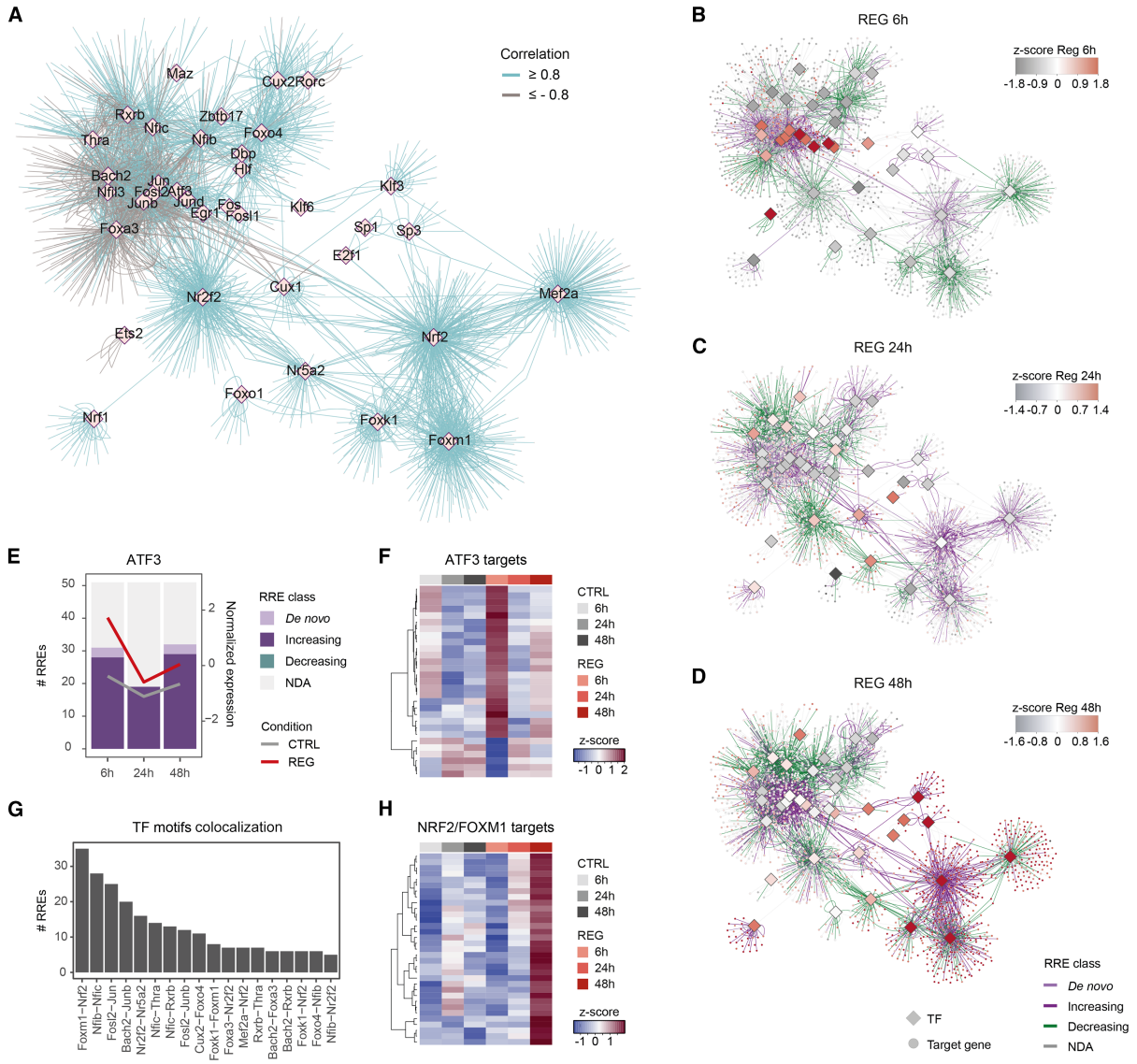

Figure 5. Early regeneration GRN

(A) GRN with edges colored by TF-target Pearson's correlation coefficient (blue, ≥0.8; gray, ≤ −0.8). While most correlations are positive, negative interactions are predicted for some TFs.

(B) GRN at 6 h: Nodes are colored by target gene normalized expression and edges by RRE classification at 6 h.

(C) GRN at 24 h: same as (B), but for 24 h.

(D) GRN at 48 h: same as (B), but for 48 h.

(E) Number and type of RREs with ATF3 motifs (left axis) and *Atf3* expression in *Z* scores (right axis) (REG in red, CTRL in gray).

(F) Expression of predicted target genes linked to ATF3 motif-containing RREs. Each column is one condition (average across replicates), gene expression as *Z* scores.

(G) Number of RREs containing TF motif pairs.

(H) Expression of predicted target genes associated with RREs with co-localization of the NRF2 and FOXM1 motifs. Each column is one condition (average across replicates), gene expression as *Z* scores. See also Figure S5.

hepatocytes at 24 and 48 h post PHx (Figure S6C), with a similar expression pattern observed for its known target genes, *Hmox1* and *Aldh1a7* (Figures S6D and S6E). Overall, NRF2 target genes, identified by the GRN and validated by ChIP-seq, showed significantly higher expression in *Nrf2*-expressing cells compared with non-expressing ones in the scRNA-seq data (Figure S6B).

Please cite this article in press as: Llorens-Giralt et al., Sequential activation of transcription factors promotes liver regeneration through specific and developmental enhancers, Cell Genomics (2025), https://doi.org/10.1016/j.xgen.2025.100887

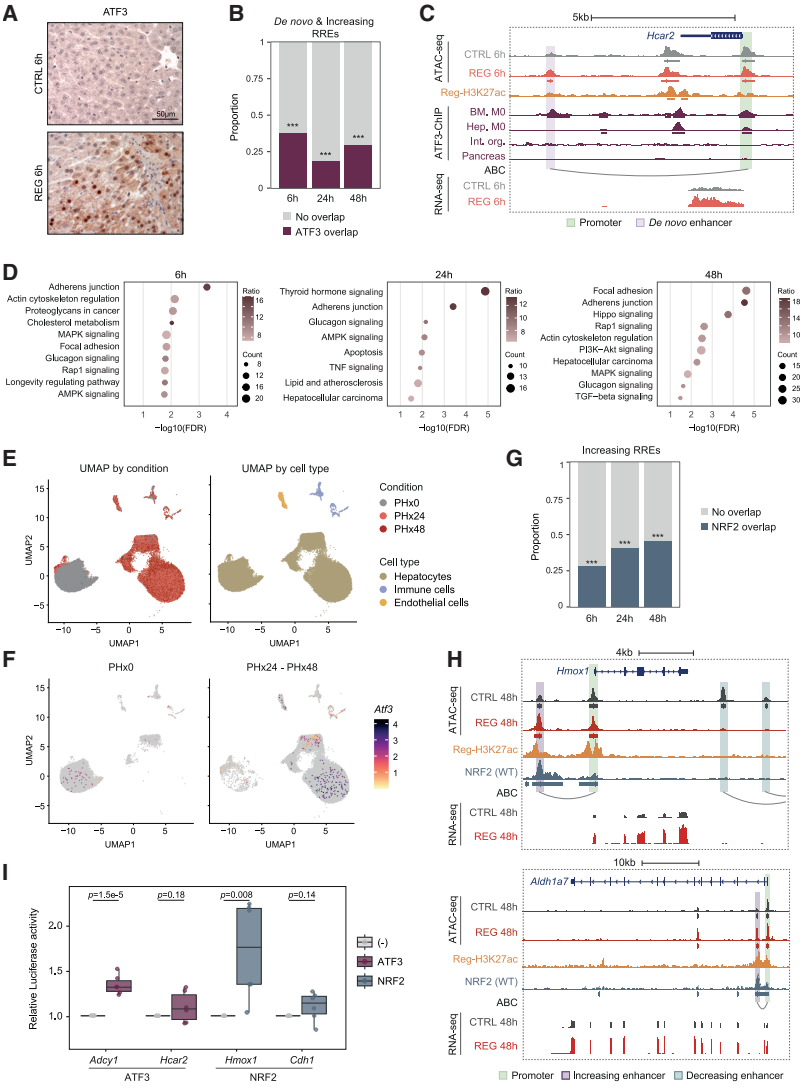

Figure 6. ATF3 and NRF2 bind to *de novo* and increasing RREs to activate the expression of regeneration-associated genes

(A) Representative ATF3 immunostaining images in control and regenerating livers at 6 h post surgery. No positive nuclei observed in controls.

(B) Proportion of *de novo* and increasing RREs overlapping ATF3 ChIP-seq peaks at each time point. Fisher's exact test (***$p_{adjusted} < 0.001$).

(C) Genome browser screenshot of the *Hcar2* locus at 6h. Promoter shows ATF3 binding and is linked to an ATF3-bound *de novo* enhancer.

(D) Kyoto Encyclopedia of Genes and Genomes (KEGG) Pathway analysis of target genes from ATF3-bound *de novo* and increasing RREs ($p_{adjusted} < 0.05$).

(E) UMAP of cells from quiescent (PHx0) and regenerating (PHx24–PHx48) livers, colored by condition (left) or annotated cell type (right).

(F) Feature plot of *Atf3* expression at PHx0 and PHx24–PHx48.

(G) Proportion of increasing RREs overlapping NRF2 ChIP-seq peaks at each time point. Fisher's exact test (***$p_{adjusted} < 0.001$).

(H) Genome browser views of *Hmox1* and *Aldh1a7* loci at 48 h. Both promoters show NRF2 binding and are linked to NRF2-bound increasing enhancers.

(I) Relative luciferase activity of candidate enhancers co-transfected with ATF3 or NRF2 vectors, or alone (−), in hepatocyte cultures. One-way ANOVA with Tukey's HSD ($p < 0.05$). See also Figure S6.

Functional analysis of NRF2-bound increasing RRE targets revealed enrichment in wound healing, kinase activity, apoptosis, angiogenesis, and epithelial proliferation (Figure S6F; Table S5). As expected, when all target genes were considered, there was enrichment for oxidative stress response (GO: 0006979; $p_{adjusted} = 2.10e^{-03}$). This suggests NRF2 may bind both promoters and enhancers of regeneration-related genes under normal conditions, but during regeneration increased *Nrf2* expression and RRE accessibility likely promote NRF2 binding to RREs, leading to target gene upregulation. In contrast, DBP, which is downregulated during regeneration according to our transcriptomics analysis (Figure 4B) and the published scRNA-seq data[31] (Figure S6G), likely detaches from RREs, contributing to their closure and reduced gene expression.

To confirm that ATF3 and NRF2 act as transcriptional activators of liver regeneration through RREs, we co-transfected expression vectors for these TFs with luciferase reporter vectors containing candidate enhancers. For ATF3, we tested RREs associated with *Hcar2* (Figure 6C) and *Adcy1* (Figure S3C), both identified by the GRN as ATF3 targets. As candidate NRF2-regulated enhancers, we selected the *Hmox1*-linked enhancer (Figure 6I) and an intronic enhancer associated with *Cdh1*, a gene upregulated at 48 h post PHx and predicted by the GRN as a potential NRF2 target. Transient co-transfection assays in hepatocyte cultures revealed a significant increase in luciferase expression in ATF3-expressing cells with the *Adcy1*-associated RRE and in NRF2-expressing cells with the *Hmox1* RRE, compared with non-expressing control cells (-ANOVA with Tukey's HSD; $p < 0.05$) (Figure 6I). Additionally, the *Hcar2* and *Cdh1* enhancers showed a trend toward increased luciferase activity upon ATF3 and NRF2 overexpression, respectively. These results support ATF3 and NRF2 as transcriptional activators of RREs.

Interplay of regeneration-specific and developmental regulatory elements

While liver regeneration and development share some molecular mechanisms, the two processes differ significantly. For instance, their cellular origins are distinct: liver regeneration after

Please cite this article in press as: Llorens-Giralt et al., Sequential activation of transcription factors promotes liver regeneration through specific and developmental enhancers, Cell Genomics (2025), https://doi.org/10.1016/j.xgen.2025.100887

CellPress
OPEN ACCESS

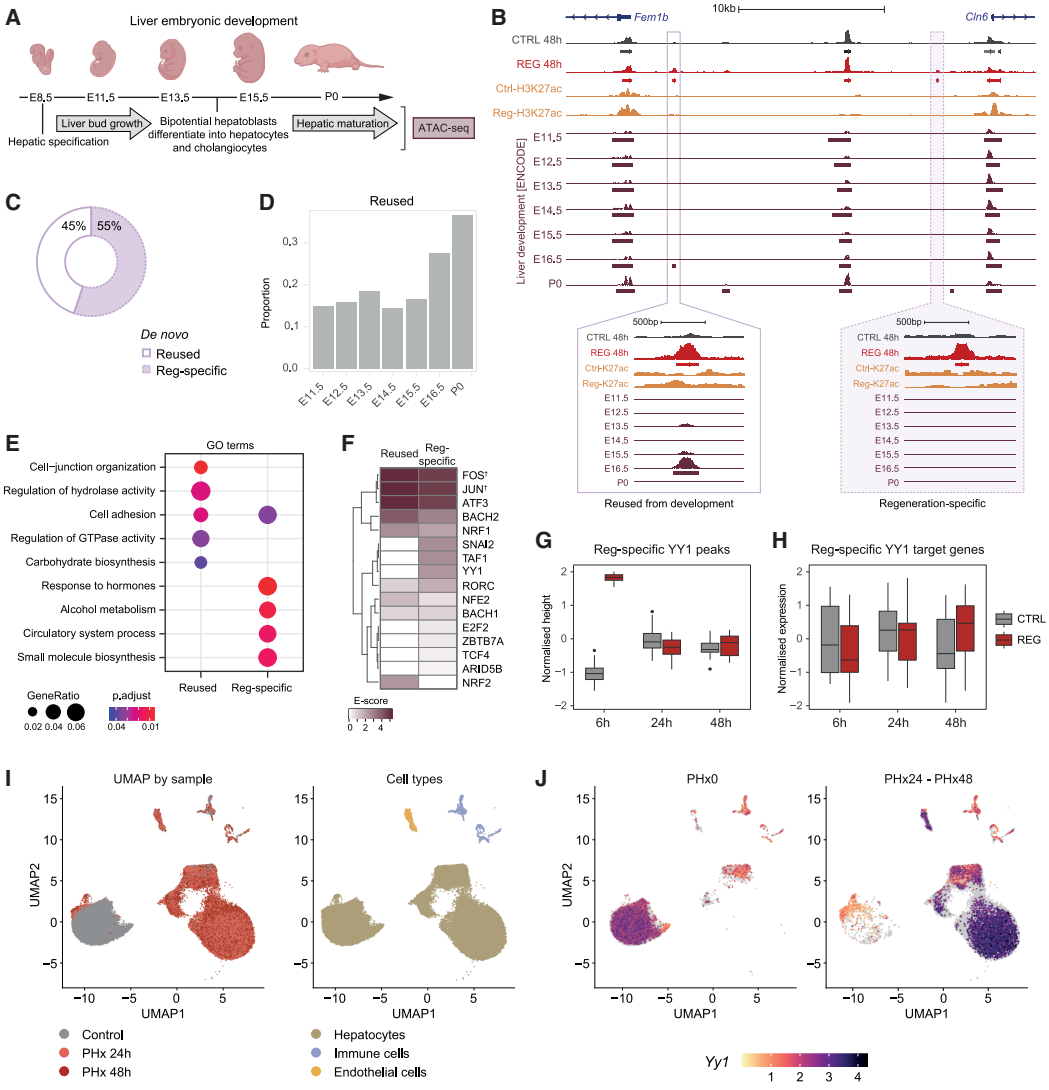

Figure 7. Enhancers from development are repurposed in the adult liver to activate the expression of regeneration genes

(A) Liver developmental stages used for ATAC-seq data in the comparative analysis with *de novo* RREs.

(B) Genome browser views of a *de novo* enhancer overlapping a developmental enhancer (Reused) and one specific to regeneration (REG specific).

(C) Proportion of *de novo* RREs classified as reused or REG specific.

(D) Proportion of *de novo* peaks overlapping developmental enhancers at each developmental stage.

(E) GO term analysis of target genes from reused vs. REG-specific *de novo* RREs ($p_{adjusted} < 0.05$).

(F) Heatmap of enriched TF motifs in reused and REG-specific *de novo* RREs. Scaled enrichment E-score shown. †All family members included.

(G) Normalized accessibility of REG-specific *de novo* peaks with YY1 motifs.

(H) Normalized expression of REG-specific YY1 putative target genes.

(I) UMAP of gene expression from quiescent (PHx0) and regenerating livers (PHx24, PHx48), colored by condition (left) and annotated cell type (right).

(J) Feature plot of *Yy1* expression in PHx0 and PHx24-PHx48. See also Figure S7.

PHx is primarily driven by mature hepatocytes, whereas during embryonic development, hepatocytes originate from hepatoblasts—bipotential precursors that also give rise to biliary epithelial cells.[19] To determine if the gene expression changes observed during liver regeneration rely on the same regulatory mechanisms used during liver development or involve unique, regeneration-specific regulatory networks, we analyzed chromatin accessibility data from mouse liver development, spanning embryonic day 11.5 (E11.5) to postnatal day 0 (P0)[58] (Figure 7A). This period encompasses the stages of accelerated liver bud growth (E10–E13), hepatoblast differentiation into hepatocytes (E14), and hepatocyte maturation (E15–P0), a process

Please cite this article in press as: Llorens-Giralt et al., Sequential activation of transcription factors promotes liver regeneration through specific and developmental enhancers, Cell Genomics (2025), https://doi.org/10.1016/j.xgen.2025.100887

that continues after birth.[19] We specifically examined whether *de novo* RREs—regions uniquely accessible in regenerating livers but not in uninjured ones—were also accessible during any stage of liver development. Such overlap would indicate the reuse of developmental enhancers for regeneration. Conversely, regions exclusively accessible during regeneration, with no accessibility during development, would suggest the presence of regeneration-specific enhancers (Figure 7B). Our analysis revealed that 45% of *de novo* RREs were developmental enhancers repurposed for regeneration (Reused), while the remaining 55% were enhancers exclusive to regeneration (REG specific) (Figure 7C). Among the Reused enhancers, most were either repurposed from late developmental stages (E16.5 and P0) (Figures 7B–7D) or were active throughout all stages of liver development (Figures S7A and S7B). To further characterize these regulatory elements, we explored their distribution in the genome. While both subtypes of *de novo* RREs were predominantly located in distal regions, consistent with the general distribution of all RREs, their proportions in proximal and promoter regions differed significantly (chi-square $p < 2.2e{-}16$). Specifically, Reused RREs were more abundant in proximal (2%) and promoter (6%) regions, compared with REG-specific regulatory elements (1% and 2%, respectively). These findings suggest that regeneration-specific regulatory mechanisms primarily function through distal enhancers.

GO term enrichment analysis of *de novo* RRE target genes revealed distinct functional categories. Reused RRE genes were enriched in cell-cell interactions and carbohydrate biosynthesis, including gluconeogenesis genes like *Sik1* (Figures 7E and S7C), a process regulated during both regeneration and birth.[59] In contrast, REG-specific targets were enriched in liver-related functions, such as alcohol metabolism and hormone responses, including insulin, leptin, and growth hormone signaling, such as peroxisome proliferator-activated receptor gamma (*Pparg*) gene (Figures 7E, S7D, and S7E). These pathways act as auxiliary mitogens, delaying but not impairing regeneration when disrupted.[18]

Next, we performed TF motif enrichment between REG-specific and Reused *de novo* RREs (Figure 7F). Although many TFs were shared between these two groups, distinct TF signatures were identified. For instance, NRF2 was exclusively enriched in Reused enhancers, while other TFs, such as the transcriptional repressor YY1, were uniquely enriched in REG-specific enhancers. We focused on YY1 due to its well-established role in intestinal stem cell renewal[60] and its involvement in hepatic lipid metabolism.[61] YY1 overexpression promotes the growth of immortalized, non-tumorigenic human hepatocytes, whereas its depletion inhibits the growth of hepatocellular carcinoma cells.[62] We observed that the YY1 binding motif was predominantly enriched in REG-specific *de novo* RREs that became accessible at 6 h after PHx (Figure 7G), while its predicted target genes were generally downregulated at this time point (Figure 7H). Pearson's correlation coefficient analysis between the accessibility of these REG-specific RREs with YY1 motifs and the expression of their associated target genes revealed that nearly 70% exhibited a negative correlation (Figure S7F). This suggests that these regions might function as REG-specific silencers rather than enhancers, consistent with the role of YY1 as a transcriptional repressor.[63] To determine which cells express *Yy1* during regeneration, we analyzed a published scRNA-seq dataset from livers collected at 0, 24, and 48 h post-PHx.[31] We found that *Yy1* was highly expressed in hepatocytes and endothelial cells during regeneration, with lower levels of expression observed in quiescent hepatocytes and immune cells (Figures 7I and 7J). Altogether, our results suggest that liver regeneration involves a collaborative interplay between regeneration-specific regulatory elements and developmental enhancers repurposed in adulthood, each governed by distinct regulatory mechanisms and linked to specific biological functions.

DISCUSSION

The mammalian liver possesses an exceptional capacity for compensatory growth following injury or PHx, a process driven by transcriptional reprogramming and epigenetic modifications.[21,24] In quiescent hepatocytes, pro-regenerative genes are maintained in active or permissive chromatin states,[27,64] enabling rapid and widespread transcriptional changes in response to injury.[65] During regeneration, some hepatocytes preserve their original chromatin landscape, while others shift toward a fetal-like state.[30,31] Despite significant progress in understanding the epigenetic events of liver regeneration, the mechanisms regulating chromatin architecture, specific enhancers, and transcriptional networks that control regenerative programs remain unclear.

Here, we identify the regulatory elements that are dynamically modulated during early liver regeneration after PHx (RREs) and uncover new TFs potentially regulating their activity. RREs mainly function as enhancers activating the expression of regeneration-associated genes, particularly those involved in key signaling and cell cycle pathways. However, RREs also include regions that become inactive during regeneration, which may lead to a global downregulation of liver-specific homeostatic functions, such as the biosynthesis of bile acids and retinol. This suggests that hepatocytes suppress energy-intensive metabolic programs characteristic of quiescent hepatocytes to prioritize proliferation. An inverse correlation between hepatocyte proliferation and metabolic function during liver regeneration has been previously proposed.[65,66] A similar shift in chromatin accessibility has been observed in chronic liver injury,[28] and spatially resolved transcriptomics during liver regeneration further confirm an initial downregulation of metabolic genes, concurrent with hepatocyte priming and proliferation.[32] Consistently, single-cell studies show that regenerating hepatocytes undergo reprogramming after PHx, shifting from metabolic to developmental functions.[30,31] However, a subset of hepatocytes retains the chromatin landscape of metabolically active uninjured cells.[30,31] Consequently, changes in RRE accessibility may occur selectively within specific hepatocyte populations.

Hepatocyte metabolic reprogramming in the injured liver is essential for meeting energy demands, supplying anabolic precursors, and regulating signaling pathways that drive tissue repair.[67] Our findings suggest that, during regeneration, hepatocytes suppress bile acid biosynthesis and undergo changes in cholesterol metabolism through transcriptional and chromatin regulation. While lipid utilization increases during regeneration

Please cite this article in press as: Llorens-Giralt et al., Sequential activation of transcription factors promotes liver regeneration through specific and developmental enhancers, Cell Genomics (2025), https://doi.org/10.1016/j.xgen.2025.100887

to support the synthesis of phospholipids and cholesterol, both essential for cell membrane formation,[68] repression of *Cyp7a1* post PHx limits bile acid production from cholesterol, despite Cyp7a1 protein levels remaining stable.[36,69] Furthermore, the ubiquitin ligase Uhrf2-mediated suppression of cholesterol biosynthesis genes is essential for regeneration,[70] and a hypercholesterolemic diet impairs liver repair.[71] Further studies are warranted to elucidate the relationship between steroid metabolic regulation and hepatic regeneration.

Our study also identifies potential transcriptional regulators orchestrating liver regeneration. The AP-1 complex emerges as a key factor driving the transcriptional response at the chromatin level, especially during the priming phase. In particular, the AP-1 subunit JUN is a critical regulator of hepatocyte proliferation, as studies have shown that liver regeneration is impaired in mice lacking JUN.[72] The role of AP-1 appears to be conserved across various regenerative models,[73] including *Drosophila* wing discs[8] and zebrafish heart,[74] as well as killifish and zebrafish fin regeneration,[6] in which AP-1 motifs are essential for the activation of RREs. Consequently, the AP-1 complex may serve as a master regulator, collaborating with tissue-specific TFs, to facilitate the opening of *de novo* RREs as a pioneer factor and activate gene expression during regeneration. Significantly, recent evidence suggests that AP-1 can act as a pioneer factor in hepatocytes by contributing to global changes in chromatin accessibility after *in vivo* reprogramming by the Yamanaka factors.[75] Furthermore, our findings suggest a cascade of TF activation after PHx, with ATF3, alongside JUN and FOS, driving the transcriptional response during the priming stage of liver regeneration. While the role of ATF3 in liver regeneration remains unclear, it is rapidly induced after PHx in rats[76] and has been implicated in various processes, including hepatic proliferation,[77] the inhibition of gluconeogenesis,[78] a liver-specific function that is initially downregulated during liver regeneration,[79] and the regulation of lipoprotein and bile acid metabolism,[80] processes that undergo alterations during liver regeneration, as observed in our study. Here, we propose that ATF3 selectively binds to the promoters and enhancers of genes essential for the initiation of regeneration, while NRF2 and FOXM1 likely mediate gene upregulation during the proliferation stage. Significantly, it has been demonstrated that the absence of NRF2 impairs liver regeneration,[81] while its ectopic activation enhances regenerative capacity.[82] Moreover, previous studies have shown that FOXM1 is essential for hepatocyte mitosis by stimulating the expression of cell cycle genes during liver regeneration.[83]

A long-standing question in regenerative biology is whether regeneration recapitulates embryonic development. Research in animals with a high regenerative potential has shown that the genes involved in development are frequently reactivated after injury and are essential for successful regeneration.[84,85] However, evidence also suggests that the regulatory networks controlling tissue regeneration and proliferation in wounded tissues differ from those involved in developmental growth.[1] In the liver, recent studies indicate that a subset of hepatocytes undergo reversible reprogramming after PHx, activating the same gene expression programs that are used for physiological growth during the postnatal stage of development.[30,31] At the same time, STAT3 binding to injury-specific enhancers, rather than developmental enhancers, to activate reprogramming-related genes[86] suggests distinct regulatory networks between regeneration and development. Our findings indicate that the regenerating liver is capable of reactivating developmental enhancers, preferentially from the postnatal or late developmental stages, to regulate genes associated with cell junctions and glucose metabolism. Significantly, hepatocytes acquire junctional integrity and polarity and undergo changes in glucose metabolism during the maturation stage of liver development, a process that takes place around the perinatal period.[19] These changes bear resemblance to those observed during liver regeneration after PHx.

In summary, our study provides a genome-wide atlas of enhancer-gene interactions and highlights key transcriptional regulators in early liver regeneration. These findings could be a valuable resource for researchers aiming to target regulatory elements involved in liver regeneration, with significant implications for regenerative medicine. Potential applications include the ectopic activation of regeneration enhancers to exert temporal and spatial control over the expression of pro-regenerative factors within an injured area, as proposed by Yan et al.[16] The addition of regenerative TFs could also be used to enhance the regenerative potential, particularly in the context of liver failure.

Limitations of the study

While this study provides key insights into liver regeneration, more biological replicates would improve robustness, and additional time points could provide a more comprehensive understanding of the process. *In vivo* transgenic reporter assays could further clarify enhancer function during regeneration. However, compliance with stringent European regulations on animal research limits the inclusion of additional replicates, time points or transgenic models. Future studies could also benefit from experiments such as ChIP-seq for TFs identified in our GRN. The lack of high-quality antibodies, particularly for TFs with less characterized roles in liver regeneration, has limited our ability to generate ChIP-seq data using liver tissue from hepatectomies. The absence of detectable changes in chromatin accessibility does not necessarily indicate that specific enhancers or regulatory regions are non-functional; therefore, complementary approaches, such as histone modification profiling or Hi-C, are needed to fully understand enhancer dynamics during liver regeneration. Finally, CRISPR-Cas9-mediated enhancer modifications could provide direct evidence of enhancer function in liver regeneration.

RESOURCE AVAILABILITY

Lead contact

Further information and requests for resources and reagents should be directed to and will be fulfilled by the lead contact, Montserrat Corominas (mcorominas@ub.edu).

Materials availability

This study did not generate new unique reagents.

Data and code availability

- The RNA-seq and ATAC-seq raw and processed data from this study are available at NCBI Gene Expression Omnibus under the accession numbers GEO: GSE181476 (RNA-seq)[33] and GEO: GSE266402 (ATAC-seq). This study did not generate any unique code.

- A Catalan version of the abstract, highlights, and graphical abstract is available at: https://doi.org/10.5281/zenodo.15267786

ACKNOWLEDGMENTS

We thank A.S. Nacht, T. Quesada-López, and E. Bertran for technical support; R. Corces for guidance on ATAC-seq; J. and P. Nieto for scRNA-seq advice; and the CRG Genomics Unit for assistance. We are also grateful to C. Camilleri-Robles for helpful discussions and manuscript revision. This project was funded by PID2021-123300NB-100 from MCIN/AEI/10.13039/501100011033/FEDER, UE to F.S and M.C.; 2021SGR00293 from the Agency for the Management of University and Research Grants (Generalitat de Catalunya) to M.C.; PID2021-122551OB-100 from MCIN/AEI/10.13039/501100011033/FEDER, UE to I.F.; and FPU20/01473 from the Spanish Ministerio de Universidades to P.L.G. We thank R. Guigó for financial support to M.R.R. and R.N. through grant PID2021-128956NB-I00 funded by MCIN/AEI/10.13039/501100011033/FEDER, UE. M.R.R. and R.N. acknowledge the support of the Spanish Ministry of Science and Innovation through the Centro de Excelencia Severo Ochoa (CEX2020-001049-S and MCIN/AEI/10.13039/501100011033) and the Generalitat de Catalunya through the CERCA program.

AUTHOR CONTRIBUTIONS

P.L.G., I.F., and M.C. conceived and designed the experiments. P.L.G. and M.H.I. performed the experiments. P.L.G., M.R.R., and R.N. analyzed the data. G.P.V. provided reagents and advice for the ATAC-seq experiments. P.L.G. and M.C. wrote the manuscript. P.L.G., M.R.R., G.P.V., F.S., I.F., R.N., and M.C. revised the manuscript. F.S., I.F., and M.C. acquired funding.

DECLARATION OF INTERESTS

The authors declare no competing interests.

DECLARATION OF GENERATIVE AI AND AI-ASSISTED TECHNOLOGIES

During the preparation of this work, the authors used ChatGPT to enhance the readability and language of the manuscript. After using this tool, the authors carefully reviewed and edited the content as needed and they take full responsibility for the content of the published article.

STAR★METHODS

Detailed methods are provided in the online version of this paper and include the following:

- KEY RESOURCES TABLE
- EXPERIMENTAL MODEL AND STUDY PARTICIPANT DETAILS
  - Animal procedures
- METHOD DETAILS
  - ATAC sequencing
  - Immunohistochemistry
  - Reporter assays
  - RNA sequencing data analysis
  - ATAC sequencing data analysis
  - ChIP sequencing data analysis
  - Hi-C data analysis
  - Enhancer-gene pair association
  - Single-cell RNA sequencing analysis
  - Transcription factor motif enrichment analysis
  - Gene coexpression regulatory network
  - Developmental analysis
- QUANTIFICATION AND STATISTICAL ANALYSIS

SUPPLEMENTAL INFORMATION

Supplemental information can be found online at https://doi.org/10.1016/j.xgen.2025.100887.

Received: July 7, 2024
Revised: March 10, 2025
Accepted: April 28, 2025
Published: May 22, 2025

REFERENCES

1. Goldman, J.A., and Poss, K.D. (2020). Gene regulatory programmes of tissue regeneration. Nat. Rev. Genet. *21*, 511–525. https://doi.org/10.1038/s41576-020-0239-7.
2. Rodriguez, A.M., and Kang, J. (2020). Regeneration enhancers: Starting a journey to unravel regulatory events in tissue regeneration. Semin. Cell Dev. Biol. *97*, 47–54. https://doi.org/10.1016/j.semcdb.2019.04.003.
3. Goldman, J.A., Kuzu, G., Lee, N., Karasik, J., Gemberling, M., Foglia, M. J., Karra, R., Dickson, A.L., Sun, F., Tolstorukov, M.Y., and Poss, K.D. (2017). Resolving Heart Regeneration by Replacement Histone Profiling. Dev. Cell *40*, 392–404.e5. https://doi.org/10.1016/j.devcel.2017.01.013.
4. Begeman, I.J., Shin, K., Osorio-Méndez, D., Kurth, A., Lee, N., Chamberlain, T.J., Pelegri, F.J., and Kang, J. (2020). Decoding an Organ Regeneration Switch by Dissecting Cardiac Regeneration Enhancers. Development *147*, dev.194019. https://doi.org/10.1242/dev.194019.
5. Kang, J., Hu, J., Karra, R., Dickson, A.L., Tornini, V.A., Nachtrab, G., Gemberling, M., Goldman, J.A., Black, B.L., and Poss, K.D. (2016). Modulation of tissue repair by regeneration enhancer elements. Nature *532*, 201–206. https://doi.org/10.1038/nature17644.
6. Wang, W., Hu, C.-K., Zeng, A., Alegre, D., Hu, D., Gotting, K., Ortega Granillo, A., Wang, Y., Robb, S., Schnittker, R., et al. (2020). Changes in regeneration-responsive enhancers shape regenerative capacities in vertebrates. Science *369*, eaaz3090. https://doi.org/10.1126/science.aaz3090.
7. Mokalled, M.H., Patra, C., Dickson, A.L., Endo, T., Stainier, D.Y.R., and Poss, K.D. (2016). Injury-induced *ctgfa* directs glial bridging and spinal cord regeneration in zebrafish. Science *354*, 630–634. https://doi.org/10.1126/science.aaf2679.
8. Harris, R.E., Setiawan, L., Saul, J., and Hariharan, I.K. (2016). Localized epigenetic silencing of a damage-activated WNT enhancer limits regeneration in mature Drosophila imaginal discs. Elife *5*, e11588. https://doi.org/10.7554/eLife.11588.
9. Vizcaya-Molina, E., Klein, C.C., Serras, F., Mishra, R.K., Guigó, R., and Corominas, M. (2018). Damage-responsive elements in *Drosophila* regeneration. Genome Res. *28*, 1852–1866. https://doi.org/10.1101/gr.233098.117.
10. Aguilar, C.A., Pop, R., Shcherbina, A., Watts, A., Matheny, R.W., Cacchiarelli, D., Han, W.M., Shin, E., Nakhai, S.A., Jang, Y.C., et al. (2016). Transcriptional and Chromatin Dynamics of Muscle Regeneration after Severe Trauma. Stem Cell Rep. *7*, 983–997. https://doi.org/10.1016/j.stemcr.2016.09.009.
11. Hung, H.A., Sun, G., Keles, S., and Svaren, J. (2015). Dynamic Regulation of Schwann Cell Enhancers after Peripheral Nerve Injury. J. Biol. Chem. *290*, 6937–6950. https://doi.org/10.1074/jbc.M114.622878.
12. Naik, S., Larsen, S.B., Gomez, N.C., Alaverdyan, K., Sendoel, A., Yuan, S., Polak, L., Kulukian, A., Chai, S., and Fuchs, E. (2017). Inflammatory memory sensitizes skin epithelial stem cells to tissue damage. Nature *550*, 475–480. https://doi.org/10.1038/nature24271.
13. Ge, Y., Gomez, N.C., Adam, R.C., Nikolova, M., Yang, H., Verma, A., Lu, C.P.-J., Polak, L., Yuan, S., Elemento, O., and Fuchs, E. (2017). Stem Cell Lineage Infidelity Drives Wound Repair and Cancer. Cell *169*, 636–650.e14. https://doi.org/10.1016/j.cell.2017.03.042.

14. Huang, G.N., Thatcher, J.E., McAnally, J., Kong, Y., Qi, X., Tan, W., DiMaio, J.M., Amatruda, J.F., Gerard, R.D., Hill, J.A., et al. (2012). C/EBP Transcription Factors Mediate Epicardial Activation During Heart Development and Injury. Science *338*, 1599–1603. https://doi.org/10.1126/science.1229765.

15. Vieira, J.M., Howard, S., Villa Del Campo, C., Bollini, S., Dubé, K.N., Masters, M., Barnette, D.N., Rohling, M., Sun, X., Hankins, L.E., et al. (2017). BRG1-SWI/SNF-dependent regulation of the Wt1 transcriptional landscape mediates epicardial activity during heart development and disease. Nat. Commun. *8*, 16034. https://doi.org/10.1038/ncomms16034.

16. Yan, R., Cigliola, V., Oonk, K.A., Petrover, Z., DeLuca, S., Wolfson, D.W., Vekstein, A., Mendiola, M.A., Devlin, G., Bishawi, M., et al. (2023). An enhancer-based gene-therapy strategy for spatiotemporal control of cargoes during tissue repair. Cell Stem Cell *30*, 96–111.e6. https://doi.org/10.1016/j.stem.2022.11.012.

17. Taub, R. (2004). Liver regeneration: from myth to mechanism. Nat. Rev. Mol. Cell Biol. *5*, 836–847. https://doi.org/10.1038/nrm1489.

18. Michalopoulos, G.K., and Bhushan, B. (2021). Liver regeneration: biological and pathological mechanisms and implications. Nat. Rev. Gastroenterol. Hepatol. *18*, 40–55. https://doi.org/10.1038/s41575-020-0342-4.

19. López-Luque, J., and Fabregat, I. (2018). Revisiting the liver: from development to regeneration - what we ought to know. Int. J. Dev. Biol. *62*, 441–451. https://doi.org/10.1387/ijdb.170264JL.

20. Blake, M.J., and Steer, C.J. (2023). Liver Regeneration in Acute on Chronic Liver Failure. Clin. Liver Dis. *27*, 595–616. https://doi.org/10.1016/j.cld.2023.03.005.

21. Arechederra, M., Berasain, C., Avila, M.A., and Fernández-Barrena, M.G. (2020). Chromatin dynamics during liver regeneration. Semin. Cell Dev. Biol. *97*, 38–46. https://doi.org/10.1016/j.semcdb.2019.03.004.

22. Zhang, C., Sun, C., Zhao, Y., Ye, B., and Yu, G. (2024). Signaling pathways of liver regeneration: Biological mechanisms and implications. iScience *27*, 108683. https://doi.org/10.1016/j.isci.2023.108683.

23. Bangru, S., and Kalsotra, A. (2020). Cellular and molecular basis of liver regeneration. Semin. Cell Dev. Biol. *100*, 74–87. https://doi.org/10.1016/j.semcdb.2019.12.004.

24. Aloia, L. (2021). Epigenetic Regulation of Cell-Fate Changes That Determine Adult Liver Regeneration After Injury. Front. Cell Dev. Biol. *9*, 643055. https://doi.org/10.3389/fcell.2021.643055.

25. Sato, Y., Katoh, Y., Matsumoto, M., Sato, M., Ebina, M., Itoh-Nakadai, A., Funayama, R., Nakayama, K., Unno, M., and Igarashi, K. (2017). Regulatory signatures of liver regeneration distilled by integrative analysis of mRNA, histone methylation, and proteomics. J. Biol. Chem. *292*, 8019–8037. https://doi.org/10.1074/jbc.M116.774547.

26. Wang, S., Zhang, C., Hasson, D., Desai, A., SenBanerjee, S., Magnani, E., Ukomadu, C., Lujambio, A., Bernstein, E., and Sadler, K.C. (2019). Epigenetic Compensation Promotes Liver Regeneration. Dev. Cell *50*, 43–56.e6. https://doi.org/10.1016/j.devcel.2019.05.034.

27. Zhang, C., Macchi, F., Magnani, E., and Sadler, K.C. (2021). Chromatin states shaped by an epigenetic code confer regenerative potential to the mouse liver. Nat. Commun. *12*, 4110. https://doi.org/10.1038/s41467-021-24466-1.

28. Wang, A.W., Wang, Y.J., Zahm, A.M., Morgan, A.R., Wangensteen, K.J., and Kaestner, K.H. (2020). The Dynamic Chromatin Architecture of the Regenerating Liver. Cell. Mol. Gastroenterol. Hepatol. *9*, 121–143. https://doi.org/10.1016/j.jcmgh.2019.09.006.

29. Merrell, A.J., Peng, T., Li, J., Sun, K., Li, B., Katsuda, T., Grompe, M., Tan, K., and Stanger, B.Z. (2021). Dynamic Transcriptional and Epigenetic Changes Drive Cellular Plasticity in the Liver. Hepatology *74*, 444–457. https://doi.org/10.1002/hep.31704.

30. Chen, T., Oh, S., Gregory, S., Shen, X., and Diehl, A.M. (2020). Single-cell omics analysis reveals functional diversification of hepatocytes during liver regeneration. JCI Insight *5*, e141024. https://doi.org/10.1172/jci.insight.141024.

31. Chembazhi, U.V., Bangru, S., Hernaez, M., and Kalsotra, A. (2021). Cellular plasticity balances the metabolic and proliferation dynamics of a regenerating liver. Genome Res. *31*, 576–591. https://doi.org/10.1101/gr.267013.120.

32. Xu, J., Guo, P., Hao, S., Shangguan, S., Shi, Q., Volpe, G., Huang, K., Zuo, J., An, J., Yuan, Y., et al. (2024). A spatiotemporal atlas of mouse liver homeostasis and regeneration. Nat. Genet. *56*, 953–969. https://doi.org/10.1038/s41588-024-01709-7.

33. Herranz-Itúrbide, M., López-Luque, J., Gonzalez-Sanchez, E., Caballero-Díaz, D., Crosas-Molist, E., Martín-Mur, B., Gut, M., Esteve-Codina, A., Jaquet, V., Jiang, J.X., et al. (2021). NADPH oxidase 4 (Nox4) deletion accelerates liver regeneration in mice. Redox Biol. *40*, 101841. https://doi.org/10.1016/j.redox.2020.101841.

34. Gralinska, E., Kohl, C., Sokhandan Fadakar, B., and Vingron, M. (2022). Visualizing Cluster-specific Genes from Single-cell Transcriptomics Data Using Association Plots. J. Mol. Biol. *434*, 167525. https://doi.org/10.1016/j.jmb.2022.167525.

35. Rib, L., Villeneuve, D., Minocha, S., Praz, V., Hernandez, N., Guex, N., and Herr, W.; CycliX Consortium (2018). Cycles of gene expression and genome response during mammalian tissue regeneration. Epigenetics Chromatin *11*, 52. https://doi.org/10.1186/s13072-018-0222-0.

36. Zhang, L., Huang, X., Meng, Z., Dong, B., Shiah, S., Moore, D.D., and Huang, W. (2009). Significance and Mechanism of CYP7a1 Gene Regulation during the Acute Phase of Liver Regeneration. Mol. Endocrinol. *23*, 137–145. https://doi.org/10.1210/me.2008-0198.

37. Zhao, Y., Ye, W., Wang, Y.-D., and Chen, W.-D. (2022). HGF/c-Met: A Key Promoter in Liver Regeneration. Front. Pharmacol. *13*, 808855. https://doi.org/10.3389/fphar.2022.808855.

38. Xu, C., Lin, F., and Qin, S. (2008). Relevance between lipid metabolism-associated genes and rat liver regeneration. Hepatol. Res. *38*, 825–837. https://doi.org/10.1111/j.1872-034X.2008.00345.x.

39. Chen, Y., Chen, L., Wu, X., Zhao, Y., Wang, Y., Jiang, D., Liu, X., Zhou, T., Li, S., Wei, Y., et al. (2023). Acute liver steatosis translationally controls the epigenetic regulator MIER1 to promote liver regeneration in a study with male mice. Nat. Commun. *14*, 1521. https://doi.org/10.1038/s41467-023-37247-9.

40. Sun, X., Chuang, J.-C., Kanchwala, M., Wu, L., Celen, C., Li, L., Liang, H., Zhang, S., Maples, T., Nguyen, L.H., et al. (2016). Suppression of the SWI/SNF Component Arid1a Promotes Mammalian Regeneration. Cell Stem Cell *18*, 456–466. https://doi.org/10.1016/j.stem.2016.03.001.

41. Shlyueva, D., Stampfel, G., and Stark, A. (2014). Transcriptional enhancers: from properties to genome-wide predictions. Nat. Rev. Genet. *15*, 272–286. https://doi.org/10.1038/nrg3682.

42. Pradeepa, M.M., Grimes, G.R., Kumar, Y., Olley, G., Taylor, G.C.A., Schneider, R., and Bickmore, W.A. (2016). Histone H3 globular domain acetylation identifies a new class of enhancers. Nat. Genet. *48*, 681–686. https://doi.org/10.1038/ng.3550.

43. Fulco, C.P., Nasser, J., Jones, T.R., Munson, G., Bergman, D.T., Subramanian, V., Grossman, S.R., Anyoha, R., Doughty, B.R., Patwardhan, T.A., et al. (2019). Activity-by-contact model of enhancer–promoter regulation from thousands of CRISPR perturbations. Nat. Genet. *51*, 1664–1669. https://doi.org/10.1038/s41588-019-0538-0.

44. Furlan-Magaril, M., Ando-Kuri, M., Arzate-Mejía, R.G., Morf, J., Cairns, J., Román-Figueroa, A., Tenorio-Hernández, L., Poot-Hernández, A.C., Andrews, S., Várnai, C., et al. (2021). The global and promoter-centric 3D genome organization temporally resolved during a circadian cycle. Genome Biol. *22*, 162. https://doi.org/10.1186/s13059-021-02374-3.

45. Falick Michaeli, T., Sabag, O., Azria, B., Fok, R., Abudi, N., Abramovitch, R., Monin, J., Gielchinsky, Y., Cedar, H., and Bergman, Y. (2024). Hepatocyte regeneration is driven by embryo-like DNA methylation reprogramming. Proc. Natl. Acad. Sci. USA *121*, e2314885121. https://doi.org/10.1073/pnas.2314885121.

46. López-Luque, J., Caballero-Díaz, D., Martinez-Palacián, A., Roncero, C., Moreno-Càceres, J., García-Bravo, M., Grueso, E., Fernández, A., Crosas-Molist, E., García-Álvaro, M., et al. (2016). Dissecting the role of epidermal growth factor receptor catalytic activity during liver regeneration and hepatocarcinogenesis. Hepatology *63*, 604–619. https://doi.org/10.1002/hep.28134.

47. Li, Z., Schulz, M.H., Look, T., Begemann, M., Zenke, M., and Costa, I.G. (2019). Identification of transcription factor binding sites using ATAC-seq. Genome Biol. *20*, 45. https://doi.org/10.1186/s13059-019-1642-2.

48. Argemí, J., Kress, T.R., Chang, H.C.Y., Ferrero, R., Bértolo, C., Moreno, H., González-Aparicio, M., Uriarte, I., Guembe, L., Segura, V., et al. (2017). X-box Binding Protein 1 Regulates Unfolded Protein, Acute-Phase, and DNA Damage Responses During Regeneration of Mouse Liver. Gastroenterology *152*, 1203–1216.e15. https://doi.org/10.1053/j.gastro.2016.12.040.

49. McLeay, R.C., and Bailey, T.L. (2010). Motif Enrichment Analysis: a unified framework and an evaluation on ChIP data. BMC Bioinf. *11*, 165. https://doi.org/10.1186/1471-2105-11-165.

50. Catarino, R.R., and Stark, A. (2018). Assessing sufficiency and necessity of enhancer activities for gene expression and the mechanisms of transcription activation. Genes Dev. *32*, 202–223. https://doi.org/10.1101/gad.310367.117.

51. Ertosun, M.G., Hapil, F.Z., and Osman Nidai, O. (2016). E2F1 transcription factor and its impact on growth factor and cytokine signaling. Cytokine Growth Factor Rev. *31*, 17–25. https://doi.org/10.1016/j.cytogfr.2016.02.001.

52. Li, W., Liang, X., Kellendonk, C., Poli, V., and Taub, R. (2002). STAT3 Contributes to the Mitogenic Response of Hepatocytes during Liver Regeneration. J. Biol. Chem. *277*, 28411–28417. https://doi.org/10.1074/jbc.M202807200.

53. Soubeyrand, S., Lau, P., and McPherson, R. (2023). Regulation of TRIB1 abundance in hepatocyte models in response to proteasome inhibition. Sci. Rep. *13*, 9320. https://doi.org/10.1038/s41598-023-36512-7.

54. Nault, R., Doskey, C.M., Fader, K.A., Rockwell, C.E., and Zacharewski, T. (2018). Comparison of Hepatic NRF2 and Aryl Hydrocarbon Receptor Binding in 2,3,7,8-Tetrachlorodibenzo- *p* -dioxin–Treated Mice Demonstrates NRF2-Independent PKM2 Induction. Mol. Pharmacol. *94*, 876–884. https://doi.org/10.1124/mol.118.112144.

55. Itoh, K., Chiba, T., Takahashi, S., Ishii, T., Igarashi, K., Katoh, Y., Oyake, T., Hayashi, N., Satoh, K., Hatayama, I., et al. (1997). An Nrf2/Small Maf Heterodimer Mediates the Induction of Phase II Detoxifying Enzyme Genes through Antioxidant Response Elements. Biochem. Biophys. Res. Commun. *236*, 313–322. https://doi.org/10.1006/bbrc.1997.6943.

56. Ishida, K., Kaji, K., Sato, S., Ogawa, H., Takagi, H., Takaya, H., Kawaratani, H., Moriya, K., Namisaki, T., Akahane, T., and Yoshiji, H. (2021). Sulforaphane ameliorates ethanol plus carbon tetrachloride-induced liver fibrosis in mice through the Nrf2-mediated antioxidant response and acetaldehyde metabolization with inhibition of the LPS/TLR4 signaling pathway. J. Nutr. Biochem. *89*, 108573. https://doi.org/10.1016/j.jnutbio.2020.108573.

57. Leonard, M.O., Kieran, N.E., Howell, K., Burne, M.J., Varadarajan, R., Dhakshinamoorthy, S., Porter, A.G., O'Farrelly, C., Rabb, H., and Taylor, C.T. (2006). Reoxygenation-specific activation of the antioxidant transcription factor Nrf2 mediates cytoprotective gene expression in ischemia-reperfusion injury. FASEB J. *20*, 2624–2626. https://doi.org/10.1096/fj.06-5097fje.

58. Gorkin, D.U., Barozzi, I., Zhao, Y., Zhang, Y., Huang, H., Lee, A.Y., Li, B., Chiou, J., Wildberg, A., Ding, B., et al. (2020). An atlas of dynamic chromatin landscapes in mouse fetal development. Nature *583*, 744–751. https://doi.org/10.1038/s41586-020-2093-3.

59. Kalhan, S., and Parimi, P. (2000). Gluconeogenesis in the fetus and neonate. Semin. Perinatol. *24*, 94–106. https://doi.org/10.1053/sp.2000.6360.

60. Perekatt, A.O., Valdez, M.J., Davila, M., Hoffman, A., Bonder, E.M., Gao, N., and Verzi, M.P. (2014). YY1 is indispensable for Lgr5+ intestinal stem cell renewal. Proc. Natl. Acad. Sci. USA *111*, 7695–7700. https://doi.org/10.1073/pnas.1400128111.

61. Pan, G., Diamanti, K., Cavalli, M., Lara Gutiérrez, A., Komorowski, J., and Wadelius, C. (2021). Multifaceted regulation of hepatic lipid metabolism by YY1. Life Sci. Alliance *4*, e202000928. https://doi.org/10.26508/lsa.202000928.

62. Zhang, S., Jiang, T., Feng, L., Sun, J., Lu, H., Wang, Q., Pan, M., Huang, D., Wang, X., Wang, L., and Jin, H. (2012). Yin Yang-1 suppresses differentiation of hepatocellular carcinoma cells through the downregulation of CCAAT/enhancer-binding protein alpha. J. Mol. Med. *90*, 1069–1077. https://doi.org/10.1007/s00109-012-0879-y.

63. Verheul, T.C.J., Van Hijfte, L., Perenthaler, E., and Barakat, T.S. (2020). The Why of YY1: Mechanisms of Transcriptional Regulation by Yin Yang 1. Front. Cell Dev. Biol. *8*, 592164. https://doi.org/10.3389/fcell.2020.592164.

64. Li, W., Yang, L., He, Q., Hu, C., Zhu, L., Ma, X., Ma, X., Bao, S., Li, L., Chen, Y., et al. (2019). A Homeostatic Arid1a-Dependent Permissive Chromatin State Licenses Hepatocyte Responsiveness to Liver-Injury-Associated YAP Signaling. Cell Stem Cell *25*, 54–68.e5. https://doi.org/10.1016/j.stem.2019.06.008.

65. Walesky, C.M., Kolb, K.E., Winston, C.L., Henderson, J., Kruft, B., Fleming, I., Ko, S., Monga, S.P., Mueller, F., Apte, U., et al. (2020). Functional compensation precedes recovery of tissue mass following acute liver injury. Nat. Commun. *11*, 5785. https://doi.org/10.1038/s41467-020-19558-3.

66. Chen, F., Schönberger, K., and Tchorz, J.S. (2023). Distinct hepatocyte identities in liver homeostasis and regeneration. JHEP Rep. *5*, 100779. https://doi.org/10.1016/j.jhepr.2023.100779.

67. Ma, X., Huang, T., Chen, X., Li, Q., Liao, M., Fu, L., Huang, J., Yuan, K., Wang, Z., and Zeng, Y. (2025). Molecular mechanisms in liver repair and regeneration: from physiology to therapeutics. Signal Transduct. Target. Ther. *10*, 63. https://doi.org/10.1038/s41392-024-02104-8.

68. Solhi, R., Lotfinia, M., Gramignoli, R., Najimi, M., and Vosough, M. (2021). Metabolic hallmarks of liver regeneration. Trends Endocrinol. Metab. *32*, 731–745. https://doi.org/10.1016/j.tem.2021.06.002.

69. Uriarte, I., Santamaria, E., López-Pascual, A., Monte, M.J., Argemí, J., Latasa, M.U., Adán-Villaescusa, E., Irigaray, A., Herranz, J.M., Arechederra, M., et al. (2024). New insights into the regulation of bile acids synthesis during the early stages of liver regeneration: A human and experimental study. Biochim. Biophys. Acta BBA - Mol. Basis Dis. *1870*, 167166. https://doi.org/10.1016/j.bbadis.2024.167166.

70. Slabber, C.F., Bachofner, M., Speicher, T., Kuklin, A., Fearon, A.E., Padrissa-Altés, S., Bogorad, R., Horváth Rudigier, C., Wüst, D., Krautbauer, S., et al. (2023). The ubiquitin ligase Uhrf2 is a master regulator of cholesterol biosynthesis and is essential for liver regeneration. Sci. Signal. *16*, eade8029. https://doi.org/10.1126/scisignal.ade8029.

71. Živný, P., Živná, H., Palička, V., Žaloudková, L., Mocková, P., Cermanová, J., and Mičuda, S. (2018). Modulation of Rat Liver Regeneration after Partial Hepatectomy by Dietary Cholesterol. Acta Medica Hradec Kralove Czech Repub *61*, 22–28. https://doi.org/10.14712/18059694.2018.19.

72. Behrens, A., Sibilia, M., David, J.P., Möhle-Steinlein, U., Tronche, F., Schütz, G., and Wagner, E.F. (2002). Impaired postnatal hepatocyte proliferation and liver regeneration in mice lacking c-jun in the liver. EMBO J. *21*, 1782–1790. https://doi.org/10.1093/emboj/21.7.1782.

73. Jia, X., Lin, W., and Wang, W. (2023). Regulation of chromatin organization during animal regeneration. Cell Regen. *12*, 19. https://doi.org/10.1186/s13619-023-00162-x.

74. Cao, Y., Xia, Y., Balowski, J.J., Ou, J., Song, L., Safi, A., Curtis, T., Crawford, G.E., Poss, K.D., and Cao, J. (2022). Identification of enhancer regulatory elements that direct epicardial gene expression during zebrafish

heart regeneration. Development *149*, dev200133. https://doi.org/10.1242/dev.200133.

75. Hishida, T., Yamamoto, M., Hishida-Nozaki, Y., Shao, C., Huang, L., Wang, C., Shojima, K., Xue, Y., Hang, Y., Shokhirev, M., et al. (2022). In vivo partial cellular reprogramming enhances liver plasticity and regeneration. Cell Rep. *39*, 110730. https://doi.org/10.1016/j.celrep.2022.110730.

76. Hsu, J.C., Laz, T., Mohn, K.L., and Taub, R. (1991). Identification of LRF-1, a leucine-zipper protein that is rapidly and highly induced in regenerating liver. Proc. Natl. Acad. Sci. USA *88*, 3511–3515. https://doi.org/10.1073/pnas.88.9.3511.

77. Allan, A.L., Albanese, C., Pestell, R.G., and LaMarre, J. (2001). Activating Transcription Factor 3 Induces DNA Synthesis and Expression of Cyclin D1 in Hepatocytes. J. Biol. Chem. *276*, 27272–27280. https://doi.org/10.1074/jbc.M103196200.

78. Cui, A., Ding, D., and Li, Y. (2021). Regulation of Hepatic Metabolism and Cell Growth by the ATF/CREB Family of Transcription Factors. Diabetes *70*, 653–664. https://doi.org/10.2337/dbi20-0006.

79. Milland, J., and Schreiber, G. (1991). Transcriptional activity of the phosphoenolpyruvate carboxykinase gene decreases in regenerating rat liver. FEBS Lett. *279*, 184–186. https://doi.org/10.1016/0014-5793(91)80144-R.

80. Xu, Y., Li, Y., Jadhav, K., Pan, X., Zhu, Y., Hu, S., Chen, S., Chen, L., Tang, Y., Wang, H.H., et al. (2021). Hepatocyte ATF3 protects against atherosclerosis by regulating HDL and bile acid metabolism. Nat. Metab. *3*, 59–74. https://doi.org/10.1038/s42255-020-00331-1.

81. Beyer, T.A., Xu, W., Teupser, D., Auf Dem Keller, U., Bugnon, P., Hildt, E., Thiery, J., Kan, Y.W., and Werner, S. (2008). Impaired liver regeneration in Nrf2 knockout mice: role of ROS-mediated insulin/IGF-1 resistance. EMBO J. *27*, 212–223. https://doi.org/10.1038/sj.emboj.7601950.

82. Chan, B.K.Y., Elmasry, M., Forootan, S.S., Russomanno, G., Bunday, T. M., Zhang, F., Brillant, N., Starkey Lewis, P.J., Aird, R., Ricci, E., et al. (2021). Pharmacological Activation of Nrf2 Enhances Functional Liver Regeneration. Hepatology *74*, 973–986. https://doi.org/10.1002/hep.31859.

83. Wang, X., Kiyokawa, H., Dennewitz, M.B., and Costa, R.H. (2002). The Forkhead Box m1b transcription factor is essential for hepatocyte DNA replication and mitosis during mouse liver regeneration. Proc. Natl. Acad. Sci. USA *99*, 16881–16886. https://doi.org/10.1073/pnas.252570299.

84. Suzuki, N., and Ochi, H. (2020). Regeneration enhancers: A clue to reactivation of developmental genes. Dev. Growth Differ. *62*, 343–354. https://doi.org/10.1111/dgd.12654.

85. Harris, R.E. (2022). Regeneration enhancers: a field in development. Am. J. Physiol. Cell Physiol. *323*, C1548–C1554. https://doi.org/10.1152/ajpcell.00403.2022.

86. Li, L., Cui, L., Lin, P., Liu, Z., Bao, S., Ma, X., Nan, H., Zhu, W., Cen, J., Mao, Y., et al. (2023). Kupffer-cell-derived IL-6 is repurposed for hepatocyte dedifferentiation via activating progenitor genes from injury-specific enhancers. Cell Stem Cell *30*, 283–299.e9. https://doi.org/10.1016/j.stem.2023.01.009.

87. Dobin, A., Davis, C.A., Schlesinger, F., Drenkow, J., Zaleski, C., Jha, S., Batut, P., Chaisson, M., and Gingeras, T.R. (2013). STAR: ultrafast universal RNA-seq aligner. Bioinformatics *29*, 15–21. https://doi.org/10.1093/bioinformatics/bts635.

88. Li, B., and Dewey, C.N. (2011). RSEM: accurate transcript quantification from RNA-Seq data with or without a reference genome. BMC Bioinf. *12*, 323. https://doi.org/10.1186/1471-2105-12-323.

89. Yu, G., Wang, L.-G., Han, Y., and He, Q.-Y. (2012). clusterProfiler: an R Package for Comparing Biological Themes Among Gene Clusters. OMICS A J. Integr. Biol. *16*, 284–287. https://doi.org/10.1089/omi.2011.0118.

90. Love, M.I., Huber, W., and Anders, S. (2014). Moderated estimation of fold change and dispersion for RNA-seq data with DESeq2. Genome Biol. *15*, 550. https://doi.org/10.1186/s13059-014-0550-8.

91. Bolger, A.M., Lohse, M., and Usadel, B. (2014). Trimmomatic: a flexible trimmer for Illumina sequence data. Bioinformatics *30*, 2114–2120. https://doi.org/10.1093/bioinformatics/btu170.

92. Langmead, B., and Salzberg, S.L. (2012). Fast gapped-read alignment with Bowtie 2. Nat. Methods *9*, 357–359. https://doi.org/10.1038/nmeth.1923.

93. Tarasov, A., Vilella, A.J., Cuppen, E., Nijman, I.J., and Prins, P. (2015). Sambamba: fast processing of NGS alignment formats. Bioinforma. Oxf. Engl. *31*, 2032–2034. https://doi.org/10.1093/bioinformatics/btv098.

94. Zhang, Y., Liu, T., Meyer, C.A., Eeckhoute, J., Johnson, D.S., Bernstein, B.E., Nusbaum, C., Myers, R.M., Brown, M., Li, W., and Liu, X.S. (2008). Model-based analysis of ChIP-Seq (MACS). Genome Biol. *9*, R137. https://doi.org/10.1186/gb-2008-9-9-r137.

95. Pohl, A., and Beato, M. (2014). bwtool: a tool for bigWig files. Bioinforma. Oxf. Engl. *30*, 1618–1619. https://doi.org/10.1093/bioinformatics/btu056.

96. Li, H., and Durbin, R. (2009). Fast and accurate short read alignment with Burrows–Wheeler transform. Bioinformatics *25*, 1754–1760. https://doi.org/10.1093/bioinformatics/btp324.

97. Durand, N.C., Shamim, M.S., Machol, I., Rao, S.S.P., Huntley, M.H., Lander, E.S., and Aiden, E.L. (2016). Juicer Provides a One-Click System for Analyzing Loop-Resolution Hi-C Experiments. Cell Syst. *3*, 95–98. https://doi.org/10.1016/j.cels.2016.07.002.

98. Hao, Y., Stuart, T., Kowalski, M.H., Choudhary, S., Hoffman, P., Hartman, A., Srivastava, A., Molla, G., Madad, S., Fernandez-Granda, C., and Satija, R. (2024). Dictionary learning for integrative, multimodal and scalable single-cell analysis. Nat. Biotechnol. *42*, 293–304. https://doi.org/10.1038/s41587-023-01767-y.

99. Korsunsky, I., Millard, N., Fan, J., Slowikowski, K., Zhang, F., Wei, K., Baglaenko, Y., Brenner, M., Loh, P.R., and Raychaudhuri, S. (2019). Fast, sensitive and accurate integration of single-cell data with Harmony. Nat. Methods *16*, 1289–1296. https://doi.org/10.1038/s41592-019-0619-0.

100. Danecek, P., Bonfield, J.K., Liddle, J., Marshall, J., Ohan, V., Pollard, M. O., Whitwham, A., Keane, T., McCarthy, S.A., Davies, R.M., and Li, H. (2021). Twelve years of SAMtools and BCFtools. GigaScience *10*, giab008. https://doi.org/10.1093/gigascience/giab008.

101. Shannon, P., Markiel, A., Ozier, O., Baliga, N.S., Wang, J.T., Ramage, D., Amin, N., Schwikowski, B., and Ideker, T. (2003). Cytoscape: A Software Environment for Integrated Models of Biomolecular Interaction Networks. Genome Res. *13*, 2498–2504. https://doi.org/10.1101/gr.1239303.

102. Higgins, M., and Anderson, R.M. (1931). Experimental pathology of liver: restoration of liver of white rat following partial surgical removal. Arch. Pathol. Lab Med. *12*, 186–202.

103. Corces, M.R., Trevino, A.E., Hamilton, E.G., Greenside, P.G., Sinnott-Armstrong, N.A., Vesuna, S., Satpathy, A.T., Rubin, A.J., Montine, K.S., Wu, B., et al. (2017). An improved ATAC-seq protocol reduces background and enables interrogation of frozen tissues. Nat. Methods *14*, 959–962. https://doi.org/10.1038/nmeth.4396.

104. Buenrostro, J.D., Wu, B., Chang, H.Y., and Greenleaf, W.J. (2015). ATAC-seq: A Method for Assaying Chromatin Accessibility Genome-Wide. Curr. Protoc. Mol. Biol. *109*, 21.29.1–21.29.9. https://doi.org/10.1002/0471142727.mb2129s109.

105. Fazio, E.N., Young, C.C., Toma, J., Levy, M., Berger, K.R., Johnson, C.L., Mehmood, R., Swan, P., Chu, A., Cregan, S.P., et al. (2017). Activating transcription factor 3 promotes loss of the acinar cell phenotype in response to cerulein-induced pancreatitis in mice. Mol. Biol. Cell *28*, 2347–2359. https://doi.org/10.1091/mbc.e17-04-0254.

Please cite this article in press as: Llorens-Giralt et al., Sequential activation of transcription factors promotes liver regeneration through specific and developmental enhancers, Cell Genomics (2025), https://doi.org/10.1016/j.xgen.2025.100887

106. Nguyen, H.C.B., Adlanmerini, M., Hauck, A.K., and Lazar, M.A. (2020). Dichotomous engagement of HDAC3 activity governs inflammatory responses. Nature *584*, 286–290. https://doi.org/10.1038/s41586-020-2576-2.

107. Seidman, J.S., Troutman, T.D., Sakai, M., Gola, A., Spann, N.J., Bennett, H., Bruni, C.M., Ouyang, Z., Li, R.Z., Sun, X., et al. (2020). Niche-Specific Reprogramming of Epigenetic Landscapes Drives Myeloid Cell Diversity in Nonalcoholic Steatohepatitis. Immunity *52*, 1057–1074.e7. https://doi.org/10.1016/j.immuni.2020.04.001.

108. Huang, M., Wang, X., Zhang, M., Liu, Y., and Chen, Y.-G. (2024). METTL3 restricts RIPK1-dependent cell death via the ATF3-cFLIP axis in the intestinal epithelium. Cell Regen. *13*, 14. https://doi.org/10.1186/s13619-024-00197-8.

Please cite this article in press as: Llorens-Giralt et al., Sequential activation of transcription factors promotes liver regeneration through specific and developmental enhancers, Cell Genomics (2025), https://doi.org/10.1016/j.xgen.2025.100887

CellPress
OPEN ACCESS

STAR★METHODS

KEY RESOURCES TABLE

REAGENT or RESOURCE	SOURCE	IDENTIFIER
Antibodies		
Anti-ATF3 antibody [EPR19488]	Abcam	ab207434; RRID: AB_2734728
Critical commercial assays		
Nano-GLO® Dual-Luciferase Reporter Assay Kit	Promega	N1610
Optiprep Density Gradient Medium	Sigma-Aldrich	D1556
Deposited data		
RNA-seq liver regeneration post-PHx (6h, 24h, 48h)	https://doi.org/10.1016/j.redox.2020.101841	GEO: GSE181476
ATAC-seq liver regeneration post-PHx (6h, 24h, 48h)	Present study	GEO: GSE266402
ChIP-seq H3K27ac in liver pre-PHx (0 h)	https://doi.org/10.1038/s41467-023-37247-9	GEO: GSE188742
ChIP-seq H3K27ac in liver, post-PHx (40 h)	https://doi.org/10.1016/j.stem.2016.03.001	GEO: GSE76935
ChIP-seq Atf3 in Intestinal organoids	https://doi.org/10.1186/s13619-024-00197-8	GEO: GSE262282
ChIP-seq Atf3 in bone marrow macrophages	https://doi.org/10.1038/s41586-020-2576-2	GEO: GSE140581
ChIP-seq Atf3 in hepatic macrophages	https://doi.org/10.1016/j.immuni.2020.04.001	GEO: GSE128336
ChIP-seq Atf3 in pancreatic tissue	https://doi.org/10.1091/mbc.e17-04-0254	GEO: GSE60250
ChIP-seq Nrf2 in liver	https://doi.org/10.1124/mol.118.112144	GEO: GSE109865
Hi-C liver	https://doi.org/10.1186/s13059-021-02374-3	GEO: GSE155158
scRNA-seq liver regeneration post-PHx (0h, 24h, 48h)	https://doi.org/10.1101/gr.267013.120	GEO: GSE151309
ATAC-seq liver development	https://doi.org/10.1038/s41586-020-2093-3	GEO: GSE172627
Experimental models: Cell lines		
Immortalised hepatocytes	López-Luque et al.[46]	https://doi.org/10.1002/hep.28134
Experimental models: Organisms/strains		
Mouse: C57BL/6J	The Jackson Laboratory	RRID: IMSR_JAX:000664
Oligonucleotides		
Primer: ATACseqPeak_39376 cloning primer forward: GTAGCTAGCGGAATGGGATGGGGAGACAG	This paper	N/A
Primer: ATACseqPeak_39376 cloning primer reverse: ATGAAGCTTCTCAGCCCAAATTCAGATGG	This paper	N/A
Primer: ATACseqPeak_76443 cloning primer forward: GTAGCTAGCGCTTGCCTGAACCCTTCTCC	This paper	N/A
Primer: ATACseqPeak_76443 cloning primer reverse: ATGAAGCTTCCTAAGCCCGTAACAGGACC	This paper	N/A
Primer: ATACseqPeak_69905 cloning primer forward: GTAGCTAGCCAGCTTTGGACTGTCTGCTC	This paper	N/A
Primer: ATACseqPeak_69905 cloning primer reverse: ATGAAGCTTGTGTGTACCAGTTCGAAGTG	This paper	N/A
Primer: ATACseqPeak_9588 cloning primer forward: GTAGCTAGCCAGGACGAGTACTTCACCAG	This paper	N/A

(*Continued on next page*)

Please cite this article in press as: Llorens-Giralt et al., Sequential activation of transcription factors promotes liver regeneration through specific and developmental enhancers, Cell Genomics (2025), https://doi.org/10.1016/j.xgen.2025.100887

Continued

REAGENT or RESOURCE	SOURCE	IDENTIFIER
Primer: ATACseqPeak_9588 cloning primer reverse: ATGAAGCTTCCATGAAGAAGGGCAAGTGC	This paper	N/A
Primer: ATACseqPeak_70885 cloning primer forward: CTGCGGGCTAGCAGTAGAAG	This paper	N/A
Primer: ATACseqPeak_70885 cloning primer reverse: ATGAAGCTTGACCTGACTCCTGGTCTGTC	This paper	N/A
Primer: ATACseqPeak_57343 cloning primer forward: GTAGCTAGCTCCTCTGTGTTGAAGAAGGC	This paper	N/A
Primer: ATACseqPeak_57343 cloning primer reverse: ATGAAGCTTCCAGGCTAGGATGTGATAGC	This paper	N/A
Recombinant DNA		
Plasmid: pGL4.27[luc2P/minP/Hygro]	Promega	E8451
Plasmid: pNL1.1.TK[Nluc/TK] Vector	Promega	N1501
Plasmid: Atf3 (NM_007498) Mouse Tagged ORF Clone	Origene	MR201634
Plasmid: Nfe2l2 (NM_010902) Mouse Tagged ORF Clone	Origene	MR226717
Software and algorithms		
grape-nf	in-house	https://github.com/guigolab/grape-nf
STAR 2.4.0	Dobin et al.[87]	
RSEM	Li et al.[88]	
clusterProfiler	Yu et al.[89]	
heatmap3		https://github.com/slzhao/heatmap3
DESeq2	Love et al.[90]	N/A
Trimmomatic	Bolger et al.[91]	N/A
Bowtie2	Langmead et al.[92]	N/A
Sambamba	Tarasov et al.[93]	N/A
MACS2	Zhang et al.[94]	N/A
bwtool	Pohl et al.[95]	N/A
BWA	Li et al.[96]	N/A
Juicer	Durand et al.[97]	N/A
Activity-by-contact algorithm	Fulco et al.[43]	N/A
Seurat v5.0.3	Hao et al.[98]	N/A
Harmony v1.2.0	Korsunsky et al.[99]	N/A
HINT-ATAC	Li et al.[47]	N/A
SAMtools v.1.16	Danecek et al.[100]	N/A
MEME Suite 5.4.1	McLeay et al.[49]	N/A
Cytoscape Software v3.10.2	Shannon et al.[101]	N/A

EXPERIMENTAL MODEL AND STUDY PARTICIPANT DETAILS

Animal procedures

C57BL/6J wild-type (WT) mice were obtained from Jackson Laboratories and housed at the IDIBELL (Barcelona, Spain). All experiments complied with the EU Directive 2010/63/UE for animal experiments and the institution's guidelines (Ethics Committee for Animal Experimentation of the IDIBELL) and were approved by the General Direction of Environment and Biodiversity, Government of

Please cite this article in press as: Llorens-Giralt et al., Sequential activation of transcription factors promotes liver regeneration through specific and developmental enhancers, Cell Genomics (2025), https://doi.org/10.1016/j.xgen.2025.100887

Catalonia (experiments #4589). Animals were 8 to 16-week-old male and female mice, housed under a 12h light/dark cycle with free access to food and water. Partial hepatectomies (PHx) were performed by removing two-thirds of the adult mouse liver, as described by Higgins and Anderson (1931).[102] The mice that had undergone surgery without liver resection (sham-operated) were used as controls. The mice were euthanised 6, 24 and 48 h after surgery, and their liver lobes were immediately frozen in liquid nitrogen and stored at −80°C. The same livers used to extract RNA were used to prepare the ATAC-seq libraries. The number of animals used in the study was minimised for ethical reasons. Thus, 2 hepatectomised and 1–2 sham-operated animals were used for each time point after surgery.

METHOD DETAILS

ATAC sequencing

ATAC-seq libraries were prepared following the Omni-ATAC protocol[103] with minor modifications. Briefly, 10–20 mg of frozen liver were placed in a pre-chilled Tenbroeck tissue grinder containing 1 mL of the Omni-ATAC homogenisation buffer and let thaw for 5 min. The tissue was homogenised on ice using a glass Tenbroeck grinder and then filtered through a 70μm Flowmi strainer. Nuclei were pelleted for 5 min at 350 g and isolated using iodixanol density gradient centrifugation (OptiPrep). The nucleus band was transferred to a fresh tube and diluted in ATAC-seq resuspension buffer (ATAC-RSB)-Tween. Nuclei were counted using trypan blue staining and 50,000 nuclei were aliquoted per sample and resuspended in 50 μL of the transposition mixture (25 μL of 2× TD buffer (Illumina, San Francisco, CA), 2.5 μL of transposase (Illumina, San Francisco, CA), 16.5 μL of PBS, 0.5 μL of 1% digitonin, 0.5 μL of 10% Tween 20 and 5 μL of H_2O). Transposition reactions were incubated at 37°C for 30 min in a thermomixer at 1,000 RPM. Reactions were cleaned up with the Qiagen MinElute PCR Purification Kit (Qiagen, Frederick, MD) and eluted into 10 μL of the elution buffer. Purified DNA was used to prepare the ATAC-seq libraries, as described previously.[104] The quality of the tagmented libraries was visualised with the Agilent Bioanalyzer High Sensitivity DNA Assay (Agilent Technologies, Savage, DE) and sequenced on the HiSeq2500 platform at the Center for Genomic Regulation (CRG) sequencing facility in Barcelona, Spain. A minimum of 49 million paired-end 50-bp-long reads were obtained per sample.

Immunohistochemistry

Paraffin-embedded tissues were cut into 4-μm-thick sections. Immunohistochemical (IHC) analyses were performed using standard procedures.[33] Sections were incubated overnight at 4°C with a recombinant anti-ATF3 antibody (1:100; ab207434, Abcam). Binding was developed with the VECTASTAIN ABC HRP Kit (rabbit IgG; PK-4001, Vector Laboratories). Tissues were visualised and imaged under a microscope.

Reporter assays

Candidate RREs were amplified from mouse genomic DNA using the primers listed in key resources table and cloned into the pGL4.27[luc2P/minP/Hygro] plasmid (Promega). NheI and HindIII restriction sites were added to the 5′ ends of the forward and reverse primers, respectively, to facilitate directional cloning. The amplified PCR products of RREs and the pGL4.27 plasmid were double digested with NheI-HF and HindIII-HF restriction enzymes (New England Biolabs), followed by dephosphorylation of the 5′ ends of the digested plasmid using calf intestinal alkaline phosphatase (0.01u CIAP/pmol of DNA ends). After digestion, the PCR-amplified inserts and the linearized vector were purified and then ligated at a 1:3 vector-to-insert ratio using T4 DNA ligase (New England Biolabs), following the manufacturer's instructions. The ligation products were transformed into DH5α competent cells (Invitrogen), and successfully transformed Ampicillin-resistant colonies were confirmed by sequencing.

In-house immortalised hepatocyte cell line[46] was grown in Dulbecco's Modified Eagle Medium (DMEM) supplemented with 10% fetal bovine serum (FBS) (Sera Laboratories International Ltd, West Sussex, UK), Penicillin (100 U/mL), Streptomycin (100 μg/mL), Amphotericin (2.5 μg/mL) and L-glutamine (2 mM), and maintained in a humidified atmosphere of 37°C, 5% CO2. Cells seeded in 12-well plates at a density of 3 x 10^4 cells per well were transiently cotransfected using polyethylenimine (3μL PEI/μg DNA) with 995 ng/mL of DNA reporter of interest per well (recombinant pGL4.24 [luc2P/minP/Hygro]) and 5 ng/mL of NanoLuc plasmid (N1501, Promega, Madison, WI, USA) in complete media. 16 h post-transfection, the medium was replaced, and cells were serum-starved for 24 h. After, cells were either switched to complete medium with 10% FBS or continued serum starvation for an additional 3 h. Cells were then harvested, lysed, and luciferase activities were measured using the Nano-GLO Dual-Luciferase Reporter Assay Kit (Promega, Madison, WI, USA) following the manufacturer's instructions. Firefly luciferase signal was divided by the NanoLuc signal to determine relative luciferase activity. The activity for each luciferase construct was normalised for the activity of the minimal promoter (minP). The constructs were measured in two independent experiments in a total of six biological replicates. Statistical significance was assessed using two-way ANOVA followed by Tukey's Honest Significant Difference (Tukey's HSD) test to compare each construct against minP, and to compare between starvation and FBS-treatment. Normality and homogeneity of variance were assumed. All tests were two-sided. Differences were considered statistically significant when p-value was <0.05.

Validation of transcriptional activators was performed following the same experimental conditions with minor modifications. Cells were transiently cotransfected with 800 ng/mL of luciferase reporter, 195 ng of mouse ATF3 plasmid (MR201634, Origene) or mouse Nfe2l2 plasmid (MR226717, Origene), and 5 ng/mL of NanoLuc plasmid (N1501, Promega, Madison, WI, USA) in complete media. 16 h post-transfection, the medium was replaced and 24 h later cells were harvested, lysed, and luciferase activities were measured

Please cite this article in press as: Llorens-Giralt et al., Sequential activation of transcription factors promotes liver regeneration through specific and developmental enhancers, Cell Genomics (2025), https://doi.org/10.1016/j.xgen.2025.100887

using the Nano-GLO Dual-Luciferase Reporter Assay Kit (Promega, Madison, WI, USA) following the manufacturer's instructions. The constructs were measured in two independent experiments in a total of six biological replicates. Statistical significance was assessed using one-way ANOVA followed by Tukey's HSD. Normality and homogeneity of variance were assumed. All tests were two-sided. Differences were considered statistically significant when p-value was <0.05.

RNA sequencing data analysis

RNA-seq raw data for WT mice at 6, 24 and 48 h after PHx were downloaded from GEO accession number GSE181476[33] and processed using the in-house pipeline grape-nf (available at https://github.com/guigolab/grape-nf). RNA-seq reads were aligned to the *Mus musculus* genome assembly GRCm39 using the STAR 2.4.0 software[87] allowing up to 4 mismatches per paired alignment. We used the mouse genome GENCODE annotation vM27. Only alignments for reads mapping to ten or fewer loci were reported. Genes and transcripts per kilobase million (TPMs) were quantified using RSEM.[88] Tracks were visualised with the UCSC Genome Browser. From the RNA-seq data, the expression values for 55,360 annotated genes were estimated and the gene expression matrix was quantile normalised. Only genes with >1 TPM in at least one condition were considered for subsequent analyses (11,512 genes). Correspondence analysis and association plots[34] were used to cluster and identify the genes with differential expression profiles during early liver regeneration. Briefly, we used the APL R package, considering 5 dimensions and clusters were defined setting a threshold of Sα score > -0.05. Normalised expression values as z-scores were used to visualise differential expressed genes using line plots or hierarchical clustering from heatmap3 R package. Gene Ontology enrichment analysis of the clusters of interest was performed using the Bioconductor package clusterProfiler,[89] one-sided Fisher's exact test was applied and p-adjust <0.05 was used as cut-off, no assumptions about the underlying distribution of gene expression data was done. Differential gene expression analysis of the TFs from Figure 4 was performed using DESeq2[90] using Wald test, assuming negative binomial distribution.

ATAC sequencing data analysis

Reads were trimmed *in silico* to remove adapter sequences and low-quality reads using Trimmomatic[91] while FastQC was used to check their quality. The reads were aligned to the mouse (mm39) reference genome using Bowtie2.[92] Duplicate reads were removed using Picard (http://broadinstitute.github.io/picard/), and the mitochondrial reads and the reads mapping to the ENCODE blacklisted regions were filtered out using BEDTools2. Sambamba[93] was used to eliminate fragments larger than 400 bp. Peak calling was performed using a MACS2[94] run in the pair-end mode, requesting an p-adjust <0.01. Read depth-normalised values (pileup) were generated by MACS2 and stored in bigWig files. All the ATAC-seq samples were checked for the library complexity and PCR bottlenecking following ENCODE standards https://www.encodeproject.org/data-standards/terms/#library (Table S6). Each replicate, time point and condition in the ATAC-seq data was processed independently. However, we combined the data, processing together the read alignments from all 6 experiments in the regenerated livers. The peaks that had at least 50% overlap in each replicate in at least one condition were retained, while the peaks with an overlap smaller than 25 nucleotides were discarded. The maximum heights of all the peaks were then quantified for each sample using bwtool.[95] These values were quantile-normalised among the samples and the peak heights were averaged between replicates (Table S7). Differentially accessible regions were identified using an absolute fold-change larger than 1.7 as the cut-off between regeneration and control at each time point. These regions were classified into *de novo* (open regions detected exclusively in REG), increasing (both in CTRL and REG, and at least 1.7-fold higher in REG) or decreasing peaks (1.7-fold lower in REG). Finally, the peaks were classified into promoters (+-500 bp around the TSS), proximal enhancers (+-500 bp away from promoters) or distal enhancers (>1 kb from the TSS), considering all possible protein-coding and non-coding isoforms from the GENCODE mouse annotation vM27.

ChIP sequencing data analysis

ChIP-seq raw read data corresponding to H3K27ac histone modification pre-PHx[39] and post-PHx[40] as well as NRF2 binding in intact liver[54] and ATF3 binding in different tissues[105–108] were obtained from NCBI GEO. Reads were aligned to the *Mus musculus* genome assembly GRCm39 with BWA.[96] Peak calling was performed using MACS2,[94] applying a cut-off of 0.05 for the FDR. Fold changes in relation to input control data were calculated and converted into the BigWig format. All the ChIP-seq samples were checked for the library complexity and PCR bottlenecking following ENCODE standards https://www.encodeproject.org/data-standards/terms/#library (Table S6). The presence of H3K27ac around RREs was analyzed by extending the ATAC-seq peaks to 500 bp to incorporate the flanking nucleosomes and using BEDTools2 intersectBed with default conditions. The overlap between ATAC-seq peaks and NRF2 and ATF3 ChIP-seq peaks was analyzed using BEDTools intersectBed with default conditions. The statistical significance of this overlap between the ATF3 peaks and the *de novo* and increasing peaks, and between the NRF2 peaks and the increasing peaks was calculated using BEDTools2 Fisher's exact test.

Hi-C data analysis

Raw read sequences for *in situ* and promoter-capture Hi-C from intact livers[44] were downloaded from NCBI GEO under the accession number GSE155161. The Juicer pipeline[97] was used to process these data. In brief, paired-end reads were mapped to the *Mus musculus* genome assembly GRCm39 with BWA,[96] keeping the most 5′ alignment block. The custom-made Juicer script "chimeric_blacklist.awk" was used to select the proper pair alignments. These alignments in turn were sorted and duplicates were removed. Hi-C matrices were generated with the Juicer Pre command, using standard resolutions of up to 5 kb and the SCALE normalisation

Please cite this article in press as: Llorens-Giralt et al., Sequential activation of transcription factors promotes liver regeneration through specific and developmental enhancers, Cell Genomics (2025), https://doi.org/10.1016/j.xgen.2025.100887

method. To calculate the contact probability of the promoter and enhancer regions, these regions were projected onto particular 5-kb genomic intervals and before calculating the probability as a fraction of the normalised read counts supporting the interaction of the promoter and enhancer intervals (n-th diagonal) divided by the normalised read counts supporting the interaction of the promoter with itself (zero-diagonal). The generated Hi-C contact matrices were also used to calculate the background contact probabilities by averaging contact probabilities genome-wide across contacting regions at the same distance and using these average values to impute contact probabilities to the regions that are absent in the Hi-C matrices due to their low mappability.

Enhancer-gene pair association

Proximal peaks were classified as proximal enhancers and associated with the nearby promoters directly. For distal peaks, the activity-by-contact (ABC) algorithm[43] was implemented. The activity of the corresponding regions was calculated as a geometric mean of the ATAC-seq and H3K27ac signals. The maximum pileup signal across all the regeneration samples combined (see above) was used as a source of the ATAC-seq data. The maximum fold-change from the regenerated livers (GEO: GSE76935)[40] was used as a source of H3K27ac data. H3K27ac was determined in nucleosomes adjusted to the open chromatin regions, extending these regions by 250 bp in both directions. All enhancers lying closer than 2 Mb up- or downstream of the corresponding promoter were considered candidate regulatory elements. The maximum value from the *in situ* Hi-C, promoter-capture Hi-C or the same distance background control was used to calculate the contact probabilities of the promoter and enhancer regions. The activity of the promoter was included in the prediction model, assuming the contact probability of the promoter with itself to be equal to one. ABC scores were calculated for the promoter and each candidate enhancer by multiplying the activity value with the contact probability. Finally, the ABC scores were normalised for each enhancer by the sum of the ABC scores for all the enhancers and promoter. For each enhancer, the interaction with the highest ABC score was selected, filtering for expressed genes only (>1 TPM in at least one condition) (Tables S2 and S3). Gene Ontology Biological Process enrichment for the annotated genes was performed using the Bioconductor package clusterProfiler,[89] one-sided Fisher's exact test was applied with a p-adjust <0.05 as a cut-off, no assumptions about the underlying distribution of gene expression data was done. Pearson's correlation coefficient was determined between the enhancer profile and the gene expression profile. Statistical differences were calculated using one-way analysis of variance (ANOVA) with Tukey's HSD for multiple comparisons (p-value <0.05). To identify gene expression differences between the *de novo*, increasing and decreasing RRE-associated candidate target genes, two-way ANOVA with Tukey's HSD test for multiple comparisons was performed for each type of element (promoter, proximal and distal) (p-value <0.05).

Single-cell RNA sequencing analysis

The single-cell RNA-seq dataset generated from mouse livers collected at 0, 24 and 48 h post-PHx was retrieved from GEO: GSE151309.[31] The standard 10× Genomics Cell Ranger output was downloaded and imported using the Read10× function in Seurat v5.0.3.[98] The genes detected in 10 or fewer cells were filtered out. Cells with unique gene counts exceeding 500 for PHx0, 300 for PHx24, and 200 for PHx48 were retained, while cells with total gene counts above 4,000 or a mitochondrial gene percentage greater than 30% were filtered out. Seurat objects were then normalised and scaled to remove unwanted sources of variation, enhancing comparability among the samples. The top 2,000 variable genes were identified using the FindVariableFeatures function in Seurat for subsequent principal component analysis (PCA). To address potential batch effects, the RunHarmony function of Harmony v1.2.0[99] was applied to integrate the merged Seurat object. The clustering of cells was performed using the FindNeighbors and FindClusters functions in Seurat with a resolution parameter set to 0.4. Dimensionality reduction was achieved through Uniform Manifold Approximation and Projection (UMAP). Cell clusters were annotated based on the expression of marker genes in accordance with Chembazhi et al. (2021).[31] Visualisation plots were generated using scCustomize v2.1.2 to facilitate interpretation and analysis.

Transcription factor motif enrichment analysis

TF differential binding analysis was performed with HINT-ATAC,[47] a computational footprinting tool tailored for ATAC-seq data. As input, BAMs of biological replicate samples were merged with SAMtools v.1.16[100] and differentially accessible peaks were used as input regions for each time point. The resulting footprints were searched for motif enrichment using the HOCOMOCO v11 database. The analysis focused exclusively on the TFs expressed in the RNA-seq data (>1 TPM). Only the TF motifs with a HINT-ATAC absolute fold change activity value greater than 1.5 and an associated p-value <0.05 were considered significant (visualised by volcano plots). TF footprints were also visualised as lineplots, showing the mean of the ATAC-seq signal (adjusted for Tn5 cutting-bias) in the 200 bp window centered at each occupied motif.

For TF motif analysis, the Analysis of Motif Enrichment (AME) tool from the MEME suite v5.4.1[49] was used, using the HOCOMOCO v11 database and default parameters. To check for differential TF binding between the promoter and enhancer regulatory elements, the peaks located within 500 bp upstream or downstream of the transcriptional start site were considered promoter peaks and the rest were considered putative enhancer peaks. Only the TFs that were significantly enriched (Mann–Whitney U test, p-adjust <0.05) and expressed in the RNA-seq data (>1 TPM) were considered a hit, with the redundant hits removed. Only the top 10 TF motifs for each time point and peak class were represented in the heatmaps from Figure 4C.

Please cite this article in press as: Llorens-Giralt et al., Sequential activation of transcription factors promotes liver regeneration through specific and developmental enhancers, Cell Genomics (2025), https://doi.org/10.1016/j.xgen.2025.100887

Gene coexpression regulatory network

To construct the early regeneration gene coexpression regulatory network (GRN), we computed the correlation of expression across all samples between target genes linked to RREs (RRE-linked targets) and potential regulatory TFs, based on the presence of their motifs within these RREs. The GRN was generated using the expression values of 1,805 RRE-linked targets and 37 TFs. Only TF-target gene pairs containing the TF motif present in the RRE and those with absolute values of Pearson's correlation coefficient equal to or higher than 0.8 were considered as reliable. The resulting GRN included 1,829 nodes, of which 37 were source nodes (selected TFs), interconnected by 3,794 edges representing *de novo*, increasing and decreasing regulatory interactions. Network visualisation was performed using Cytoscape Software v3.10.2.[101] Nodes were displayed according to Edge-weighted Spring-Embedded Layout analysis of TF-target correlation of expression (Pearson's correlation coefficient between TF and target expression). Node size was adjusted to denote TFs and colored by normalised expression values calculated as z-scores for each time point. Edges were colored depending on TF-target correlation of expression (negative or positive) or based on RREs classification at each time point. Edge transparency was adjusted depending on RRE classification at each time point for visualisation purposes (Non-differentially accessible peaks were made more transparent).

Developmental analysis

To determine if the regeneration enhancers were repurposed from development, ATAC-seq data from mouse livers at different embryonic stages were obtained from the ENCODE development series ENCSR326DKM.[58] The ATAC-seq postnatal dataset was obtained from the reference epigenome ENCSR687SNT.[58] Peak coordinates were converted from mm10 to mm39 using the liftOver tool from the UCSC Genome Browser. *De novo* peaks overlapping open regions in the fetal or postnatal day 0 livers were considered to be reused. This overlap was calculated using BEDTools2 intersectBed.

QUANTIFICATION AND STATISTICAL ANALYSIS

The quantitative and statistical analyses are described in the relevant sections of the method details or in the figure legends.

APPENDIX II
Publication (Llorens-Giralt *et al*., 2021)

cells

MDPI

Review

Chromatin Organization and Function in *Drosophila*

Palmira Llorens-Giralt, Carlos Camilleri-Robles, Montserrat Corominas and Paula Climent-Cantó *

Departament de Genètica, Microbiologia i Estadística, Facultat de Biologia and Insitut de Biomedicina (IBUB), Universitat de Barcelona, 08028 Barcelona, Catalonia, Spain; pllorens@ub.edu (P.L.-G.); carloscamilleri@ub.edu (C.C.-R.); mcorominas@ub.edu (M.C.)
* Correspondence: pcliment@ub.edu

Abstract: Eukaryotic genomes are packaged into high-order chromatin structures organized in discrete territories inside the cell nucleus, which is surrounded by the nuclear envelope acting as a barrier. This chromatin organization is complex and dynamic and, thus, determining the spatial and temporal distribution and folding of chromosomes within the nucleus is critical for understanding the role of chromatin topology in genome function. Primarily focusing on the regulation of gene expression, we review here how the genome of *Drosophila melanogaster* is organized into the cell nucleus, from small scale histone–DNA interactions to chromosome and lamina interactions in the nuclear space.

Keywords: chromatin composition; chromatin organization; gene regulation; 3D genome structure; nuclear architecture

Citation: Llorens-Giralt, P.; Camilleri-Robles, C.; Corominas, M.; Climent-Cantó, P. Chromatin Organization and Function in *Drosophila*. *Cells* **2021**, *10*, 2362. https://doi.org/10.3390/cells10092362

Academic Editor: Peter Askjaer

Received: 12 August 2021
Accepted: 6 September 2021
Published: 8 September 2021

1. Introduction

In eukaryotic cells, nuclear organization refers to the spatial distribution of nuclear contents and components. The cell nucleus contains DNA, which is organized as multiple long linear molecules in a complex with a large variety of proteins, such as histones, to form chromatin and chromosomes. Thus, the eukaryotic genome is packaged into higher-order chromatin structures and organized in a manner that accommodates highly dynamic processes such as DNA replication, gene transcription, and DNA repair.

There are many different levels of nuclear organization and whether they affect gene function or just reflect this function is still unclear. Here, we focus on *Drosophila melanogaster*, a pre-eminent animal model system for genetic studies. Starting from basic DNA composition, we review what is currently known about the general structure of chromatin, chromosomes, and nuclear organization.

2. The *Drosophila* Genome

The first annotated whole genome sequence of the fruit fly *Drosophila* was published more than two decades ago, when it was estimated to contain around 13,600 genes [1,2]. The most recent version of the *Drosophila* genome identifies 13,969 protein-coding genes and 2545 long non-coding RNA genes, with a GC percentage of ~42% [3] (FlyBase r6.40, June 2021).

The *Drosophila* genome is divided into four chromosomes: the X and Y sex chromosomes, the autosomal chromosomes 2 and 3, and a tiny chromosome 4 containing no more than 100 genes and known as the "dot chromosome". In *Drosophila*, like in other Diptera species, polytene chromosomes can be observed in the interphase nuclei of certain tissues such as the salivary glands. This highly specialized form of chromosomes develops by endoreduplication of the chromosomes of diploid nuclei, producing multiple chromatids of each chromosome. Polytene chromosomes have been very useful in cytogenetic studies due to their distinct patterns of bands and interbands showing different degrees of condensation, gene expression profiles, and protein composition [4,5].

3. Chromatin Composition and Structure

Eukaryotic DNA molecules, together with proteins and RNA, are packaged into a compact structure called chromatin. Different chromatin states have long been recognized, with chromatin classically divided into euchromatin (which decondenses regularly during the cell cycle, consists primarily of single-copy sequences, and is transcriptionally active) and heterochromatin (which is condensed throughout the cell cycle, consists mainly of repetitive sequences, and can silence gene expression) [6,7]. In *Drosophila*, heterochromatin comprises approximately a third of the genome and is organized primarily into pericentromeric and telomeric blocks [8]. Pericentromeric heterochromatin is mainly composed of repetitive sequences, including fragments of various transposable elements (TEs) and satellite DNAs (satDNA), which are large blocks of tandemly repeated DNA sequences [9]. Heterochromatin protein 1 (HP1a in *Drosophila*) is a conserved eukaryotic chromosomal protein that is associated with pericentromeric heterochromatin and mediates the concomitant gene silencing [10]. Despite its association with gene repression, it was reported recently that a significant part of the constitutive heterochromatin in *Drosophila* is, in fact, occupied by active genes [11]. Moreover, an RNAi screen conducted in flies revealed that heterochromatin is structurally complex and contains many dynamic smaller subdomains [12]. Beyond the binary classification of chromatin into euchromatin and heterochromatin, several groups have partitioned the *Drosophila* genome into different chromatin types or states based on a combinatorial signature of bound proteins, histone modifications and integrative analysis with other chromatin data [13] (discussed below).

3.1. Nucleosome Dynamics

The basic unit of chromatin is the nucleosome, which consists of an octamer composed of two copies of each of the core histones (H2A, H2B, H3, and H4) that is wrapped by 145–147 bp of DNA in a left-handed superhelical turn [14,15]. The core histones interact with DNA through the highly conserved histone-fold domain, while the N-terminal tail participates in nucleosome stabilization [15,16]. The different nucleosomes are separated by linker DNA and the resulting arrangement is an 11-nm chromatin fiber that resembles a beads-on-a-string structure [17]. Linker histones, such as H1, bind to DNA at the entry/exit site of the nucleosome, seal the structure, and protect an extra 20 bp of DNA [18–20]. The resulting structure is called a "chromatosome" [21]. Several studies have addressed the role of H1 in chromatin folding, showing that H1 promotes and stabilizes the compaction of nucleosomes into a 30-nm chromatin fiber [22,23]. However, the 30-nm fiber is only observed as short fragments in vivo, since nucleosomes are found in clutches of various sizes separated by nucleosome-depleted regions [24].

The organization of nucleosomes varies across the genome and plays a central role in controlling DNA accessibility. Nucleosome-depleted regions are characteristic of active chromatin sites and adjacent regions show a regular placement of nucleosomes. More irregular positions are commonly found elsewhere [25–27]. The determinants of nucleosome positioning were defined some years ago as a combination of DNA sequences, ATP-dependent chromatin remodeling enzymes, transcription factors (TFs), and elongating RNA polymerase II (RNAPII) [28]. A comparative analysis between *Drosophila* cell lines identified genomic regions that exhibited cell line-specific nucleosome enrichment or depletion. The same study revealed that nucleosomes were positioned in accordance with previously known DNA–nucleosome interactions, with helically repeating A/T dinucleotide pairs arranged within nucleosomal DNA and AT-rich pentamers generally excluded from nucleosomal DNA [29].

Nucleosomes are highly dynamic structures and the partial unwrapping of DNA from the octamer leads to exposure of the different regions for protein recognition [30,31]. Nucleosome dynamics are controlled by a complex cooperation between different histones, histone post-translational modifications, nucleosome occupancy and positioning [32,33]. In recent years, the development of genome-wide mapping approaches has provided a vast amount of information regarding the genomic location of chromatin-associated

proteins, such as histones, as well as of several of their modifications. A large number of these modifications have been implicated in the regulation of gene expression, as we will discuss below.

3.2. Core Histones and Their Variants

Drosophila contains five canonical histones (H1, H2A, H2B, H3, and H4), usually referred to as replication-coupled histones since they are mostly incorporated during DNA replication. The canonical histone genes are clustered into a highly repeated unit that contains one copy of each gene, although H4 is also encoded by another gene outside the cluster (*H4r*) [34].

In addition to the canonical histones, the fly genome encodes four histone variants (BigH1, H2Av, H3.3, and cenH3), with H2B and H4 being the only histones lacking variants. Histone variants confer different structural properties and carry out specialized functions in numerous processes [35]. The unique *Drosophila* H2A variant, H2Av, combines the features of the H2A.X and H2A.Z eukaryotic variants and has been linked to transcription, DNA repair, and heterochromatin [36]. H2Av may also have a role in chromosome organization, since the depletion of the machinery responsible for its incorporation results in the alteration of chromosome structure in salivary glands and S2 cells [37,38]. H2Av is broadly distributed in the *Drosophila* genome and nucleosomes with H2Av are particularly enriched downstream of the transcription start site (TSS) of active genes, which correlates positively with transcription levels [25,39]. It has been proposed that H2Av may facilitate the progression of RNAPII, since a reduction of H2Av levels results in an increase in RNAPII stalling [40]. In addition, H2Av has been implicated in gene silencing through the Polycomb group (PcG) of proteins. H2Av seems to participate in Polycomb (Pc) recruitment since Pc sites are lost in polytene chromosomes from H2Av mutants [41]. Moreover, H2Av is also found in heterochromatin [25,42] and HP1a binding may depend on the presence of H2Av [41].

The H3 replacement variant H3.3 is encoded by two genes, H3.3A and H3.3B, which are ubiquitously expressed throughout all the tissues and developmental stages [43]. H3.3 is usually enriched in active chromatin, such as active promoters and gene bodies of transcribed genes [44,45], and in sites with high nucleosome turnover rates [46]. However, clonally removing H3.3 in cells from the *Drosophila* wing disc does not affect gene expression [47]. Furthermore, H3.3 null mutant flies are viable and show no phenotypic alterations, except for infertility [47]. Interestingly, regions of H3.3 enrichment are generally depleted of H1 and knocking down H3.3 leads to increased H1 association at these sites [48].

3.3. Linker Histones

Drosophila contains only one somatic H1 [49] and one embryonic and germline-specific variant, BigH1 [50]. H1 is broadly distributed throughout the genome [48,51]. Its loss results in the misexpression of only a small subset of genes [52,53], mainly those located in heterochromatin [54,55]. The changes in gene expression include the upregulation of TEs [52,53,56]. In mammals, linker histones are also widely distributed [57–60] and, similar to flies, only a small number of genes are affected in triple knock-out mouse embryonic stem cells (ESCs) with 50% total H1 depletion [61] or in human cells with reduced H1 levels [59,62,63]. Moreover, these changes in gene expression mainly affect heterochromatic regions [57,59,62,64].

BigH1 is expressed in both male and female germlines with similar expression patterns [50,65,66]. While the function in the female germline is not known, in males, BigH1 is important for germ stem cell maintenance and spermatocyte differentiation [65]. BigH1 is retained in precellular embryos, where it is important in maintaining the silencing of the zygotic genome [50]. Recent studies have focused on the different properties of the two linker histones and have found that BigH1 has a greater repression ability than

the somatic H1 due to its higher content in acidic residues [66]. Moreover, nucleosomes containing BigH1 are more stable, but show higher mobility than H1-nucleosomes [67].

4. Covalent Modifications of Chromatin

Covalent modifications play an essential role in the nucleosome–nucleosome interactions that dictate chromatin folding and dynamics. These modifications, occurring both in DNA and histones, have the potential to form a complex combinatorial regulatory system and are fundamental in regulating all processes that use DNA as a template, such as transcription, DNA repair, and replication.

4.1. DNA Methylation

Methylation of the carbon C5 of cytosine to form 5-methylcytosine (5mC) is probably the best-known modification of DNA in eukaryotes. Despite the general role 5mC plays in the repression of vertebrate gene expression, the situation may be different for invertebrates. There is evidence in favor of cytosine C5 methylation in *Drosophila*, although its source is still elusive [68]. Although 5mC is rare, methylation on N6 adenine (6mA) seems prevalent in *Caenorhabditis elegans* and *Drosophila* [69,70]. Recent studies have confirmed that NMAD-1 (MT-A70 family) and DMAD (DNA 6mA demethylase, TET ortholog) are 6mA demethylases in *C. elegans* and *Drosophila* respectively [71]. The *Drosophila* DMAD regulates 6mA levels during embryo development and oogenesis. DNA immunoprecipitation studies in ovaries from DMAD mutants show that 6mA is enriched in transposon regions and seems to promote their expression [70]. More recently, He and coworkers (2019) have shown that, in *Drosophila* embryos, 6 mA is found not only in transposon regions but also in zygotic genes. This modification can be read by the TF Jumu, which controls the activation of the zygotic genome (ZGA) through the regulation of *zelda*, among other genes [72].

4.2. Histone Modifications

Several residues in histones are susceptible to modification. The most well studied modifications are the ones occurring at the N-terminal tails of the core histones, although modifications of the globular domains have been gaining more attention [73,74]. The N-terminal tails of the core histones protrude outside the nucleosome and contact with adjacent nucleosomes. Thus, modifications in this region can directly affect nucleosome–nucleosome interactions and alter the chromatin structure. This is the case for H4K16 and H4K20. While acetylation of H4K16 reduces the level of compaction in vitro [75,76], the di- and tri-methylation of H4K20 has the opposite effect and enhances chromatin condensation in vitro [77]. However, modifications at the N-terminal tails also mediate the recruitment of effector proteins [78]. Recognition of these modifications is achieved through specialized domains present in "reader" proteins, which can be remodeling complexes, other modifying enzymes or scaffolds of the transcription machinery [78]. Some of the effector proteins and the enzymes that catalyze or remove these modifications are part of the PcG or Trithorax group (TrxG), which are chromatin-modifying complexes implicated in the maintenance of repressed or active gene expression states [79].

There are some modifications that correlate with gene activity [80]. The clearest example is the acetylation of histones H3 and H4, which is associated with active transcription. Acetylation of lysine (K) partially neutralizes the positive charge of histones, thus weakening the interaction between histones and DNA [81]. Methylation is, by far, more complex, and its correlation with gene expression depends not only on which amino acid is modified, but also on the degree of methylation (mono, di or tri). The hypothesis of the "histone code" proposes that the combination of different modifications is important in regulating gene expression and other DNA processes [82]. Recent studies, however, challenge the instructive role of histone modifications and suggest that those modifications traditionally associated with active genes do not directly trigger transcriptional activation [83]. Indeed, typical histone modifications only have a few roles in regulating transcription [84]. A study using different developmental time points showed that the transcription of genes

temporally regulated during fly and worm development occurred in the absence of canonically active histone modifications [85]. Similarly, another study using genetic approaches and mutant derivatives found that transcriptional regulation can occur in the complete absence of H3K4 methylation [86]. Likewise, the depletion of H3K27ac in mouse ESCs does not alter chromatin accessibility or transcription, indicating that this modification is dispensable for enhancer activity in mouse ESCs [87]. These modifications might instead be necessary for sustained transcription, since there is a correlation between the amount of these modifications and the stability of expression [85].

Another example of transcription without the typical active histone modifications is the first wave of transcription of the ZGA, which is characterized by the enrichment of H4K8ac, H3K18ac, and H3K27ac in active genes [88]. Other modifications commonly associated with active genes, such as H3K4me3, H3K9ac, H3K36me3, and H3K4me1, do not become enriched until mitotic cycle 14 [88,89], indicating again that these modifications are not required for transcriptional competence, at least during the first wave of transcription. Recently, H3K14ac was shown to be important for the transcription of active genes that lack H3K9ac, H3K27ac, and H3K4me3 during *Drosophila* embryo development and in imaginal wing discs [90]. Moreover, modifications in the globular domain may have a role in regulating gene expression and other processes, since mutations of the H3 residues K56, K115, K122, T80, and T118 induce lethality at different developmental stages in *Drosophila* [91].

5. Functional Organization of the Genome

5.1. Segmentation of the Genome into Chromatin States

As mentioned above, several groups have attempted to classify chromatin into different types. Filion et al. (2010) proposed the segmentation of the genome of *Drosophila* cells into five types of chromatin based on genome-wide binding maps of selected chromatin components, with histone modification profiles used for independent validation (Figure 1A). These chromatin states, labeled as GREEN, BLUE, BLACK, RED, and YELLOW, are distributed throughout the genome in discrete domains with a length usually ranging from ~1 to 52 kb. The GREEN and BLUE chromatin types correspond to classic heterochromatic regions and are characterized by the binding of HP1 and HP1-interacting proteins or of PcG proteins, respectively. While GREEN chromatin is marked with H3K9me2 and usually corresponds to pericentromeric regions, BLUE chromatin is highly enriched in H3K27me3 and developmentally regulated genes. The last type of silent chromatin is BLACK chromatin, which covers about half of the genome and tends to have longer domains. BLACK chromatin is thus the predominant type and is characterized by being poor in genes and producing very low levels of mRNA. Interestingly, the genes within this type of chromatin can become active in specific cell types or tissues, suggesting that BLACK domains can be remodeled into a different chromatin type during development. Moreover, some of the proteins that mark this type of chromatin are histone H1, auroraB (AurB), Suppressor of Underreplication (SUUR), the AT-hook protein D1, and lamin (LAM), indicating a role of the nuclear lamina in the regulation of BLACK chromatin. The two remaining types of chromatin, RED and YELLOW, correspond to active regions and are characterized by the extensive binding of histone deacetylases (HDACs) and ASH2, as well as enrichment in H3K4me2, H3K79me3, and RNAPII. RED chromatin is also bound by several other proteins, including TFs such as the GAGA factor (GAF) and Jun-related antigen (JRA). Instead, YELLOW chromatin is uniquely marked by H3K36me3 and its reader protein MRG15. The genes located in RED and YELLOW chromatin are also different: the genes in RED chromatin have specific expression patterns and functions, such as signaling and TF activity, whereas those in YELLOW chromatin are ubiquitously expressed and have more general functions, such as DNA repair and metabolism [13].

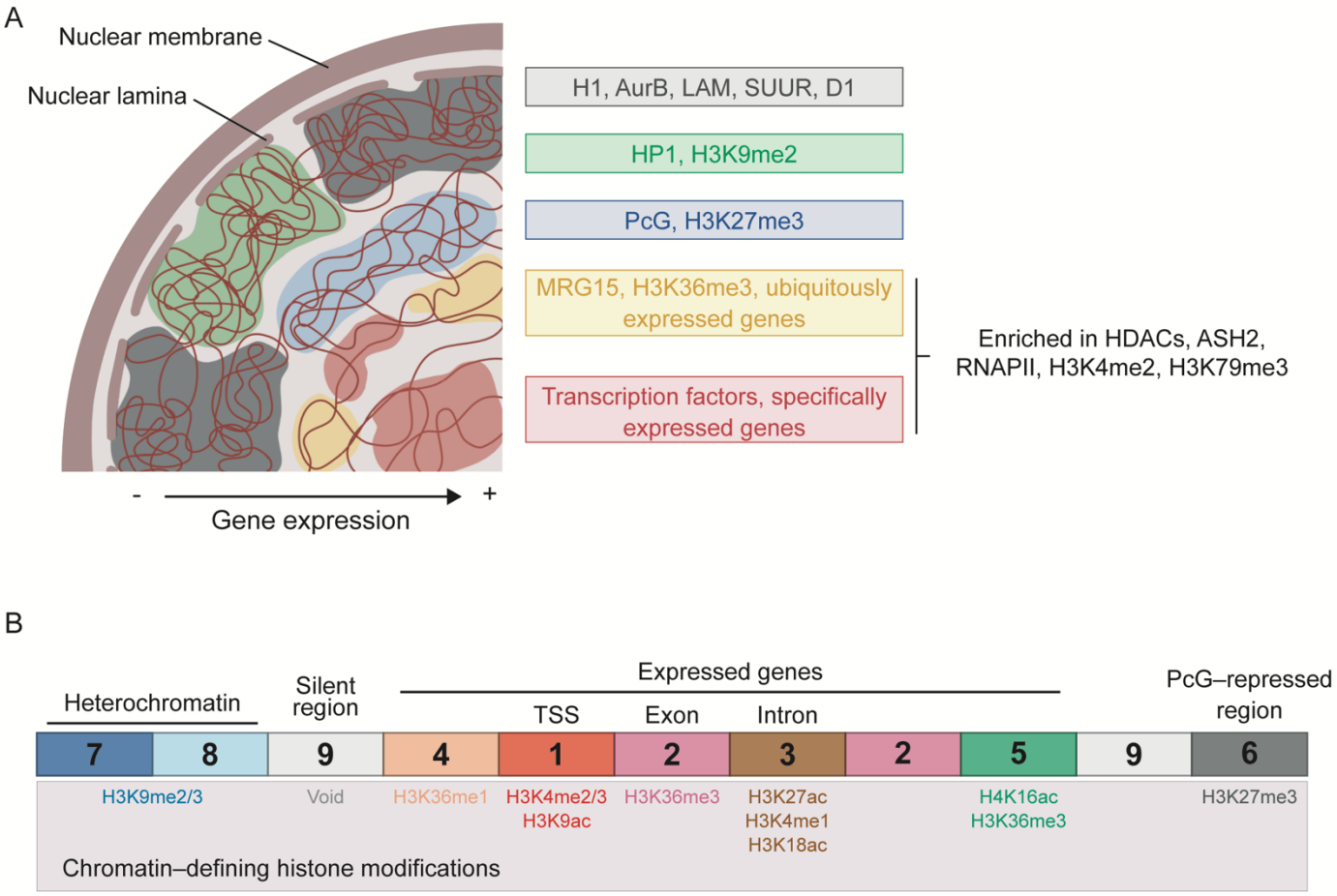

Figure 1. Classification of the chromatin landscape in *Drosophila*. (**A**) Chromatin segmentation into 5 types according to combinatorial protein binding. BLACK, GREEN, and BLUE chromatin types correspond to repressed and silenced domains, whereas YELLOW and RED chromatin types represent active regions. The more repressed regions tend to localize at the periphery of the nucleus, with BLACK and GREEN chromatin interacting with the nuclear lamina. Only the most characteristic components of each chromatin type are indicated. Based on Filion et al. [13]. (**B**) Division of chromatin into 9 states attending to histone modification patterns. States 1, 2, and 5 are associated with actively transcribed genes; states 3 and 4 with putative regulatory regions; state 6 with PcG-repressed regions; states 7 and 8 with heterochromatin; and state 9 corresponds to silent regions. The most enriched histone modifications are indicated for each chromatin state. Based on Karchkenko et al. [92].

Following a similar approach, Kharchenko et al. (2011) used histone modifications to determine nine distinct chromatin states in the *Drosophila* genome (Figure 1B). To functionally characterize these states, the authors integrate data from non-histone proteins, chromosome accessibility, transcription analyses, and short RNA production. In the 9-state model, transcriptionally active regions fall into more than two chromatin states, some of which can be observed at different regions of a particular gene. State 1 (red) is characterized by the enrichment of H3K4me3/me2 and H3K9ac, and is found at active promoters and TSSs. State 2 (purple) contains high levels of H3K36me3, an elongation mark enriched towards the 3′ end of the genes. State 3 (brown) is usually found within intronic regions and is enriched in H3K27ac, H3K4me1 and H3K18ac. Open chromatin regions are mainly associated with states 1 and 3, which are bound by different components of chromatin remodeling factors, such as NURF301 and MRG15 in the case of state 1, or SPT16 and dMI-2 in state 3. The authors propose a regulatory role for the state 3 domains, since they are also enriched in dCBP/p300 and almost half of them are bound by GAF and developmental TFs. State 4 (coral) resembles state 3, but lacks H3K27ac and is also marked by the presence of H3K36me1. Chromosome X is particularly enriched in state 5 (green), which is defined

by high levels of H4K16ac and the modifications also present in state 2, probably reflecting a distinct mechanism of transcriptional regulation required for dosage compensation in male cells. State 6 (dark grey) is enriched in H3K27me3 and corresponds to PcG-repressed regions. Heterochromatic regions are depicted by state 7 (dark blue) and 8 (light blue), which are characterized by an enrichment in H3K9me2/m3, although levels are higher in state 7. Finally, the authors consider a last chromatin state characterized by the presence of low levels of the histone modifications considered in the study, the state 9 (light grey) [92].

These different types of chromatin have been related to physical domains of chromosome folding. For example, PcG-bound chromatin (BLUE chromatin or state 6) has been shown to form small subnuclear structures called PcG bodies or PcG-repressed domains [93,94]. As we discuss below, there is a strong link between chromatin activity and chromosome architecture.

5.2. 3D Organization of the Genome

Technical advances such as the high-throughput derivative of chromosome conformation capture (Hi-C) have enabled the analysis of the three-dimensional architecture of genomes (Figure 2A) [95–97]. Chromatin interaction maps generated by Hi-C assays in *Drosophila*, mice, and humans have revealed that the genome is composed of several layers of structure that are organized in a hierarchical manner [98–101]. At the higher level of genome topology, chromatin is partitioned into two multimegabase compartments with distinct transcriptional activity: an active compartment (A) that is dense in expressed genes and correlates with histone modifications generally associated with active transcription, and an inactive compartment (B) that is gene-poor and heterochromatic [97,100]. The genome is further organized into sub-megabase domains called topologically associating domains (TADs), which are defined by a higher interaction frequency within the region than with those located outside of the TAD [98,102,103]. In mammals, TADs are likely to be formed from the active extrusion of chromatin loops mediated by the cohesin complex [104,105], and are insulated at the borders by the architectural chromatin protein CCCTC-binding factor (CTCF) [103,106]. Depletion of cohesin in mammalian cells results in the loss of the majority of TADs [107], while deleting CTCF sites or inverting their orientation reduces TAD insulation and facilitates crosstalk between adjacent TADs [108–110].

In *Drosophila,* high-resolution Hi-C data from Rowley et al. (2017) suggested that TADs and compartments occur at a much lower scale than previously proposed. According to that study, the main topological features are compartmental domains, which represent small discrete regions of ~10 kb that preferentially interact within themselves and correlate with transcriptional activity states [111], thus indicating that *Drosophila* TADs actually correspond to smaller A/B compartments. This is consistent with the segmentation of the fly genome into the domains of the particular chromatin types mentioned above [13]. Thus, A compartmental domains would correspond to RED and YELLOW chromatin, while B compartmental domains would include BLUE, GREEN and BLACK chromatin types. These compartmental domains can be accurately modeled using only transcriptional data, while both CTCF and transcription-based simulations are required to generate an accurate human Hi-C map [111]. Significantly, the experimental inhibition of transcription in *Drosophila* cells by triptolide or heat shock results in a decrease in domain architecture that is more pronounced when RNAPII binding is also depleted [111]. In another study from Hug et al. (2017), Hi-C maps generated during fly embryogenesis showed that most TADs are formed concomitantly with the start of transcription. Inhibiting transcription before ZGA results in reduced contact density within domains and a significant loss of interdomain insulation, although TADs are not entirely eliminated [112].

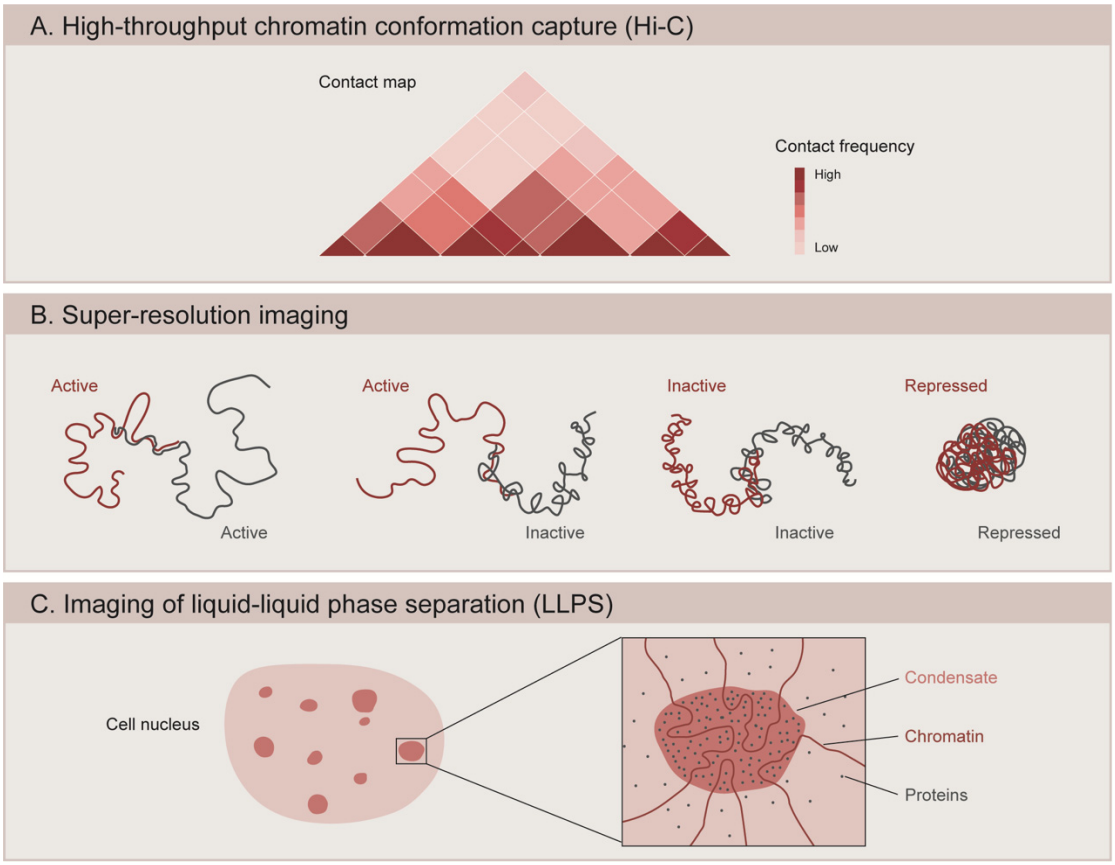

Figure 2. Methods to study the 3D organization of the genome. (**A**) High-throughput chromatin conformation capture (Hi-C) generates contact maps that represent the interaction frequency between genomic loci. Studies using Hi-C have revealed that chromatin is organized into topologically associating domains (TADs). (**B**) Super-resolution microscopy is used to image the spatial organization of different chromatin domains: transcriptionally active (Active), inactive (Inactive), and Polycomb-repressed (Repressed). While active and inactive regions can partially intermix with one another, repressed domains show a more compact configuration and do not overlap with other neighboring domains. (**C**) Microscopy-based methods are used to assess the ability of chromatin components to form condensates through liquid–liquid phase separation (LLPS). Condensate formation is mediated by the biochemical properties of the macromolecules and their interactions.

Unlike in mammals, the majority of *Drosophila* domain borders coincide with active promoters or active gene minidomains rather than with CTCF sites [111,113]. Accordingly, domain boundaries are mostly unaffected by the loss of CTCF, as has been observed in *Drosophila* neurons [114]. CTCF mutant flies can progress through embryogenesis and larval stages, although they display strong homeotic defects [115]. Instead, many other insulator proteins have been described in *Drosophila*; however, their role in shaping chromatin domains is still unclear [116]. In recent studies using Hi-C data from *Drosophila* cell lines, significantly enriched DNA motifs have been identified at domain boundaries, including the motifs for the Suppressor of Hairy wing [Su(Hw)], the Boundary Element Associated Factor (BEAF-32), and the Motif-1 binding protein (M1BP) [113,117]. Interestingly, loss of BEAF-32 has no major effect on chromosome structure, while depletion of M1BP results in cell arrest and dramatic genome reorganization [113]. Another study revealed an essential role for the pioneer TF Zelda in establishing insulation at domain borders, at least partially, during embryogenesis [112]. That study showed that Zelda-depleted embryos display major chromatin conformation defects, although they are mostly locus-specific, i.e., at former Zelda-bound domain boundaries [112]. Furthermore, Zelda mutant embryos show loss of long-range gene interactions [118], suggesting a role of this pioneer factor in chromatin looping during *Drosophila* embryogenesis. Significantly, Zelda-dependent sites that fail to interact in mutant embryos are associated with the specific depletion of

RNAPII binding [118]. Overall, these results suggest that compartmentalization in the fly genome is mostly driven by transcriptional activity and/or RNAPII presence, while CTCF looping is also required for domain formation in mammals. A recent study has proposed that mammalian TADs are subdivided into chromatin nanodomains of similar size to *Drosophila* TADs. These nanodomains, like *Drosophila* TADs, are mostly unaffected by CTCF or cohesin depletion [119].

The recent application of super-resolution microscopy coupled to DNA labeling has revealed that *Drosophila* TADs correlate well with epigenetic states, usually classified into transcriptionally active (associated with H3K4me3, H3K36me3 and acetylated histones), PcG-repressed (enriched in PcG proteins and H3K27me3), and inactive (devoid of specific marks) (Figure 2B). Using a combination of fluorescent in situ hybridization (FISH) and 3D-structured illumination microscopy (3D-SIM), Szabo and colleagues (2018) showed that the chromatin fiber is segmented into globular domains defined as nanocompartments [120]. These structures correspond to PcG or inactive TADs, and are interspersed by regions of less condensed active chromatin [120]. Similarly, 3D stochastic optical reconstruction microscopy (3D-STORM) of labeled chromatin revealed distinct spatial organization for each chromatin state, where PcG-repressed chromatin forms small compact domains that are distinct from the transcriptionally inactive regions [94]. Interestingly, active and inactive domains show less condensation and partial intermixing with each other, while PcG-repressed domains exhibit more compact packaging and a stronger tendency to spatially exclude neighboring active chromatin [94]. These PcG domains depend on Polycomb repressive complex 1 (PRC1), since knockdown of the Polyhomeotic (Ph) component of PRC1 leads to domain loss and an increased expression of PcG-target genes [94]. Similarly, genome editing of Polycomb responsive elements (PRE) caused the aberrant formation of TADs and a decreased silencing during *Drosophila* embryogenesis [118]. In mammals, PcG-bound chromatin also forms small dense domains in which developmentally regulated genes targeted by PRC1 are corepressed [121]. These domains are functionally lost upon the activation of PRC1-target genes or upon the PRC1 unbinding of target genes during cell fate specification [121]. The function of Ph in domain formation is also conserved for the mammalian ortholog Phc1, since knocking out Phc1 in mouse ESCs leads to domain loss and subsequent gene de-repression [121]. A recent study used Optical Reconstruction of Chromatin Architecture (ORCA), a method that combines high resolution microscopy with Oligopaint and RNA-FISH, to observe the 3D chromatin organization of the bithorax-complex (BX-C) inside the nuclei of individual cells from *Drosophila* embryos. The study revealed segment-specific organization of the BX-C and identified TADs exclusive to each body segment [122]. The boundaries of these segment-specific TADs often coincide with changes in chromatin states, such as at the edge of a H3K27me3 domain or at the border between transcriptionally active and inactive regions. However, the same study found adjacent TADs with the same epigenetic states that were independent of H3K27me3. The borders of these TADs might be determined by cohesins and CTCF, since the deletion of border regions marked by these proteins results in TADs fusion. Nevertheless, these deletions also include active genes, which could influence the structure of TADs [122]. Finally, another study showed that the boundaries of most Polycomb domains in *Drosophila* consist of active regions and that actively transcribed genes can stop the spreading of H3K27me3, since ectopic addition of a transcriptional terminator caused the extension of the PcG domain [123].

The results discussed above indicate that the fly genome is divided into functional domains in which regulatory contacts are spatially restricted. However, this model requires TADs to be physical units when they could instead represent statistical frequencies of chromatin interactions within cell populations [124]. Single-cell Hi-C (scHi-C) has been recently introduced to overcome the limitations of bulk Hi-C, but have shown contrasting results in this respect. The contact maps generated for single *Drosophila* nuclei bore striking resemblance to the TAD profile in bulk Hi-C, with over 40% of TAD boundaries conserved between individual cells [125]. However, the long-range interactions within and

between TADs were very heterogeneous, suggesting substantial stochasticity in the folding of chromatin into domains [125]. Another study using human cell lines showed high cell-to-cell variations in contact patterns, where single-cell contact clusters did not match population TADs [126]. These scHi-C maps averaged into TADs when they were pooled together, suggesting that TADs merely reflect the tendencies of measured interactions within a population of cells [126]. Using 3D-SIM and DNA-labeling in *Drosophila*, contact probabilities within TADs were shown to be higher for all cells compared to contacts between neighboring TADs [127]. This preferent confinement of interactions within domains indicates the presence of TADs in individual cells. Furthermore, Cattoni and colleagues (2017) showed that active and repressive chromatin form discrete nanocompartments at the single-cell level, whereas stable looping between TAD borders is infrequent. This suggests that TAD assembly in flies is not the result of long-term stable interactions, but rather can be explained by the stochastic contacts between regions of similar chromatin types [127]. In agreement with this, Szabo and colleagues (2018) observed that TADs are generally consistent between cells, despite variable intra- and interdomain contacts, further suggesting that TADs are true physical entities of the fly genome [120]. Likewise, super-resolution microscopy of mouse ESCs showed significant variability at the TAD scale between individual cells, although chromatin contacts were more frequent within TADs than between adjacent TADs [119]. Further evidence in favor of TADs is the observation that bands from *Drosophila* polytene chromosomes strongly correlate with TADs, whereas the decondensed polytene regions, named interbands, mostly correspond to inter-TADs or TAD borders [128,129]. This finding reveals a direct relationship between sequencing-inferred chromatin structure and chromosome condensation observed by light microscopy [128,129], suggesting that TADs are a stable and conserved unit of chromosome folding.

5.3. Regulation of Gene Expression by Chromatin Organization

While there is an increasing amount of evidence showing that transcriptional activity plays a prominent role in chromatin organization [111,130–132], it is still rather controversial how—and if—genome topology modulates gene expression [133]. In a recent study, the simultaneous analysis of enhancer–promoter interactions and transcription in *Drosophila* embryos showed that the sustained proximity of the enhancer to its target gene was required for activation [131]. Moreover, the *Drosophila* Hox gene clusters Antennapedia and Bithorax, which are separated by 10 Mb in the linear genome, are thought to be corepressed by a PcG-mediated physical interaction, with mutations in one complex resulting in the de-repression of the genes in the other complex [93]. Interestingly, the absence of either one of the two PRC1 subunits Ph or Pc affects chromatin organization prior to ectopic Hox gene transcription, suggesting that PRC1 maintains gene silencing by compacting chromatin into domains [134]. In agreement with these results, disruption of the TAD structure has been found to cause misexpression in some cases. For instance, the deletion or inversion of the TAD boundary at the *Epha4* locus causes ectopic interactions between promoters and enhancers, leading to aberrant gene expression and a pathogenic phenotype in mammalian limbs [135]. Furthermore, deletion of domain boundaries in the *Notch* locus of *Drosophila* results in TAD fusion and transcriptional changes, together with a decreased binding of RNAPII [136].

However, there is also significant evidence questioning the role of the chromatin structure modulating gene expression [133,137]. In *Drosophila*, the analysis of gene expression in balancers (highly rearranged chromosomes) showed that disruption of TADs has little effect on gene activity and only a subset of genes is sensitive to structural alterations [138]. Similarly, a recent study using *Drosophila* dorsoventral patterning as a model system indicated that genome topology and transcription are independent [139]. Following fly embryonic development, the study demonstrated that chromatin conformation is generally maintained across cell types, even if transcriptional profiles change dramatically [139]. Likewise, single-cell spatial genomics in *Drosophila* embryos revealed that developmentally relevant enhancer–promoter interactions appear before TAD formation and remain invariant during

cell fate specification [140]. Finally, sonic hedgehog (*Shh*) gene expression during mouse limb development was shown to be robust to perturbations in the TAD structure and was only altered when the Shh limb enhancers were deleted [141]. Altogether, these results suggest that chromatin organization can play a role in regulating gene expression, but it is most likely to be one of many modulators and not the main regulatory factor.

5.4. Nuclear Lamina and Pericentromeric Heterochromatin

The functional organization of the genome is also influenced by the existing contacts between the chromatin and the nuclear lamina (NL) (Figure 1A) [142]. The NL is a dense meshwork composed of A- and B-type lamins and lamin-associated proteins that, together with the outer and inner membranes and the nuclear pore complexes, form the nuclear envelope. The NL functions as a support for multiple chromatin anchoring sites and it is suggested that NL proteins tether heterochromatin to the nuclear periphery. In fact, *Drosophila* genes that interact with B-type lamin are transcriptionally silent and late replicating [143]. During the differentiation of mouse ESCs, genes that move away from the lamina are activated, whereas the others remain inactive and become activated in the next differentiation step [144].

Lamin B receptor, located at the inner nuclear membrane, provides a tethering mechanism for heterochromatin by binding to HP1a, which is preferentially located in the H3K9me3-rich heterochromatic region [145–147]. Hi-C data have also confirmed that the inactive chromatin compartment is strongly enriched in NL contacts [148,149]. In addition, transcriptional repressors, such as HDACs, are known to bind to lamina proteins [150–152], raising the question of whether the contacts with the NL make the chromatin in lamina-associated domains (LADs) compact and inactive. Evidence indicates that the NL contacts can play a role in gene repression. In vitro experiments on *Drosophila* cell lines have demonstrated that knocking down lamin proteins decreases the compactness of inactive chromatin domains, increases the accessibility of the promoters located in heterochromatic regions, enhances the levels of histone H3 acetylation, and increases gene expression [144,153–155]. Similarly, in mouse ESCs, the expression of reporter genes inserted into LADs is remarkably lower when compared to inter-LADs, which is only partially explained by chromatin compaction, therefore pointing towards a repressive environment near the NL where transcription is less permissive [156]. Additionally, several studies on cell differentiation have revealed that the activation of tissue-specific gene expression is associated with translocations of loci from the NL to the nuclear interior [144,149,157,158]. For instance, the ectopic release of cardiac genes from the nuclear periphery in mouse ESCs leads to a premature myogenesis, providing a clear example of the relevance of gene positioning in the nuclear periphery during organogenesis [159]. Together, these findings indicate that the NL is essential for the positioning of the heterochromatin in the nuclear periphery, establishing a transcriptionally repressed domain near the nuclear envelope and a transcriptionally active domain in the nuclear interior [160].

Apart from the heterochromatin contacts with the NL, interactions between different heterochromatic regions, most likely mediated by the affinity between repetitive elements [161,162] or heterochromatin-associated proteins [163,164], could be essential for heterochromatin compartmentalization within the nucleus [165]. Contacts between pericentromeric heterochromatin (PCH) regions, which are located near the centromere and are enriched in HP1a and repetitive elements [166,167], have been proposed to contribute to the global genome architecture in the nucleus [168]. In *Drosophila*, the PCH regions from the four chromosomes cluster in the 3D nucleus, forming membraneless structures called chromocenters that were first described in the 1970s [169–171]. Although recent studies have found HP1a to be crucial for PCH clustering in *Drosophila* embryos [172], the mechanism driving this clustering in differentiated cells in mice does not depend on HP1a, indicating an alternative mechanism for PCH coalescence [173]. However, PCH contacts are not only restricted to other PCH regions. It was recently found that PCH can interact with euchromatic regions enriched in H3K9me2/3. Genes located in PCH-contacting

euchromatin show higher expression than those located in euchromatin not contacting PCH [168]. Since HP1a is the reader of H3K9me2/3, the most probable scenario is that PCH-euchromatic interactions are driven by HP1a.

5.5. Nuclear Pore Complexes

Besides the nuclear lamina, chromatin can also interact with the nuclear pore complexes (NPCs) located in the nuclear envelope and whose canonical function is to mediate nucleocytoplasmic transport. NPCs are composed of multiple nucleoporins (Nups), for which ~30 different subtypes have been described [174]. Depending on the Nup subtype, the association to the NPC can be stable or dynamic, as certain Nups can be found freely within the nucleoplasm. In *Drosophila*, as well as in mammals, chromatin binding maps show differential binding preferences for different Nup subtypes. For instance, Nup153 and Megator (Mtor) are known to bind to the fly genome in continuous domains enriched in marks of active transcription [175]. In fact, the depletion of Nup153 results in the altered expression of thousands of genes, suggesting a role in transcriptional regulation [175]. However, not all Nup subtypes bind preferentially to active regions. An interesting example is the antagonistic binding preferences of core nuclear pore proteins Nup93 and Nup107 in *Drosophila* cells; while Nup107 is mainly found at active genes, Nup93 is located preferentially at repressed chromatin regions, bound by PcG proteins [176]. Indeed, the depletion of Nup93 leads to de-clustering of distant Polycomb regions that previously coalesced, and to de-repression of PcG target genes [176]. These findings point towards Nup93 as a key mediator of long-range Polycomb interactions, as well as a necessary factor for proper silencing of PcG-associated target genes.

Dynamic Nups can also interact with the genome within the nucleoplasm, outside the NPC. This is the case of Nup98, which binds genes both at the NPC and within the nucleoplasm [177,178]. The association involving nucleoplasmic Nup98 correlates with a higher degree of target gene activation compared to NPC-bound Nup98. The expression of these target genes depends on the levels of Nup98, as their expression increases upon the ectopic overexpression of Nup98, and decreases upon Nup98 depletion [178]. In line with these findings, the interacting partners of Nup98 include several proteins implicated in gene activation, including Thritorax (Trx), suggesting a role of Nup98 in maintaining active gene expression [179].

NPCs also seem to play a role in genome architecture. Multiple studies have demonstrated that NPC components contribute to the formation of long-range genomic contacts [180–182]. In *Drosophila*, as well as in mammals, several Nups are found targeting a subset of promoters and enhancers. These contacts are preferentially located in NPC-bound Nups rather than nucleoplasmic Nups, and occur regardless of the transcriptional state of the genes, suggesting that NPCs can target silent or poised genes and enhancers [180,181]. Particularly, Nup98 was found to bind promoters and enhancers of ecdysone-inducible genes and, upon its depletion, the enhancer–promoter loops induced by ecdysone were destabilized [180]. Moreover, NPC-bound Nup98 was also observed to bind at a subset of TAD boundary regions, and was identified as a physical interactor to insulator proteins such as CTCF [113]. Altogether, these findings suggest that NPCs not only bind to specific regions in the genome, but may also participate in the formation or maintenance of promoter-enhancer loops as well as in the formation of TAD borders.

6. Liquid–Liquid Phase Separation

Functional compartmentalization of the cell nucleus plays an important role in the regulation of genome activity. Recent evidence suggests that liquid–liquid phase separation (LLPS) underlies the formation of membraneless compartments in the nucleus [183]. These membraneless compartments are formed as a result of distinct biochemical properties that segregate macromolecules into a concentrated liquid phase and a dilute phase, referred to as condensates [184]. This non-covalent form of fluid compartmentalization is triggered by weak multivalent interactions between proteins, RNA, and DNA. Specifically, proteins are

thought to mediate phase separation through interactions between domains that are called low-complexity domains (LDRs) or intrinsically disordered domains (IDRs) [184,185]. Recent studies suggest that chromatin compartments might be formed and organized through LLPS (Figure 2C). In *Drosophila*, HP1a undergoes liquid phase separation in vitro and can form condensates suggested to facilitate heterochromatin formation in early embryos [164]. Indeed, partial knock-down of HP1a causes major alterations in chromatin organization in *Drosophila* embryos, such as a reduced contact frequency within heterochromatic regions and increased crosstalk between active and inactive domains [172]. HP1a depletion in differentiated cells does not affect genome structure, suggesting that HP1a is required for establishing 3D structure in early embryos, but not for the maintenance of compartmentalization during cell differentiation [172]. The human counterpart, HP1α, is also capable of compacting heterochromatin through phase separation in an in vitro model system [163]. However, a recent study using mouse fibroblasts showed that HP1α has a weak capacity to form liquid droplets in living cells and that the compaction and maintenance of heterochromatin foci occur independently of HP1α [173].

Other proteins have been suggested to facilitate chromatin condensation through LLPS, including histones and transcriptional regulators. The linker histone H1 was recently shown to promote the phase separation of reconstituted chromatin into denser and less dynamic droplets [186]. On the other hand, acetylation of histone tails gradually reduces chromatin droplet density until its dissolution. This acetylated chromatin, which is unable to undergo phase separation by itself, undergoes LLPS after the addition of multi-bromodomain proteins in vitro [186]. Similarly, the Chromobox 2 (CBX2) component of PRC1 was recently proposed to mediate the phase separation of PcG-repressed chromatin in mice. In an in vitro model, reconstituted PRC1 can undergo phase separation into droplets, but fails to do so when CBX2 is mutated in its LDR [187]. The same mutations in CBX2 had been previously shown to decrease chromatin compaction and transcriptional repression in mouse cells [188]. Finally, superenhancers, which are clusters of enhancers that are able to recruit high levels of transcriptional regulators and can strongly activate gene expression [189,190], are also thought to assemble through LLPS [191]. Indeed, recent studies suggest that TFs and coactivators can form phase-separated condensates, in which the transcription machinery is highly concentrated and facilitates the expression of genes in both flies and mammals [191–193]. Interestingly, the carboxy-terminal domain of RNAPII, an LDR, can undergo phase separation in vitro even in the absence of other proteins [194]. Moreover, the activation domains of several TFs can form liquid droplets in vitro with the coactivator mediator subunit MED1, which results in gene activation [195]. Altogether, the evidence suggests that chromatin has an intrinsic capacity to undergo phase separation into functionally distinct, but physically adjacent domains. However, the precise contribution of LLPS to the formation of chromatin domains and genome function is still unclear.

7. Conclusions and Future Perspectives

In this review, we aimed to highlight what is known about the genome of *Drosophila melanogaster* regarding chromatin composition and 3D organization, mostly related to the regulation of gene expression. As we have discussed, the role that chromatin modifications play in transcription is still unclear, and new studies are now focusing on the effects of local chromatin environment and genome folding. In spite of several open questions, the 3D organization of the genome in nuclear compartments is increasingly recognized as a major feature of gene regulation. How these nuclear compartments are formed and what is their importance regarding gene function remains to be elucidated.

Over the last decade, numerous studies have used chromosome conformation capture techniques to analyze the 3D architecture of genomes [95]. In *Drosophila*, these studies have revealed that the genome is organized into physical domains of particular chromatin states named TADs. However, Hi-C experiments reflect averaged information coming from cell populations, and thus cannot account for individual heterogeneity between cells, cell-types or tissues. To overcome this limitation, new methodologies have been developed,

including scHi-C [126] and microscopy-based techniques, which couple super-resolution imaging with DNA labeling [120,122,196,197]. These emerging microscopy methods not only enable the visualization of the 3D genome organization at the single-cell level, but also maintain the spatial information within tissues or organisms. Furthermore, they allow the incorporation of RNA probes to distinguish cell types and to link chromatin structure to gene expression [122,196,197]. Other technical approaches to study the relationship between genome organization and gene expression include gene silencing by RNA interference (RNAi) and genomic engineering with CRISPR/Cas9 technology [198]. In *Drosophila*, CRISPR/Cas9 screens have recently been used to identify factors involved in genome architecture, including chromatin-binding proteins and functional cis-regulatory elements, such as enhancers and boundary elements or insulators [198]. Furthermore, the development of new methods based on a nuclease-dead Cas9 (dCas9) coupled with live imaging is allowing researchers to study the 4D genome, changes in 3D chromatin structure over time [199]. In the CRISPR/dCas9 system, there is specific recruitment of a fluorescently labelled dCas9 to the genomic region of interest, which allows the tracking of the contact and folding dynamics of this region by live microscopy [199].

Sequencing-based technologies rely on the available version of the genome and, in the case of *Drosophila*, the assembly of heterochromatic regions is still incomplete. New technologies based on long-read sequencing will improve the current genome assembly and thus increase the quality of Hi-C maps. In the field of microscopy, one of the major limitations is the number of loci that can be probed simultaneously. Recent advances including ORCA [122], Hi-M [197], and OligoFISSEQ [200] allow the sequential labeling and imaging of multiple genomic sequences, but still require long acquisition times and are very expensive. Altogether, the development of these techniques is encouraging, and further optimization will allow us to resolve the chromatin dynamics of whole genomes and to uncover the degree of heterogeneity inside cell populations.

Funding: This work was supported by grants PGC2018-099763-B100 and 2017SGR1455 from AGAUR (Generalitat de Catalunya) to M.C., C.C.-R. holds a predoctoral FPI contract from the Spanish Government (Ministerio de Ciencia e Innovación) and P.L.-G. is a predoctoral fellow of FI, Generalitat de Catalunya.

Institutional Review Board Statement: Not applicable.

Acknowledgments: We thank Jordi Bernués for critical reading of the manuscript and we apologize to colleagues whose work could not be cited here due to space limitations. Figures were created using Illustrator.

Conflicts of Interest: The authors declare no conflict of interest.

References

1. Adams, M.D.; Celniker, S.E.; Holt, R.A.; Evans, C.A.; Gocayne, J.D.; Amanatides, P.G.; Scherer, S.E.; Li, P.W.; Hoskins, R.A.; Galle, R.F.; et al. The Genome Sequence of *Drosophila melanogaster*. *Science* **2000**, *287*, 2185–2195. [CrossRef]
2. Myers, E.W. A Whole-Genome Assembly of Drosophila. *Science* **2000**, *287*, 2196–2204. [CrossRef]
3. Hoskins, R.A.; Carlson, J.W.; Wan, K.H.; Park, S.; Mendez, I.; Galle, S.E.; Booth, B.W.; Pfeiffer, B.D.; George, R.A.; Svirskas, R.; et al. The Release 6 reference sequence of the *Drosophila melanogaster* genome. *Genome Res.* **2015**, *25*, 445–458. [CrossRef]
4. Zhimulev, I.F.; Belyaeva, E.S.; Vatolina, T.Y.; Demakov, S.A. Banding patterns in *Drosophila melanogaster* polytene chromosomes correlate with DNA-binding protein occupancy. *BioEssays* **2012**, *34*, 498–508. [CrossRef]
5. Zykova, T.Y.; Levitsky, V.G.; Belyaeva, E.S.; Zhimulev, I.F. Polytene Chromosomes—A Portrait of Functional Organization of the Drosophila Genome. *Curr. Genom.* **2018**, *19*, 179–191. [CrossRef]
6. Grewal, S.I.S.; Elgin, S.C.R. Heterochromatin: New possibilities for the inheritance of structure. *Curr. Opin. Genet. Dev.* **2002**, *12*, 178–187. [CrossRef]
7. Craig, J.M. Heterochromatin? many flavours, common themes. *BioEssays* **2005**, *27*, 17–28. [CrossRef]
8. Pimpinelli, S.; Wakimoto, B.T. Expanding the boundaries of heterochromatin. *Genetica* **2003**, *117*, 111–116. [CrossRef]
9. Pimpinelli, S.; Berloco, M.; Fanti, L.; Dimitri, P.; Bonaccorsi, S.; Marchetti, E.; Caizzi, R.; Caggese, C.; Gatti, M. Transposable elements are stable structural components of *Drosophila melanogaster* heterochromatin. *Proc. Natl. Acad. Sci. USA* **1995**, *92*, 3804–3808. [CrossRef]

10. Eissenberg, J.C.; Elgin, S.C.R. HP1a: A structural chromosomal protein regulating transcription. *Trends Genet.* **2014**, *30*, 103–110. [CrossRef]
11. Marsano, R.M.; Giordano, E.; Messina, G.; Dimitri, P. A New Portrait of Constitutive Heterochromatin: Lessons from *Drosophila melanogaster*. *Trends Genet.* **2019**, *35*, 615–631. [CrossRef]
12. Swenson, J.M.; Colmenares, S.U.; Strom, A.R.; Costes, S.V.; Karpen, G.H. The composition and organization of Drosophila heterochromatin are heterogeneous and dynamic. *eLife* **2016**, *5*, e16096. [CrossRef]
13. Filion, G.J.; van Bemmel, J.G.; Braunschweig, U.; Talhout, W.; Kind, J.; Ward, L.D.; Brugman, W.; de Castro, I.J.; Kerkhoven, R.M.; Bussemaker, H.J.; et al. Systematic Protein Location Mapping Reveals Five Principal Chromatin Types in Drosophila Cells. *Cell* **2010**, *143*, 212–224. [CrossRef]
14. Kornberg, R.D. Chromatin Structure: A Repeating Unit of Histones and DNA. *Science* **1974**, *184*, 868–871. [CrossRef]
15. Luger, K.; Mäder, A.W.; Richmond, R.K.; Sargent, D.F.; Richmond, T.J. Crystal structure of the nucleosome core particle at 2.8 Å resolution. *Nature* **1997**, *389*, 251–260. [CrossRef]
16. Iwasaki, W.; Miya, Y.; Horikoshi, N.; Osakabe, A.; Taguchi, H.; Tachiwana, H.; Shibata, T.; Kagawa, W.; Kurumizaka, H. Contribution of histone N-terminal tails to the structure and stability of nucleosomes. *FEBS Open Bio* **2013**, *3*, 363–369. [CrossRef]
17. Cutter, A.R.; Hayes, J.J. A brief review of nucleosome structure. *FEBS Lett.* **2015**, *589*, 2914–2922. [CrossRef]
18. Allan, J.; Hartman, P.G.; Crane-Robinson, C.; Aviles, F.X. The structure of histone H1 and its location in chromatin. *Nature* **1980**, *288*, 675–679. [CrossRef]
19. Thoma, F.; Koller, T. Influence of histone H1 on chromatin structure. *Cell* **1977**, *12*, 101–107. [CrossRef]
20. Thoma, F.; Koller, T.; Klug, A. Involvement of histone H1 in the organization of the nucleosome and of the salt-dependent superstructures of chromatin. *J. Cell Biol.* **1979**, *83*, 403–427. [CrossRef]
21. Simpson, R.T. Structure of the chromatosome, a chromatin particle containing 160 base pairs of DNA and all the histones. *Biochemistry* **1978**, *17*, 5524–5531. [CrossRef]
22. Bednar, J.; Garcia-Saez, I.; Boopathi, R.; Cutter, A.R.; Papai, G.; Reymer, A.; Syed, S.H.; Lone, I.N.; Tonchev, O.; Crucifix, C.; et al. Structure and Dynamics of a 197 bp Nucleosome in Complex with Linker Histone H1. *Mol. Cell* **2017**, *66*, 384–397.e8. [CrossRef]
23. Cutter, A.R.; Hayes, J.J. Linker histones: Novel insights into structure-specific recognition of the nucleosome. *Biochem. Cell Biol.* **2017**, *95*, 171–178. [CrossRef]
24. Ricci, M.A.; Manzo, C.; García-Parajo, M.F.; Lakadamyali, M.; Cosma, M.P. Chromatin Fibers Are Formed by Heterogeneous Groups of Nucleosomes In Vivo. *Cell* **2015**, *160*, 1145–1158. [CrossRef]
25. Mavrich, T.N.; Ioshikhes, I.P.; Venters, B.J.; Jiang, C.; Tomsho, L.P.; Qi, J.; Schuster, S.C.; Albert, I.; Pugh, B.F. A barrier nucleosome model for statistical positioning of nucleosomes throughout the yeast genome. *Genome Res.* **2008**, *18*, 1073–1083. [CrossRef]
26. Kaplan, N.; Moore, I.K.; Fondufe-Mittendorf, Y.; Gossett, A.J.; Tillo, D.; Field, Y.; LeProust, E.M.; Hughes, T.R.; Lieb, J.D.; Widom, J.; et al. The DNA-encoded nucleosome organization of a eukaryotic genome. *Nature* **2009**, *458*, 362–366. [CrossRef]
27. Yuan, G.C.; Liu, Y.-J.; Dion, M.F.; Slack, M.D.; Wu, L.F.; Altschuler, S.J.; Rando, O.J. Genome-Scale Identification of Nucleosome Positions in S. cerevisiae. *Science* **2005**, *309*, 626–630. [CrossRef]
28. Struhl, K.; Segal, E. Determinants of nucleosome positioning. *Nat. Struct. Mol. Biol.* **2013**, *20*, 267–273. [CrossRef]
29. Martin, R.L.; Maiorano, J.; Beitel, G.J.; Marko, J.F.; McVicker, G.; Fondufe-Mittendorf, Y.N. A comparison of nucleosome organization in Drosophila cell lines. *PLoS ONE* **2017**, *12*, e0178590. [CrossRef]
30. Li, G.; Levitus, M.; Bustamante, C.; Widom, J. Rapid spontaneous accessibility of nucleosomal DNA. *Nat. Struct. Mol. Biol.* **2005**, *12*, 46–53. [CrossRef]
31. Poirier, M.G.; Oh, E.; Tims, H.S.; Widom, J. Dynamics and function of compact nucleosome arrays. *Nat. Struct. Mol. Biol.* **2009**, *16*, 938–944. [CrossRef]
32. Zhou, K.; Gaullier, G.; Luger, K. Nucleosome structure and dynamics are coming of age. *Nat. Struct. Mol. Biol.* **2019**, *26*, 3–13. [CrossRef] [PubMed]
33. Lai, W.K.M.; Pugh, B.F. Understanding nucleosome dynamics and their links to gene expression and DNA replication. *Nat. Rev. Mol. Cell Biol.* **2017**, *18*, 548–562. [CrossRef] [PubMed]
34. Horard, B.; Loppin, B. Histone storage and deposition in the early Drosophila embryo. *Chromosoma* **2015**, *124*, 163–175. [CrossRef]
35. Talbert, P.B.; Henikoff, S. Histone variants at a glance. *J. Cell Sci.* **2021**, *134*, jcs244749. [CrossRef] [PubMed]
36. Baldi, S.; Becker, P.B. The variant histone H2A.V of Drosophila—Three roles, two guises. *Chromosoma* **2013**, *122*, 245–258. [CrossRef]
37. Prozzillo, Y.; Cuticone, S.; Ferreri, D.; Fattorini, G.; Messina, G.; Dimitri, P. In Vivo Silencing of Genes Coding for dTip60 Chromatin Remodeling Complex Subunits Affects Polytene Chromosome Organization and Proper Development in *Drosophila melanogaster*. *Int. J. Mol. Sci.* **2021**, *22*, 4525. [CrossRef]
38. Messina, G.; Damia, E.; Fanti, L.; Atterrato, M.T.; Celauro, E.; Mariotti, F.R.; Accardo, M.C.; Walther, M.; Vernì, F.; Picchioni, D.; et al. *Yeti*, a *Drosophila melanogaster* essential gene, encodes a protein required for chromatin organization. *J. Cell Sci.* **2014**, *127*, 2577–2588. [CrossRef]
39. Weber, C.M.; Henikoff, J.G.; Henikoff, S. H2A.Z nucleosomes enriched over active genes are homotypic. *Nat. Struct. Mol. Biol.* **2010**, *17*, 1500–1507. [CrossRef]
40. Weber, C.M.; Ramachandran, S.; Henikoff, S. Nucleosomes are context-specific, H2A.Z-Modulated barriers to RNA polymerase. *Mol. Cell* **2014**, *53*, 819–830. [CrossRef]

41. Swaminathan, J.; Baxter, E.M.; Corces, V.G. The role of histone H2Av variant replacement and histone H4 acetylation in the establishment of Drosophila heterochromatin. *Genes Dev.* **2005**, *19*, 65–76. [CrossRef]
42. Leach, T.J.; Mazzeo, M.; Chotkowski, H.L.; Madigan, J.P.; Wotring, M.G.; Glaser, R.L. Histone H2A.Z is widely but nonrandomly distributed in chromosomes of *Drosophila melanogaster*. *J. Biol. Chem.* **2000**, *275*, 23267–23272. [CrossRef]
43. Akhmanova, A.S.; Bindels, P.C.T.; Xu, J.; Miedema, K.; Kremer, H.; Hennig, W.; Xu, J.; Hennig, W. Structure and expression of histone H3.3 genes in *Drosophila melanogaster* and *Drosophila hydei*. *Genome* **1995**, *38*, 586–600. [CrossRef]
44. Ahmad, K.; Henikoff, S. The Histone Variant H3.3 Marks Active Chromatin by Replication-Independent Nucleosome Assembly. *Mol. Cell* **2002**, *9*, 1191–1200. [CrossRef]
45. Goldberg, A.D.; Banaszynski, L.A.; Noh, K.-M.; Lewis, P.W.; Elsaesser, S.J.; Stadler, S.; Dewell, S.; Law, M.; Guo, X.; Li, X.; et al. Distinct Factors Control Histone Variant H3.3 Localization at Specific Genomic Regions. *Cell* **2010**, *140*, 678–691. [CrossRef]
46. Mito, Y.; Henikoff, J.G.; Henikoff, S. Histone Replacement Marks the Boundaries of cis-Regulatory Domains. *Science* **2007**, *315*, 1408–1411. [CrossRef]
47. Hödl, M.; Basler, K. Transcription in the Absence of Histone H3.3. *Curr. Biol.* **2009**, *19*, 1221–1226. [CrossRef]
48. Braunschweig, U.; Hogan, G.J.; Pagie, L.; van Steensel, B. Histone H1 binding is inhibited by histone variant H3.3. *EMBO J.* **2009**, *28*, 3635–3645. [CrossRef] [PubMed]
49. Nagel, S.; Grossbach, U. Histone H1 Genes and Histone Gene Clusters in the Genus Drosophila. *J. Mol. Evol.* **2000**, *51*, 286–298. [CrossRef]
50. Pérez-Montero, S.; Carbonell, A.; Morán, T.; Vaquero, A.; Azorín, F. The embryonic linker histone H1 variant of *Drosophila*, dBigH1, regulates zygotic genome activation. *Dev. Cell* **2013**, *26*, 578–590. [CrossRef]
51. Nalabothula, N.; McVicker, G.; Maiorano, J.; Martin, R.; Pritchard, J.K.; Fondufe-Mittendorf, Y.N. The chromatin architectural proteins HMGD1 and H1 bind reciprocally and have opposite effects on chromatin structure and gene regulation. *BMC Genomics* **2014**, *15*, 92. [CrossRef]
52. Lu, X.; Wontakal, S.N.; Kavi, H.; Kim, B.J.; Guzzardo, P.M.; Emelyanov, A.V.; Xu, N.; Hannon, G.J.; Zavadil, J.; Fyodorov, D.V.; et al. Drosophila H1 Regulates the Genetic Activity of Heterochromatin by Recruitment of Su(var)3-9. *Science* **2013**, *340*, 78–81. [CrossRef]
53. Vujatovic, O.; Zaragoza, K.; Vaquero, A.; Reina, O.; Bernués, J.; Azorín, F. *Drosophila melanogaster* linker histone dH1 is required for transposon silencing and to preserve genome integrity. *Nucleic Acids Res.* **2012**, *40*, 5402–5414. [CrossRef]
54. Lu, X.; Wontakal, S.N.; Emelyanov, A.V.; Morcillo, P.; Konev, A.Y.; Fyodorov, D.V.; Skoultchi, A.I. Linker histone H1 is essential for Drosophila development, the establishment of pericentric heterochromatin, and a normal polytene chromosome structure. *Genes Dev.* **2009**, *23*, 452–465. [CrossRef]
55. Siriaco, G.; Deuring, R.; Chioda, M.; Becker, P.B.; Tamkun, J.W. Drosophila ISWI Regulates the Association of Histone H1 with Interphase Chromosomes in Vivo. *Genetics* **2009**, *182*, 661–669. [CrossRef]
56. Bayona-Feliu, A.; Casas-Lamesa, A.; Reina, O.; Bernués, J.; Azorín, F. Linker histone H1 prevents R-loop accumulation and genome instability in heterochromatin. *Nat. Commun.* **2017**, *8*, 283. [CrossRef]
57. Cao, K.; Lailler, N.; Zhang, Y.; Kumar, A.; Uppal, K.; Liu, Z.; Lee, E.K.; Wu, H.; Medrzycki, M.; Pan, C.; et al. High-Resolution Mapping of H1 Linker Histone Variants in Embryonic Stem Cells. *PLoS Genet.* **2013**, *9*, e1003417. [CrossRef]
58. Izzo, A.; Kamieniarz-Gdula, K.; Ramírez, F.; Noureen, N.; Kind, J.; Manke, T.; van Steensel, B.; Schneider, R. The Genomic Landscape of the Somatic Linker Histone Subtypes H1.1 to H1.5 in Human Cells. *Cell Rep.* **2013**, *3*, 2142–2154. [CrossRef]
59. Mayor, R.; Izquierdo-Bouldstridge, A.; Millán-Ariño, L.; Bustillos, A.; Sampaio, C.; Luque, N.; Jordan, A. Genome Distribution of Replication-independent Histone H1 Variants Shows H1.0 Associated with Nucleolar Domains and H1X Associated with RNA Polymerase II-enriched Regions. *J. Biol. Chem.* **2015**, *290*, 7474–7491. [CrossRef]
60. Millán-Ariño, L.; Islam, A.B.M.M.K.; Izquierdo-Bouldstridge, A.; Mayor, R.; Terme, J.-M.; Luque, N.; Sancho, M.; López-Bigas, N.; Jordan, A. Mapping of six somatic linker histone H1 variants in human breast cancer cells uncovers specific features of H1.2. *Nucleic Acids Res.* **2014**, *42*, 4474–4493. [CrossRef]
61. Fan, Y.; Nikitina, T.; Zhao, J.; Fleury, T.J.; Bhattacharyya, R.; Bouhassira, E.E.; Stein, A.; Woodcock, C.L.; Skoultchi, A.I. Histone H1 Depletion in Mammals Alters Global Chromatin Structure but Causes Specific Changes in Gene Regulation. *Cell* **2005**, *123*, 1199–1212. [CrossRef]
62. Izquierdo-Bouldstridge, A.; Bustillos, A.; Bonet-Costa, C.; Aribau-Miralbés, P.; García-Gomis, D.; Dabad, M.; Esteve-Codina, A.; Pascual-Reguant, L.; Peiró, S.; Esteller, M.; et al. Histone H1 depletion triggers an interferon response in cancer cells via activation of heterochromatic repeats. *Nucleic Acids Res.* **2017**, *45*, 11622–11642. [CrossRef]
63. Sancho, M.; Diani, E.; Beato, M.; Jordan, A. Depletion of Human Histone H1 Variants Uncovers Specific Roles in Gene Expression and Cell Growth. *PLoS Genet.* **2008**, *4*, e1000227. [CrossRef]
64. Healton, S.E.; Pinto, H.D.; Mishra, L.N.; Hamilton, G.A.; Wheat, J.C.; Swist-Rosowska, K.; Shukeir, N.; Dou, Y.; Steidl, U.; Jenuwein, T.; et al. H1 linker histones silence repetitive elements by promoting both histone H3K9 methylation and chromatin compaction. *Proc. Natl. Acad. Sci. USA* **2020**, *117*, 14251–14258. [CrossRef]
65. Carbonell, A.; Pérez-Montero, S.; Climent-Cantó, P.; Reina, O.; Azorín, F. The Germline Linker Histone dBigH1 and the Translational Regulator Bam Form a Repressor Loop Essential for Male Germ Stem Cell Differentiation. *Cell Rep.* **2017**, *21*, 3178–3189. [CrossRef]

66. Climent-Cantó, P.; Carbonell, A.; Tamirisa, S.; Henn, L.; Pérez-Montero, S.; Boros, I.M.; Azorín, F. The tumour suppressor brain tumour (Brat) regulates linker histone dBigH1 expression in the Drosophila female germline and the early embryo. *Open Biol.* **2021**, *11*, 200408. [CrossRef]
67. Henn, L.; Szabó, A.; Imre, L.; Román, Á.; Ábrahám, A.; Vedelek, B.; Nánási, P.; Boros, I.M. Alternative linker histone permits fast paced nuclear divisions in early Drosophila embryo. *Nucleic Acids Res.* **2020**, *48*, 9007–9018. [CrossRef]
68. Dunwell, T.L.; Gerd, P.P. Drosophila genomic methylation: New evidence and new questions. *Epigenomics* **2014**, *6*, 459–461. [CrossRef]
69. Greer, E.L.; Blanco, M.A.; Gu, L.; Sendinc, E.; Liu, J.; Aristizábal-Corrales, D.; Hsu, C.-H.; Aravind, L.; He, C.; Shi, Y. DNA Methylation on N6-Adenine in *C. elegans*. *Cell* **2015**, *161*, 868–878. [CrossRef]
70. Zhang, G.; Huang, H.; Liu, D.; Cheng, Y.; Liu, X.; Zhang, W.; Yin, R.; Zhang, D.; Zhang, P.; Liu, J.; et al. N6-methyladenine DNA modification in Drosophila. *Cell* **2015**, *161*, 893–906. [CrossRef]
71. Yu, G.; Wu, Q.; Gao, Y.; Chen, M.; Yang, M. The Epigenetics of Aging in Invertebrates. *Int. J. Mol. Sci.* **2019**, *20*, 4535. [CrossRef] [PubMed]
72. He, S.; Zhang, G.; Wang, J.; Gao, Y.; Sun, R.; Cao, Z.; Chen, Z.; Zheng, X.; Yuan, J.; Luo, Y.; et al. 6mA-DNA-binding factor Jumu controls maternal-to-zygotic transition upstream of Zelda. *Nat. Commun.* **2019**, *10*, 2219. [CrossRef]
73. Lawrence, M.; Daujat, S.; Schneider, R. Lateral Thinking: How Histone Modifications Regulate Gene Expression. *Trends Genet.* **2016**, *32*, 42–56. [CrossRef]
74. Tessarz, P.; Kouzarides, T. Histone core modifications regulating nucleosome structure and dynamics. *Nat. Rev. Mol. Cell Biol.* **2014**, *15*, 703–708. [CrossRef]
75. Akhtar, A.; Becker, P.B. Activation of Transcription through Histone H4 Acetylation by MOF, an Acetyltransferase Essential for Dosage Compensation in Drosophila. *Mol. Cell* **2000**, *5*, 367–375. [CrossRef]
76. Shogren-Knaak, M.; Haruhiko, I.; Sun, J.-M.; Pazin, M.; Davie, J.R.; Peterson, C.L. Histone H4-K16 Acetylation Controls Chromatin Structure and Protein Interactions. *Science* **2006**, *311*, 844–847. [CrossRef]
77. Lu, X.; Simon, M.D.; Chodaparambil, J.V.; Hansen, J.C.; Shokat, K.M.; Luger, K. The effect of H3K79 dimethylation and H4K20 trimethylation on nucleosome and chromatin structure. *Nat. Struct. Mol. Biol.* **2008**, *15*, 1122–1124. [CrossRef]
78. Bannister, A.J.; Kouzarides, T. Regulation of chromatin by histone modifications. *Cell Res.* **2011**, *21*, 381–395. [CrossRef]
79. Schuettengruber, B.; Bourbon, H.-M.; Di Croce, L.; Cavalli, G. Genome Regulation by Polycomb and Trithorax: 70 Years and Counting. *Cell* **2017**, *171*, 34–57. [CrossRef]
80. Zhang, T.; Cooper, S.; Brockdorff, N. The interplay of histone modifications—Writers that read. *EMBO Rep.* **2015**, *16*, 1467–1481. [CrossRef]
81. Verdin, E.; Ott, M. 50 years of protein acetylation: From gene regulation to epigenetics, metabolism and beyond. *Nat. Rev. Mol. Cell Biol.* **2015**, *16*, 258–264. [CrossRef]
82. Strahl, B.D.; Allis, C.D. The language of covalent histone modifications. *Nature* **2000**, *403*, 41–45. [CrossRef] [PubMed]
83. Morgan, M.A.J.; Shilatifard, A. Reevaluating the roles of histone-modifying enzymes and their associated chromatin modifications in transcriptional regulation. *Nat. Genet.* **2020**, *52*, 1271–1281. [CrossRef] [PubMed]
84. Talbert, P.B.; Henikoff, S. The Yin and Yang of Histone Marks in Transcription. *Annu. Rev. Genom. Hum. Genet.* **2021**, *22*, 147–170. [CrossRef] [PubMed]
85. Pérez-Lluch, S.; Blanco, E.; Tilgner, H.; Curado, J.; Ruiz-Romero, M.; Corominas, M.; Guigó, R. Absence of canonical marks of active chromatin in developmentally regulated genes. *Nat. Genet.* **2015**, *47*, 1158–1167. [CrossRef]
86. Hödl, M.; Basler, K. Transcription in the Absence of Histone H3.2 and H3K4 Methylation. *Curr. Biol.* **2012**, *22*, 2253–2257. [CrossRef]
87. Zhang, T.; Zhang, Z.; Dong, Q.; Xiong, J.; Zhu, B. Histone H3K27 acetylation is dispensable for enhancer activity in mouse embryonic stem cells. *Genome Biol.* **2020**, *21*, 45. [CrossRef]
88. Li, X.-Y.; Harrison, M.M.; Villalta, J.E.; Kaplan, T.; Eisen, M.B. Establishment of regions of genomic activity during the Drosophila maternal to zygotic transition. *eLife* **2014**, *3*, e03737. [CrossRef]
89. Chen, K.; Johnston, J.; Shao, W.; Meier, S.; Staber, C.; Zeitlinger, J. A global change in RNA polymerase II pausing during the Drosophila midblastula transition. *eLife* **2013**, *2*, e00861. [CrossRef] [PubMed]
90. Regadas, I.; Dahlberg, O.; Vaid, R.; Ho, O.; Belikov, S.; Dixit, G.; Deindl, S.; Wen, J.; Mannervik, M. A unique histone 3 lysine 14 chromatin signature underlies tissue-specific gene regulation. *Mol. Cell* **2021**, *81*, 1766–1780.e10. [CrossRef]
91. Graves, H.K.; Wang, P.; Lagarde, M.; Chen, Z.; Tyler, J.K. Mutations that prevent or mimic persistent post-translational modifications of the histone H3 globular domain cause lethality and growth defects in Drosophila. *Epigenet. Chromatin* **2016**, *9*, 9. [CrossRef] [PubMed]
92. Kharchenko, P.V.; Alekseyenko, A.A.; Schwartz, Y.B.; Minoda, A.; Riddle, N.C.; Ernst, J.; Sabo, P.J.; Larschan, E.; Gorchakov, A.A.; Gu, T.; et al. Comprehensive analysis of the chromatin landscape in *Drosophila melanogaster*. *Nature* **2011**, *471*, 480–485. [CrossRef]
93. Bantignies, F.; Roure, V.; Comet, I.; Leblanc, B.; Schuettengruber, B.; Bonnet, J.; Tixier, V.; Mas, A.; Cavalli, G. Polycomb-Dependent Regulatory Contacts between Distant Hox Loci in *Drosophila*. *Cell* **2011**, *144*, 214–226. [CrossRef] [PubMed]
94. Boettiger, A.N.; Bintu, B.; Moffitt, J.R.; Wang, S.; Beliveau, B.J.; Fudenberg, G.; Imakaev, M.; Mirny, L.A.; Wu, C.; Zhuang, X. Super-resolution imaging reveals distinct chromatin folding for different epigenetic states. *Nature* **2016**, *529*, 418–422. [CrossRef] [PubMed]

95. Kempfer, R.; Pombo, A. Methods for mapping 3D chromosome architecture. *Nat. Rev. Genet.* **2020**, *21*, 207–226. [CrossRef]
96. Dekker, J.; Marti-Renom, M.A.; Mirny, L.A. Exploring the three-dimensional organization of genomes: Interpreting chromatin interaction data. *Nat. Rev. Genet.* **2013**, *14*, 390–403. [CrossRef]
97. Lieberman-Aiden, E.; van Berkum, N.L.; Williams, L.; Imakaev, M.; Ragoczy, T.; Telling, A.; Amit, I.; Lajoie, B.R.; Sabo, P.J.; Dorschner, M.O.; et al. Comprehensive Mapping of Long-Range Interactions Reveals Folding Principles of the Human Genome. *Science* **2009**, *326*, 289–293. [CrossRef]
98. Sexton, T.; Yaffe, E.; Kenigsberg, E.; Bantignies, F.; Leblanc, B.; Hoichman, M.; Parrinello, H.; Tanay, A.; Cavalli, G. Three-dimensional folding and functional organization principles of the Drosophila genome. *Cell* **2012**, *148*, 458–472. [CrossRef]
99. Bonev, B.; Cavalli, G. Organization and function of the 3D genome. *Nat. Rev. Genet.* **2016**, *17*, 661–678. [CrossRef]
100. Rao, S.S.P.; Huntley, M.H.; Durand, N.C.; Stamenova, E.K.; Bochkov, I.D.; Robinson, J.T.; Sanborn, A.L.; Machol, I.; Omer, A.D.; Lander, E.S.; et al. A 3D map of the human genome at kilobase resolution reveals principles of chromatin looping. *Cell* **2014**, *159*, 1665–1680. [CrossRef]
101. Misteli, T. The Self-Organizing Genome: Principles of Genome Architecture and Function. *Cell* **2020**, *183*, 28–45. [CrossRef] [PubMed]
102. Nora, E.P.; Lajoie, B.R.; Schulz, E.G.; Giorgetti, L.; Okamoto, I.; Servant, N.; Piolot, T.; van Berkum, N.L.; Meisig, J.; Sedat, J.; et al. Spatial partitioning of the regulatory landscape of the X-inactivation centre. *Nature* **2012**, *485*, 381–385. [CrossRef] [PubMed]
103. Dixon, J.R.; Selvaraj, S.; Yue, F.; Kim, A.; Li, Y.; Shen, Y.; Hu, M.; Liu, J.S.; Ren, B. Topological domains in mammalian genomes identified by analysis of chromatin interactions. *Nature* **2012**, *485*, 376–380. [CrossRef] [PubMed]
104. Wutz, G.; Várnai, C.; Nagasaka, K.; Cisneros, D.A.; Stocsits, R.R.; Tang, W.; Schoenfelder, S.; Jessberger, G.; Muhar, M.; Hossain, M.J.; et al. Topologically associating domains and chromatin loops depend on cohesin and are regulated by CTCF, WAPL, and PDS5 proteins. *EMBO J.* **2017**, *36*, 3573–3599. [CrossRef] [PubMed]
105. Davidson, I.F.; Bauer, B.; Goetz, D.; Tang, W.; Wutz, G.; Peters, J. DNA loop extrusion by human cohesin. *Science* **2019**, *366*, 1338–1345. [CrossRef]
106. Fudenberg, G.; Imakaev, M.; Lu, C.; Goloborodko, A.; Abdennur, N.; Mirny, L.A. Formation of Chromosomal Domains by Loop Extrusion. *Cell Rep.* **2016**, *15*, 2038–2049. [CrossRef]
107. Rao, S.S.P.; Huang, S.-C.; Glenn St Hilaire, B.; Engreitz, J.M.; Perez, E.M.; Kieffer-Kwon, K.-R.; Sanborn, A.L.; Johnstone, S.E.; Bascom, G.D.; Bochkov, I.D.; et al. Cohesin Loss Eliminates All Loop Domains. *Cell* **2017**, *171*, 305–320.e24. [CrossRef]
108. de Wit, E.; Vos, E.S.M.; Holwerda, S.J.B.; Valdes-Quezada, C.; Verstegen, M.J.A.M.; Teunissen, H.; Splinter, E.; Wijchers, P.J.; Krijger, P.H.L.; de Laat, W. CTCF Binding Polarity Determines Chromatin Looping. *Mol. Cell* **2015**, *60*, 676–684. [CrossRef]
109. Hanssen, L.L.P.; Kassouf, M.T.; Oudelaar, A.M.; Biggs, D.; Preece, C.; Downes, D.J.; Gosden, M.; Sharpe, J.A.; Sloane-Stanley, J.A.; Hughes, J.R.; et al. Tissue-specific CTCF–cohesin-mediated chromatin architecture delimits enhancer interactions and function in vivo. *Nat. Cell Biol.* **2017**, *19*, 952–961. [CrossRef]
110. Nora, E.P.; Goloborodko, A.; Valton, A.-L.; Gibcus, J.H.; Uebersohn, A.; Abdennur, N.; Dekker, J.; Mirny, L.A.; Bruneau, B.G. Targeted Degradation of CTCF Decouples Local Insulation of Chromosome Domains from Genomic Compartmentalization. *Cell* **2017**, *169*, 930–944. [CrossRef]
111. Rowley, M.J.; Nichols, M.H.; Lyu, X.; Ando-Kuri, M.; Rivera, I.S.M.; Hermetz, K.; Wang, P.; Ruan, Y.; Corces, V.G. Evolutionarily Conserved Principles Predict 3D Chromatin Organization. *Mol. Cell* **2017**, *67*, 837–852. [CrossRef]
112. Hug, C.B.; Grimaldi, A.G.; Kruse, K.; Vaquerizas, J.M. Chromatin Architecture Emerges during Zygotic Genome Activation Independent of Transcription. *Cell* **2017**, *169*, 216–228. [CrossRef] [PubMed]
113. Ramírez, F.; Bhardwaj, V.; Arrigoni, L.; Lam, K.C.; Grüning, B.A.; Villaveces, J.; Habermann, B.; Akhtar, A.; Manke, T. High-resolution TADs reveal DNA sequences underlying genome organization in flies. *Nat. Commun.* **2018**, *9*, 189. [CrossRef] [PubMed]
114. Kaushal, A.; Mohana, G.; Dorier, J.; Özdemir, I.; Omer, A.; Cousin, P.; Semenova, A.; Taschner, M.; Dergai, O.; Marzetta, F.; et al. CTCF loss has limited effects on global genome architecture in Drosophila despite critical regulatory functions. *Nat. Commun.* **2021**, *12*, 1011. [CrossRef] [PubMed]
115. Gambetta, M.C.; Furlong, E.E.M. The Insulator Protein CTCF Is Required for Correct Hox Gene Expression, but Not for Embryonic Development in Drosophila. *Genetics* **2018**, *210*, 129–136. [CrossRef]
116. Schwartz, Y.B.; Cavalli, G. Three-dimensional genome organization and function in Drosophila. *Genetics* **2017**, *205*, 5–24. [CrossRef]
117. Wang, Q.; Sun, Q.; Czajkowsky, D.M.; Shao, Z. Sub-kb Hi-C in D. melanogaster reveals conserved characteristics of TADs between insect and mammalian cells. *Nat. Commun.* **2018**, *9*, 188. [CrossRef]
118. Ogiyama, Y.; Schuettengruber, B.; Papadopoulos, G.L.; Chang, J.-M.; Cavalli, G. Polycomb-Dependent Chromatin Looping Contributes to Gene Silencing during Drosophila Development. *Mol. Cell* **2018**, *71*, 73–88. [CrossRef]
119. Szabo, Q.; Donjon, A.; Jerković, I.; Papadopoulos, G.L.; Cheutin, T.; Bonev, B.; Nora, E.P.; Bruneau, B.G.; Bantignies, F.; Cavalli, G. Regulation of single-cell genome organization into TADs and chromatin nanodomains. *Nat. Genet.* **2020**, *52*, 1151–1157. [CrossRef]
120. Szabo, Q.; Jost, D.; Chang, J.-M.; Cattoni, D.I.; Papadopoulos, G.L.; Bonev, B.; Sexton, T.; Gurgo, J.; Jacquier, C.; Nollmann, M.; et al. TADs are 3D structural units of higher-order chromosome organization in *Drosophila*. *Sci. Adv.* **2018**, *4*, eaar8082. [CrossRef]

121. Kundu, S.; Ji, F.; Sunwoo, H.; Jain, G.; Lee, J.T.; Sadreyev, R.I.; Dekker, J.; Kingston, R.E. Polycomb Repressive Complex 1 Generates Discrete Compacted Domains that Change during Differentiation. *Mol. Cell* **2017**, *65*, 432–446. [CrossRef]
122. Mateo, L.J.; Murphy, S.E.; Hafner, A.; Cinquini, I.S.; Walker, C.A.; Boettiger, A.N. Visualizing DNA folding and RNA in embryos at single-cell resolution. *Nature* **2019**, *568*, 49–54. [CrossRef]
123. De, S.; Gehred, N.D.; Fujioka, M.; Chan, F.W.; Jaynes, J.B.; Kassis, J.A. Defining the Boundaries of Polycomb Domains in *Drosophila*. *Genetics* **2020**, *216*, 689–700. [CrossRef]
124. Szabo, Q.; Bantignies, F.; Cavalli, G. Principles of genome folding into topologically associating domains. *Sci. Adv.* **2019**, *5*, eaaw1668. [CrossRef]
125. Ulianov, S.V.; Razin, S.V. The two waves in single-cell 3D genomics. *Semin. Cell Dev. Biol.* **2021**. [CrossRef]
126. Flyamer, I.M.; Gassler, J.; Imakaev, M.; Brandão, H.B.; Ulianov, S.V.; Abdennur, N.; Razin, S.V.; Mirny, L.A.; Tachibana-Konwalski, K. Single-nucleus Hi-C reveals unique chromatin reorganization at oocyte-to-zygote transition. *Nature* **2017**, *544*, 110–114. [CrossRef]
127. Cattoni, D.I.; Cardozo Gizzi, A.M.; Georgieva, M.; Di Stefano, M.; Valeri, A.; Chamousset, D.; Houbron, C.; Déjardin, S.; Fiche, J.-B.; González, I.; et al. Single-cell absolute contact probability detection reveals chromosomes are organized by multiple low-frequency yet specific interactions. *Nat. Commun.* **2017**, *8*, 1753. [CrossRef] [PubMed]
128. Eagen, K.P.; Hartl, T.A.; Kornberg, R.D. Stable Chromosome Condensation Revealed by Chromosome Conformation Capture. *Cell* **2015**, *163*, 934–946. [CrossRef]
129. Ulianov, S.V.; Khrameeva, E.E.; Gavrilov, A.A.; Flyamer, I.M.; Kos, P.; Mikhaleva, E.A.; Penin, A.A.; Logacheva, M.D.; Imakaev, M.V.; Chertovich, A.; et al. Active chromatin and transcription play a key role in chromosome partitioning into topologically associating domains. *Genome Res.* **2016**, *26*, 70–84. [CrossRef] [PubMed]
130. Hou, C.; Li, L.; Qin, Z.S.; Corces, V.G. Gene Density, Transcription, and Insulators Contribute to the Partition of the Drosophila Genome into Physical Domains. *Mol. Cell* **2012**, *48*, 471–484. [CrossRef] [PubMed]
131. Chen, H.; Levo, M.; Barinov, L.; Fujioka, M.; Jaynes, J.B.; Gregor, T. Dynamic interplay between enhancer–promoter topology and gene activity. *Nat. Genet.* **2018**, *50*, 1296–1303. [CrossRef]
132. van Steensel, B.; Furlong, E.E.M. The role of transcription in shaping the spatial organization of the genome. *Nat. Rev. Mol. Cell Biol.* **2019**, *20*, 327–337. [CrossRef]
133. Misteli, T.; Finn, E.H. Chromatin architecture is a flexible foundation for gene expression. *Nat. Genet.* **2021**, *53*, 426–427. [CrossRef]
134. Cheutin, T.; Cavalli, G. Loss of PRC1 induces higher-order opening of Hox loci independently of transcription during Drosophila embryogenesis. *Nat. Commun.* **2018**, *9*, 3898. [CrossRef]
135. Lupiáñez, D.G.; Kraft, K.; Heinrich, V.; Krawitz, P.; Brancati, F.; Klopocki, E.; Horn, D.; Kayserili, H.; Opitz, J.M.; Laxova, R.; et al. Disruptions of Topological Chromatin Domains Cause Pathogenic Rewiring of Gene-Enhancer Interactions. *Cell* **2015**, *161*, 1012–1025. [CrossRef]
136. Arzate-Mejía, R.G.; Josué Cerecedo-Castillo, A.; Guerrero, G.; Furlan-Magaril, M.; Recillas-Targa, F. In situ dissection of domain boundaries affect genome topology and gene transcription in Drosophila. *Nat. Commun.* **2020**, *11*, 894. [CrossRef] [PubMed]
137. Cavalheiro, G.R.; Pollex, T.; Furlong, E.E. To loop or not to loop: What is the role of TADs in enhancer function and gene regulation? *Curr. Opin. Genet. Dev.* **2021**, *67*, 119–129. [CrossRef] [PubMed]
138. Ghavi-Helm, Y.; Jankowski, A.; Meiers, S.; Viales, R.R.; Korbel, J.O.; Furlong, E.E.M. Highly rearranged chromosomes reveal uncoupling between genome topology and gene expression. *Nat. Genet.* **2019**, *51*, 1272–1282. [CrossRef]
139. Ing-Simmons, E.; Vaid, R.; Bing, X.Y.; Levine, M.; Mannervik, M.; Vaquerizas, J.M. Independence of chromatin conformation and gene regulation during Drosophila dorsoventral patterning. *Nat. Genet.* **2021**, *53*, 487–499. [CrossRef] [PubMed]
140. Espinola, S.M.; Götz, M.; Bellec, M.; Messina, O.; Fiche, J.-B.; Houbron, C.; Dejean, M.; Reim, I.; Cardozo Gizzi, A.M.; Lagha, M.; et al. Cis-regulatory chromatin loops arise before TADs and gene activation, and are independent of cell fate during early Drosophila development. *Nat. Genet.* **2021**, *53*, 477–486. [CrossRef]
141. Williamson, I.; Kane, L.; Devenney, P.S.; Flyamer, I.M.; Anderson, E.; Kilanowski, F.; Hill, R.E.; Bickmore, W.A.; Lettice, L.A. Developmentally regulated Shh expression is robust to TAD perturbations. *Development* **2019**, *146*, dev179523. [CrossRef]
142. Shevelyov, Y.Y.; Ulianov, S.V. The Nuclear Lamina as an Organizer of Chromosome Architecture. *Cells* **2019**, *8*, 136. [CrossRef] [PubMed]
143. Pickersgill, H.; Kalverda, B.; de Wit, E.; Talhout, W.; Fornerod, M.; van Steensel, B. Characterization of the *Drosophila melanogaster* genome at the nuclear lamina. *Nat. Genet.* **2006**, *38*, 1005–1014. [CrossRef] [PubMed]
144. Peric-Hupkes, D.; Meuleman, W.; Pagie, L.; Bruggeman, S.W.M.; Solovei, I.; Brugman, W.; Gräf, S.; Flicek, P.; Kerkhoven, R.M.; van Lohuizen, M.; et al. Molecular Maps of the Reorganization of Genome-Nuclear Lamina Interactions during Differentiation. *Mol. Cell* **2010**, *38*, 603–613. [CrossRef] [PubMed]
145. Nikolakaki, E.; Mylonis, I.; Giannakouros, T. Lamin B Receptor: Interplay between Structure, Function and Localization. *Cells* **2017**, *6*, 28. [CrossRef] [PubMed]
146. Pindyurin, A.V.; Ilyin, A.A.; Ivankin, A.V.; Tselebrovsky, M.V.; Nenasheva, V.V.; Mikhaleva, E.A.; Pagie, L.; van Steensel, B.; Shevelyov, Y.Y. The large fraction of heterochromatin in Drosophila neurons is bound by both B-type lamin and HP1a. *Epigenet. Chromatin* **2018**, *11*, 65. [CrossRef] [PubMed]

147. Solovei, I.; Wang, A.S.; Thanisch, K.; Schmidt, C.S.; Krebs, S.; Zwerger, M.; Cohen, T.V.; Devys, D.; Foisner, R.; Peichl, L.; et al. LBR and Lamin A/C Sequentially Tether Peripheral Heterochromatin and Inversely Regulate Differentiation. *Cell* **2013**, *152*, 584–598. [CrossRef]
148. Zhu, J.; Adli, M.; Zou, J.Y.; Verstappen, G.; Coyne, M.; Zhang, X.; Durham, T.; Miri, M.; Deshpande, V.; De Jager, P.L.; et al. Genome-wide Chromatin State Transitions Associated with Developmental and Environmental Cues. *Cell* **2013**, *152*, 642–654. [CrossRef]
149. Kind, J.; Pagie, L.; de Vries, S.S.; Nahidiazar, L.; Dey, S.S.; Bienko, M.; Zhan, Y.; Lajoie, B.; de Graaf, C.A.; Amendola, M.; et al. Genome-wide Maps of Nuclear Lamina Interactions in Single Human Cells. *Cell* **2015**, *163*, 134–147. [CrossRef]
150. Briand, N.; Collas, P. Lamina-associated domains: Peripheral matters and internal affairs. *Genome Biol.* **2020**, *21*, 85. [CrossRef]
151. Somech, R.; Shaklai, S.; Geller, O.; Amariglio, N.; Simon, A.J.; Rechavi, G.; Gal-Yam, E.N. The nuclear-envelope protein and transcriptional repressor LAP2β interacts with HDAC3 at the nuclear periphery, and induces histone H4 deacetylation. *J. Cell Sci.* **2005**, *118*, 4017–4025. [CrossRef]
152. Demmerle, J.; Koch, A.J.; Holaska, J.M. The Nuclear Envelope Protein Emerin Binds Directly to Histone Deacetylase 3 (HDAC3) and Activates HDAC3 Activity. *J. Biol. Chem.* **2012**, *287*, 22080–22088. [CrossRef] [PubMed]
153. Milon, B.C.; Cheng, H.; Tselebrovsky, M.V.; Lavrov, S.A.; Nenasheva, V.V.; Mikhaleva, E.A.; Shevelyov, Y.Y.; Nurminsky, D.I. Role of Histone Deacetylases in Gene Regulation at Nuclear Lamina. *PLoS ONE* **2012**, *7*, e49692. [CrossRef] [PubMed]
154. Verboon, J.M.; Rincon-Arano, H.; Werwie, T.R.; Delrow, J.J.; Scalzo, D.; Nandakumar, V.; Groudine, M.; Parkhurst, S.M. Wash Interacts with Lamin and Affects Global Nuclear Organization. *Curr. Biol.* **2015**, *25*, 804–810. [CrossRef] [PubMed]
155. Ulianov, S.V.; Doronin, S.A.; Khrameeva, E.E.; Kos, P.I.; Luzhin, A.V.; Starikov, S.S.; Galitsyna, A.A.; Nenasheva, V.V.; Ilyin, A.A.; Flyamer, I.M.; et al. Nuclear lamina integrity is required for proper spatial organization of chromatin in Drosophila. *Nat. Commun.* **2019**, *10*, 1176. [CrossRef]
156. Akhtar, W.; de Jong, J.; Pindyurin, A.V.; Pagie, L.; Meuleman, W.; de Ridder, J.; Berns, A.; Wessels, L.F.A.; van Lohuizen, M.; van Steensel, B. Chromatin Position Effects Assayed by Thousands of Reporters Integrated in Parallel. *Cell* **2013**, *154*, 914–927. [CrossRef]
157. Shevelyov, Y.Y.; Lavrov, S.A.; Mikhaylova, L.M.; Nurminsky, I.D.; Kulathinal, R.J.; Egorova, K.S.; Rozovsky, Y.M.; Nurminsky, D.I. The B-type lamin is required for somatic repression of testis-specific gene clusters. *Proc. Natl. Acad. Sci. USA* **2009**, *106*, 3282–3287. [CrossRef]
158. Kind, J.; Pagie, L.; Ortabozkoyun, H.; Boyle, S.; de Vries, S.S.; Janssen, H.; Amendola, M.; Nolen, L.D.; Bickmore, W.A.; van Steensel, B. Single-Cell Dynamics of Genome-Nuclear Lamina Interactions. *Cell* **2013**, *153*, 178–192. [CrossRef]
159. Poleshko, A.; Shah, P.P.; Gupta, M.; Babu, A.; Morley, M.P.; Manderfield, L.J.; Ifkovits, J.L.; Calderon, D.; Aghajanian, H.; Sierra-Pagán, J.E.; et al. Genome-Nuclear Lamina Interactions Regulate Cardiac Stem Cell Lineage Restriction. *Cell* **2017**, *171*, 573–587.e14. [CrossRef]
160. van Steensel, B.; Belmont, A.S. Lamina-Associated Domains: Links with Chromosome Architecture, Heterochromatin, and Gene Repression. *Cell* **2017**, *169*, 780–791. [CrossRef]
161. Tang, S.-J. Chromatin Organization by Repetitive Elements (CORE): A Genomic Principle for the Higher-Order Structure of Chromosomes. *Genes* **2011**, *2*, 502–515. [CrossRef]
162. van de Werken, H.J.G.; Haan, J.C.; Feodorova, Y.; Bijos, D.; Weuts, A.; Theunis, K.; Holwerda, S.J.B.; Meuleman, W.; Pagie, L.; Thanisch, K.; et al. Small chromosomal regions position themselves autonomously according to their chromatin class. *Genome Res.* **2017**, *27*, 922–933. [CrossRef] [PubMed]
163. Larson, A.G.; Elnatan, D.; Keenen, M.M.; Trnka, M.J.; Johnston, J.B.; Burlingame, A.L.; Agard, D.A.; Redding, S.; Narlikar, G.J. Liquid droplet formation by HP1α suggests a role for phase separation in heterochromatin. *Nature* **2017**, *547*, 236–240. [CrossRef]
164. Strom, A.R.; Emelyanov, A.V.; Mir, M.; Fyodorov, D.V.; Darzacq, X.; Karpen, G.H. Phase separation drives heterochromatin domain formation. *Nature* **2017**, *547*, 241–245. [CrossRef] [PubMed]
165. Falk, M.; Feodorova, Y.; Naumova, N.; Imakaev, M.; Lajoie, B.R.; Leonhardt, H.; Joffe, B.; Dekker, J.; Fudenberg, G.; Solovei, I.; et al. Heterochromatin drives compartmentalization of inverted and conventional nuclei. *Nature* **2019**, *570*, 395–399. [CrossRef] [PubMed]
166. Riddle, N.C.; Minoda, A.; Kharchenko, P.V.; Alekseyenko, A.A.; Schwartz, Y.B.; Tolstorukov, M.Y.; Gorchakov, A.A.; Jaffe, J.D.; Kennedy, C.; Linder-Basso, D.; et al. Plasticity in patterns of histone modifications and chromosomal proteins in *Drosophila* heterochromatin. *Genome Res.* **2011**, *21*, 147–163. [CrossRef] [PubMed]
167. Smith, C.D.; Shu, S.; Mungall, C.J.; Karpen, G.H. The Release 5.1 Annotation of *Drosophila melanogaster* Heterochromatin. *Science* **2007**, *316*, 1586–1591. [CrossRef]
168. Lee, Y.C.G.; Ogiyama, Y.; Martins, N.M.C.; Beliveau, B.J.; Acevedo, D.; Wu, C.-T.; Cavalli, G.; Karpen, G.H. Pericentromeric heterochromatin is hierarchically organized and spatially contacts H3K9me2 islands in euchromatin. *PLoS Genet.* **2020**, *16*, e1008673. [CrossRef]
169. Jagannathan, M.; Cummings, R.; Yamashita, Y.M. The modular mechanism of chromocenter formation in Drosophila. *eLife* **2019**, *8*, e43938. [CrossRef]
170. Zhang, P.; Spradling, A.C. The Drosophila salivary gland chromocenter contains highly polytenized subdomains of mitotic heterochromatin. *Genetics* **1995**, *139*, 659–670. [CrossRef]

171. Jones, K.W. Chromosomal and Nuclear Location of Mouse Satellite DNA in Individual Cells. *Nature* **1970**, *225*, 912–915. [CrossRef] [PubMed]
172. Zenk, F.; Zhan, Y.; Kos, P.; Löser, E.; Atinbayeva, N.; Schächtle, M.; Tiana, G.; Giorgetti, L.; Iovino, N. HP1 drives de novo 3D genome reorganization in early Drosophila embryos. *Nature* **2021**, *593*, 289–293. [CrossRef] [PubMed]
173. Erdel, F.; Rademacher, A.; Vlijm, R.; Tünnermann, J.; Frank, L.; Weinmann, R.; Schweigert, E.; Yserentant, K.; Hummert, J.; Bauer, C.; et al. Mouse Heterochromatin Adopts Digital Compaction States without Showing Hallmarks of HP1-Driven Liquid-Liquid Phase Separation. *Mol. Cell* **2020**, *78*, 236–249.e7. [CrossRef] [PubMed]
174. Beck, M.; Hurt, E. The nuclear pore complex: Understanding its function through structural insight. *Nat. Rev. Mol. Cell Biol.* **2017**, *18*, 73–89. [CrossRef]
175. Vaquerizas, J.M.; Suyama, R.; Kind, J.; Miura, K.; Luscombe, N.M.; Akhtar, A. Nuclear Pore Proteins Nup153 and Megator Define Transcriptionally Active Regions in the Drosophila Genome. *PLoS Genet.* **2010**, *6*, e1000846. [CrossRef] [PubMed]
176. Gozalo, A.; Duke, A.; Lan, Y.; Pascual-Garcia, P.; Talamas, J.A.; Nguyen, S.C.; Shah, P.P.; Jain, R.; Joyce, E.F.; Capelson, M. Core Components of the Nuclear Pore Bind Distinct States of Chromatin and Contribute to Polycomb Repression. *Mol. Cell* **2020**, *77*, 67–81.e7. [CrossRef]
177. Capelson, M.; Liang, Y.; Schulte, R.; Mair, W.; Wagner, U.; Hetzer, M.W. Chromatin-Bound Nuclear Pore Components Regulate Gene Expression in Higher Eukaryotes. *Cell* **2010**, *140*, 372–383. [CrossRef]
178. Kalverda, B.; Pickersgill, H.; Shloma, V.V.; Fornerod, M. Nucleoporins Directly Stimulate Expression of Developmental and Cell-Cycle Genes Inside the Nucleoplasm. *Cell* **2010**, *140*, 360–371. [CrossRef]
179. Pascual-Garcia, P.; Jeong, J.; Capelson, M. Nucleoporin Nup98 Associates with Trx/MLL and NSL Histone-Modifying Complexes and Regulates Hox Gene Expression. *Cell Rep.* **2014**, *9*, 433–442. [CrossRef]
180. Pascual-Garcia, P.; Debo, B.; Aleman, J.R.; Talamas, J.A.; Lan, Y.; Nguyen, N.H.; Won, K.J.; Capelson, M. Metazoan Nuclear Pores Provide a Scaffold for Poised Genes and Mediate Induced Enhancer-Promoter Contacts. *Mol. Cell* **2017**, *66*, 63–76. [CrossRef]
181. Ibarra, A.; Benner, C.; Tyagi, S.; Cool, J.; Hetzer, M.W. Nucleoporin-mediated regulation of cell identity genes. *Genes Dev.* **2016**, *30*, 2253–2258. [CrossRef]
182. Tan-Wong, S.M.; Wijayatilake, H.D.; Proudfoot, N.J. Gene loops function to maintain transcriptional memory through interaction with the nuclear pore complex. *Genes Dev.* **2009**, *23*, 2610–2624. [CrossRef]
183. Strom, A.R.; Brangwynne, C.P. The liquid nucleome—Phase transitions in the nucleus at a glance. *J. Cell Sci.* **2019**, *132*, jcs235093. [CrossRef]
184. Banani, S.F.; Lee, H.O.; Hyman, A.A.; Rosen, M.K. Biomolecular condensates: Organizers of cellular biochemistry. *Nat. Rev. Mol. Cell Biol.* **2017**, *18*, 285–298. [CrossRef]
185. King, J.T.; Shakya, A. Phase separation of DNA: From past to present. *Biophys. J.* **2021**, *120*, 1139–1149. [CrossRef]
186. Gibson, B.A.; Doolittle, L.K.; Schneider, M.W.G.; Jensen, L.E.; Gamarra, N.; Henry, L.; Gerlich, D.W.; Redding, S.; Rosen, M.K. Organization of Chromatin by Intrinsic and Regulated Phase Separation. *Cell* **2019**, *179*, 470–484.e21. [CrossRef] [PubMed]
187. Plys, A.J.; Davis, C.P.; Kim, J.; Rizki, G.; Keenen, M.M.; Marr, S.K.; Kingston, R.E. Phase separation of polycomb-repressive complex 1 is governed by a charged disordered region of CBX2. *Genes Dev.* **2019**, *33*, 799–813. [CrossRef] [PubMed]
188. Lau, M.S.; Schwartz, M.G.; Kundu, S.; Savol, A.J.; Wang, P.I.; Marr, S.K.; Grau, D.J.; Schorderet, P.; Sadreyev, R.I.; Tabin, C.J.; et al. Mutation of a nucleosome compaction region disrupts Polycomb-mediated axial patterning. *Science* **2017**, *355*, 1081–1084. [CrossRef]
189. Whyte, W.A.; Orlando, D.A.; Hnisz, D.; Abraham, B.J.; Lin, C.Y.; Kagey, M.H.; Rahl, P.B.; Lee, T.I.; Young, R.A. Master Transcription Factors and Mediator Establish Super-Enhancers at Key Cell Identity Genes. *Cell* **2013**, *153*, 307–319. [CrossRef] [PubMed]
190. Pott, S.; Lieb, J.D. What are super-enhancers? *Nat. Genet.* **2015**, *47*, 8–12. [CrossRef]
191. Sabari, B.R.; Dall'Agnese, A.; Boija, A.; Klein, I.A.; Coffey, E.L.; Shrinivas, K.; Abraham, B.J.; Hannett, N.M.; Zamudio, A.V.; Manteiga, J.C.; et al. Coactivator condensation at super-enhancers links phase separation and gene control. *Science* **2018**, *361*, eaar3958. [CrossRef]
192. Cho, W.-K.; Spille, J.-H.; Hecht, M.; Lee, C.; Li, C.; Grube, V.; Cisse, I.I. Mediator and RNA polymerase II clusters associate in transcription-dependent condensates. *Science* **2018**, *361*, 412–415. [CrossRef] [PubMed]
193. Mir, M.; Stadler, M.R.; Ortiz, S.A.; Hannon, C.E.; Harrison, M.M.; Darzacq, X.; Eisen, M.B. Dynamic multifactor hubs interact transiently with sites of active transcription in Drosophila embryos. *eLife* **2018**, *7*, e40497. [CrossRef] [PubMed]
194. Boehning, M.; Dugast-Darzacq, C.; Rankovic, M.; Hansen, A.S.; Yu, T.; Marie-Nelly, H.; McSwiggen, D.T.; Kokic, G.; Dailey, G.M.; Cramer, P.; et al. RNA polymerase II clustering through carboxy-terminal domain phase separation. *Nat. Struct. Mol. Biol.* **2018**, *25*, 833–840. [CrossRef] [PubMed]
195. Boija, A.; Klein, I.A.; Sabari, B.R.; Dall'Agnese, A.; Coffey, E.L.; Zamudio, A.V.; Li, C.H.; Shrinivas, K.; Manteiga, J.C.; Hannett, N.M.; et al. Transcription Factors Activate Genes through the Phase-Separation Capacity of Their Activation Domains. *Cell* **2018**, *175*, 1842–1855. [CrossRef] [PubMed]
196. Cardozo Gizzi, A.M.; Cattoni, D.I.; Fiche, J.-B.; Espinola, S.M.; Gurgo, J.; Messina, O.; Houbron, C.; Ogiyama, Y.; Papadopoulos, G.L.; Cavalli, G.; et al. Microscopy-Based Chromosome Conformation Capture Enables Simultaneous Visualization of Genome Organization and Transcription in Intact Organisms. *Mol. Cell* **2019**, *74*, 212–222. [CrossRef] [PubMed]
197. Cardozo Gizzi, A.M.; Espinola, S.M.; Gurgo, J.; Houbron, C.; Fiche, J.-B.; Cattoni, D.I.; Nollmann, M. Direct and simultaneous observation of transcription and chromosome architecture in single cells with Hi-M. *Nat. Protoc.* **2020**, *15*, 840–876. [CrossRef]

198. Askjaer, P.; Harr, J.C. Genetic approaches to revealing the principles of nuclear architecture. *Curr. Opin. Genet. Dev.* **2021**, *67*, 52–60. [CrossRef]
199. Jerkovic, I.; Cavalli, G. Understanding 3D genome organization by multidisciplinary methods. *Nat. Rev. Mol. Cell Biol.* **2021**, *22*, 511–528. [CrossRef]
200. Nguyen, H.Q.; Chattoraj, S.; Castillo, D.; Nguyen, S.C.; Nir, G.; Lioutas, A.; Hershberg, E.A.; Martins, N.M.C.; Reginato, P.L.; Hannan, M.; et al. 3D mapping and accelerated super-resolution imaging of the human genome using in situ sequencing. *Nat. Methods* **2020**, *17*, 822–832. [CrossRef]

APPENDIX III

Publication (Camilleri-Robles *et al*., 2024)

FEBS Letters

FEBS PRESS science publishing by scientists

RESEARCH LETTER

A shift in chromatin binding of phosphorylated p38 precedes transcriptional changes upon oxidative stress

Carlos Camilleri-Robles, Paula Climent-Cantó*, Palmira Llorens-Giralt, Cecilia C. Klein, Florenci Serras and Montserrat Corominas

Departament de Genètica, Microbiologia i Estadística, Facultat de Biologia and Institut de Biomedicina (IBUB), Universitat de Barcelona, Spain

Correspondence
M. Corominas, Departament de Genètica, Microbiologia i Estadística, Facultat de Biologia and Institut de Biomedicina (IBUB), Universitat de Barcelona, Diagonal 643, 08028 Barcelona, Catalonia, Spain
Tel: +34 934037003
E-mail: mcorominas@ub.edu

Present address
*Hereditary Cancer Program, IDIBELL, L'Hospitalet de Llobregat, Barcelona, Spain

(Received 17 June 2024, revised 24 July 2024, accepted 2 August 2024)

doi:10.1002/1873-3468.15006

Edited by Francesc Posas

P38 mitogen-activated protein kinases are key in the regulation of the cellular response to stressors. P38 is known to regulate transcription, mRNA processing, stability, and translation. The transcriptional changes mediated by phosphorylated p38 (P-p38) in response to extracellular stimuli have been thoroughly analyzed in many tissues and organisms. However, the genomic localization of chromatin-associated P-p38 remains poorly understood. Here, we analyze the chromatin binding of activated P-p38 and its role in the response to reactive oxygen species (ROS) in *Drosophila* S2 cells. We found that P-p38 is already bound to chromatin in basal conditions. After ROS exposure, chromatin-associated P-p38 relocates towards genes involved in the recovery process. Our findings highlight the role of P-p38 dynamic chromatin binding in orchestrating gene expression responses to oxidative stress.

Keywords: *Drosophila*; p38; ROS; stress; transcription

Many intracellular signaling pathways that are activated by environmental stimuli rely on the post-translational modifications of proteins, such as phosphorylation, driven by the balance between kinases and phosphatases. Mitogen-activated protein kinases (MAPKs) are highly conserved serine/threonine protein kinases involved in multiple signal transduction pathways [1]. MAPKs undergo sequential phosphorylation and activation by upstream kinases. They function both in the cytoplasm and in the nucleus, where they may interact with chromatin through direct binding to DNA or chromatin-associated substrates [2]. Exposure of cells to stress results in the rapid activation of the MAPKs JNK and p38, also known as stress-activated protein kinases (SAPKs) [1,3,4]. P38 is activated by several physical and chemical stressors and is involved in a broad range of cellular processes, such as proliferation, differentiation, regeneration, migration, and apoptosis [3–11].

In response to extracellular stimuli, specific upstream kinases phosphorylate p38 to activate its kinase domain and, subsequently, phosphorylated p38 (P-p38) will phosphorylate its substrates either in the cytoplasm or in the nucleus [1,4–6,12]. The nuclear translocation of p38 depends on p38 phosphorylation and on the action of importins [13–17]. In the nucleus, P-p38 substrates include different transcription factors (TFs), chromatin-modifying enzymes and remodelers, and core elements of the transcriptional machinery [18–23]. Moreover, p38

Abbreviations
ChIP-seq, chromatin immunoprecipitation sequencing; CTL, control; FDR, false discovery rate; GO, gene ontology; H_2O_2, hydrogen peroxide; H3K4me3, histone H3 lysine 4 trimethylation; MAPKs, mitogen-activated protein kinases; P-p38, phosphorylated p38; qPCR, quantitative PCR; SAPKs, stress-activated protein kinases; STR, stress; TES, transcription end site; TF, transcription factor; TSS, transcription start site.

can also localize at chromatin [24,25], indicating a direct regulation of gene expression and function at the chromatin level. The transcriptional response mediated by p38 has been analyzed in several organisms. P38 signaling is critical to elicit the early gene expression program required for mouse embryonic fibroblasts adaptation to stress [26]. In yeast, p38 homolog Hog1 plays a key role in global gene regulation under saline stress [27]. Additionally, p38 mediates changes in gene expression in cellular processes unrelated to stress. It regulates TEF-1 and C/EBPbeta transcriptional activity in proliferating cardiomyocytes [18], promotes muscle-specific gene expression [28], and mediates tumor necrosis factor alpha signaling [29].

The production of reactive oxygen species (ROS), as byproducts of metabolism, is a source of oxidative stress that can be harmful for the cell. However, at physiological levels, ROS are also considered beneficial as they can act as signaling molecules [30–32]. ROS can be produced during aerobic respiration in the mitochondria as well as by several enzymes located in different cellular compartments, including peroxisomes, the endoplasmic reticulum, and the plasma membrane [32]. The most abundant type of ROS inside the cell is hydrogen peroxide (H_2O_2), which is produced by different stimuli [32]. In *Drosophila*, physiological levels of ROS have been shown to control key cellular and developmental processes, such as neuronal plasticity, stem cell proliferation and maintenance, and differentiation of immune cells upon infection [32–34]. A role for P-p38 by reducing ROS levels has also been reported during embryonic wound repair in flies [35]. Moreover, ROS-induced JNK and p38 signaling are required to activate the cytokines Unpaired (Upd) during regeneration of wing imaginal discs [10] and to mediate the regenerative response in the adult midgut [36]. In this study, we explore the chromatin localization of P-p38 in response to oxidative stress in *Drosophila* S2 cells. We find that P-p38 is already bound to chromatin in control conditions, but it changes its localization in the genome after exposure to H_2O_2.

A Catalan version of the article's abstract is available at: https://doi.org/10.5281/zenodo.13388878

Materials and methods

Induction of oxidative stress in Drosophila S2 cells

Drosophila S2 cells (ATCC CRL-1963) were grown in Schneider's medium (Sigma-Aldrich, St. Louis, MO, USA) supplemented with 10% FBS (Gibco, Waltham, MA, USA), 100 mg·mL^{-1} of streptomycin, and 100 mg·mL^{-1} of penicillin at 25 °C. For the induction of oxidative stress, cells were grown to 5 × 10^6 cells·mL^{-1} and incubated with three different concentrations of H_2O_2 (Sigma-Aldrich, 516813) diluted in Schneider's medium: 5, 10, or 20 mM. The same volume of Schneider's medium was added to the control cells. Cells were incubated at 25 °C for the indicated time. To calculate the cell survival upon H_2O_2 treatment, we stained the cells using Trypan Blue and counted the number of living and dead cells using a Neubauer chamber.

Antibodies

The antibodies used in these experiments were: anti-P-p38 (Cell Signaling Technology, Danvers, MA, USA, 9211), anti-histone H3 trimethyl Lys4 (H3K4me3; Abcam, Cambridge, UK, ab8580), anti-histone H3 (Abcam, ab1791), and anti-α-tubulin (Invitrogen, Waltham, MA, USA, A11126). The commercial secondary antibodies used were coupled to horseradish peroxidase (Jackson ImmunoResearch, West Grove, PA, USA) or Alexa fluorophores (Invitrogen).

Immunostaining

For the immunostaining experiments, cells were attached to slides previously treated with concanavalin A (0.5 mg·mL^{-1}; Sigma, C5275), washed with PBS for 10 min with agitation and fixed in 4% paraformaldehyde for 15 min. After fixation, cells were washed with agitation for 15 min in PBS, and in PBST (PBS-0.3% Triton X-100) containing 0.2% BSA for 10 min twice. The anti-P-p38 (1 : 100) primary antibody was diluted in PBST-0.2% BSA and added to the cells, which were incubated overnight with slow agitation at 4 °C. The next day, cells were washed three times with PBST-0.2% BSA and incubated with the secondary antibody (1 : 200) diluted in PBST-0.2% BSA for 1 h at room temperature with agitation. Cells were then washed twice for 10 min in PBST and incubated with Phalloidin (1 : 75; Invitrogen, A12379) for 30 min. Cells were then washed four times with PBS and mounted in SlowFade Diamond Antifade Mountant with DAPI (Invitrogen, S36964).

Images were recorded on a Zeiss LSM 880 microscope. Nuclear and cytoplasmic P-p38 signal intensity was measured for 10 cells per condition. Two-way ANOVA followed by Sidak's multiple comparison test were used to address differences in cytoplasmic and nuclear P-p38 signal among different conditions. One-way ANOVA followed by Sidak's multiple comparison test were used to address differences in the nuclear to cytoplasmic P-p38 signal among different conditions.

Chromatin immunoprecipitation (ChIP)

Cells were collected and fixed in 1% formaldehyde for 10 min at room temperature by gentle mixing. Glycine was added to a final concentration of 125 mM to stop

crosslinking. After 5 min, cells were spun down for 2 min at 1500 ***g*** and washed with 5 mL of PBS. Cells were then resuspended in 10 mL of wash buffer A (10 mM HEPES pH 7.9, 10 mM EDTA, 0.5 mM EGTA, and 0.25% Triton X-100) and incubated for 10 min at 4 °C on a rotating wheel. Cells were spun down again and resuspended in 10 mL of wash buffer B (10 mM HEPES, pH 7.9, 100 mM NaCl, 1 mM EDTA, 0.5 mM EGTA, and 0.01% Triton X-100), incubated for 10 min on a rotating wheel at 4 °C and spun down again. Cells were lysed in 5 mL of TE (10 mM Tris–HCl, pH 8, and 1 mM EDTA) and 1% SDS. Chromatin was washed three times with 5 mL of TE and resuspended in TE containing 1 mM phenylmethanesulfonyl fluoride (PMSF) and 0.1% SDS. Chromatin was sonicated in a Bioruptor sonicator (Diagenode, Seraing, Belgium) to obtain fragments of 200–500 bp. Lysates were adjusted with 1% Triton X-100, 0.1% sodium deoxycholate (DOC), and 140 mM NaCl, before being incubated for 10 min on a rotating wheel at 4 °C. Chromatin was then recovered by centrifugation.

For each experiment, 40 µL of chromatin were used for the input sample, while two aliquots of 400 µL were used for the immunoprecipitation (IP) of P-p38 and H3K4me3. IPs were carried out using RIPA buffer (140 mM NaCl, 10 mM Tris–HCl, pH 8, 1 mM EDTA, 1% Triton X-100, 0.01% SDS, and 0.1% DOC). The preclearing of chromatin samples was performed on a rotating wheel for 1 h at 4 °C with 30 µL of 50% (v/v) protein A-Sepharose CL4B beads (GE Healthcare, Chicago, IL, USA, 17-0780-01) previously blocked with RIPA-1% BSA. The antibody was added, and the incubation was performed overnight at 4 °C on a rotating wheel. IPs were performed by adding 40 µL of 50% (v/v) protein A-Sepharose CL4B beads previously blocked with RIPA-1% BSA and incubating the samples on a rotating wheel for 3 h at 4 °C. Beads were washed five times for 5 min in 1 mL of RIPA, once for 5 min in 250 mM LiCl buffer (250 mM LiCl, 10 mM Tris–HCl, pH 8, 1 mM EDTA, 0.5% NP-40, and 0.5% DOC) and twice for 5 min in TE. Then, the beads were resuspended in 40 µL of TE, and DNase-free RNase A was added at 0.25 $\mu g \cdot mL^{-1}$ to the IPs and input samples and incubated for 30 min at 37 °C. Samples were adjusted with 1% SDS, 0.1 M $NaHCO_3$, and 0.2 $mg \cdot mL^{-1}$ of Proteinase K and incubated overnight at 65 °C for decrosslinking. DNA was purified with phenol-chloroform extraction. The antibodies used were anti-P-p38 and anti-H3K4me3. Library preparation and sequencing using the HiSeq 2500 system were undertaken at the CRG Genomics Unit (Barcelona, Spain). Two biological replicates and their corresponding inputs were sequenced per condition.

ChIP-seq data processing and analysis

Data were processed using the chip-nf pipeline (https://github.com/guigolab/chip-nf; revision: 47c471b6f4 [v0.2.3]; NEXTFLOW v19.07.0). Reads were continuously mapped to the fly genome (dm6), with up to two mismatches using the GEM mapper [37]. Only alignments for reads mapping to 10 or fewer loci were reported. Duplicated reads were removed using Picard (http://broadinstitute.github.io/picard/). The fragment length was set to 200 bp. We ran MACS2 [38] to identify the regions significantly enriched on ChIP-Seq reads from each sample in comparison to the normalized input control. We retained peaks that had at least 50% overlap in each replicate using the BEDTOOLS INTERSECTBED tool [39]. Peak scores were rescaled to conform to the format supported by the UCSC genome browser (score must be < 1000). Peaks spanning < 50 bp or located in non-canonical chromosomes were discarded. Peaks showing ≥ 50% overlap in control and stress conditions were considered the same peak. Coordinates of identified P-p38 and H3K4me3 peaks are shown in Table S1 and Table S2, respectively.

P-p38 peaks were classified based on their genomic location into: promoter, if the peak center was positioned within −500 bp and +100 bp from the TSS of a gene; gene body, if the peak overlapped at least 1 bp with a gene body; and intergenic, if none of the previous applied. H3K4me3 peaks were classified into: promoter, if the peak overlapped at least 1 bp with the region located ±500 bp from a TSS; and gene body, if the peak overlapped at least 1 bp with a gene body. Intergenic H3K4me3 peaks were not considered. Peak classification was mutually exclusive in the following rank: promoter > gene body > intergenic.

Average plots and heatmaps were calculated for identified promoter, gene body, and intergenic P-p38 peaks in Fig. S2, and for promoter and gene body H3K4me3 peaks in Fig. S3. Bigwig files from input and experimental replicates for control and stress conditions were used. Metagene plots for genes associated with P-p38 and H3K4me3 peaks shown in Fig. 2C,F, respectively, were generated using the bigwig average of the two experimental replicates per condition.

RNA extraction and quantitative PCR (qPCR)

For expression analysis, total RNA was isolated from 10^7 cells using Trizol (Ambion, Waltham, MA, USA) and the RNA Clean and Concentrator kit (Zymo Research, Irvine, CA, USA). A total of 1 µg of RNA was used as template for cDNA synthesis using Moloney Murine Leukemia Virus reverse transcriptase (M-MLV) (Invitrogen).

Reactions containing FastStart Universal SYBR Green Master (Rox) (Roche, Basel, Switzerland), the appropriate cDNA, and primers were run in a 7500 Real-Time PCR System (Applied Biosystems, Foster City, CA, USA). The levels of *sply* were used to normalize the samples, and relative RNA expression was calculated using the ddCt method. Three technical replicates were used for each reaction, and three separate biological replicates were collected

for each experiment. Primer sequences used are shown in Table S3.

RNA-seq library preparation, data processing, and analysis

Sequencing libraries were prepared using the TruSeq Stranded mRNA Library Prep kit (Illumina, San Diego, CA, USA), following the manufacturer's instructions. Paired-end sequencing was performed in a HiSeq 2500 sequencer. Library preparation and sequencing were undertaken at the CRG Genomics Unit (Barcelona, Spain). Three biological replicates were sequenced per condition.

Data were processed using grape-nf (available at https://github.com/guigolab/grape-nf; revision: 5fb9c88236 [v0.2.1]; NEXTFLOW version 19.07.0). RNA-seq reads were aligned to the fly genome (dm6) using the STAR 2.4.0j software [40], with up to 4 mismatches per paired alignment using the FlyBase genome annotation r6.36 [41]. Only alignments for reads mapping to 10 or fewer loci were reported. Gene and transcript TPMs were quantified using RSEM [42]. Differential gene expression analysis (DEA) was performed using DESeq2 [43]. Low count genes (less than 10 counts across all samples) were filtered out before DEA. No outlier sample was indicated by Cook's distance method available in DESeq2. Shrinkage of log fold change values was performed using ashr method [44]. A fold change $\geq |1.5|$ and an adjusted P-value < 0.05 were used to consider a gene to be differentially expressed. Kruskal–Wallis test followed by Dunn's test for multiple comparisons were used to analyze differences in gene expression between groups. A minimum P value < 0.05 was set for significance. The list of differentially expressed genes is shown in Table S4.

Hierarchical clustering of genes associated with P-p38

For gene clustering, we used available RNA-seq data from S2 cells in control conditions (Pre-treatment), after 3 h of sodium arsenite exposure (Post-treatment), and after 3 h of recovery in control media (Recovery) [45]. Three biological replicates were used for each condition. We discarded genes that were not expressed in any sample by removing all genes whose sum of counts was < 10. Complete hierarchical clustering of genes associated with P-p38 was based on the Euclidean distance calculated using z-scores for each gene. Three main dendrogram branches were used for the assignment of genes into Clusters 1, 2, and 3.

Functional annotation of genes and motif enrichment analysis

We used the CLUSTERPROFILER tool version 3.10.1 [46] from Bioconductor to identify the enriched Gene Ontology (GO) terms in our study. We searched for enriched biological process terms setting a < 0.01 P-value cutoff and using False Discovery Rate (FDR) as adjustment method.

We used the AME TOOL version 5.5.3 [47] to search for significantly enriched motifs in P-p38 peaks. We selected the input motifs from the JASPAR 2022 Insects database [48]. We selected a < 10 E-score to consider significant hits and used the default options for the analysis. Only motifs from TFs expressed at least 1 TPM in at least one condition (Pre-treatment, Post-treatment, or Recovery) were considered.

Statistical analysis

To analyze differences across different treatments in Figs 1F,G, 2I and 3A', and S1, we used a two-way ANOVA followed by Dunnett's test for multiple comparisons. For evaluating differences in proportions among the different groups depicted in Figs 2B,E,H and 3C, we used a contingency table followed by a Chi-squared test with Bonferroni correction for multiple comparisons.

All statistical tests were two-tailed, with significance determined at P-values less than 0.05. All statistical tests were conducted using GRAPHPAD PRISM 9 (GraphPad Software, Boston, MA, USA) or R.

Results and Discussion

P-p38 accumulates in the nucleus upon oxidative stress

To explore the response of P-p38 to oxidative stress, we used *Drosophila* S2 cells, a model system previously employed to investigate p38 activation in stress conditions [49–51]. In agreement with prior research [49,51], we observed low levels of P-p38 in S2 cells under control conditions, predominantly located in the nucleus (Fig. 1A). To investigate the effect of oxidative stress in the nuclear localization of P-p38, we first determined the survival curve at various hydrogen peroxide (H_2O_2) concentrations and incubation times (Fig. S1). A low dose of 5 mM H_2O_2 did not induce changes in the P-p38 signal after a short exposure of 30 min (Fig. 1B,F), but it significantly increased the nuclear signal of P-p38 after 1 h of incubation (Fig. 1C,F). Conversely, a higher dose of 10 mM H_2O_2 significantly increased the nuclear signal of P-p38 after 30 min of treatment (Fig. 1D,F), but these levels did not show further increase after a longer exposure time (Fig. 1E,F).

In response to oxidative stress, we observed a dose- and time-dependent nuclear accumulation of P-p38, which aligns with earlier studies describing a rapid

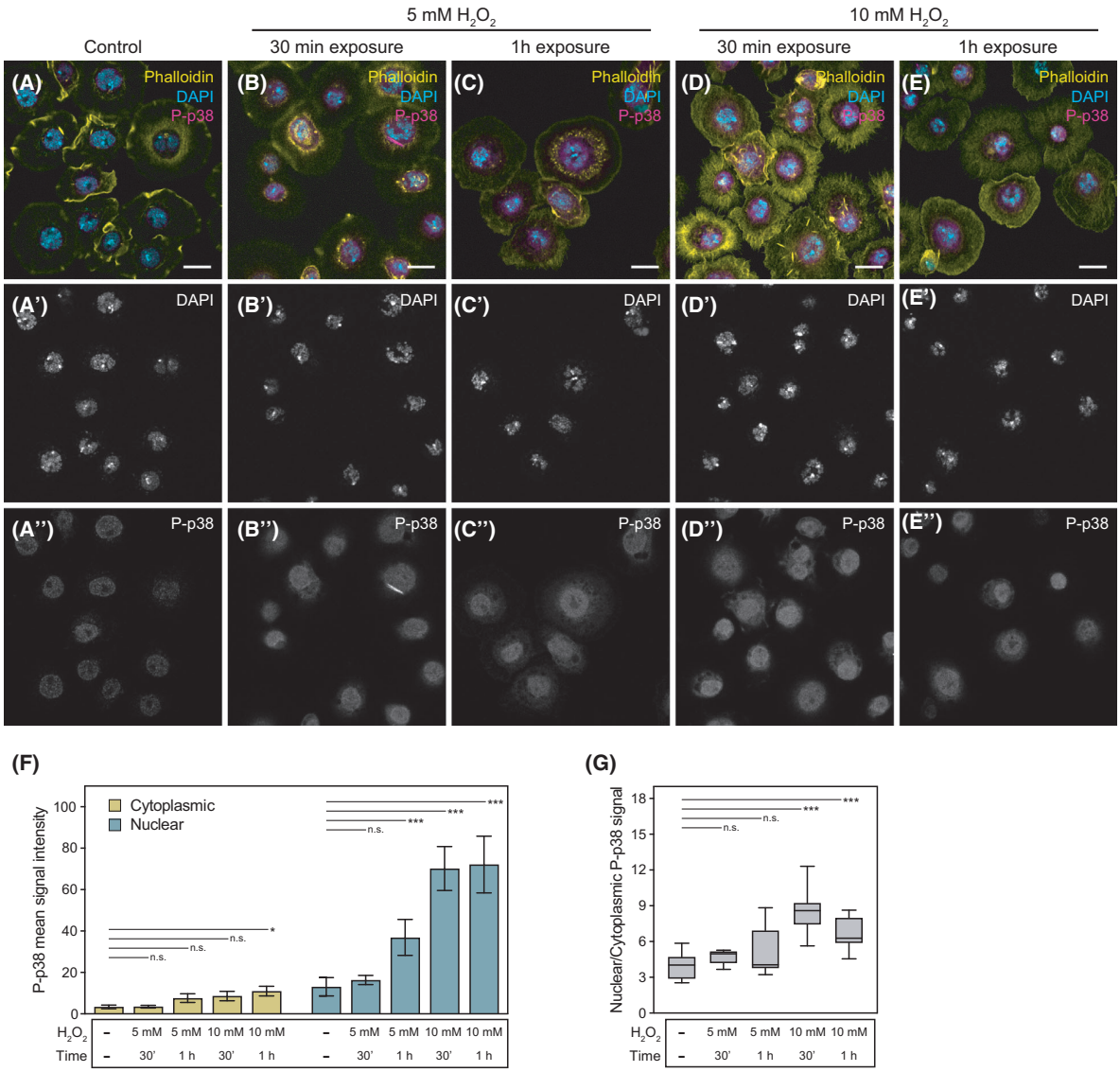

Fig. 1. Phosphorylated p38 accumulates in the nucleus upon exposure to H_2O_2. (A–E) Immunostaining of S2 cells after incubation with control media (A), after incubation with 5 mM H_2O_2 for 30 min (B) or 1 h (C), and after incubation with 10 mM H_2O_2 for 30 min (D) or 1 h (E). Top row (A–E) shows Phalloidin labeling the cytoplasm in yellow, DAPI labeling the nuclei in blue, and P-p38 signal in magenta. Middle row (A′–E′) shows DAPI. Bottom row (A″–E″) shows P-p38. Scale bar = 10 μm. (F) Quantification of P-p38 immunostaining. Mean signal intensity of P-p38 in the cytoplasm and in the nucleus is shown. Error bars represent the standard error (SD) of $N = 10$ cells. (G) Nuclear to cytoplasmic P-p38 signal ratio. Median and interquartile range of $N = 10$ cells are represented. Two-way ANOVA and Dunnett's test for multiple comparisons were used to assess significance in F and G. ***$P < 0.001$; *$P < 0.05$; n.s., non-significant.

nuclear translocation of active p38 in reaction to various stimuli [6]. We also found that subjecting S2 cells to a higher dose of 10 mM H_2O_2 for a short duration of 30 min maximized the P-p38 nuclear to cytoplasmic signal ratio (Fig. 1G). Consequently, subsequent experiments involved a 30-min incubation of S2 cells with 10 mM H_2O_2.

Oxidative stress induces changes in the chromatin localization of P-p38

Next, we analyzed the chromatin-binding profile of nuclear P-p38 by chromatin immunoprecipitation sequencing (ChIP-seq) in untreated cells (Control) and in 10 mM H_2O_2-treated cells (Stress). We found that

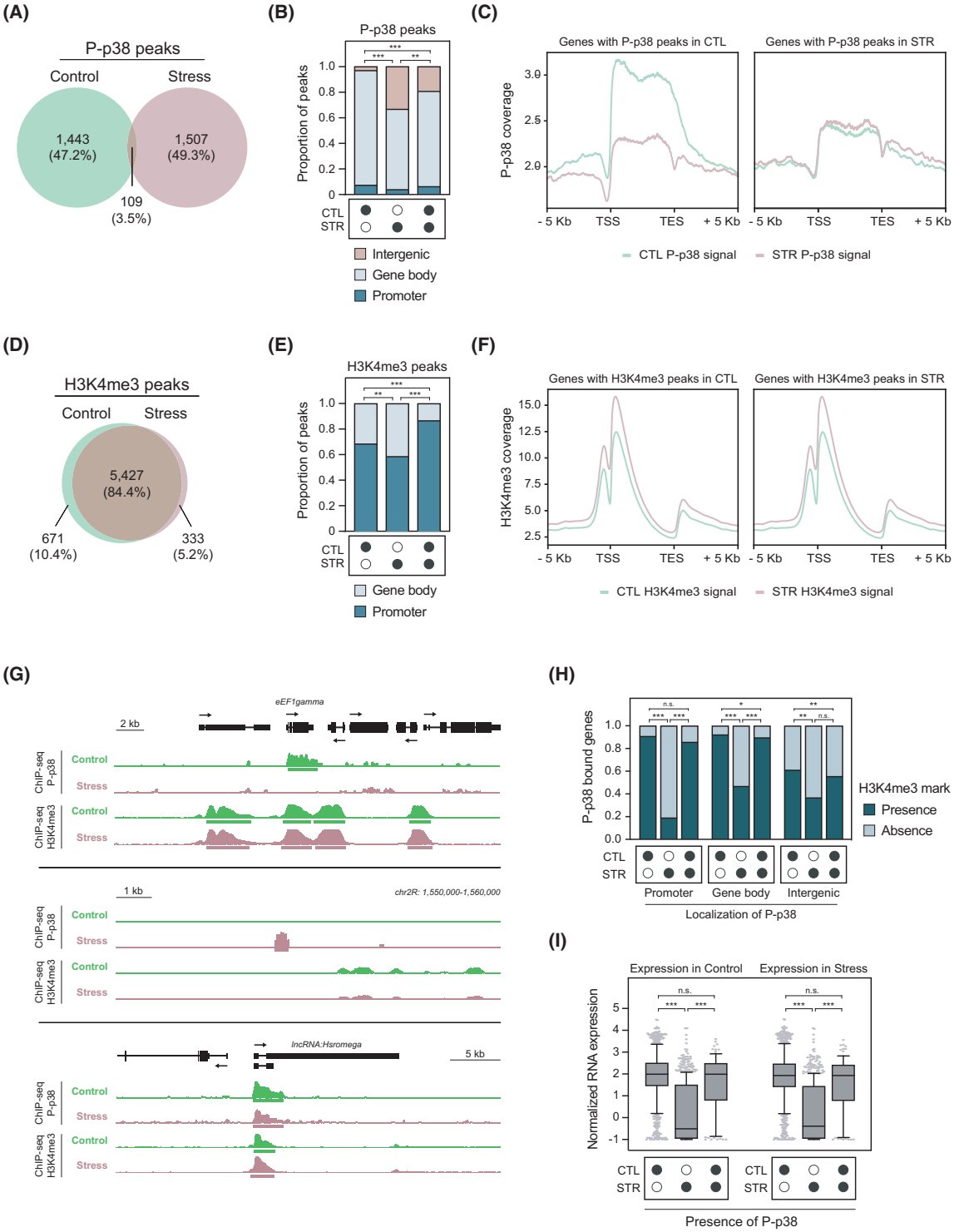

Fig. 2. P-p38 chromatin localization changes upon oxidative stress. (A) Number of P-p38 chromatin peaks identified in untreated control cells (Control), upon H_2O_2 exposure (Stress), and in both conditions. (B) Genomic distribution of P-p38 chromatin peaks for each condition. (C) Metagene plot showing the distribution of P-p38 signal along the genes associated with P-p38 peaks in control (left plot) and in stress (right plot). (D) Number of H3K4me3 chromatin peaks identified in untreated control cells (Control), upon H_2O_2 exposure (Stress), and in both conditions. (E) Genomic distribution of H3K4me3 chromatin peaks for each condition. (F) Metagene plot showing the distribution of H3K4me3 signal along the genes associated with H3K4me3 peaks in control (left plot) and in stress (right plot). (G) Screenshots of the UCSC Genome Browser showing P-p38 and H3K4me3 ChIP-seq tracks in Control and Stress conditions. Screenshot on top shows a P-p38 control peak present at the gene body of *eEF1gamma*. Screenshot at the middle shows a P-p38 stress peak in an intergenic region of chr 2R. Screenshot at the bottom shows a P-p38 peak present in control and stress conditions at the promoter of the *lncRNA:Hsromega*. ChIP-seq tracks shown are normalized to input. (H) Proportion of genes associated with P-p38 that contain H3K4me3 marks at their promoter or gene body. Proportions are calculated separately for genes associated with P-p38 in the promoter, gene body, or intergenic regions. (I) Expression of genes associated with P-p38 in the control, upon stress, or in both conditions. Relative gene expression in the control and after 30 min of 10 mM H_2O_2 exposure is shown and is represented as the $\log_{10}$ of TPMs plus a pseudocount of 0.1. CTL, control; STR, stress. Chi-squared test with Bonferroni correction for multiple comparisons was used to assess significance in B, E, and H. Two-way ANOVA and Dunnett's test for multiple comparisons were used to assess significance in I. ***$P < 0.001$; n.s., non-significant.

the number of P-p38 chromatin peaks was comparable in both conditions: 1552 peaks in the control and 1616 peaks in the stressed cells, with only 109 peaks shared between them (3.5% of the total identified P-p38 peaks) (Fig. 2A; Fig. S2). We classified peaks according to their position relative to the transcription start site (TSS) of their closest annotated gene and defined 3 types of peaks: promoter peaks (located −500 bp to +100 bp from the TSS), gene body peaks (overlapping exons or introns), and intergenic peaks. In control conditions, we found 7.3% of P-p38 peaks associated with promoter regions, 89.6% localized in the gene body, and only 3.1% in intergenic regions (Fig. 2B). However, exposure to H_2O_2 induced a redistribution of chromatin P-p38 across the genome, leading to an increase of intergenic peaks (33.3%), and a concurrent reduction of promoter and gene body peaks to 3.9% and 62.8%, respectively (Fig. 2B). Peaks present in both conditions showed intermediate percentages between control and stress peaks (Fig. 2B). Metagene plots reveal that the P-p38 signal is found along the entire gene body region, from the TSS to the transcription end site (TES) (Fig. 2C). Our results lead to two main conclusions: (a) P-p38 primarily associates with gene body regions, and (b) oxidative stress induces a redistribution of P-p38 to intergenic regions.

The major presence of P-p38 in gene body regions suggests that it may operate not only in the initiation, but also in the elongation of transcription. In yeast and mammals, p38 is present along the coding sequence and interacts with different elongation factors and the RNA polymerase machinery [21,24,52]. Indeed, in yeast, the phosphorylation of the transcription elongation factor Spt4 by p38 homolog Hog1 facilitates transcriptional elongation after osmotic shock [21]. A similar situation may occur in S2 cells, although further experiments are required to corroborate this hypothesis, as there have been no reports yet on the interaction of p38 and Spt4 in *Drosophila*. After stress, however, there is an increase in P-p38 bound to intergenic regions, suggesting a potential role for these regions as enhancers.

As a first approach to relate chromatin-associated P-p38 to gene expression, we examined the tri-methylation of lysine 4 on histone H3 (H3K4me3) by ChIP-seq in control and stressed cells. H3K4me3 is a chromatin modification typically restricted to narrow regions around the TSS of expressed genes, although it can also be found covering extensively the coding regions of some genes [53]. The majority of H3K4me3 peaks identified were present in both conditions (5427 peaks; 84.4% of total), while a small fraction was present only in control (671 peaks; 10.4%) or stress (333 peaks; 5.2%) (Fig. 2D; Fig. S3). As expected, most H3K4me3 peaks were primarily located close to the TSS (Fig. 2E,F). The presence of H3K4me3 marks in almost identical positions in control and stressed cells suggests that very few changes in gene expression occurred after 30 min of H_2O_2 exposure (Fig. 2D–F).

Next, we analyzed the correlation between P-p38 and H3K4me3. We observed that genes associated with P-p38 in the promoter or gene body after stress were less marked by H3K4me3 than genes containing P-p38 in the same genomic regions in control or in both conditions (Fig. 2G,H). This suggests that, upon stress, P-p38 preferentially binds to lowly expressed genes. We then assigned P-p38 intergenic peaks to the nearest gene [54]. We found that these genes also displayed lower levels of H3K4me3 in their promoter and gene body regions (Fig. 2G,H), indicating less expression. To further link P-p38 binding to gene expression, we performed RNA-seq. In accordance with the levels of H3K4me3, we observed that the expression of genes associated with P-p38 under stress was significantly

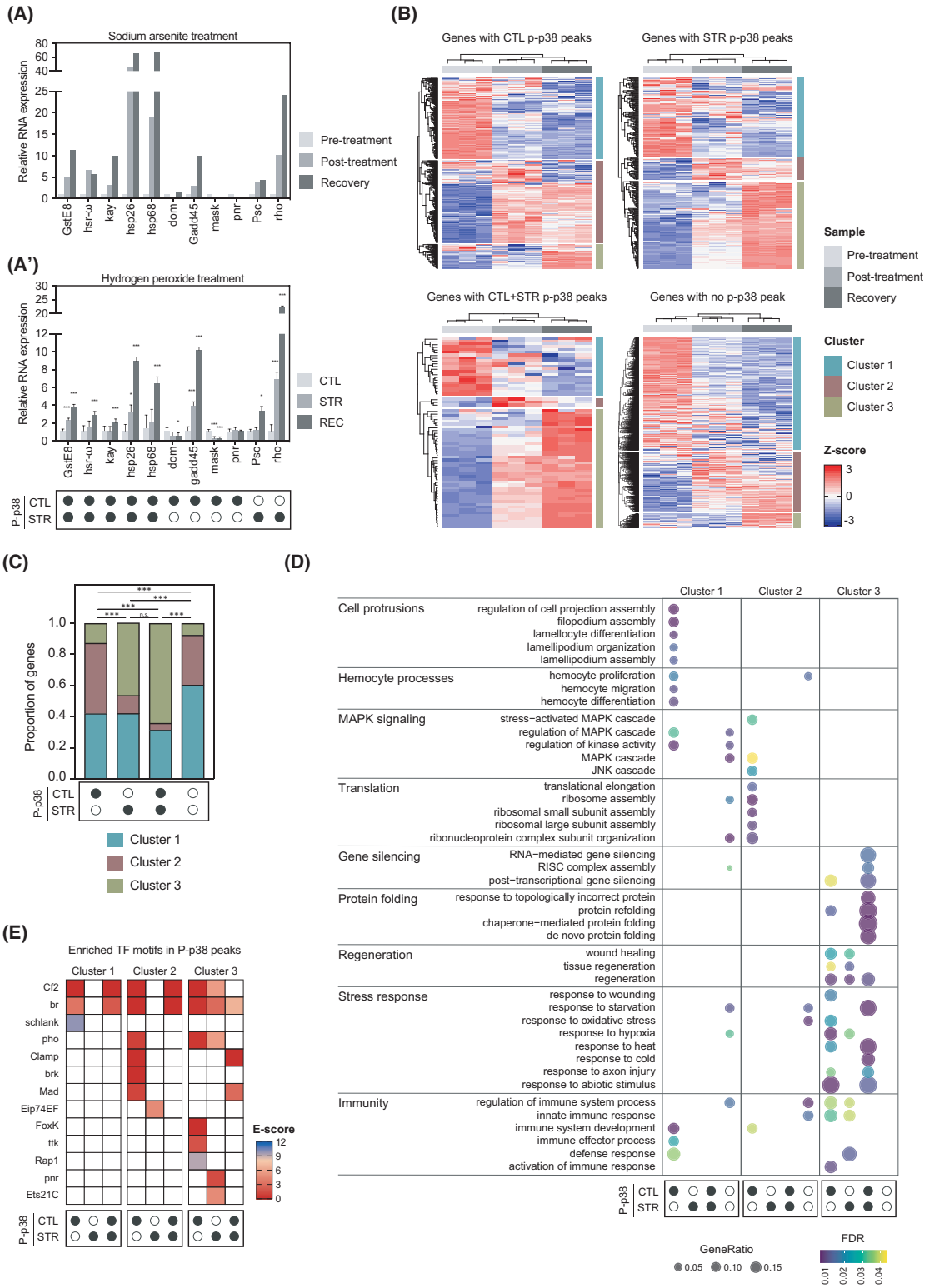

Fig. 3. Stress recovery genes are more associated with P-p38. (A, A') Expression of genes associated with P-p38 peaks. Fold change of TPMs from RNA-seq experiments using S2 cells in control media (Pre-treatment), after 3 h of sodium arsenite exposure (Post-treatment), and after 3 h of recovery in control media (Recovery) are shown from Singh and colleagues [45] (A). Normalized ddCt from the qPCR of S2 cells incubated with control media (CTL), after 30 min of 10 mM H_2O_2 incubation (STR), and after 1 h of recovery in control media (REC) (A'). Error bars in A' represent the standard deviation (SD) of 3 biological replicates. (B) Heatmap of genes containing P-p38 only in the control, only upon stress, in control and stress conditions, and of genes not associated with P-p38. RNA-seq data from Singh *et al.* [45]. Three biological replicates are represented per condition. Normalized *Z*-score is shown for each gene. Complete hierarchical clustering was used to generate gene and sample dendrograms. (C) Proportion of genes assigned to each cluster separated by their association with chromatin P-p38. (D) Selected Gene Ontology (GO) biological process terms enriched in each cluster and condition. Major biological processes are shown for each group of GO terms. Gene Ratio is represented as bubble sizes, while bubble color represents the false discovery rate (FDR). (E) Selected TF motifs enriched in P-p38 chromatin peaks for each cluster. Only TFs expressed Pre-treatment, Post-treatment or in Recovery samples were considered. Two-way ANOVA and Dunnett's test for multiple comparisons were used to assess significance in A'. Chi-squared test with Bonferroni correction for multiple comparisons was used to assess significance in C. ***$P < 0.001$; *$P < 0.05$; n.s., non-significant.

lower than that of genes bound by P-p38 in the control or in both conditions (Fig. 2I). Probably due to the short exposure time to H_2O_2 (30 min), we found very few differential-expressed genes (202 genes; 2.6% of all expressed genes). Altogether, our results suggest that the shift observed in P-p38 binding towards intergenic regions upon stress may occur prior to changes in gene expression.

P-p38 targets recovery genes in response to oxidative stress

To get more insight into the expression profiles of genes associated with P-p38 in response to stress, we used available RNA-seq data obtained from *Drosophila* S2 cells after acute oxidative stress [45]. These data include three different conditions: cells incubated in standard media (Pre-treatment), cells subjected to acute oxidative stress through exposure to sodium arsenite for 3 h (Post-treatment), and cells incubated in control media for 3 h after the sodium arsenite exposure (Recovery). First, we selected several genes associated with chromatin P-p38 and plotted their expression following sodium arsenite treatment from the available RNA-seq (Fig. 3A). Next, we analyzed the expression of the same genes after incubation with H_2O_2 using qPCR (Fig. 3A'). To mimic the sodium arsenite recovery stage, we treated S2 cells with control media for 1 h after H_2O_2 exposure (REC). We noted consistent expression patterns for most tested genes: *hsp26*, *hsp68*, *gadd45*, and *rho* highly increased their expression after oxidative stress, particularly during the recovery stage, whereas the expression of *dom*, *pnr*, and *Psc* remained relatively similar to control in both treatments (Fig. 3A,A'). Given the concordance in transcriptional changes following both oxidative treatments, we subsequently used the RNA-seq data obtained after sodium arsenite incubation [45] to further explore the putative function of P-p38 chromatin-associated genes.

We removed non-expressed genes and defined 4 different gene sets: (a) genes associated with P-p38 chromatin peaks in the control (708 genes), (b) genes associated with P-p38 peaks upon stress (355 genes), (c) genes associated with P-p38 peaks present in both conditions (67 genes), and (d) genes not associated with P-p38 (15 070 genes). Then, each set was subjected to complete hierarchical clustering, revealing 3 separated gene clusters based on their expression: genes upregulated pre-treatment (Cluster 1), genes upregulated post-treatment (Cluster 2), most of which remain activated in recovery, and genes mainly upregulated in the recovery phase (Cluster 3) (Fig. 3B; Fig. S4). The 3 clusters were observed in the four gene sets, but the proportion of genes belonging to each cluster clearly differed. The percentage of Cluster 1 genes was higher among genes not associated with P-p38 compared to any other gene set (Fig. 3C), while genes associated with P-p38 belonged preferentially to Clusters 2 (genes bound by P-p38 only in the control) and 3 (genes bound by P-p38 only under stress or in both conditions) (Fig. 3C). These differences point to distinct trends of gene expression based on P-p38 binding: (a) genes not bound by P-p38 tended to be downregulated upon stress, (b) genes associated with P-p38 only in the control were preferentially upregulated post-treatment, and (c) genes associated with P-p38 upon stress or in both conditions were mainly upregulated in the recovery stage.

We next performed a Gene Ontology (GO) term enrichment analysis of genes belonging to each cluster. In the set of genes associated with P-p38 only in control conditions, Cluster 1 was enriched in biological processes that usually occur on hemocytes, such as the formation of cell protrusions, proliferation, migration, differentiation, and immunity-related processes

(Fig. 3D). These findings were consistent with S2 cells originating from a macrophage-like lineage [55]. On the other hand, Cluster 2 genes were specifically enriched in translation-related processes, including ribosome assembly and translational elongation (Fig. 3D). Genes from Clusters 1 and 2 that were associated with P-p38 only in the control were enriched in the MAPK cascade, which includes p38 itself. While genes from Cluster 1 that were not bound by P-p38 also showed enrichment in the regulation of MAPK signaling, only genes from Cluster 2 showed enrichment in stress-activated MAPKs (Fig. 3D). Probably due to the smaller number of genes, no relevant enrichment was found for genes associated with P-p38 upon stress belonging to Cluster 2. Finally, Cluster 3 genes were enriched in multiple processes occurring during the recovery process upon stress exposure, including gene silencing, protein folding, stress response, and immunity-related terms (Fig. 3D). Interestingly, Cluster 3 genes lacking P-p38 were not enriched in any of these GO terms, suggesting that P-p38 may bind preferentially to genes involved in the recovery process.

Although MAPKs, including p38, lack a DNA binding domain, previous studies have reported their potential interaction with chromatin through the binding to chromatin-associated substrates, such as TFs, RNA polymerase subunits, histone modifying complexes, and ATP-dependent chromatin modifiers [2]. In mammals, TFs are involved in the anchoring of p38 to the chromatin [52]. Because similar mechanisms may exist in *Drosophila*, we searched for TF motifs within the P-p38 chromatin peaks associated with genes in each cluster (Fig. 3E). P-p38 peaks from Cluster 1 genes contained a small number of motifs mostly found in peaks from other clusters. In contrast, P-p38 peaks from genes of Clusters 2 and 3 showed enrichment in specific motifs, with clear differences between control and stress conditions. TFs enriched exclusively in stress-related P-p38 peaks included *pannier* (*pnr*), a gene of the GATA family, whose members are known for their role in the *C. elegans* response to oxidative stress [56], and *Ets at 21C* (*Ets21C*), which coordinates a regeneration-specific gene regulatory network activated by apoptosis in *Drosophila* imaginal discs [57]. The burst of ROS resulting from injuries in these discs is known to be required for the activation of the JNK and p38 signaling pathways, necessary for regenerative growth [58].

Several studies have investigated the relationship between p38 and chromatin [22,25,52] but, to our knowledge, this is the first report on chromatin-associated P-p38. In yeast and mammalian cells, the early stages of the response to various stimuli, including oxidative stress, have been shown to be highly dependent on p38 [26,27]. Hog1, the yeast homolog of p38, controls stress responses by regulating the expression of genes required for a rapid stress response and for the adaptation to future exposure [59,60]. Similarly, in *Drosophila* S2 cells, we found that P-p38 in chromatin was primarily associated with genes that were upregulated after stress exposure and during recovery. Furthermore, a fraction of the chromatin P-p38 is associated with genes involved in major S2 cell functions, such as the formation of cell protrusions, migration, or differentiation. This indicates that, similar to mammalian cells [18,20,29], *Drosophila* P-p38 also plays a role in cellular processes unrelated to stress. Finally, as previously reported for p38 [18,25–29] we found that P-p38 binds to both up and downregulated genes upon exposure to stress, which suggests that the phosphorylated form of p38 may also be involved in the activation and repression of transcription.

Acknowledgements

The authors would like to thank the Genomics Unit at the CRG for assistance with the sequencing and Ivan Sopena-Majós for his help in taking fluorescent images. This research was funded by the Spanish Ministerio de Ciencia, Innovación y Universidades (PID2021-123300NB-100 to F.S. and M.C.) and by the Agència de Gestió d'Ajuts Universitaris i de Recerca (2021SGR00293 to M.C.).

Author contributions

CC-R, PC-C, and MC conceived and designed the experiments. CC-R, PC-C, and PL-G performed the experiments. CCK pre-processed the sequencing data. CC-R, PC-C, and PL-G analyzed the data. CC-R, PC-C, and MC wrote the manuscript. CC-R, PC-C, PL-G, FS, and MC revised and edited the manuscript. FS and MC acquired the funding.

Peer review

The peer review history for this article is available at https://www.webofscience.com/api/gateway/wos/peer-review/10.1002/1873-3468.15006.

Data accessibility

Raw and processed ChIP-seq and RNA-seq data from this study have been submitted to GEO under the accession number GSE220761. Processed BigWig files

used to generate the plots in Figs S2 and S3 are available in Zenodo repository under the DOI number 10.5281/zenodo.13292560.

References

1 Cargnello M and Roux PP (2011) Activation and function of the MAPKs and their substrates, the MAPK-activated protein kinases. *Microbiol Mol Biol Rev* **75**, 50–83.
2 Klein AM, Zaganjor E and Cobb MH (2013) Chromatin-tethered MAPKs. *Curr Opin Cell Biol* **25**, 272–277.
3 Canovas B and Nebreda AR (2021) Diversity and versatility of p38 kinase signalling in health and disease. *Nat Rev Mol Cell Biol* **22**, 346–366.
4 Martínez-Limón A, Joaquin M, Caballero M, Posas F and de Nadal E (2020) The p38 pathway: from biology to cancer therapy. *Int J Mol Sci* **21**, 1–18.
5 Cuadrado A and Nebreda AR (2010) Mechanisms and functions of p38 MAPK signalling. *Biochem J* **429**, 403–417.
6 Maik-Rachline G, Lifshits L and Seger R (2020) Nuclear p38: roles in physiological and pathological processes and regulation of nuclear translocation. *Int J Mol Sci* **21**, 1–23.
7 Nebreda AR and Porras A (2000) p38 MAP kinases: beyond the stress response. *Trends Biochem Sci* **25**, 257–260.
8 Osaki L and Gama P (2013) MAPKs and signal transduction in the control of gastrointestinal epithelial cell proliferation and differentiation. *Int J Mol Sci* **14**, 10143–10161.
9 Rodríguez-Carballo E, Gámez B and Ventura F (2016) p38 MAPK signaling in osteoblast differentiation. *Front Cell Dev Biol* **4**, 1–20.
10 Santabárbara-Ruiz P, López-Santillán M, Martínez-Rodríguez I, Binagui-Casas A, Pérez L, Milán M, Corominas M and Serras F (2015) ROS-induced JNK and p38 signaling is required for unpaired cytokine activation during drosophila regeneration. *PLoS Genet* **11**, 1–26.
11 Segalés J, Perdiguero E and Muñoz-Cánoves P (2016) Regulation of muscle stem cell functions: a focus on the p38 MAPK signaling pathway. *Front Cell Dev Biol* **4**, 1–15.
12 de Nadal E, Ammerer G and Posas F (2011) Controlling gene expression in response to stress. *Nat Rev Genet* **12**, 833–845. doi: 10.1038/nrg3055
13 Ferrigno P, Posas F, Koepp D, Saito H and Silver PA (1998) Regulated nucleo/cytoplasmic exchange of HOG1 MAPK requires the importin β homologs NMD5 and XPO1. *EMBO J* **17**, 5606–5614.
14 Flores K and Seger R (2013) Stimulated nuclear import by β-like importins. *F1000Prime Rep* **5**, 1–7. doi: 10.12703/P5-41
15 Gong X, Ming X, Deng P and Jiang Y (2010) Mechanisms regulating the nuclear translocation of p38 MAP kinase. *J Cell Biochem* **110**, 1420–1429.
16 Wood CD, Thornton TM, Sabio G, Davis RA and Rincon M (2009) Nuclear localization of p38 MAPK in response to DNA damage. *Int J Biol Sci* **5**, 428–437.
17 Zehorai E and Seger R (2019) Beta-like importins mediate the nuclear translocation of MAPKs. *Cell Physiol Biochem* **52**, 802–821.
18 Ambrosino C, Iwata T, Scafoglio C, Mallardo M, Klein R and Nebreda AR (2006) TEF-1 and C/EBPβ are major p38α MAPK-regulated transcription factors in proliferating cardiomyocytes. *Biochem J* **396**, 163–172.
19 Cuadrado A, Corrado N, Perdiguero E, Lafarga V, Mũoz-Canoves P and Nebreda AR (2010) Essential role of p18Hamlet/SRCAP-mediated histone H2A.Z chromatin incorporation in muscle differentiation. *EMBO J* **29**, 2014–2025.
20 Lluís F, Ballestar E, Suelves M, Esteller M and Muñoz-Cánoves P (2005) E47 phosphorylation by p38 MAPK promotes MyoD/E47 association and muscle-specific gene transcription. *EMBO J* **24**, 974–984.
21 Silva A, Cavero S, Sarah V, Solé C, Böttcher R, Chávez S, Posas F and de Nadal E (2017) Regulation of transcription elongation in response to osmostress. *PLoS Genet* **13**, 1–24.
22 Simone C, Forcales SV, Hill DA, Imbalzano AN, Latella L and Puri PL (2004) p38 pathway targets SWI-SNF chromatin-remodeling complex to muscle-specific loci. *Nat Genet* **36**, 738–743.
23 Trempolec N, Dave-Coll N and Nebreda AR (2013) SnapShot: p38 MAPK signaling. *Cell* **152**, 656–656.e1.
24 Proft M, Pascual-Ahuir A, De Nadal E, Arño J, Serrano R and Posas F (2001) Regulation of the Sko1 transcriptional repressor by the Hog1 MAP kinase in response to osmotic stress. *EMBO J* **20**, 1123–1133.
25 Segalés J, Islam ABMMK, Kumar R, Liu QC, Sousa-Victor P, Dilworth FJ, Ballestar E, Perdiguero E and Muñoz-Cánoves P (2016) Chromatin-wide and transcriptome profiling integration uncovers p38α MAPK as a global regulator of skeletal muscle differentiation. *Skelet Muscle* **6**, 1–15.
26 Ferreiro I, Joaquin M, Islam A, Gomez-Lopez G, Barragan M, Lombardía L, Domínguez O, Pisano DG, Lopez-Bigas N, Nebreda AR *et al.* (2010) Whole genome analysis of p38 SAPK-mediated gene expression upon stress. *BMC Genomics* **11**, 144.
27 Posas F, Chamber JR, Heyman JA, Hoeffler JP, De Nadal E and Ariño J (2000) The transcriptional response of yeast to saline stress. *J Biol Chem* **275**, 17249–17255.
28 Lluís F, Perdiguero E, Nebreda AR and Muñoz-Cánoves P (2006) Regulation of skeletal muscle gene expression by p38 MAP kinases. *Trends Cell Biol* **16**, 36–44.

29 Zer C, Sachs G and Shin JM (2007) Identification of genomic targets downstream of p38 mitogen-activated protein kinase pathway mediating tumor necrosis factor-α signaling. *Physiol Genomics* **31**, 343–351.
30 Bigarella CL, Liang R and Ghaffari S (2014) Stem cells and the impact of ROS signaling. *Development* **141**, 4206–4218.
31 Sies H and Jones DP (2020) Reactive oxygen species (ROS) as pleiotropic physiological signalling agents. *Nat Rev Mol Cell Biol* **21**, 363–383.
32 Sinenko SA, Starkova TY, Kuzmin AA and Tomilin AN (2021) Physiological signaling functions of reactive oxygen species in stem cells: from flies to man. *Front Cell Dev Biol* **9**, 1–21.
33 Oswald MCW, Garnham N, Sweeney ST and Landgraf M (2018) Regulation of neuronal development and function by ROS. *FEBS Lett* **592**, 679–691.
34 Serras F (2022) The sooner, the better: ROS, kinases and nutrients at the onset of the damage response in drosophila. *Front Cell Dev Biol* **10**, 1–8.
35 Scepanovic G, Hunter MV, Kafri R and Fernandez-Gonzalez R (2021) p38-mediated cell growth and survival drive rapid embryonic wound repair. *Cell Rep* **37**, 109874.
36 Patel PH, Pénalva C, Kardorff M, Roca M, Pavlović B, Thiel A, Teleman AA and Edgar BA (2019) Damage sensing by a Nox-Ask1-MKK3-p38 signaling pathway mediates regeneration in the adult drosophila midgut. *Nat Commun* **10**, 1–14. doi: 10.1038/s41467-019-12336-w
37 Marco-Sola S, Sammeth M, Guigó R and Ribeca P (2012) The GEM mapper: fast, accurate and versatile alignment by filtration. *Nat Methods* **9**, 1185–1188.
38 Zhang Y, Liu T, Meyer CA, Eeckhoute J, Johnson DS, Bernstein BE, Nusbaum C, Myers RM, Brown M, Li W *et al.* (2008) Model-based analysis of ChIP-seq (MACS). *Genome Biol* **9**, R137.
39 Quinlan AR and Hall IM (2010) BEDTools: a flexible suite of utilities for comparing genomic features. *Bioinformatics* **26**, 841–842.
40 Dobin A, Davis CA, Schlesinger F, Drenkow J, Zaleski C, Jha S, Batut P, Chaisson M and Gingeras TR (2013) STAR: ultrafast universal RNA-seq aligner. *Bioinformatics* **29**, 15–21.
41 Thurmond J, Goodman JL, Strelets VB, Attrill H, Gramates LS, Marygold SJ, Matthews BB, Millburn G, Antonazzo G, Trovisco V *et al.* (2019) FlyBase 2.0: the next generation. *Nucleic Acids Res* **47**, D759–D765.
42 Li B and Dewey CN (2011) RSEM: accurate transcript quantification from RNA-seq data with or without a reference genome. *BMC Bioinformatics* **12**, 323.
43 Love MI, Huber W and Anders S (2014) Moderated estimation of fold change and dispersion for RNA-seq data with DESeq2. *Genome Biol* **15**, 1–21.
44 Stephens M (2017) False discovery rates: a new deal. *Biostatistics* **18**, 275–294.
45 Singh A, Kandi AR, Jayaprakashappa D, Thuery G, Purohit DJ, Huelsmeier J, Singh R, Pothapragada SS, Ramaswami M and Bakthavachalu B (2022) The transcriptional response to oxidative stress is independent of stress-granule formation. *Mol Biol Cell* **33**, 1–16.
46 Yu G, Wang LG, Han Y and He QY (2012) ClusterProfiler: an R package for comparing biological themes among gene clusters. *Omi A J Integr Biol* **16**, 284–287.
47 McLeay RC and Bailey TL (2010) Motif enrichment analysis: a unified framework and an evaluation on ChIP data. *BMC Bioinformatics* **11**, 165.
48 Castro-Mondragon JA, Riudavets-Puig R, Rauluseviciute I, Berhanu Lemma R, Turchi L, Blanc-Mathieu R, Lucas J, Boddie P, Khan A, Manosalva Pérez N *et al.* (2022) JASPAR 2022: the 9th release of the open-access database of transcription factor binding profiles. *Nucleic Acids Res* **50**, D165–D173.
49 Ryabinina OP, Subbian E and Iordanov MS (2006) D-MEKK1, the drosophila orthologue of mammalian MEKK4/MTK1, and Hemipterous/D-MKK7 mediate the activation of D-JNK by cadmium and arsenite in Schneider cells. *BMC Cell Biol* **7**, 1–10.
50 Chen J, Xie C, Tian L, Hong L, Wu X and Han J (2010) Participation of the p38 pathway in drosophila host defense against pathogenic bacteria and fungi. *Proc Natl Acad Sci USA* **107**, 20774–20779.
51 Cully M, Genevet A, Warne P, Treins C, Liu T, Bastien J, Baum B, Tapon N, Leevers SJ and Downward J (2010) A role for p38 stress-activated protein kinase in regulation of cell growth via TORC1. *Mol Cell Biol* **30**, 481–495.
52 Ferreiro I, Barragan M, Gubern A, Ballestar E, Joaquin M and Posas F (2010) The p38 SAPK is recruited to chromatin via its interaction with transcription factors. *J Biol Chem* **285**, 31819–31828.
53 Beacon TH, Delcuve GP, López C, Nardocci G, Kovalchuk I, van Wijnen AJ and Davie JR (2021) The dynamic broad epigenetic (H3K4me3, H3K27ac) domain as a mark of essential genes. *Clin Epigenetics* **13**, 138.
54 Kim TK, Hemberg M, Gray JM, Costa AM, Bear DM, Wu J, Harmin DA, Laptewicz M, Barbara-Haley K, Kuersten S *et al.* (2010) Widespread transcription at neuronal activity-regulated enhancers. *Nature* **465**, 182–187.
55 Echalier G (1997) Drosophila Cells in Culture. Academic Press, San Diego, CA.
56 Hu Q, D'Amora DR, MacNeil LT, Walhout AJM and Kubiseski TJ (2017) The oxidative stress response in *Caenorhabditis elegans* requires the GATA transcription factor ELT-3 and SKN-1/Nrf2. *Genetics* **206**, 1909–1922.
57 Worley MI, Everetts NJ, Yasutomi R, Chang RJ, Saretha S, Yosef N and Hariharan IK (2022) Ets21C

sustains a pro-regenerative transcriptional program in blastema cells of drosophila imaginal discs. *Curr Biol* **32**, 3350–3364.e6.
58 Serras F (2016) The benefits of oxidative stress for tissue repair and regeneration. *Fly (Austin)* **10**, 128–133.
59 Nadal-Ribelles M, Conde N, Flores O, González-Vallinas J, Eyras E, Orozco M, de Nadal E and Posas F (2012) Hog1 bypasses stress-mediated down-regulation of transcription by RNA polymerase II redistribution and chromatin remodeling. *Genome Biol* **13**, 1–11.
60 De Nadal E and Posas F (2015) Osmostress-induced gene expression – a model to understand how stress-activated protein kinases (SAPKs) regulate transcription. *FEBS J* **282**, 3275–3285.

Supporting information

Additional supporting information may be found online in the Supporting Information section at the end of the article.

Fig. S1. Survival curve of S2 cells in control conditions and after exposure to 5 mM, 10 mM, and 20 mM H_2O_2.
Fig. S2. Analyses of P-p38 ChIP-seq peaks.
Fig. S3. Analyses of H3K4me3 ChIP-seq peaks.
Fig. S4. Expression analyses of genes bound by P-p38.
Table S1. List of P-p38 peaks and coordinates.
Table S2. List of H3K4me3 peaks and coordinates.
Table S3. List of oligonucleotides used in this work.
Table S4. List of differentially expressed genes.

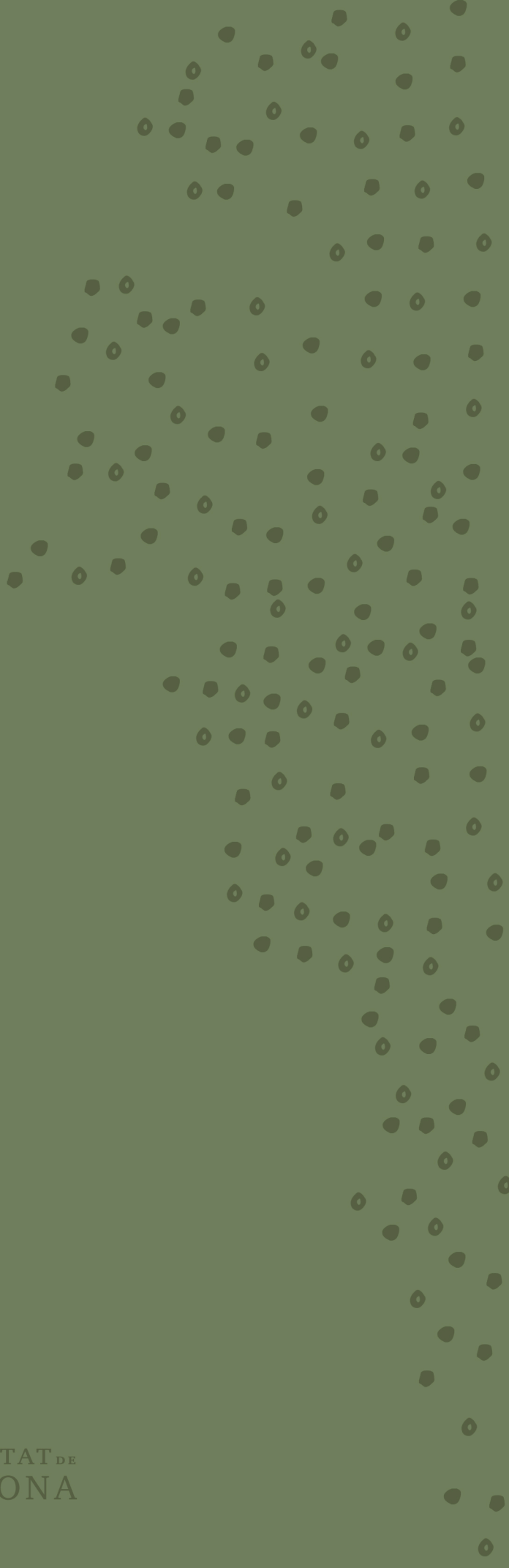

UNIVERSITAT DE BARCELONA